Design of mechanoresponsive surfaces and materials

César Rios Neyra

UNIVERSITÉ DE STRASBOURG

ÉCOLE DOCTORALE DE PHYSIQUE ET CHIMIE PHYSIQUE

INSTITUT CHARLES SADRON

THÈSE

présentée par :

César RIOS NEYRA

Soutenance prévue le : **26 septembre 2013**

pour obtenir le grade de : **Docteur de l'Université de Strasbourg**

Discipline/ Spécialité : Chimie-Physique

DESIGN OF MECHANORESPONSIVE SURFACES AND MATERIALS

THÈSE dirigée par :

M. SCHAAF Pierre	Professeur, Université de Strasbourg

RAPPORTEURS :

Mme. COCHE-GUERENTE Liliane	Maître de Conférences, Université Joseph Fourier, Grenoble 1
M. NARDIN Michel	Directeur de recherches, Institut des sciences des matériaux de Mulhouse

EXAMINATEUR :

M. SCHLATTER Guy	Professeur, Université de Strasbourg

INVITES :

M. JIERRY Loïc	Maître de Conférences, Université de Strasbourg
M. LAVALLE Philippe	Directeur de recherches, INSERM

A mi familia,

Acknowledgements

This PhD work was conducted at the laboratories of the Institut Charles Sadron, UPR 22 CNRS within the “Ingénierie Macromoléculaire aux Interfaces” team and at the INSERM Unit UMR-S 1121 “Biomatériaux et Bioingénierie” in Strasbourg, France.

I would like to express my deepest appreciation to all those that helped and supported me, thus contributing to the accomplishment of my PhD.

I would like to start by expressing my sincere gratitude to Professor Pierre Schaaf, my PhD advisor, for giving me the opportunity to be part of his research group. His continuous support and guidance during my doctoral research was highly appreciated and helpful to work in this challenging topic.

I would like to express my entire gratitude to my co-advisor, Dr. Loïc Jierry, for the interesting scientific discussions, personal advices, motivation and patience during my research work.

I would like to extend my entire gratitude to Dr. Philippe Lavalle, concerning the fluorescence experiments on the confocal microscope, fluorescence microscope and spectrofluorimeter that I performed at INSERM labs. His quality of work, scientific discussions, patience, time and motivation were very appreciated during my thesis.

I also want to thank Dr. Fouzia Boulmedais and Dr. Jean-Claude Voegel for their scientific discussions during the group meetings, advice and patience during my doctoral thesis.

I would also like to thank Dr. Liliane Coche-Guerente and Dr. Michel Nardin for having accepted to act as referees for my thesis work and for providing interesting suggestions. I am also grateful to Professor Guy Schlatter for his participation as president of the advisory committee.

I would also want to thank the directors of the Institut Charles Sadron, Professor Jean-François Legrand and Dr. Jean-Michel Guenet for accepting me as a PhD student at the institut.

I express my sincere gratitude to Dr. Joseph Hemmerlé and Monsieur Karim Benmligh for the design and implementation of the different stretching devices used during my uncountable experiments.

I would not forget the important contribution of Dr. Bernard Senger for the scientific discussions during the group meetings, the FRAP analysis and data treatment of the fluorescence experiments.

I would like to thank Dr. Joseph Selb for his great help during the fluorescence and rheological experiments together with the interpretations of the results and scientific discussions.

I would also like to thank Dr. Jacques Drutz for his time, for teaching me how to use the UV and IR machines as well as the discussion of the results.

I would like to thank Dr. Pascal Marie for the interesting scientific discussions about polydimethylsiloxane substrates and polymerization techniques.

I would like to thank Dr. Andreas Reisch and Dr. Benoît Frisch for teaching me the chemical modification of enzymes and polyelectrolytes and their respective analysis used during my experiments.

I would like to thank all my colleagues that I met during my thesis work with whom I worked or shared the fume hoods and had some fun:

My colleagues from my former lab at ISIS: Patty, Jonathan, Adrian, Anton and Vincent.

My colleagues from INSERM lab: Armelle, Géraldine, Christophe, Morgane, Julien, Engin, Christian, Cédric, Damien, Dominique and Vincent.

My colleagues from IMI lab: Lydie, Johan, Eloïse, Tony, Elodie, Alexandre, Fabien, Thanh, Clément, Cécile, Gaulthier, Mathias, Gwenaëlle, Audrey, Emmanuelle, Nathalie, Jean-Nicolas and Prasad.

I would like also to thank my great friends for all the good times in and out of the ICS:
Maria, Diana, Lara, Johanna, David, Patty, Martin, Gaby, Christi, Andru, Franck, Stéphanie, Akkiz, Dominique, Rémi, Alliny, Nathalie, Anna, Mirella, Olga, Paul, Marek, Souvik, Christophe, Joseph, Gladys, Tam, Hatice, Christiane, Francine, Heveline, Yasmine, Patrycja, Arnaud, Camille, Laure, Sisouk and Daniel, I would never forget that good friends are there when we need them.

Finally, I would like to express my sincere gratefulness to the people who motivate me and trust me during all this time in France, my family:

My parents Maria and Alberto (R.I.P), my brothers P. Alberto Cristian and Carlos and my aunt Carmen for the support, advice and enthusiasm during this adventure since it started in 2006 in France for my studies, especially my PhD.

My dear Rebecca, for sharing my life every day, for the support I get from you when I'm down, the jokes you tell that makes me laugh and for just being like you are.

Abstract

In nature, there are plants that can be folded when being touched by animals or insects. At a lower scale, cells are known to probe the mechanical properties of the surface and adhere on it if it is appropriate for them. It is also well described that some kinds of proteins can exhibit hidden cryptic sites to specific ligands when a mechanical stretch is undergone by these proteins. In all these three examples, a mechanical stimulus starts a cascade of chemical transformations leading to the response of the living organism, the cell, or the protein, respectively.

In the last decade, these mechanosensitive transduction processes have inspired the scientific community and the design of smart materials and surfaces has emerged as a growing and very active field of research. Yet the work described up to now does concern mainly the color switching of materials when stretched or squeezed. In this context, the goal of my thesis was **to develop new routes to design chemo-mechanoresponsive materials**, i.e. materials that respond chemically to a mechanical stress, in a reversible way.

All the systems designed during my PhD thesis were based on the functionalization of silicone sheets: a first way was to create *cryptic site surfaces* by embedding ligands (biotin) into PEG brushes. The couple streptavidin/biotin was used as a model system. At rest, the surface so-prepared was antifouling and biotin ligands were specifically recognized by the streptavidin when the surface was stretched at 50%. Unfortunately, in this first approach, the mechanosensitive surface did not lead to a reversible process. In a second approach, we modified the silicone surface by using the polyelectrolyte multilayer (PEM) film deposition. This strategy was based on the covalent cross-linking of modified enzyme, the *β*-galactosidase, into the PEM. We succeeded in modulating the enzyme activity in the film under stretching and this approach appears as partially reversible under stretching/unstretching cycles. **This work represents the first reported system where enzymatic activity can be modulated by stretching due to modulation of the enzyme conformation**. In a last approach, we also designed a mixed system consisting of a silicone sheet onto which a polyacrylamide hydrogel is covalently attached with the goal to create a stretchable gel into which one can covalently attach enzymes or chemical mechanophores. These enzymes or mechanophores can thus be put under mechanical stress. We succeeded in creating a system that can be stretched up to 150% without detachment of the gel from the silicone and without inducing cracks in the gel.

Résumé

Dans la nature, il existe des plantes capables de se mouvoir quand elles sont touchées par des animaux ou des insectes. A une échelle plus petite, il est connu que les cellules sondent leur environnement pour estimer les propriétés mécaniques de celui-ci et décider d'y adhérer ou non. Il a même été démontré que lorsque certaines protéines sont étirées sous l'effet d'un stress mécanique, elles exhibent des sites cryptiques permettant l'adhésion spécifique de ligands. Dans chacun de ses trois exemples, une cascade de transformations chimiques est amorcée par un stimulus mécanique qui permet une réponse de la plante, de la cellule ou d'une protéine, respectivement.

Au cours des dix dernières années, ces processus de transduction mécano-sensible ont inspiré la communauté scientifique et ont participé au développement d'une nouvelle classe de matériaux dits « intelligents », un domaine très actif et en constante évolution. Il faut cependant noter que dans le cas des matériaux mécano-sensibles, seul des matériaux capables de changer de couleur sous l'effet d'une contrainte mécanique ont été décrits. Dans ce contexte, le but de ma thèse a été de **mettre au point de nouvelles voies d'accès à des matériaux chimio-mécano répondants**, autrement dit, des matériaux capables de permettre une transformation chimique réversible lorsqu'ils sont soumis à un stress mécanique.

Tous les systèmes conçus au cours de ma thèse ont été développés sur des substrats en silicone : une première approche a consisté à créer des *surfaces à sites cryptiques* où une biotine est enfouie dans des brosses de chaines de poly(éthylène glycol) (PEG). Le système streptavidine/biotine a été utilisé comme modèle. Ces surfaces sont anti-adsorbantes à la streptavidine sauf lorsqu'elles sont étirées à hauteur de 50% où cette fois la biotine est reconnue. Ces surfaces mécanorépondantes se sont révélées non réversibles. Dans une seconde approche, nous avons modifiés la surface du silicone par adsorption d'une multicouche de polyélectrolytes. Cette stratégie est basée sur la réticulation covalente du film par une enzyme préalablement modifiée. L'enzyme choisie est la β-galactosidase. Nous sommes ainsi parvenus à créer une surface présentant une activité catalytique modulable par l'étirement mécanique, et ce, d'une façon partiellement réversible. Ce travail représente **le premier exemple d'un système où une contrainte mécanique imposée à un matériau permet la déformation conformationnelle d'une enzyme, à l'origine de la diminution de l'activité catalytique du matériau**. Dans une dernière approche, nous avons conçu un système mixte composé d'un substrat de silicone sur lequel une couche d'épaisseur macroscopique d'un gel de polyacrylamide est greffée de façon covalente. Des enzymes ou d'autres mécanophores pourront ainsi être inclus dans le réseau polymérique du gel de polyacrylamide et ainsi être étirés. Nous sommes parvenus à préparer de tels systèmes où l'hydrogel reste solidaire du film de silicone, sans apparition de craquelures jusqu'à 150% d'étirement.

Table of contents

Chapter 3: Investigation of a bispyrene unit used as a mechanical sensor or a pH probe

Abbreviations

β-Gal	β-Galactosidase
β-Gal^{FITC}	β-Galactosidase labeled with fluorescein
β-Gal-mal	β-Galactosidase-maleimide
β-Gal-mal^{FITC}	β-Galactosidase-maleimide labeled with fluorescein
Biotin-Mal	biotine modified with maleimide groups
CA	contact angle
CLSM	confocal laser scanning microscope
DCC	N, N'-Dicyclohexylcarbodiimide
EDC	N-(3-Dimethylaminopropyl)-N'-ethylcarbodiimide hydrochloride
FDG	fluorescein di(β-D-galactopyranoside)
FITC	fluorescein isothiocyonate
FTIR	fourier transform infrared spectroscopy
HA	hyaluronic acid
LbL	layer by layer
MPS	3-mercaptopropyltrimethoxysilane
NHS	N-Hydroxysuccinimide sodium salt
NMR	nuclerar magnetic resonance spectroscopy
PBS	phosphate buffered saline
PEG	poly(ethylene glycol)
PEG-Mal	poly(ethylene glycol) modified with maleimide groups
PEM	polyelectrolyte multilayers

PLL	poly(L-lysine)
PLL^{FITC}	poly(L-lysine) labeled with fluorescein
PLL-S-TP	poly(L-lysine) modified with thiopyridone groups
PDMS	poly(dimethylsiloxane)
QCM	quartz crystal microbalance
$Strepta^{FITC}$	Streptavidin labeled with fluorescein
TCEP	tris(2-carboxyethyl)phosphine hydrochloride
TRIS	tris(hydroxymethyl)aminomethane
UVO	ultraviolet ozone

General introduction

Material science has received over the last years considerable attention due, in particular, to potential technological applications. Enormous amount of progress has been made in the improvement in materials of high yield strength, materials with high electrical storage capacity or in bioactive biomaterials. One also assists in the emergence of new type of materials called "smart materials", "adaptative materials" or "stimuli responsive materials". These are materials whose properties adapt to changes of their environment[1]. In the area of responsive materials aimed at biomedical applications, the most studied stimuli are temperature, pH, ionic strength and protein concentration. Also investigated are materials that respond to an applied magnetic or electric field. A particularly illustrative example of this type of material is that of surfaces covered by lower critical solution temperature (LCST) polymers such as poly(N-isoprolacrylamide) (PNIPAM). For this polymer, water is a good solvent at low temperature (T < LCST ≈ 30°C) and becomes a poor solvent at temperatures above this value. PNIPAM chains thus adopt an extended conformation at low temperature and a globular conformation above the LCST. Surfaces covered by such a polymer can thus be used to adhere cells at 37°C, a temperature at which water is a poor solvent and to release the cells when the temperature is lowered below the LCST, restoring the initial surface.[2] Another example of application of these PNIPAM polymers is by modifying them chemically by anchoring crown ethers onto them. The interaction of these polymers with different ions changes their LCST. Thus, when working at constant temperature, an increase of ion concentration can render water a good solvent, decreasing the ion concentration can render water a poor solvent. This then directly affects the polymer conformation which adopts an extended coil at high ion concentration and a globule conformation at low ion concentration. By anchoring these polymers onto porous materials one can create an ion gate that closes as soon as the concentration of specific ions reaches a critical concentration.[3]

Using proteins that change conformation in the presence of specific ligand molecules allows creating another type of responsive materials namely materials that change shape in the presence of the ligands. Sui et *al*. used for example calmodulin, a protein that undergoes a rapid but reversible transformation from an extended dumbbell to a collapsed conformation in response to binding of small drug or peptide molecules. They created a material where calmodulin molecules were linked by poly(ethyleneglycol) chains and that changes shape reversibly in the presence of calmodulin ligands.[4] Recently the group of Kumacheva reported

a hydrogel that can undergo two different shape changes when submitted to two different triggers namely a change in temperature and a change in the CO_2 concentration of the contacting liquid.[5] These examples represent only a few of a numerous list of reported stimuli responsive materials.

Despite the great activity in this field, only very few works report materials that respond to a mechanical stress such as a stretching. Such materials are called ***mechanoresponsive***. Most of the mechanoresponsive materials reported so far change color under a mechanical stimulus. This color change can result from structural changes of the material[6] or chemical reactions induced by the mechanical stress[7]. Since more than 8 years the group of P. Schaaf at the Institut Charles Sadron in collaboration with the Unité INSERM "Biomatériaux et bioingénierie" and the Institut des Surfaces et Matériaux de Mulhouse tries to develop systems that respond chemically or biologically by promoting cell adhesion triggered by a mechanical stimulus, namely triggered by stretching. Such systems can be called *chemo* and/or *cyto-mechanoresponsive*. Two types of systems can be envisioned: "bulk" systems and responsive surfaces. In "bulk" systems the active molecules are embedded in the bulk of the material. These molecules either change their chemical nature or their conformation during stretching or interact with other molecules that diffuse from outside into the material, these processes taking place only when the material is under stretching. As far as surfaces are concerned they can be rendered mechanically active either by becoming accessible to "ligands" with which they interact or by changing conformation during stretching.

In order to develop such systems one relies on elastomers. Their surface can be functionalized to become mechanically responsive or the elastomer can play the role of mechanical support for another material which is more fragile. Cross-linked poly(dimethylsiloxane) (PDMS) sheets (silicone) constitute elastomers that appear at first sight as a good choice to develop such systems: silicones are highly elastic with a high ultimate strain, they are fairly transparent which is of importance for microscopy techniques and they are biocompatible which can be of interest for cellular experiments. Yet silicones have also some drawbacks: they are chemically inert and thus difficult to functionalize. Even when functionalized, their properties change slowly with time due to diffusion of low molecular weight PDMS chains out of the material. Nevertheless, we have chosen this material as substrate to develop mechanically responsive systems. Two main strategies were followed in the past in our laboratory to modify the silicone surface. The first strategy consists in creating systems based on polyelectrolyte multilayers that are deposited onto the silicone

sheets. By stretching the silicone sheet, the multilayers are also stretched. If active molecules are embedded in these films they can become accessible to their environment. The other strategy consists of modifying the silicone sheets by polymer plasma in order to be able to further functionalize them with polymer brushes. By stretching one modifies the brush density and eventually exhibits active sites.

The goal of my thesis was to develop new strategies and processes to design **chemo-mechanoresponsive surfaces**. Plasma polymerization is a very powerful technique for surface modification of polymeric materials. Yet it requires a special experimental set-up and an experience that is not usually available in research laboratories. Our first task was thus to find an alternative of surface treatment of the silicone substrates that allows grafting polymer brushes and that leaves the silicone surface elastic (no cracks while stretching). We have developed a method based on UV-Ozone (UVO) surface exposition and further chemical surface modification leading to the introduction of versatile chemical groups on substrate: thiol or methacrylate groups. This way of chemical grafting has been done through a silanization step realized immediately after the UVO treatment. Several techniques like IR, contact angle measurements, optical, electronic and atomic force microscopies were investigated to characterize the resulting modified surface at rest and under stretching. Thus, by anchoring maleimide-poly(ethylene glycol) (Mal-PEG) chains and maleimide-biotin ligands onto thiols-covered substrates (by using the maleimide-thiol click reaction) we created substrates that become adsorptive to streptavidin under stretching (and antifouling at rest). Yet, our systems were not reversible when returning to the non-stretched state. Moreover, we could not obtain surfaces that were fully homogeneous. This work is described in chapter 4.

Next we wanted to develop **bulk materials** that respond to stretching. We selected poly(acrylamide) (PAM) hydrogels into which we wanted to covalently attach enzymes or mechanophore molecules. This kind of chemical gel is a very common hydrogel that has been intensively used to introduce covalent entities in its polymeric network. When stretching the PAM gel, the enzymes or the mechanophore molecules should change conformation and thus change their activity or emission spectrum respectively. Polyacrylamide gels prove to be very fragile and are thus difficult to stretch. For this reason we tried to covalently anchor PAM gels onto silicone substrates which provide the mechanical resistance. Based on the UV-ozone silicone treatment introduced to create brush systems, we thus developed a method that allows getting covalently attached PAM gels onto silicone sheets. A layer of methacrylate groups was introduced on the silicone substrate through chemical silanization. Then, in presence of all the constituting partners of the PAM in water, and the methacrylate-modified silicone

substrate, the radical polymerisation is initiated. The resulting PAM hydrogel is thus covalently and strongly attached on the silicone sheet. Under stretching, the gels do not crack and remain firmly attached to the substrate. This is, to our knowledge, the first reported method that allows to covalently attach a macroscopic sized hydrogel onto a silicone substrate. This work is presently under preparation for publication and will be described in details in chapter 6.

Next we wanted to incorporate mechanophores into this gel. As mechanophore model we selected bispyrene molecules which can be found in two conformations characterized by two separate fluorescent emissions: a "closed" or stacked conformation with a characteristic excimer emission spectrum and an "open" conformation with a characteristic monomer spectrum. We thus synthesized bispyrene molecules which can both play the role of mechanophore and pH sensor. These molecules are constituted of two pyrene rings linked through a triamine linker and flanked by two arms that allow linkage to the polyacrylamide or eventually to another polymer matrix. The idea was that when the polyacrylamide gel is in the non-stretched state, the bispyrene molecules adopt a stacked conformation and when brought under stretching, they adopt an open conformation. Unfortunately our model of mechanophore has adopted an open conformation already rest. They could thus not be used as an effective mechanophores. However, in order to value our molecules we used their properties to be bifunctional and pH sensitive. By ending their two lateral arms with azide moieties, we could use them as bifunctional linkers to be clicked with alkyne bearing polyelectrolytes. We made use of such a system to investigate the behaviour of the one-pot morphogen film driven constructions, a concept recently introduced by our group and that allows building films at an electrode by generating Cu(I) from Cu(II). Cu(I) acts as a catalyst for the azide/alkyne click reaction and allows films to build under the presence of an electrochemical trigger, exclusively from the substrate. Using our bispyrene molecules which can be found in two conformations, open and closed according to pH, we have shown that poly(acrylic acid) based film is not sensitive to the external pH on a large scale and has an interesting swelling/deswelling behaviour during pH variation. This work let to a publication in "Soft Matter" which is presented in chapter 3.

We also modified enzymes, β-Galactosidase, by grafting on their outer lysine groups, arms that allow covalently attaching them in a polyacrylamide hydrogel. Unfortunately we did not achieve creating an enzymatically active polyacrylamide gel. One of the reasons that we envision for this failure is that the exothermic reaction that takes place during the gel formation denatures the enzymes. We thus finally decided to use reticulated poly(L-

lysine)/hyaluronic acid (PLL/HA) polyelectrolyte multilayers as gel and to covalently attach the enzymes inside of it, in order to create an enzymatically-mechanoresponsive systems (chapter 5). An orthogonal bis-reticulation must be used to cross-link the PLL/HA multilayer on one side, and then, to graft later the modified enzymes into the multilayer film by using another kind of coupling chemistry. In order to achieve this goal, one has to proceed in three steps: first, cross-linking the film by using the carbodiimide chemistry, let diffusing the enzymes into the film and finally cross-linking the enzymes into the film through the maleimide-thiol click chemistry already used in a previous part of my manuscript (chapter 4). With this system we achieved creating enzymatically active films whose activity decreases when stretched. This system appears to be partially reversible when returning to the non-stretched state. The results relative to this system are currently under preparation for publication. These results will be presented in details.

Finally, in the chapter 1 will describe the context of my PhD work, including a short historical development of the mechanoresponsive systems since the end of the 19th century up to now. A description of the mechanosensitive processes in biological systems and the contribution of my group in the field of mechanoresponsive systems will complete this first chapter.

The material and the general methods used to realize the work presented in the chapters 3, 4, 5 and 6 are reported in chapter 2. It must be noted that to avoid repeating experimental sections in this chapter, the *Material and Methods* already described in the drafts of publication (chapter 5 and 6) or in published work (chapter 3) have not been repeated in chapter 2.

Chapter 1

State of the art

1.1 A historical perspective

Mechanical force is a notion that is taught in physics courses but that is rarely mentioned in chemistry. Does it mean that mechanical forces have no influence on chemical reactions or chemical processes? Biology proves the contrary. At the end of the 19th century, Julius Wolff made the first observation that bones develop their structure along force lines.[8] This means that cells involved in bone development must be able to sense forces. More recently researchers became aware of the fact that stem cells develop different phenotypes depending on the mechanical properties of their environment.[9] Again, this requires that stem cells are able to sense the mechanical properties of a substrate and transduce mechanical information into intra-cellular chemical signals. The understanding of the molecular mechanisms behind these sensing processes of cells has become a very active field of research and these mechanisms can be a source of inspiration to develop mechanoresponsive systems. We will shortly discuss some of these mechanisms later. Yet, even if chemists seldom refer to mechanical forces, as early as 1930 Staudinger mentioned a reduction in the molecular weight of polymers in response to mastication and he suggested that this might be due to homolytic carbon-carbon bond cleavage induced by mechanical forces.[10] Later, in 1940, Kauzmann and Eyring predicted that stretching specific bonds within a molecule could result in lowering the activation barrier associated with homolytic dissociation by altering the potential energy landscape of the reaction coordinates.[11] This prediction was further validated experimentally since and it was found that bond cleavage induced by mechanical stress exerted on polymer chains occurs more easily for certain chemical bonds than for others. For example, by applying ultrasounds onto polymeric systems Encina and co-workers have shown that peroxide links break ten times faster than carbon-carbon bonds.[12] Very recently the group of Fernandez showed, through elegant AFM force experiments, that reduction of disulfide bonds catalyzed by *Escherichia coli* thioreredoxin is enhanced when the bond is subjected to strong enough a pulling force.[13] The enhancement of the bond breakage seems to follow Bell type law as a function of the applied force, $r(F) = A.\exp((F.\Delta x - E_a)/k_B T)$, where $r(F)$ represents the unbinding rate as a function of the applied pulling force F, A represents a natural frequency of attempt to rupture the bond, Δx is the distance from an equilibrium position to the transition state of the reaction, E_a is the activation energy of the reaction, k_B and T are respectively the Boltzmann constant and the temperature.[14] This law was introduced by Bell in 1978 to describe ligand/receptor forces acting during cell adhesion.[15] Yet it is found that the reduction of disulfide bonds in proteins does not always increase with the applied tensile

force. In the presence of thioredoxin it is decelerated at low pulling forces (below 200 pN) and it is almost insensitive to the pulling force when the reduction reaction is catalyzed by metal ions.[16] Baldus and Gräter predicted, through hybrid quantum and molecular mechanical calculations that redox potentials of disulfide bonds increase when pulling forces are increased from 30 to 3300 pN.[17]

Ultrasounds applied on polymer chains have proven to be a very efficient source for activating reactions through mechanical force. The application of ultrasounds generates cavitation bubbles. During their creation, these bubbles violently aspirate the polymer chains which are then subject to strong mechanical stress.[18] Moore, Sottos and White started exploring this field by incorporating benzocyclobutene into poly(ethylene glycol) chains such that the relative stereochemistry of the polymer attachment points on the benzocyclobutene were either *cis* or *trans*.[19] These chains were than subjected to ultrasounds and the putative *ortho*-quinodimethide products of the mechanical activation were selectively trapped with a maleimide derivative through a [4+2] cycloaddition. Interestingly, only a single isomer was observed, regardless of the stereochemistry of the benzocyclobutene starting material. This indicates that the *cis* and *trans* substituted benzocyclobutene underwent a disrotatory electrocyclic ring opening reaction to afford the same *ortho*-quinodimethide isomer. Yet this result is in violation with the Woodward – Hoffmann rule. It thus seems that thermal activation and mechanical activation reactions do not always follow the same reaction path.

Piermattei et *al*. used also ultrasounds to show that mechanical forces can be used to break bonds between a metal and one of its ligands when incorporated into polymer chains. This can be used to activate a latent organocatalyst which catalyzes a transesterification reaction for example.[20] But most of the advances in this field concern materials that change colour upon stretching. This property is particularly interesting since it allows developping materials that report their points of weakness. This is achieved in different ways. The groups of Sottos and of Moore have incorporated mechanophores into polymer chains that under tensile stress undergo an internal chemical reaction that leads to a change of colour.[21] More precisely they have introduce spiropyran molecules into poly(methyl acrylate) chains that were cross-linked into a poly(methyl methacrylate) matrix. Under stress, spiropyran undergoes an electrocyclic ring-opening reaction and transforms into merocyanine leading to a strong colour change of the material (figure 1.1).

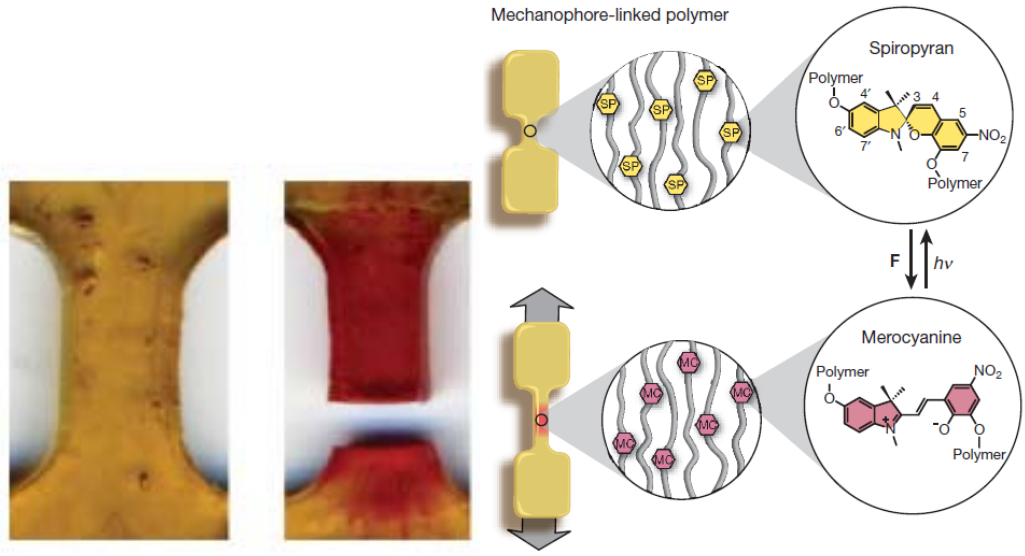

Figure 1.1: Polymethylacrylate sample into which were incorporated chains containing the mechanophore spiropyrane (left) that reacts internally to become merocyanine under stretching (right). Images taken from ref [7].

Since this pioneering work many more polymeric systems incorporating mechanophores based on electrocyclic ring opening reactions have been reported. For example, in 2009, Craig and co-workers reported that *gem*-dichlorocyclopropanes incorporated into polymer backbones could also undergo force-induced electrocyclic ring opening reactions.[22] Using a *gem*-dichlorocyclopropanated indene incorporated into a cross-linked poly(methylacrylate) material, the group of Moore reported recently a new type of material which under compression releases protons (mechanogenerated acid). This is due to a force dependent rearrangement that results in a proton elimination.[23]

Clark and co-workers reported a polymer-protein hybrid material which changes its fluorescence properties when submitted to stress (figure 1.2).[24] This material relies on a new type of protein-based nano-sensor able to report a matrix deformation. This nano-sensor is composed of two cavities that are covalently coupled one to each other and that permanently entrap a pair of donor-acceptor fluorescent proteins giving the possibility for FRET to occur. Under stress, the matrix deforms and these deformations induce a nanometer size separation of the two cavities. This then leads to a FRET reduction. This reduction is very sensitive to Angstrom separations in the material.

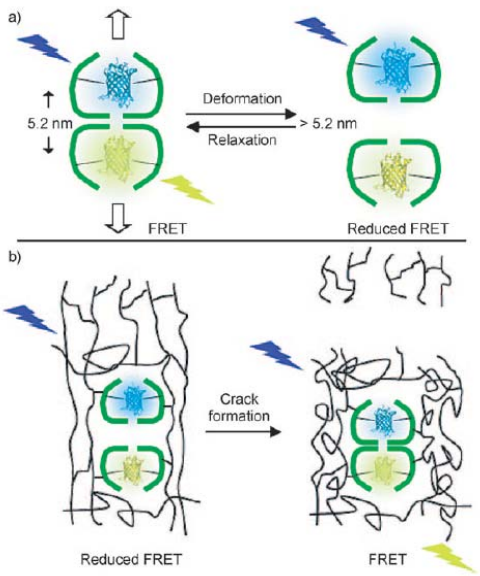

Figure 1.2: Concept of mechano-sensors based on FRET between two fluorescent proteins encapsulated in two cavities of a thermosome. Deformation increases the distance between the two fluorescent molecules resulting in a reduced FRET process. Image taken from ref. [25]

As already mentioned, AFM offers a unique opportunity to sense the effect of mechanical force onto single molecules. Gaub was the first to perform single molecule AFM experiments in which he pulled on single titin proteins. By repeatedly stretching the protein he showed the reversible unfolding of individual immunoglobulin domains (figure 1.3).[26]

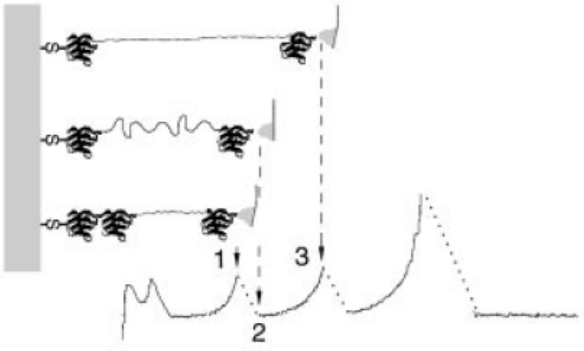

Figure 1.3: AFM stretching curve of four immunoglobulin domain. One observes the unfolding of the different domains during stretching. Image taken from ref. [26]

This work showed that one can reversibly change the conformation of proteins by AFM and opened the route towards single molecule stretching experiments. Later on Gaub and coworkers used this same technique to apply forces onto an enzyme, lipase B from

Candida Antartica. They applied a periodic stretching-release protocol on the enzyme and found that not the force but the release of the force triggers the enzymatic activity.[27] This seems to be due to the release of the constraint on the enzyme allowing the proteins to rearrange along a given path which goes through activation sites in the free energy landscape.

In 2010 Tseng at al. addressed the problem of the coupling between mechanics and chemistry in an enzyme through equilibrium experiments.[28] The enzyme was deformed through a DNA molecular spring method (figure 1.4) and the effect on the chemical reaction it catalyzes was determined.

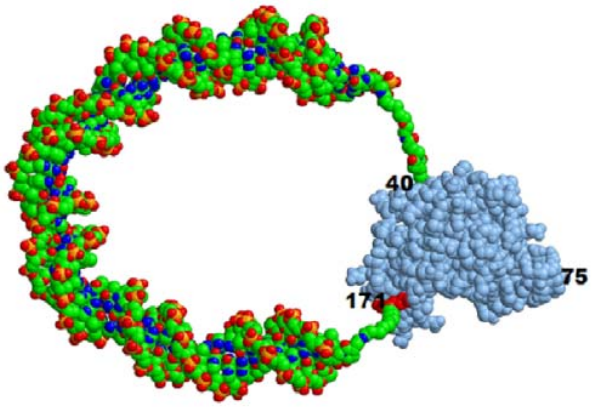

Figure 1.4: Representation of the DNA molecular spring method. A single stranded DNA is covalently coupled on an enzyme at two defined positions. When interacting with the complementary strand, the DNA stiffens inducing tension in the enzyme. The enzymatic activity of the enzyme is then measured. Image taken from ref. [28]

As enzyme they used guanylate kinase that was modified such as to create a protein-DNA chimera. Depending of the ligation position of the DNA and its length, they found that the enzyme activity was reduced and the reduction was stronger for shorter DNA (larger strength exerted by the DNA on the enzyme) even if the effect remains moderate (less than 10% reduction on the kinetic parameters).

1.2 Mechanochemistry in biological systems

One of the great differences between proteins and small molecules is their secondary, ternary and quaternary structure and their flexibility. These properties allow conformational changes of the proteins in a predetermined way under external stimuli and in particular under external forces. There are several mechanisms by which cells transform a force into a

chemical signal. One of them is based on force-induced conformational changes in proteins, and in particular in adhesive proteins. These then modify the interactions between these proteins and their ligands. There are several different ways in which a force can modify the affinity of a protein towards its ligand: (1) by modifying the conformation of a domain of the protein that allosterically regulates the binding site; (2) by exposing active sites that are buried in the native conformation (cryptic sites).

1.2.1 Enhancement of mechanical forces due to allosteric regulation

Cellular adhesion is mediated through adhesion proteins that bind ligands often in an external force responsive way. One prominent example is provided by leukocytes which, in response to an inflammatory process, are recruited from the bloodstream. The adhesion of leukocytes on blood vessels takes place through a variety of interactions, among them selectin-ligand and a subset of integrin-ligand interactions support rolling. The whole process takes place under hydrodynamic shear forces and nature has optimised the structure of the involved proteins to respond to this stress. Whereas for most ligand-receptor complexes, the lifetime decreases as a tensile force is applied on them (slip bonds), for selectin and integrins this bond lifetime first increases when the force strength increases, up to a critical force before decreasing at even higher forces (catch bonds). Selectins contain a ligand-binding lectin domain that binds in particular to the primary ligands P-selecting glycoprotein ligand 1 (PSGL-1), an epidermal growth factor-like (EGF) domain, multiple short consensus repeat domains, a transmembrane domain and a short cytoplasmic domain. They are found in two different conformations: a bent conformation in which the lectin and the EGF domains form an angle lying between 116° and 121° corresponding to a low affinity state towards PSGL-1 binding and an extended conformation in which the two domains form an angle lying between 149° and 154° and which corresponds to a high affinity state towards PSGL-1 binding [29]. Forces exerted throughout the length of the receptor/ligand complex favour energetically the extended conformation and thus induce a transition from the bent to the extended conformation and thus from the low to the high affinity state (figure 1.5). This explains the increase of the lifetime of the complex as the force increases.[29]

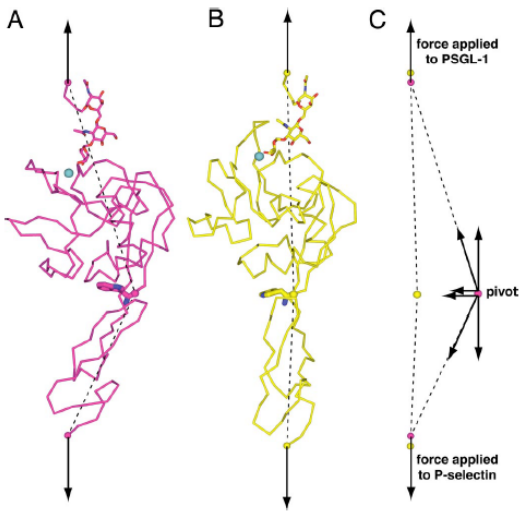

Figure 1.5: Model for the conformational change of P-selectin under tensile force. In the absence of force the protein is in a bent conformation. Under tensile force the protein takes an extended conformation. The binding to receptors is different in these two conformations. Image taken from ref. [29]

A similar force regulated binding strength takes place on integrins binding to intercellular adhesion molecule-1 (ICAM-1). Integrins are heterodimer molecules constituted of two units, α and β, which mediate cell-cell and cell-extracellular matrix interactions. The integrin subunit α contains a domain known as the integrated (I) domain which is a major binding site. This domain is constituted of seven α helices surrounding a central, six-stranded β sheet. The C- and N- termini of the α I domain are close one to each other on the "lower" face whereas the upper face is a metal-ion dependent adhesion site (MIDAS). Domain I can be found in two different states, a high-affinity and a low affinity state towards ligand.[30] When an integrin binds an ICAM-1 on a substrate in shear flow, a tensile force tends to lengthen the molecules. Due to this force, one of the α helices, α7, of the integrin is displaced axially towards its C-terminus which stabilizes the high affinity conformation of domain I.[31] A general picture of conformational changes induced by mechanical forces leading to higher receptor affinity is presented in figure 1.6.

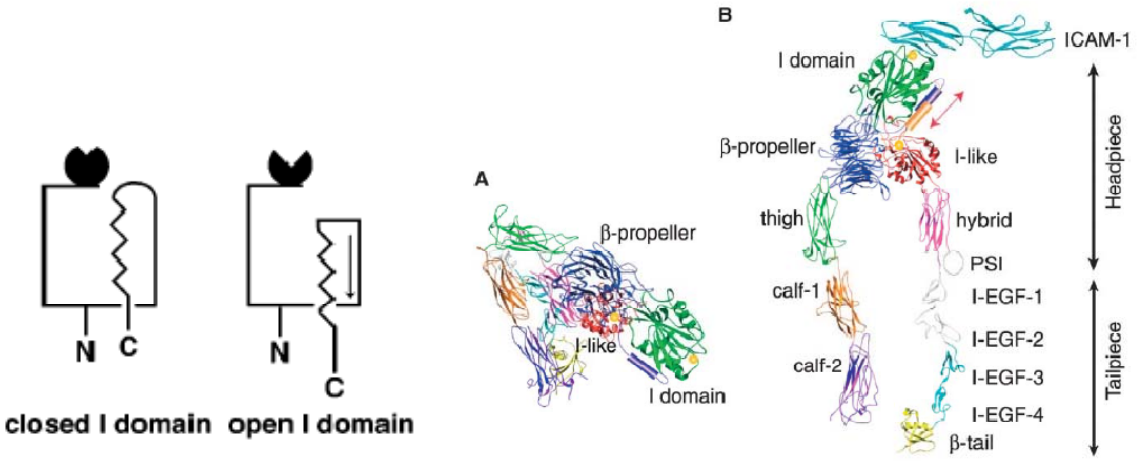

Figure 1.6: (left) schematic representation of the conformational change of domain I of $\alpha_L\beta_2$ binding to intercellular adhesion molecule-1 (ICAM-1). (right) Representation of the conformational changes of Integring domain I under tensile force : (A) Bent conformation of the $\alpha_L\beta_2$ integrin extracellular domain I with the closed headpiece and low affinity I domain; (B) Extended conformation with the open headpiece high affinity I domain and bound ICAM-1. Images taken from ref. [30, 31]

Another example of catch bonds is provided by the bacterial adhesive protein, FimH, which is the terminal adhesin on type 1 fimbriae, and which binds carbohydrate mannose and mediates weak bacterial adhesion at low flow and strong adhesion at high flow. FimH has two domains, a pilin domain that integrates FimH into the fimbriae and a lectin domain that binds to mannose. A linker chain connects the two domains. Steered Molecular Dynamics suggest that tensile forces applied on the N and C terminus of the lectin domain induce an extension in the linker domain.[32] It was also shown that the disruption between the lectin and the pilin domains by a structural mutation of the interdomain increases the affinity of the lectin for mannose by up to 300 times.[33] The interdomain thus regulates, in an allosteric way, the mannose binding domain and this also explains the increase of binding under shear force: as for selectins, the application of a force induces a conformational change in the protein which switches allosterically the binding domain from a low to a high affinity state.

1.2.2 Cryptic site proteins

Integrins play a crucial role in mechanostransduction as they are one of the major adhesion components that transfer a signal from the extracellular matrix to the cytoplasm. Outside of the cell, integrins are coupled to extracellular matrix proteins such as fibronectin;

inside of the cell they are coupled to proteins such as talin or filamins that make the link with the cytoskeleton. One way in which a force is converted into a biochemical signal, a stronger bonding for example, is by exhibiting cryptic sites. These sites are buried inside the protein in its unconstrained state whereas they become accessible when the protein is stretched under a tensile force. Fibronectin, for example, is constituted of more than 50 module repeats, many of them possessing an RGD adhesion sequence buried in their interior. Under tensile force, these modules partially unfold, exposing their adhesion site which is recognized by integrins. Moreover, the sequential unfolding of the modules can signal the magnitude of the stress that is acting on the protein.[34]

Inside of the cell one important adhesion player is talin. Talin couples the cytoskeleton to the extracellular matrix through integrins. It can bind to vinculin for assembly and reorganization of the actin cytoskeleton. Talin is constituted of a head that binds and activates integrins and of a rod that contains bundles of α-helices with up to 11 buried vinculin binding sites. These sites become exposed by the application of a tensile force that stretches the molecule by a sequential unfolding of the helical bundles (figure 1.7).[35]

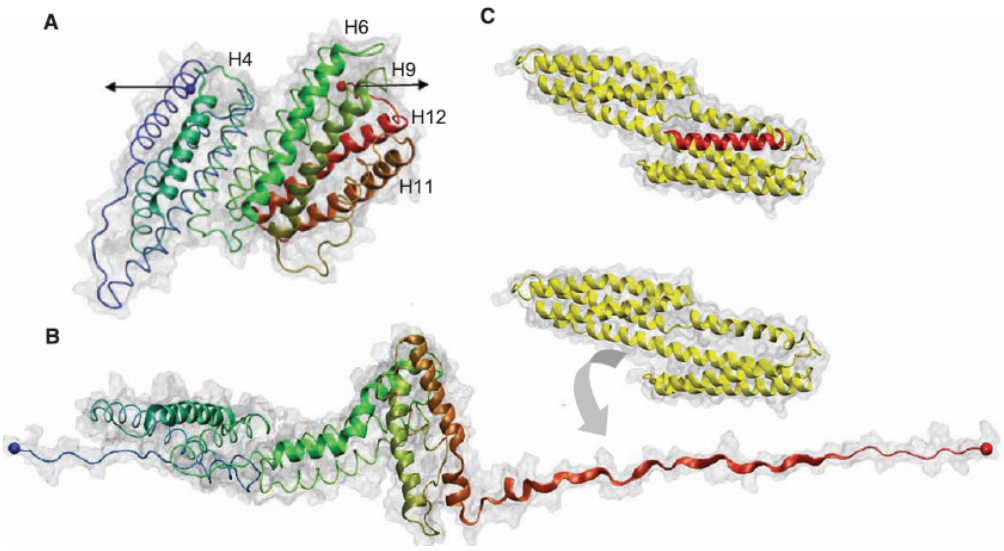

Figure 1.7: Representation of a domain of Talin (A) at rest; (B) under stretch. Under stretch the domain unfolds exhibiting an interaction domain with Vinculin (C). Image taken from ref [36].

Filamins constitute another family of proteins that connect transmembrane receptors such as integrins to actin. Filamins are dimeric proteins that consist of an N-terminal actin binding domain followed by 24 immunoglobulin-like domains (FLNa1-24).[37] Filamins bind the integrins through interactions between the cytoplasmic tails of the integrin β chains and

CD faces of FLNa19 and FLNa21. However, these CD faces are masked by the A-strand of the preceding FLNa18 and FLNa20 domains, thus inhibiting integrin binding.[14] Steered Molecular Dynamics (SMD) simulations suggest that the CD faces of FLNa19 and FLNa21 become exposed as a force applies to the filamin rod. The force induces an unraveling of the filamin fragment structure via a displacement of the A-strand and a dissociation of the domain-domain interactions. Folding of the integrin binding domains FLNa19 and FLNa21 remain intact. This process exposes the binding of filamin to the integrin cytoplasmic tail allowing for the interaction to take place.[38]

1.3 Cryptic site substrates

It thus clearly appears that the first steps of the mechanism by which cells transform mechanical information into a chemical signal involve conformational changes of proteins by which cryptic sites become accessible for interaction with other proteins. Exhibiting crytic sites or molecules by stretching a material or a surface is the strategy followed by the group in which I performed my PhD work to create chemo or cyto mechanoresponsive substrates. We will now briefly review the research done in this field since 2005 by our group. Two routes were followed to develop such substrates: one route was based on polyelectrolyte multilayers and one route was based on grafting polymer brushes directly on silicone sheets.

1.3.1 Polyelectrolyte multilayer based mechanoresponsive systems

Polyelectrolyte multilayers are obtained by bringing a substrate alternately in contact with a polyanion and a polycation solution.[39] This concept was introduced in 1991 by Decher.[40] There exist two kinds of polyelectrolyte multilayers. The first multilayers that were discovered correspond to films whose thickness increases linearly with the number of deposition steps. These films are nicely stratified[39] and no polyelectrolyte can diffuse through the film. The two most studied linearly growing polyelectrolyte multilayers are poly(styrene sulfonate)/poly(allylamine hydrochloride) (PSS/PAH) and poly(acrylic acid)/poly(diallyl dimethyl ammonium chloride) (PAA/PDADMA). In 1999 Elbert et al. discovered a second kind of multilayers, namely films whose thickness increases exponentially with the number of deposition steps.[41] Picart et al. showed that this growth behaviour is due to the fact that at least one of the two polyelectrolytes participating in the film construction diffuses in and out of the film at each bilayer deposition step.[42] These films correspond in fact to gel-like structures into which one can incorporate proteins and enzymes which can diffuse in the

film.[43] It was also found that polyelectrolyte multilayers preserve the enzymatic activity. Garza et al.[44] showed that one can deposit linearly growing films on top of exponentially growing ones and that the linearly growing film then acts as a barrier towards the diffusion of polyelectrolytes from the solution into the exponentially growing multilayer. This type of architecture is called a reservoir-barrier architecture.

In a first study two linearly growing multilayers were deposited one on top of the other, namely a poly(acrylic acid)/poly(allylamine hydrochloride) film on top of a Nafion/ poly(allylamine hydrochloride). This structure was deposited on a silicone substrate that could be stretched. Nafion being hydrophobic and the (PAA/PAH) film being hydrophilic, one observed a reversible hydrophobicity change during stretching/unstretching cycles. The amplitude of the hydrophobicity changes, measured by changes in the water contact angle, were important (variations of the water contact angle between 110 and 50°) when the ending (PAA/PAH) multilayer was constituted of two bilayers whereas changes of less than 10° were observed when the (PAA/PAH) film was constituted of 4 bilayers. The reversible change in hydrophobicity was interpreted as being due to a thinning of the ending multilayer under stretching, leading to the appearance of Nafion that comes in contact with water. Yet when the outer multilayer becomes too thick, Nafion remains always embedded under the PAA/PAH multilayer, whatever the stretching degree.[45]

Next the behaviour under stretching of reservoir-barrier structures was investigated with the idea to open the barrier under stretching and to close it again when returning to the non-stretched state. Two types of architectures were investigated (HA/PLL)-(PSS/PAH) and (HA/PLL)-(PSS/PDADMA) (HA: hyaluronic acid; PLL: poly(L-lysine)) where (HA/PLL) is an exponentially growing film which plays the role of reservoir and (PSS/PAH) and (PSS/PDADMA) are two linearly growing films which play the role of barrier. Whereas stretching the film induced cracks in the (PSS/PAH) multilayer which appears brittle, holes in the nanometer range formed with the (PSS/PDADMA) multilayer. When returning to the non-stretched state, the cracks closed and the two sides of the cracks became adjacent for (PSS/PAH) leading to a partial healing (figure 1.8).

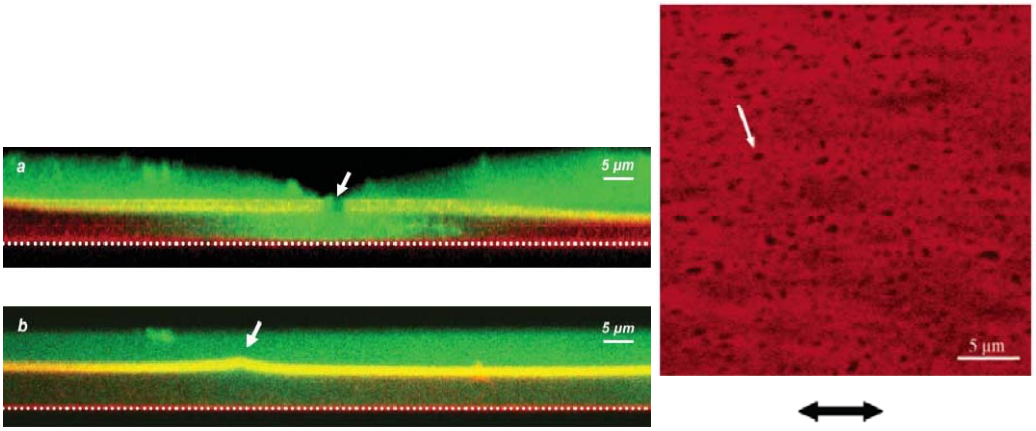

Figure 1.8: (left) Confocal laser microscopy image of a $(PLL/HA)_{30}/PLL^{Rho}/(HA/PLL)/(PSS/PAH)_{30}/(HA/PLL)_{30}(HA/PLL^{FITC})$ under stretching (top) and after coming back to rest (bottom). Image taken from ref.[46] (right): Fluorescence microscopy image of a $(PLL/HA)_{30}/PLL^{Rho}/(HA/PLL)/(PSS/PDADMA)_5/(HA/PLL)_{30}(HA/PLL^{FITC})$ film under stretching. One observes nanovalves all over the surface. Image taken from ref. [47]

For the (PSS/PDADMA) case, the holes disappeared so that the system healed totally.[46, 47] These results were obtained by bringing the film in contact with the polyelectrolyte solutions during 10 minutes during each deposition step. Yet the linearly growing film is deposited on top of an exponentially growing one into which polyelectrolytes can diffuse and even exchange with polyelectrolyte chains already present in the film. This renders the buildup process sensitive to the contact time between the film and the polyelectrolyte solutions during the deposition steps. It was shown more recently that by reducing this contact time, no holes forms anymore under stretching for the (PSS/PDADMA) barrier and the barrier can remain tied under stretching when the number of bilayers constituting the barrier exceeds four.[48, 49]

This observation led to the development of the first substrate that became enzymatically active under stretching in a partially reversible way.[48] This substrate was constituted of a (HA/PLL)-(PSS/PDADMA) architecture where an enzyme, alkaline phosphatase, was incorporated in the reservoir. The film was deposited on a silicone sheet. Alkaline phosphatase is a hydrolase enzyme responsible for dephosphorylation of many types of molecules, including fluorescein diphosphate (FDP). FDP is a non-fluorescent substrate and hydrolysis of its two phosphate substituents mediated by alkaline phosphatase yields weakly fluorescent fluorescein monophosphate followed by strongly fluorescent fluorescein. FDP was present in the solution in contact with this film. In the absence of stretching, the

(PSS/PDADMA) multilayer played the role of barrier towards FDP. When the film was stretched above 70% a strong fluorescence increase was observed in the solution indicating that the enzymes became accessible to the substrate and remained active. When returning to the non-stretched state, the enzymatic activity was again strongly (but not totally) inhibited indicating reversibility of the system. It was shown that the (PSS/PDADMA) multilayer remained tied to FDP and that the enzymes present in the reservoir were exhibited through the barrier. This system can thus be qualified as the first cryptic site substrate. It is schematically represented in figure 1.9.

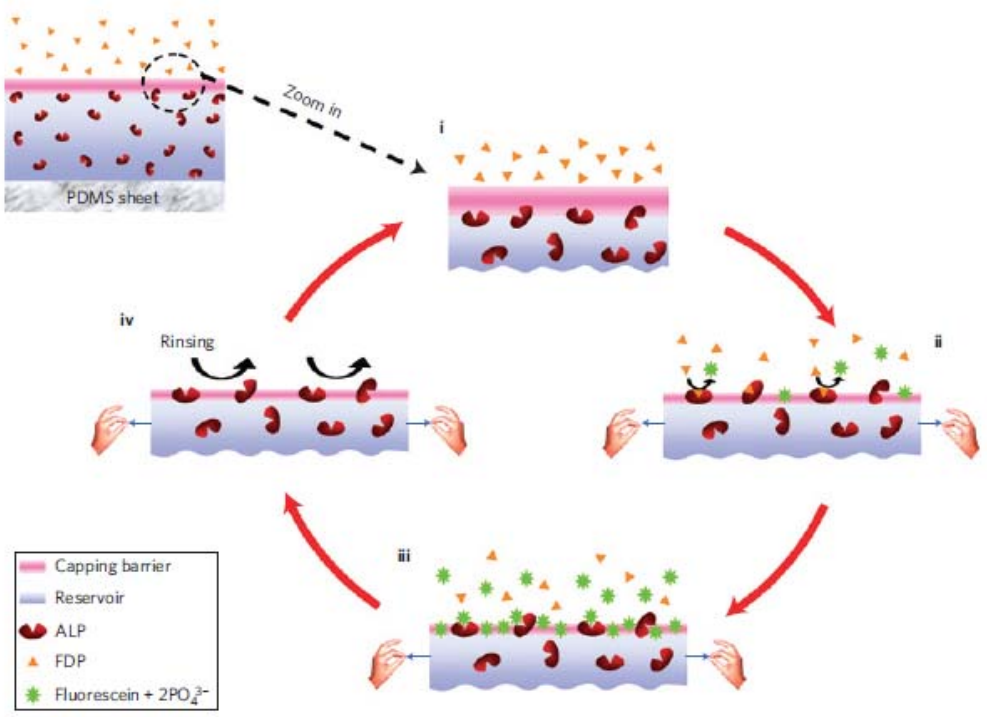

Figure 1.9: Schematic representation of the first enzymatic mechano-responsive film. Enzymes are embedded in a (HA/PLL) multilayer that is capped by a (PSS/PDADMA) multilayer playing the role of barrier towards the substrate of the enzyme. Under stretching the enzymes becomes accessible to its substrate and the reaction takes place. This system is close to reversible. Image taken ref.[48]

More recently the same concept was applied but in the reverse way, namely by incorporating the substrate FDP in the reservoir and by anchoring, on top of the (PSS/PDADMA) barrier the enzyme alkaline phosphatase.[50] At rest the film was inactive and by stretching fluorescein diffused from the film towards the solution. This was due to the fact that by stretching the FDP substrate could come in contact with the enzymes and that

fluorescein, the product of the reaction, diffused into the solution. Unfortunately this system was not reversible.

Polyelectrolyte multilayers were also used in another way to create chemoresponsive substrates. Poly(acrylic acid) chains were chemically modified by grafting onto them phosphorylcholine moieties through short ethylene oxide linkers $(EO)_3$ (PAA-PC chains). The grafting ratio was about 25%. Phosphorycholine groups cover the outer membrane of red blood cells and are responsible for their non-thrombogenic character.[51] These chains were then used to built PEI/$(PSS/PAH)_3$/PSS/$(PAH/PAA\text{-}PC)_2$ multilayer architectures which were deposited on silicone sheets. These films proved to be antifouling (no protein adsorption and no cell adhesion) at rest and under stretching at least up to a stretching degree of 50%.[52] These films were further functionalized by incorporating, between the $(PSS/PAH)_3$ and the $(PAH/PAA\text{-}PC)_2$ multilayers one layer of PAA chains modified by grafting biotin or (arginine-glycine-aspartactic acid) (RGD) peptides again linked to the PAA chains through an $(EO)_3$ linker. Biotin is a ligand of streptavidin and the biotin/streptavidin bond is one of the strongest non-covalent bonds reported in biology (for a schematic representation see figure 1.10).[53]

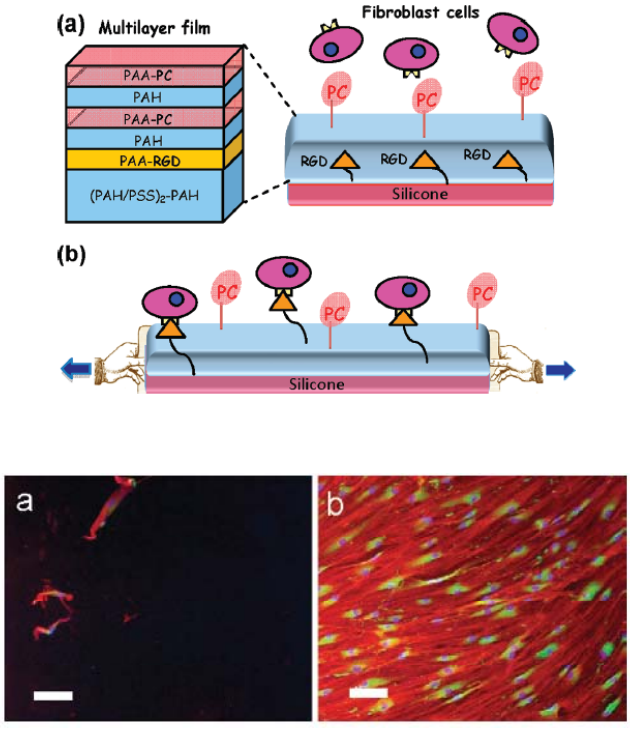

Figure 1.10: (top) Schematic representation of the fist cryptic surface film based on embedding ligands (her RGD peptides) under a multilayer (PAH/PAA-CP). (bottom left) Cells deposited on a non stretched films do not adhere; (bottom right) When stretched the film becomes cell adherent due to RGD peptide exhibition. Images taken from ref[54].

RGD peptides are known to promote cell adhesion through interactions with integrins. At rest these architectures remain antifouling and no interaction is observed with streptavidin (in the case of biotin) or cells in the case of RGD. By stretching these films up to 50%, they become specifically interacting with streptavidin and adherent to cells. The amount of streptavidin depositing on a stretched film increases linearly with the stretching degree up to 50% of stretching.[54] This shows that stretching these architectures renders ligands accessible to their receptors. Yet this system was not reversible: when returning to the non-stretched state the substrate remained interactive with streptavidin or cells.

1.3.2 Responsive systems based on poly(ethylene oxide) brushes[55]

The latter system we just described was based both on polyelectrolyte multilayers and on short PEO-PC chains extending into the solution. Another strategy to built cryptic site substrates was based on poly(ethylene oxide) chains of mass of about 2000 (45 monomers) and NH_2-$(EO)_3$-biotin or NH_2-$(EO)_3$-RGD peptides that are directly anchored onto silicone sheets. In order to achieve the grafting onto the silicone sheets, the substrate was first modified by plasma polymerization of maleic anhydride resulting in an anhydride maleic polymer film deposited on the silicone substrate. The anhydride maleic groups were then hydrolysed through contact with water resulting in a surface covered by carboxylic groups. The difficulty of this type of functionalization is to sufficiently cover the surface yet not to render the functionalized surface brittle which would result in cracks during stretching.[56] Once this functionalization was achieved, PEO chains ending by an amine group were covalently fixed onto the surface through EDC/NHS chemistry performed under stretching at 60°C. In a second step, ligands, biotin or RGD peptides, terminated by an amine were covalently anchored onto the remaining non-reacted carboxylic groups under stretching. When returning to the non-stretched state, this system appeared anti-fouling, non-interacting with streptavidin and non cell adherent. Under stretching streptavidin interacted with the surface and cells adhered readily. When returning to the non stretched state the system returned to its initial state. The postulated mechanism is schematically represented in figure 1.11. The mechanoresponsive process appears that totally reversible and this appears to be the first reversible *cyto* and *chemo mechanoresponsive* system. One of our goals was to achieve a similar system, yet without using plasma polymerisation, a technique that is readily available in most chemistry laboratories.

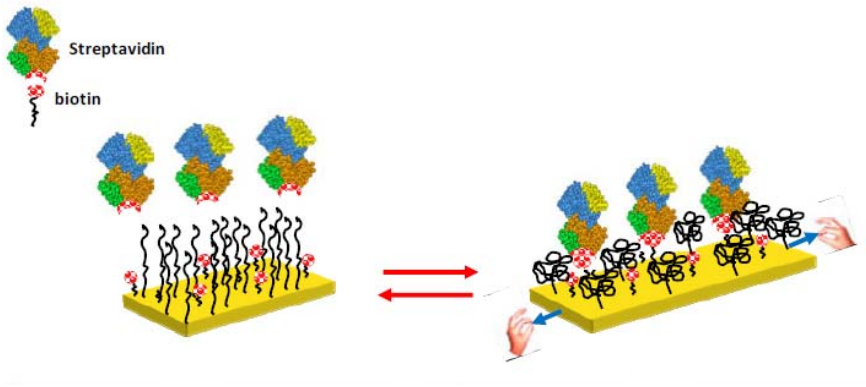

Figure 1.11: Schematic representation of the first fully reversible cyto and chemo mechano-responsive film. The grafting of the PEG chains and the biotin (or RGD) ligands is based on a first functionalization of the silicone substrate (yellow) by polymer plasma treatment. Image taken from ref. [55]

1.4 Summary

In the last decade, important breakthroughs have been reported in the field of mechanoresponsive material design. Most of these works does concern exclusively the transduction of a mechanical force into a changing of colour (or fluorescence emission) of the material. The reason for this is not a lack of originality but rather due to the impossibility to get another outcome. Indeed, the mechanophore-contained materials investigated, such as polyethylene or polymethylmethacrylate, are mainly inert to their environment: they cannot communicate with the surrounding media through exchange with solution (aqueous or organic) or air, except displaying a colour. Thus, the transformation of the mechanical stress undergone by the material cannot lead to a change of a catalytic reaction, a releasing of compounds or a recognition process: only the emission of light seems to be the response of these kinds of systems. In all these mecanoresponsive material, the strategy systematically involved is founded on the molecular incorporation of the mecanophore into the polymeric architecture of the material. Thus, the host material chosen is of crucial importance because it must be both resistant to stress and elastic to be reversibly mechanoresponsive. It most cases, this last feature is not met.

The contribution of my group is based on another strategy inspired from nature: use cryptic site pocket to design a new kind of mechanoresponsive systems. An important contribution has been reported since 2005 in the literature, as described in this first chapter. In this strategy, only the material will undergo the mechanical force. The consequence of this

force is to reveal active sites, which were not accessible before the imposition of the stress. By using multilayer films or PEG brushes, these aqueous based systems in essence can exchange and thus communicate with their environment through water. This property let hopes to design a new class of 2D or 3D mechanoresponsive systems able to recognize molecules specifically and have catalytic activity triggered by a mechanical force. This was the aim of my PhD project: "Design of mechanoresponsive surfaces and materials".

1.5 References

1. Stuart, M. A. C.; Huck, W. T. S.; Genzer, J.; Muller, M.; Ober, C.; Stamm, M.; Sukhorukov, G. B.; Szleifer, I.; Tsukruk, V. V.; Urban, M.; Winnik, F.; Zauscher, S.; Luzinov, I.; Minko, S., Emerging applications of stimuli-responsive polymer materials. *Nature Materials 9*, 101-113.

2. Yamada, N.; Okano, T.; Sakai, H.; Karikusa, F.; Sawasaki, Y.; Sakurai, Y., Thermoresponsive Polymeric Surfaces - Control of Attachment and Detachment of Cultured-Cells. *Makromol. Chem-Rapid* **1990,** *11*, 571-576.

3. Ito, T.; Hioki, T.; Yamaguchi, T.; Shinbo, T.; Nakao, S.; Kimura, S., Development of a molecular recognition ion gating membrane and estimation of its pore size control. *Journal of the American Chemical Society* **2002,** *124*, 7840-7846.

4. Sui, Z. J.; King, W. J.; Murphy, W. L., Dynamic materials based on a protein conformational change. *Advanced Materials* **2007,** *19*, 3377-3380.

5. Lukach, A.; Liu, K.; Therien-Aubin, H.; Kumacheva, E., Controlling the Degree of Polymerization, Bond Lengths, and Bond Angles of Plasmonic Polymers. *Journal of the American Chemical Society* **2013,** *134*, 18853-18859.

6. Lott, J.; Weder, C., Luminescent Mechanochromic Sensors Based on Poly(vinylidene fluoride) and Excimer-Forming p-Phenylene Vinylene Dyes. *Macromolecular Chemistry and Physics* **2010,** *211*, 28-34.

7. Davis, D. A.; Hamilton, A.; Yang, J.; Cremar, L. D.; Van Gough, D.; Potisek, S. L.; Ong, M. T.; Braun, P. V.; Martinez, T. J.; White, S. R.; Moore, J. S.; Sottos, N. R., Force-induced activation of covalent bonds in mechanoresponsive polymeric materials. *Nature* **2009,** *459*, 68 - 72.

8. Wolff, J., The law of bone remodelling, Berlin, Heidelberg, New York, Springer, 1986 (translation of the German 1892 edition)

9. Engler, A. J.; Sen, S.; Sweeney, H. L.; Discher, D. E., Matrix elasticity directs stem cell lineage specification. *Cell* **2006,** *126*, 677-689.

10. Staudinger, H.; Bondy, H. F., Uber Isopren und Kautschuk 19. Mitteil.): Uber die Molekuhlgrosse des Kautschuks und der Balata. *Ber. Dtsch. Chem. Ges.* **1930,** *63*, 734.

11. Kauzmann, W.; Eyring, H., The Viscous Flow of Large Molecules. *J. Am. Chem. Soc.* **1940,** *62*, 3113-3125.

12. Encina, M. V.; Lissi, E.; Sarasua, M.; Gargallo, L.; Radic, D., Ultrasonic Degradation of Polyvinylpyrrolidone - Effect of Peroxide Linkages. *Journal of Polymer Science Part C-Polymer Letters* **1980,** *18*, 757-760.

13. Wiita, A. P.; Perez-Jimenez, R.; Walther, K. A.; Grater, F.; Berne, B. J.; Holmgren, A.; Sanchez-Ruiz, J. M.; Fernandez, J. M., Probing the chemistry of thioredoxin catalysis with force. *Nature* **2007,** *450*, 124-130.

14. Alegre-Cebollada, J.; Perez-Jimenez, R.; Kosuri, P.; Fernandez, J. M., Single-molecule Force Spectroscopy Approach to Enzyme Catalysis. *Journal of Biological Chemistry* **2010,** *285*, 18961-18966.

15. Bell, G. I., Models for Specific Adhesion of Cells to Cells. *Science* **1978,** *200*, 618-627.

16. Perez-Jimenez, R.; Li, J. Y.; Kosuri, P.; Sanchez-Romero, I.; Wiita, A. P.; Rodriguez-Larrea, D.; Chueca, A.; Holmgren, A.; Miranda-Vizuete, A.; Becker, K.; Cho, S. H.; Beckwith, J.; Gelhaye, E.; Jacquot, J. P.; Gaucher, E.; Sanchez-Ruiz, J. M.; Berne, B. J.; Fernandez, J. M., Diversity of chemical mechanisms in thioredoxin catalysis revealed by single-molecule force spectroscopy. *Nature Structural & Molecular Biology* **2009,** *16*, 890-U120.

17. Baldus, I. B.; Grater, F., Mechanical Force Can Fine-Tune Redox Potentials of Disulfide Bonds. *Biophysical Journal* **2012,** *102*, 622-629.

18. Kryger, M. J.; Munaretto, A. M.; Moore, J. S., Structure-Mechanochemical Activity Relationships for Cyclobutane Mechanophores. *Journal of the American Chemical Society* **2011,** *133*, 18992-18998.

19. Hickenboth, C. R.; Moore, J. S.; White, S. R.; Sottos, N. R.; Baudry, J.; Wilson, S. R., Biasing reaction pathways with mechanical force. *Nature* **2007,** *446*, 423-427.

20. Piermattei, A.; Karthikeyan, S.; Sijbesma, R. P., Activating catalysts with mechanical force. *Nature Chemistry* **2009,** *1*, 133-137.

21. Davis, D. A.; Hamilton, A.; Yang, J. L.; Cremar, L. D.; Van Gough, D.; Potisek, S. L.; Ong, M. T.; Braun, P. V.; Martinez, T. J.; White, S. R.; Moore, J. S.; Sottos, N. R., Force-

induced activation of covalent bonds in mechanoresponsive polymeric materials. *Nature* **2009,** *459*, 68-72.

22. Lenhardt, J. M.; Black, A. L.; Craig, S. L., gem-Dichlorocyclopropanes as Abundant and Efficient Mechanophores in Polybutadiene Copolymers under Mechanical Stress. *Journal of the American Chemical Society* **2009,** *131*, 10818-10819.

23. Diesendruck, C. E.; Steinberg, B. D.; Sugai, N.; Silberstein, M. N.; Sottos, N. R.; White, S. R.; Braun, P. V.; Moore, J. S., Proton-Coupled Mechanochemical Transduction: A Mechanogenerated Add. *Journal of the American Chemical Society* **2012,** *134*, 12446-12449.

24. Bruns, N.; Pustelny, K.; Bergeron, L. M.; Whitehead, T. A.; Clark, D. S., Mechanical Nanosensor Based on FRET within a Thermosome: Damage-Reporting Polymeric Materials. *Angewandte Chemie-International Edition* **2009,** *48*, 5666-5669.

25. Bruns, N.; Pustelny, K.; Bergeron, L. M.; Whitehead, T. A.; Clark, D. S., Mechanical Nanosensor Based on FRET within a Thermosome: Damage-Reporting Polymeric Materials. *Angew. Chem. Int. Ed.* **2009,** *48*, 5666-5669.

26. Rief, M.; Gautel, M.; Oesterhelt, F.; Fernandez, J. M.; Gaub, H. E., Reversible unfolding of individual titin immunoglobulin domains by AFM. *Science* **1997,** *276*, 1109-1112.

27. Gumpp, H.; Puchner, E. M.; Zimmermann, J. L.; Gerland, U.; Gaub, H. E.; Blank, K., Triggering Enzymatic Activity with Force. *Nano Letters* **2009,** *9*, 3290-3295.

28. Tseng, C. Y.; Wang, A.; Zocchi, G., Mechano-chemistry of the enzyme Guanylate Kinase. *Epl* **2010,** *91*.

29. Springer, T. A., Structural basis for selectin mechanochemistry. *Proc. Natl. Acad. Sci. USA* **2009,** *106*, 91-96.

30. Jin, M.; Andricioaei, I.; Springer, T. A., Conversion between three conformational states on Integrin I domains with a C-terminal pull spring studied with molecular dynamics. *Structure* **2004,** *12*, 2137-2147.

31. Astrof, N. S.; Salas, A.; Shimaoka, M.; Chen, J.; Springer, T. A., Importance of force linkage in mechanochemistry of adhesion receptors. *Biochemistry* **2006,** *45*, 15020-15028.

32. Yakovenko, O.; Sharma, S.; Forero, M.; Tchesnokova, V.; Aprikian, P.; Kidd, B.; Mach, A.; Vogel, V.; Sokurenko, E.; Thomas, W., FimH forms catch bonds that are enhanced by mechanical force due to allosteric regulation. *J. Biol. Chem.* **2008,** *283*, 11596-11605.

33. Aprikian, P.; Tchesnokova, V.; Kidd, B.; Yakovenko, O.; Yarov-Yarovoy, V.; Trinchina, E.; Vogel, V.; Thomas, W.; Sokurenko, E., Interdomain interaction in the FimH adhesin of Escherichia coli regulates the affinity to mannose. *J. Biol. Chem.* **2007,** *282*, 23437-23446.

34. Vogel, V.; Sheetz, M., Local force and geometry sensing regulate cell functions. *Nat. Rev. Mol. Cell Biol.* **2006,** *7*, 265-275.

35. del Rio, A.; Perez-Jimenez, R.; Liu, R.; Roca-Cusachs, P.; Fernandez, J. M.; Sheetz, M. P., Stretching single talin rod molecules activates vinculin binding. *Nature* **2009,** *323*, 638-641.

36. del Rio, A.; Perez-Jimenez, R.; Liu, R.; Roca-Cusachs, P.; Fernandez, J. M.; Sheetz, M. P., Stretching single talin rod molecules activates vinculin binding. *Science* **2009,** *323*, 638-641.

37. Pudas, R.; Kiema, T.; Butler, P. J. G.; Stewart, M.; Ylänne, J., Structural basis for vertebrate filamin dimerization. *Structure* **2005,** *13*, 111-119.

38. Pentikäinen, U.; Ylänne, J., The regulation mechanism for the auto-inhibition of binding of human filamin A to integrin. *J. Mol. Biol.* **2009,** *393*, 644-657.

39. Decher, G., Fuzzy nanoassemblies: Toward layered polymeric multicomposites. *Science* **1997,** *277*, 1232-1237.

40. Decher, G.; Hong, J. D., Buildup of Ultrathin Multilayer Films by a Self-Assembly Process .2. Consecutive Adsorption of Anionic and Cationic Bipolar Amphiphiles and Polyelectrolytes on Charged Surfaces. *Berichte Der Bunsen-Gesellschaft-Physical Chemistry Chemical Physics* **1991,** *95*, 1430-1434.

41. Elbert, D. L.; Herbert, C. B.; Hubbell, J. A., Thin polymer layers formed by polyelectrolyte multilayer techniques on biological surfaces. *Langmuir* **1999,** *15*, 5355-5362.

42. Picart, C.; Mutterer, J.; Richert, L.; Luo, Y.; Prestwich, G. D.; Schaaf, P.; Voegel, J.-C.; Lavalle, P., Molecular basis for the explanation of the exponential growth of polyelectrolyte multilayers. *Proceedings of the National Academy of Sciences of the United States of America* **2002,** *99*, 12531-12535.

43. Vogt, C.; Ball, V.; Mutterer, J.; Schaaf, P.; Voegel, J. C.; Senger, B.; Lavalle, P., Mobility of Proteins in Highly Hydrated Polyelectrolyte Multilayer Films. *Journal of Physical Chemistry B* **2012,** *116*, 5269-5278.

44. Garza, J. M.; Schaaf, P.; Muller, S.; Ball, V.; Stoltz, J. F.; Voegel, J. C.; Lavalle, P., Multicompartment films made of alternate polyelectrolyte multilayers of exponential and linear growth. *Langmuir* **2004,** *20*, 7298-7302.

45. Hemmerle, J.; Roucoules, V.; Fleith, G.; Nardin, M.; Ball, V.; Lavalle, P.; Marie, P.; Voegel, J. C.; Schaaf, P., Mechanically responsive films of variable hydrophobicity made of polyelectrolyte multilayers. *Langmuir* **2005,** *21*, 10328-10331.

46. Mertz, D.; Hemmerle, J.; Boulmedais, F.; Voegel, J. C.; Lavalle, P.; Schaaf, P., Polyelectrolyte multilayer films under mechanical stretch. *Soft Matter* **2007,** *3*, 1413-1420.

47. Mertz, D.; Hemmerle, J.; Mutterer, J.; Ollivier, S.; Voegel, J. C.; Schaaf, P.; Lavalle, P., Mechanically responding nanovalves based on polyelectrolyte multilayers. *Nano Letters* **2007,** *7*, 657-662.

48. Mertz, D.; Vogt, C.; Hemmerle, J.; Mutterer, J.; Ball, V.; Voegel, J. C.; Schaaf, P.; Lavalle, P., Mechanotransductive surfaces for reversible biocatalysis activation. *Nature Materials* **2009,** *8*, 731-735.

49. Mertz, D.; Vogt, C.; Hemmerle, J.; Debry, C.; Voegel, J. C.; Schaaf, P.; Lavalle, P., Tailored design of mechanically sensitive biocatalytic assemblies based on polyelectrolyte multilayers. *Journal of Materials Chemistry* **2012,** *21*, 8324-8331.

50. Vogt, C.; Mertz, D.; Benmlih, K.; Hemmerle, J.; Voegel, J. C.; Schaaf, P.; Lavalle, P., Layer-by-Layer Enzymatic Platform for Stretched-Induced Reactive Release. *Acs Macro Letters* **2012,** *1*, 797-801.

51. Zwaal, R. F. A.; Comfurius, P.; Vandeenen, L. L. M., Membrane Asymmetry and Blood-Coagulation. *Nature* **1977,** *268*, 358-360.

52. Reisch, A.; Hemmerle, J.; Chassepot, A.; Lefort, M.; Benkirane-Jessel, N.; Candolfi, E.; Mesini, P.; Letscher-Bru, V.; Voegel, J. C.; Schaaf, P., Anti-fouling phosphorylcholine bearing polyelectrolyte multilayers: Cell adhesion resistance at rest and under stretching. *Soft Matter* **2010,** *6*, 1503-1512.

53. Teulon, J.-M.; Delcuze, Y.; Odorico, M.; Chen, S. W.; Parot, P.; Pellequer, J. L., Single and multiple bonds in (strept)avidin-biotin interactions. *J. Mol. Recognit.* **2010,** *24*, 490-502.

54. Davila, J.; Chassepot, A.; Longo, J.; Boulmedais, F.; Reisch, A.; Frisch, B.; Meyer, F.; Voegel, J. C.; Mesini, P. J.; Senger, B.; Metz-Boutigue, M. H.; Hemmerle, J.; Lavalle, P.; Schaaf, P.; Jierry, L., Cyto-mechanoresponsive Polyelectrolyte Multilayer Films. *Journal of the American Chemical Society* **2012,** *134*, 83-86.

55. Bacharouche, J.; Badique, F.; Fahs, A.; Spanedda, M. V.; Geissler, A.; Malval, J. P.; Vallat, M. F.; Anselme, K.; Francius, G.; Frisch, B.; Hemmerlé, J.; Schaaf, P.; Roucoules, V., Biomimetic Cryptic Site Surfaces for Reversible Chemo- and Cyto Mechanoresponsive Substrates. *ACS Nano* **2013,** *(in press)*.

56. Roucoules, V.; Ponche, A.; Geissler, A.; Siffer, F.; Vidal, L.; Ollivier, S.; Vallat, M. F.; Marie, P.; Voegel, J. C.; Schaaf, P.; Hemmerle, J., Changes in silicon elastomeric surface properties under stretching induced by three surface treatments. *Langmuir* **2007,** *23*, 13136-13145.

Chapter 2

Materials and methods

In this chapter the materials and methods for the assembly of polyelectrolyte multilayers and the functionalisation of PDMS surfaces are presented. Due to the fact that most chapters will be submitted as scientific articles and presented under this form in this thesis, the experiments details of the materials and methods used for chapter 3.6, chapter 5 and chapter 6 are given in page 62, 136, 155 respectively. Here, we described only the materials and methods relative to experiments that are not anticipated to be published.

2.1 Materials

2.1.1 Solutions of polyelectrolytes

The polyelectrolytes used for the construction of the multilayers were dissolved in a 0.15 M NaCl solutions prepared with ultrapure water (18.2 MΩ.cm Milli-Q plus system, Millipore). These commercial polyelectrolytes used are summarized in Table 2.1.

2.1.2 Fluorescence probes

2.1.2.1 Fluorescence polyelectrolytes

In order to visualize the polyelectrolyte films by confocal microscopy (chapter 5), we used a commercial poly(L-lysine) labeled with fluorescein isothiocyanate (PLL^{FITC}) described in Table1. PLL^{FITC} solutions were used at 1 mg/mL concentration in TRIS 10 mM / NaCl 0.15 M buffer and at pH 7.4. The solutions were stocked at -20°C until used.

2.1.2.2 Fluorescence protein

Streptavidin is obtained from cultures of the bacterium *Streptomyces avidinii.*[1] It is a tetramer of four identical subunits that are built up of 159 amino acids and have a molecular weight of 16.5 kDa each (figure 2.1). The tetramer has an approximately spherical shape with a diameter of about 5.5 nm and an overall molecular weight of 60 kDa due to postsecretory degradiation. The isoelectric point of the streptavidin lies between 5 and 6. Streptavidin can bind four equivalents of the vitamin biotine. The interaction between streptavidin and biotin is, with a binding constant of the order of 10^{15} M^{-1}, among the strongest non-covalent interaction known. The reason for its use here lies exactly in this strong and specific interaction, as will be explained in more details in chapter 4. For the experiments, streptavidin

labeled with fluorescein isothiocyanate (streptavidin^{FITC} 3-9 mol FITC per mol streptavidin) was purchased from Sigma-Aldrich and used at a concentration of 0.1 mg/mL in 10 mM TRIS buffer and the pH was adjust to 7.4. Then, the solutions were kept at -20°C until use.

Polyelectrolyte Notation	**Molecular structure**	**Mw (g/mol)**	**pKa**	**Supplier**
Poly(L-lysine) PLL	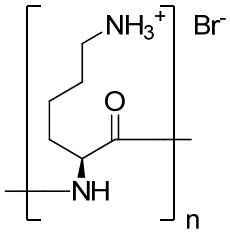	26 000	10.5	Sigma-Aldrich
Hyaluronic acid HA	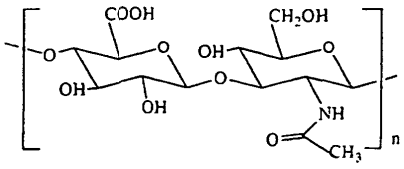	132 000	2.9	Lifecore Biomedical
Poly(L-lysine) labeled with fluorescein isothiocyanate PLL^{FITC}	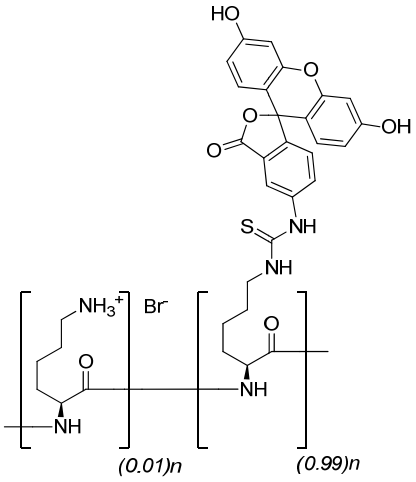	70 000	10.5	Sigma-Aldrich

Table 2.1: Polyelectrolytes used for the construction of polyelectrolyte multilayered films

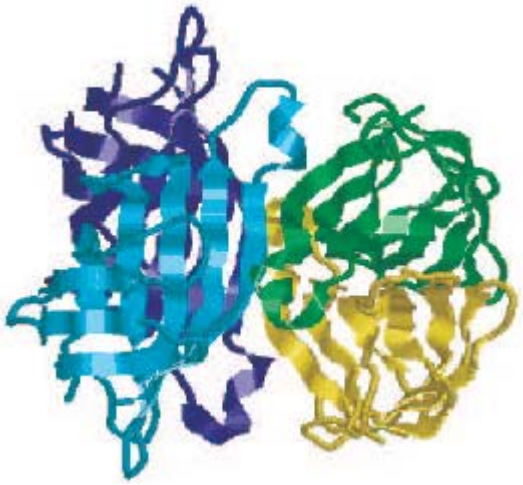

Figure 2.1: Molecular model of streptavidin tetramer (shown here is the Y43F mutand) from X-ray diffraction data.[2] The four subunits are presented in different colors, secondary structure elements are indicated.

2.1.3 Support for construction of films

2.1.3.1 Glass slides

The construction of polyelectrolyte multilayers (PEM) films were done in circular glass slides of 12 mm of diameter, 150 µm of thickness and less than 1 nm of roughness (Menzel-Gläser, Braunschweig, Germany). They were cleaned with 70% ethanol, 2% (v/v) Hellmanex® and 0.1 M HCl solutions for 10 min with rinsing steps of Milli-Q water between each treatment.

2.1.3.2 Silicone

Poly(dimethylsiloxane) (PDMS) sheets of 250 µm of thickness (Specialty Manufacturing Inc., Saginaw, Michigan, United States) were chosen as support for the grafting of biotine-poly(ethyleneglycol) brushes (chapter 4), for construction of PEM films (chapter 5) or for covalently attaching hydrogel materials (chapter 6). This material was chosen because it is transparent and presents excellent elastomeric properties (figure 2.2). The sheets were cut to fit the microscope slides in 18 x 18 mm^2 and cleaned with 70% ethanol, 2% (v/v) Hellmanex® and 0.1M HCl solutions for 10 min with rinsing steps of Milli-Q water between each treatment. They were stocked out of dust to avoid problems during the PEM films construction.

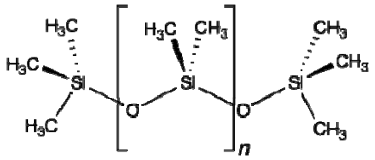

Figure 2.2: Structure of Poly(dimethylsiloxane)

2.1.4 Stretching devices

The influence of mechanical stretching on protein adsorption (chapter 4), controlled enzymatic activity (chapter 5) and covalently bonded hydrogel on silicones modified surfaces (chapter 6) were investigated. Differents kinds of homemade stretching devices presented bellow were used to carry out these experiments.

2.1.4.1 Large stretching device

The homemade stretching device used during the experiment of host guest interaction between Streptavidin and Biotin on PDMS modified surface (chapter 4) is represented in figure 2.3. It allows to stretch the PDMS in an uniaxial direction with a modulated electrical motor at a velocity of 0.5 mm/s. The stretching rate (α) is defined by the relation $\alpha = (l - l_0)/l_0$ where l and l_0 represent the length of the stretched and unstretched state respectively. All the experiments were done at room temperature with the modified side of PDMS in the upper position and in a hydrated state. For all the experiments, the stretching device was easily adapted in the microscope for fluorescence measurements.

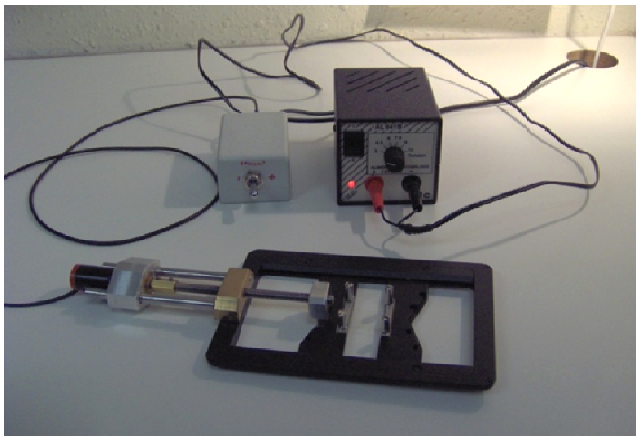

Figure 2.3: Large **s**tretching device with the modulated motor and adaptor for the fluorescence microscope.

2.1.4.2 Medium stretching device

The homemade stretching device used for the experiments of the PDMS surface modification with hydrogels (chapter 6) is presented in the figure 2.4. It is made of stainless steel and it allows stretching manually the sample in an unaxial direction.

Figure 2.4: Medium stretching device use for the stretching of PDMS-hydrogel modified surfaces.

Concerning the UVO activation and chemical modification of PDMS in a stretched state, a homemade stretching device made in poly(methylmethacrylate) (PMMA) was used, resisting to the UVO and chemical treatment (figure 2.5).

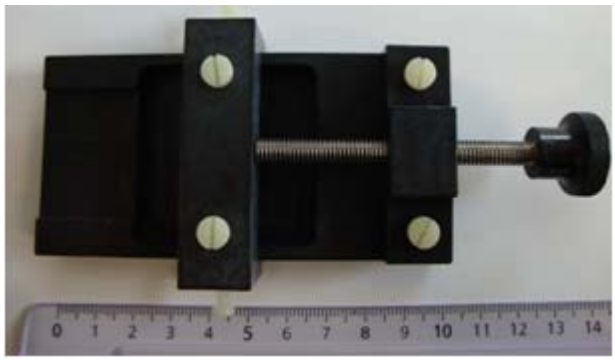

Figure 2.5: Stretching device used for the experiments where the modification of PDMS required extreme conditions as UVO activation or chemical contact.

2.1.5 Modification of silicon surfaces

2.1.5.1 UV-ozone (UVO)

A UV-ozone Pro Cleaner Bio Force Nanosciences machine that has a mercury vapor lamp wavelength of 254 nm and 185 nm with an UV intensity of 14.76 mW/cm^2 at 1 cm of distance from the sample was used for the PDMS's surface activation. The 185 nm UV

wavelength creates ozone gaz which is then transformed to atomic oxygen by the 254 nm wavelength. The oxygen radical so formed presents unpair electrons which will react in contact with the PDMS surfaces producing silanol groups and carboxylic groups depending on the exposition time of the activation. Therefore, a hydrophilic surface is obtained after treatment of the PDMS surfaces by UVO activation. Nevertheless, the formation of a thin layer of silicon oxyde (SiOx) can occur depending on the time of exposition and it will be responsible for the crack formation on the PDMS's surface under stretching.

2.1.6 Procedure to prepare PDMS Sylgard-184

Poly(dimethylsiloxane) PDMS Sylgard-184 from Dow Corning was prepared using a mixture of viscous base (part A) and curing agent (part B) in a rate of 10:1. After mixing the two components cited before they were degased for 1h in an oven under pressure. Then, the transparent solution was poured into PMMA molds and cured overnight at 90°C and 254 mmHg. Carefully, they were unmold and washed, first with a solution of n-heptane and dodecanthiol (0.01 %) for 1 h and then two times with only n-heptane for 1h each time. This washing process will remove the remaining unreacted chaines and the Pt catalyst from the material. Finally, they were dried in two steps, first under pressure at room temperature during 1h and then in the oven at 60°C for 3h. The poly(dimethylsiloxane) PDMS obtained is a transparent and elastic material that is stocked avoiding contact with dust.

2.1.6 Silanization procedure of the oxidized silicone sheet by using the 3-mercaptopropyltrimethoxysilane

After the activation of the 18 x 18 mm^2 PDMS surfaces (from SMI or PDMS Sylgard-184) by UVO for 1h30min, the samples were put in a glass bottle that contains a 1 % v/v solution of 3-mercaptopropyltrimethoxysilane (HS) in MeOH and stirred overnight at room temperature. The samples were then rinsed three times with MeOH for 1h under stirring, changing the solvent every 15 minutes and then kept in MeOH.

2.2 Methods

2.2.1 Contact angle (CA) measurements

Contact angle (CA) measurements represent the easiest and quickest method for examining the properties of surfaces. The method consists in measuring the angle between the outline tangent of a drop deposited on a solid and the surface of this solid (figure 2.6).

The static contact angle between a liquid drop and a smooth solid surface is given by Young's equation which essentially expresses the force balance between the interfacial tensions at the solid-liquid-vapor interfaces:

$$\sigma_{LV}\cos(\theta) = \sigma_{SV} - \sigma_{SL} \qquad (2.1)$$

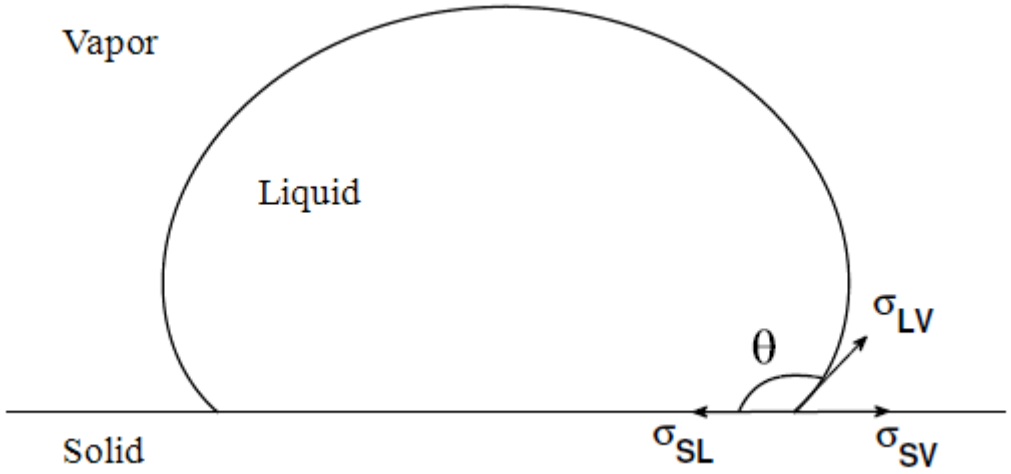

Figure 2.6: Young's model of sessile drop showing the relationship between interfacial tensions. θ is the contact angle, $\boldsymbol{\sigma_{LV}}$ is the liquid-vapor interfacial tension, $\boldsymbol{\sigma_{SV}}$ is the solid-vapor interfacial tension and $\boldsymbol{\sigma_{SL}}$ is the solid-liquid interfacial tension.

If water is used to measure the contact angle it is possible to deduce the hydrophobic (great angle, low surface energy) or hydrophilic (small angle, high surface energy) character of the surface.

CA measurements were carried out using the DIGIDROP-GBX® coupled with a charge-coupled device CCD camera and a total volume of 6 µL high-purity water dropwise. Measurements were made on both sides of the drop and were averaged. A series of three experiments were carried out for each treatment.

2.2.2 Infrared spectroscopy (FTIR)

An FT-IR spectrometer Bruker Vertex 70 equipped with DTGS detector and an Attenuated Total Reflectance ATR germanium crystal accessory was used for IR spectroscopy measurements. All spectra were acquired at 4 cm^{-1} resolution over 20 scans within the range 4000 - 600 cm^{-1}.

2.2.3 Atomic force microscopy (AFM)

Atomic force microscopy (AFM) was performed using a multimode scanning probe microscope (Veeco/Bruker, Santa Barbara, CA). The apparatus was operated in the contact mode under liquid condition. Silicon nitride cantilevers with a spring constant of 0.03 $N.m^{-1}$ were used for imaging (MSCT model, Veeco/Bruker, Santa Barbara, CA). For more details about the experiment see chapter 3.6.

2.2.4 Optical microscopy

White light microscopy images were captured with the inverted optical microscope Nikon Eclipse TE200 using a x40 objective lenses. Images were acquired with Nikon Digital Camera DS-Qi1Mc (with NIS-Elements software). This method was particular interesting to analyze the crack formation on silicone surfaces after UVO treatment under stretching (chapter 4 and chapter 6).

2.2.5 Nuclear magnetic resonance (NMR)

The nuclear magnetic resonance (NMR) spectra were recorded on a Bruker Advance 400 spectrometer operating at 400 MHz for ^{1}H and 100 MHz for ^{13}C. The NMR spectra were calibrated using residual undeuterated solvent as an internal reference. The multiplicities of the peaks were described by singlet (s), doublet (d), triplet (t), multiplet and broad (br). The degree of substitution (DS) of the polymer after modification was determined from the ratios of integrals of ^{1}H.

2.2.6 Fluorescence based microscopy methods

We mainly used, throughout this thesis, microscopy methods that rely on fluorescence experiments. We thus present in more details these methods.

2.2.6.1 Principles of fluorescence

Fluorescence is the phenomenon in which a molecule absorbs a photon of a given wavelength (or energy $h\nu_{EX}$) followed by the emission of a photon at a smaller energy ($h\nu_{EM}$) larger wavelenght (Jablonski diagram, figure 2.7). The fluorescent molecule is excited from its ground state S_0 to a state S_1'. At room temperature, the molecule loses some of its energy by vibrational relaxation or collisions with surrounding molecules, bringing it to a state of lower energy, S_1. When going back to the ground state, a photon of lower energy is emitted, compared to the excitation photon. The difference between the two wavelengths is called the Stokes shift.

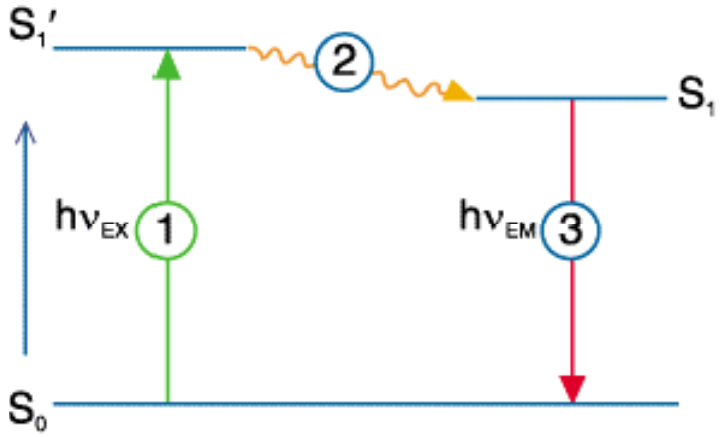

Figure 2.7: Jablonski diagram. (1) The fluorescent molecule at the ground state absorbs a photon and is promoted to the excited state S_1'. (2) It reaches the lower excited state S_1 through non-radiative energy loss. (3) On getting back to the ground state a photon of lower energy is emitted ($h\nu_{EM} < h\nu_{EX}$).

The fluorescence intensity and the excitation and emission wavelengths depend on the molecule, the so called fluorophore. In general, fluorophores are relatively small molecules that can be covalently attached to the molecules of interest. In our case these molecules of interest are polyelectrolytes or biological macromolecules like proteins, notably enzymes. The fluorophores allow for the detection of the labeled species in the polyelectrolyte multilayers by using confocal laser scanning microscopy for example. In this work the fluorescein isothiocyanate (FITC) was used as the fluorescent marker which presents a maximum absorbance and emission at 495 nm and 525 nm, respectively (figure 2.8).

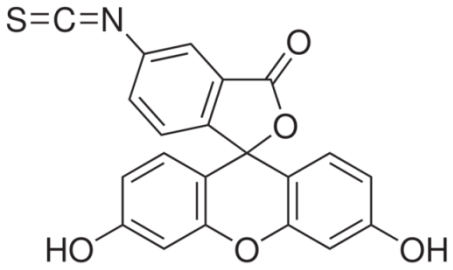

Figure 2.8: Molecular structure of the fluorescence probe fluorescein isothiocyanate (FITC) (λ_{EX} = 495 nm / λ_{EX} = 525 nm).

2.2.6.2 Fluorescence microscope

Based on the Stokes shift principle, after illumination of the specimen with one wavelength and filtering the return light, it is possible to observe fluorescent objects (figure 2.9). The sample is illuminated with light either from a mercury arc lamp or a laser directed on the sample by a dichroic mirror after passing a filter that eliminates light above a certain wavelength. The light coming from the sample is then directed through a second filter that blocks light below a given wavelength. Hence, only the light due to emission of the fluorophore is detected. The contrast corresponding to this kind of observation is superior to the contrast due to absorption.

The "classical" fluorescence microscope was used to study, in chapter 4, the ligand accessibility to the silicone surface modified with poly(ethyleneglycol) brushes, biotin and strepatvidin^{FITC} at the unstretched or stretched state. The experiments were carried out using an inverted light microscope (Nikon Microphot-FXA, Japan) equipped with a mercury lamp and operating between 470 nm and 490 nm for excitation and above 500 nm for detection. A ×10 dry objective and a digital camera were used.

Image analysis was performed using ImageJ software (Rasband, W. S., ImageJ, U. S. National Institutes of Health, Bethesda, Maryland, USA, http://imagej.nih.gov/ij/, 1997-2011).

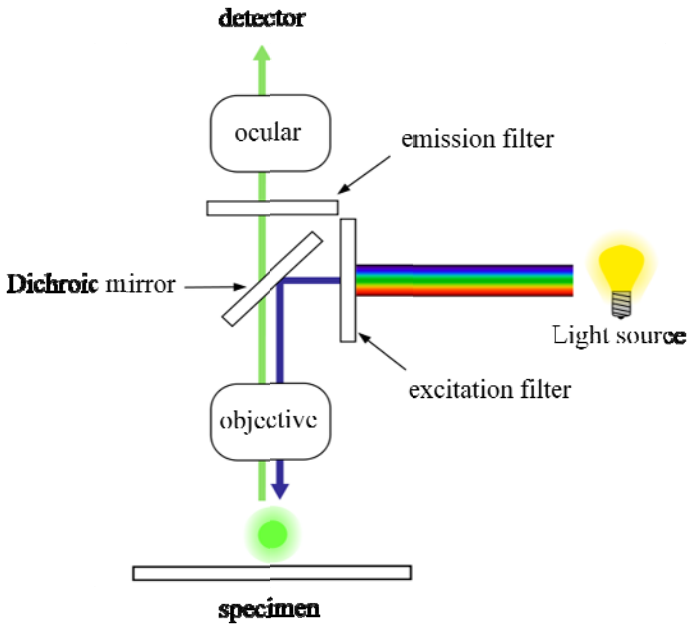

Figure 2.9: Basic set up of a fluorescence microscope.

2.2.6.3 Confocal laser scanning microscope (CLSM)

The general principle of the confocal microscope was proposed by Minsky[3]. It consists in using point illumination produced by a laser through a precise point of the sample (focal point) with an epifluorescence microscope. Nevertheless, the laser pathway throught the sample generates a parasite fluorescence out of the sample plan. Therefore, the confocal microscope uses a pinhole to eliminate light that comes from planes other than the focal planes (figure 2.10).

The confocal images are obtained by scanning the sample point per point along the x and y axes with motorized mirrors that are placed through the optical pathway of the laser. The scanning along the z axis is performed by using an objective mounted on a piezoelectric motor. So, it is possible to scan different focal planes (cross-section) and then reconstruct the 3D image of the sample. The resolution in the z direction is of the order of 500 nm for an objective with a 1.4 numerical aperture at a wavelength of 500 nm. We use this technique to visualize exponentially growing polyelectrolyte multilayer films and measure their thickness (micrometers) in aqueous environment.

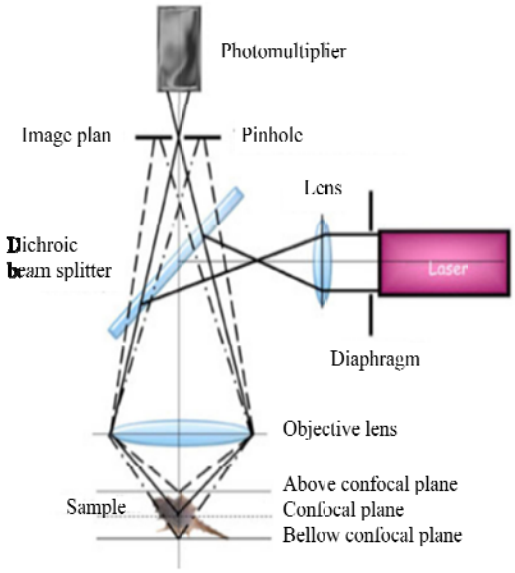

Figure 2.10: Representation of the confocal laser scanning microscope principal. The laser beam is concentrated by the dichroic beam splitter and the objective lens on a focal point on the sample. The fluorescence is then collected by the photomultiplier. In order to eliminate the parasite fuorescence (point lines), a pinhole is placed at the image plan of the objective.

The experiments were performed with the confocal microscope LSM 510 META (Carl Zeiss S.A.S., Le Pecq, France) mounted on a AxioVert 100M (Carl Zeiss S.A.S., Le Pecq, France) microscope with HeNe (543 nm) and Ar (459, 488, and 514 nm) lasers. In our experiments, we used an argon laser, with 488 nm for excitation and 520 nm for emission. A ×40 wet objective was used to visualize the polyelectrolyte multilayer films after construction on glass or silicone substrates (chapter 5).

Image analysis was performed using ImageJ software (Rasband, W. S., ImageJ, U. S. National Institutes of Health, Bethesda, Maryland, USA, http://imagej.nih.gov/ij/, 1997-2011).

2.2.6.4 Fluorescence recovery after photobleaching (FRAP)

Fluorescence recovery after photobleaching (FRAP) is a method used to quantify the mobility of fluorescent molecules in an environment that was photobleached with a powerful laser. It was developed in the seventies by Peters et al.[4]. Axelrod et al. showed that this technique allows evaluating quantitatively the diffusion coefficient of a fluorescently labeled molecule[5]. This technique was also used for example for the study of the diffusion of the

PLL^{FITC} inside of a PLL/HA film or even more the diffusion of proteins inside the PEM films of poly(allylamine) / poly(styrene sulfonate).

Experimental protocol

We used the FRAP experiments to investigate the diffusion of fluorescently labeled proteins in polyelectrolyte multilayer films. These experiments were realized with a confocal microscope.

In practice, a defined region of the sample, in our case a circular region, is illuminated with high intensity laser for 20 s causing part of the fluorophores within that region to become photobleached (permanent destruction of their fluorescence). This creates a darker, bleached region, within the sample. Then, if at least part of the labeled molecules are mobile, non-photobleached molecules from the region exterior to the disk diffuse toward the bleached region. This influx leads to an increase of the fluorescence intensity over time (figure 2.11). Note that this intensity recovery is in general incomplete because some of the fluorescent molecules may be immobile or appear as such over the time of observation.

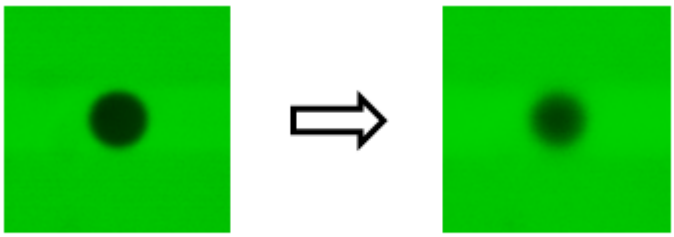

Figure 2.11: FRAP technique uses the high power of a laser to photobleach a defined region of the sample. The recovery of the fluorescence in this region indicates any kind of movement (diffusion or transport) of fluorescent molecules. The disc diameter, d, of the bleached region equals 115.17 µm.

Recovery of fluorescence in the bleached area occurs as a result of the diffusion of fluorescent molecules from the unbleached region into the bleached one. The fraction of fluorescent molecules that can participate in this exchange is referred to as the mobile fraction. On the other hand, the immobile fraction cannot contribute to the recovery.

For a FRAP experiment to provide meaningful data, it is important that the sample is not photobleached during the pre-bleach or recovery phase of the experiment and that the detector is not saturated. This is achieved by using weak laser intensities during these phases.

In this kind of experiment, we are interested in images parallel to the sample plane taken at various recovery times after the end of bleaching (t = 0). Image resolution of 512 pixels × 512 pixels was obtained with an objective x10, numerical aperture of 0.3 and numerical zoom ×2 corresponding to square images of side length equal to 460 µm. The fluorescence ratio between the bleached and the unbleached zones is plotted against the fluorescent recovery time. In chapter 5, FRAP experiments were carried out to study the diffusion of labeled enzymes with FITC within the polyelectrolyte multilayer film.

Data processing

Images such as those shown in figure 2.11 were analyzed by means of ImageJ. At a given recovery time, t, this analysis consists in measuring the light intensity within the bleached disk, $I(t)$, and the mean intensity, $I_{ref}(t)$, within four disks of equal size (i.e. same radius a located in the corners of the image. The quantity of interest is the ratio $I(t) / I_{ref}(t)$. This ratio is assumed to be equal to the concentration of fluorescent molecules inside the bleached region divided by the concentration of fluorescent molecules in regions of the image that are unaffected by the movement of fluorescent molecules toward the bleached region.

For the sake of simplicity, we assume that at t = 0, the bleached region has a perfectly sharp contour (see left image in figure 2.11 above). This means that the bleaching time was sufficiently short to avoid significant diffusion during bleaching and thereby the "corona effect"[6]. The initial condition is then expressed by

$$\frac{c(r,0)}{c_0} = \begin{cases} \alpha \text{ if } r < a \\ 1 \text{ elsewhere} \end{cases} \qquad (2.2)$$

where r means the radial distance from the center of the bleached disk, c_0 is the concentration before bleaching or far from the bleached region and α represents the proportion of non-bleached molecules within the disk at t = 0.

Again for the sake of simplicity, we assume that the fluorescent molecules are either mobile with diffusion coefficient D or immobile. The markers are therefore entirely characterized by the two parameters D and the proportion of mobile markers, p. In the special case where p = 1, the time evolution of the relative fluorescent molecule concentration within a disk of radius a centered on the center of the initially bleached disk is given by (see Appendix A of Picart C., et al.[7] for mathematical details)

$$\left.\frac{c(\tau)}{c_0}\right|_{p=1} = \alpha + (1-\alpha)\exp\left(-\frac{2}{\tau}\right)\left[\mathbf{I}_0\left(\frac{2}{\tau}\right) + \mathbf{I}_1\left(\frac{2}{\tau}\right)\right] \qquad (2.3)$$

where $\tau = \frac{4Dt}{a^2}$. $\mathbf{I}_0$ and $\mathbf{I}_1$ represent modified Bessel functions of first kind and order 0 and 1, respectively[8]. In the general case ($p \leq 1$), the intensity within the region of interest is still composed of two parts: one contribution from the non-bleached molecules (first term on the right hand side in eq. 2.3) and one contribution from the gradually incoming molecules. However, only a proportion p of the bleached fraction $1 - \alpha$ can be recovered. It follows that eq. 2.3 becomes

$$\frac{c(\tau)}{c_0} = \alpha + p(1-\alpha)\exp\left(-\frac{2}{\tau}\right)\left[\mathbf{I}_0\left(\frac{2}{\tau}\right) + \mathbf{I}_1\left(\frac{2}{\tau}\right)\right] \qquad (2.4)$$

When $t \to \infty$, the concentration ratio tends to

$$\frac{c(\infty)}{c_0} = \alpha + p(1-\alpha) \qquad (2.5)$$

which reaches unity only if $p = 1$ as could be intuitively anticipated.

At short times ($\tau < 0.15$), the concentration ratio is approximately given by

$$\frac{c(\tau)}{c_0} = \alpha + p(1-\alpha)\sqrt{\frac{\tau}{\pi}} \qquad (2.6)$$

or

$$\frac{c(t)}{c_0} = \alpha + p(1-\alpha)\frac{2}{a}\sqrt{\frac{D}{\pi}}\sqrt{t} \qquad (2.7)$$

Therefore, as long as the experimental data are located on a straight line when represented as a function of $\sqrt{t}$, only the product $p\sqrt{D}$ can be extracted. Consequently, it is necessary to follow the recovery over long enough the time to actually need the exact expression (2.4) to model the observations. Then D and p can be obtained separately.

2.3 References

(1) Waldrop, L. G., *Biotin in Encyclopedia of Life Science*. John Wiley and Sons: 2001.

(2) Le Trong, I.; Freitag, S.; Klumb, L. A.; Chu, V.; Stayton, P. S.; Stenkamp, R. E. Structural studies of hydrogen bonds in the high-affinity streptavidin-biotin complex: mutations of amino acids interacting with the ureido oxygen of biotin *Acta Crystallographica Section D-Biological Crystallography* **2003**, 59, 1567-1573.

(3) Minsky, M. Microscopy apparatus. Patent US/1961/3013467, 1961.

(4) Peters, R.; Peters, J.; Tews, K. H.; Bahr, W. A microfluorimetric study of translational diffusion in erythrocyte membranes *Biochimica et Biophysica Acta (BBA) - Biomembranes* **1974**, 367, 282-294.

(5) Axelrod, D.; Koppel, D. E.; Schlessinger, J.; Elson, E.; Webb, W. W. Mobility Measurement by Analysis of Fluorescence Photobleaching Recovery Kinetics *Biophys. J.* **1976**, 16, 1055-1069.

(6) Weiss, M. Challenges and artifacts in quantitative photobleaching experiments *Traffic* **2004**, 5, 662-671.

(7) Picart, C.; Mutterer, J.; Arntz, Y.; Voegel, J. C.; Schaaf, P.; Senger, B. Application of fluorescence recovery after photobleaching to diffusion of a polyelectrolyte in a multilayer film *Microscopy Research and Technique* **2005**, 66, 43-57.

(8) Abramowich, M.; Stegun, I., *Handbook of mathematical functions*. Dover: New York, 1970.

Chapter 3

Investigation of a bispyrene unit used as a mechanical sensor or a pH probe

3.1 Introduction

One aim of my project is to develop systems that respond chemically to a mechanical stress such as the stretching of a material. One way that we considered to realize such materials is to covalently couple enzymes into hydrogels with the idea that stretching the hydrogel induces stresses on the protein architectures leading to a switch of their conformations. It is thus important to characterize the mechanical stress that is applied at a molecular level in such a material under stretching. Also, it was postulated and recently proven that during the adhesion of cells on a substrate, cells sense the mechanical properties of the substrate by pulling on it.[1, 2] Characterizing these pulling forces at a nanometer scale in the material is thus of great interest.[3-5] In order to address these two aspects we thought to use molecules that change conformation under the influence of a pulling force and whose conformational changes can be monitored spectroscopically. We envisioned that bispyrene derivatives might be able to play this role when being covalently linked on a polymer network. These molecules present a characteristic emission spectrum of pyrene monomers when they are in an "opened" conformation. In a "closed" conformation where the two pyrene rings interact through π-π interactions they exhibit a typical excimer spectrum (see figure 3.1).

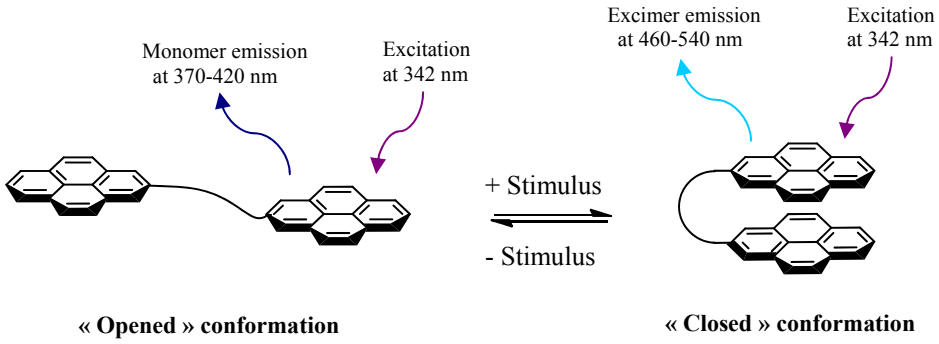

Figure 3.1: Schematic representation of a general bispyrene unit switching reversibly from an "opened" and a "closed" conformation controlled by an external stimulus. When a bispyrene molecule is excited at 342 nm, a characteristic fluorescence emission is observed according to its conformation: 460-540 nm when the bispyrene is in the "closed" conformation, 370-420 nm when the bispyrene is in the "opened" conformation.

Many stimuli allow the control of the conformational change of a bispyrene molecule: pH[6, 7], solvent polarity[8, 9], host hydrophobic compounds[10, 11] or metallic ions[12, 13] according to the chemical structure of the spacer between the two pyrene rings.Our idea was that, once

covalently linked on a polymer matrix, in the absence of stress, the bispyrene molecules are in a "closed" conformation which switches to an "opened" conformation under a mechanical stress. We have prepared and used two original bispyrene molecules **2** and **3**, whose the two pyrene rings are linked together through a diethylenetriamine linker and which can be covalently crosslinked into a polymer network through two reactive side arms: vinyl groups for the bispyrene derivative **2** and azido groups for the bispyrene **3**. These two arms are on each pyrene ring(see figure 3.2).

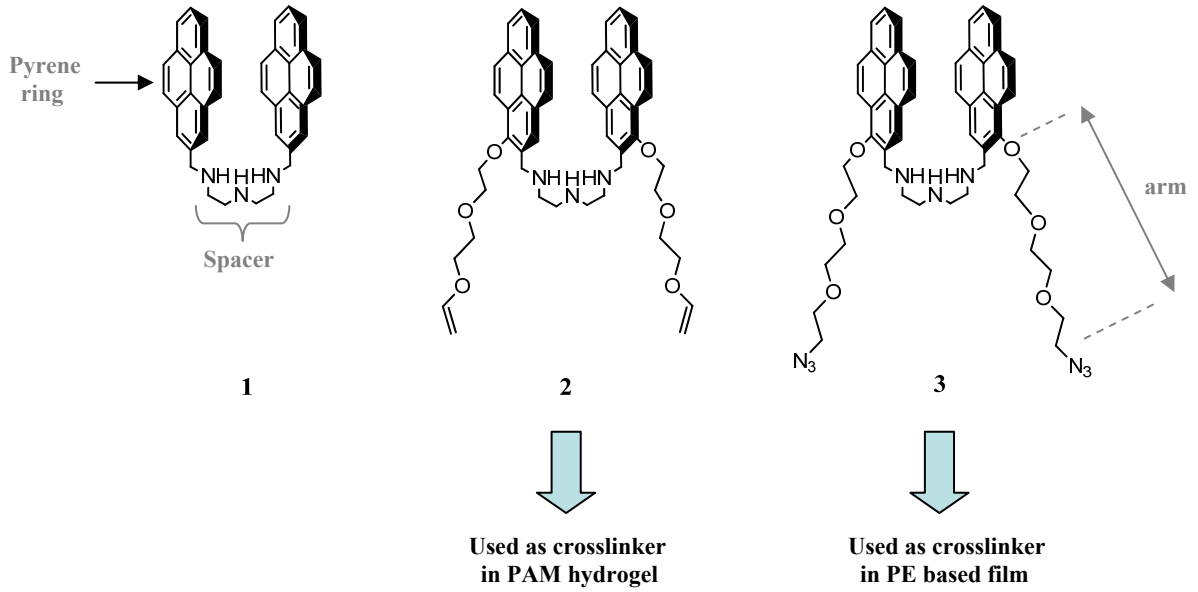

Figure 3.2: Chemical structure of the bispyrene derivatives **1**, **2** and **3**: compounds **2** and **3** are dedicated to be used in Poly(acrylamide) (PAM) hydrogels and Polyelectrolytes (PE) based films respectively.

Bispyrene units such as the compound **1** (figure 3.2), without the lateral arms on each pyrene ring, have been intensively studied in the literature[14]. It was shown that these molecules can play the role of local pH sensors because of their pH-sensitive conformation. Indeed, at high pH when the amines are not protonated, the molecules adopt a "closed" conformation whereas at low pH, when the amines of the central linker between the two pyrene rings are positively charged (ammonium groups formation) they adopt an “opened” conformation[12] due to the positive charges repulsion.

This chapter is divided in three parts: we will first describe the syntheses of the functionalized bispyrene molecules **2** and **3** bearing reactive side arms (Part 3.2). We will then describe the results relative to the incorporation of bispyrene **2** in poly(acrylamide) hydrogel

(PAM) networks with the goal to render it mechanoresponsive (Part 3.3). These experiments were performed in collaboration with a Master II student, Jean-Nicolas Tisserant. Unfortunately, as we will see, our material was not mechanoresponsive **and thus only a brief description about the results obtained in this project will be given herein**. Next, we took advantage of the fact that our bispyrene molecules, when bearing azide moieties on the two lateral arms, could serve simultaneously as crosslinking agents between polymer chains bearing alkynes moieties and pH sensors. This study was intended to better understand the properties of polyelectrolyte based films (PE) resulting from a one-pot morphogen film self-construction through covalent bonds formation between polyelectrolytes and homobifunctional spacers, a concept introduced recently in our group (Part 3.6). Such a construction was obtained by electrochemical-control of the Huisgen click-chemistry reaction between poly(acrylic acid) chains modified by attaching alkyne groups (PAA-*Alk*) and biazides ethylene glycol spacers (*Az*-EG_n-*Az*) or our modified bispyrene molecules in the presence of a $CuSO_4$ solution. The morphogen Cu(I) was generated from Cu(II) after applying a reduction electric potential and therefore the covalent films were buildup on the electrode surface. The reversible conformational switch of the bispyrene entity depending on the pH of its environment, allowed probing the real pH inside the film when the pH outside the film is changing. The results of this study led to a publication in "Soft Matter".

3.2 Design and synthesis of the bispyrenes 2 and 3

Our synthetic strategy to design the bispyrenes **2** and **3** is based on a convergent synthesis leading to the disubstitued pyrene ring **4**. Indeed, prepared from 1-bromopyrene, the compound **4** allows the grafting of the desired arms to each pyrene ring through nucleophilic substitution on the phenol group, followed by a coupling reaction (reductive amination) between the aldehyde group of the bispyrene derivatives and the diethylenetriamine linker. These two steps provide the desired bispyrene **2** and **3** (figure 3.3) which experimental details are described in Annex 1 and in the supporting information of part 3.6 respectively.

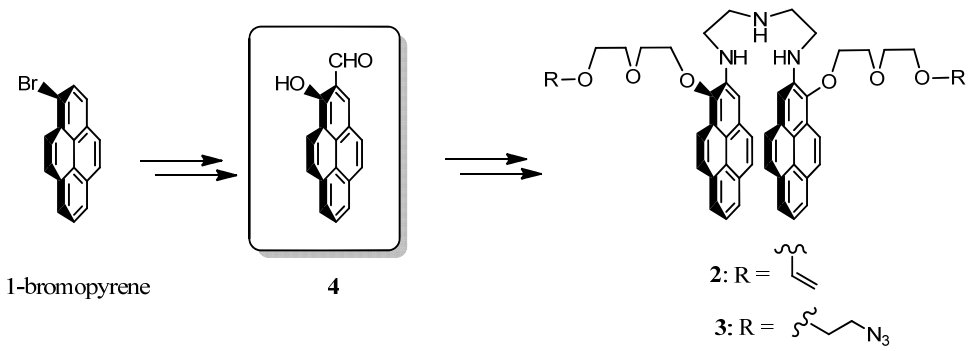

Figure 3.3: Synthetic strategy to prepare the bispyrenes **2** and **3** from 1-bromopyrene through the disubstituted precursor **4**.

The possibility to disubstitute the pyrene ring is necessary because one substitution will be involved in the coupling with the second pyrene ring, through the diethylenetriamine bridge, and the second substitution will provide the chemical group allowing the coupling into a polymeric network, vinyl (in case of compound **2**) or azide group (in case of compound **3**). Few works have been reported concerning the synthesis of pure disubstituted pyrene ring: the main difficulty encountered is to purify compounds contaminated by several regioisomers. Recently, Zhou et *al*.[15] developed a convenient preparation of the pyrene derivative **4** (figure 3.4). This pyrene **4** has two reactive functions, a phenol and an aldehyde, that can be involved for two different coupling reaction. Starting from the commercially available 1-bromopyrene, the compound **4** is prepared in three steps: Ullman coupling reaction provide the derivative **5** with 92% of yield. Then, ortholithiation in presence of butyllithium followed by the addition dimethylformamide yield to the compound **6**. Demethoxylation with aluminium chloride led to the disubstituted pyrene **4**.

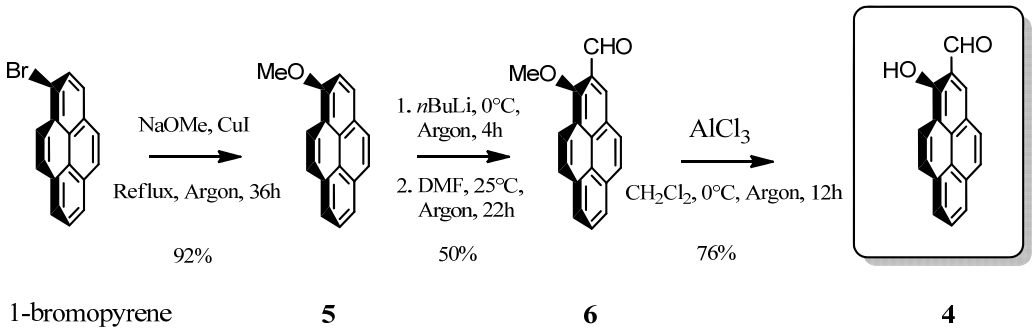

Figure 3.4: Synthesis of the disubstituted pyrene **4** in three steps from 1-bromopyrene.

Then, the arm bearing the functional groups (vinyl or azido groups) can be attached on compound **4** though the phenol. Oligoethylene glycol derivatives **7** and **8** can be prepared in

few steps according to described procedure[16]. Once the arm introduced to the disubstituted pyrene ring **9** and **10**, the coupling with the diethylentriamine can be done: a bis imine is formed and reduced *in situ* in presence of sodium borohydride to afford the desired bispyrene compounds **2** and **3** with 77% and 59% of yield respectively (figure 3.5).

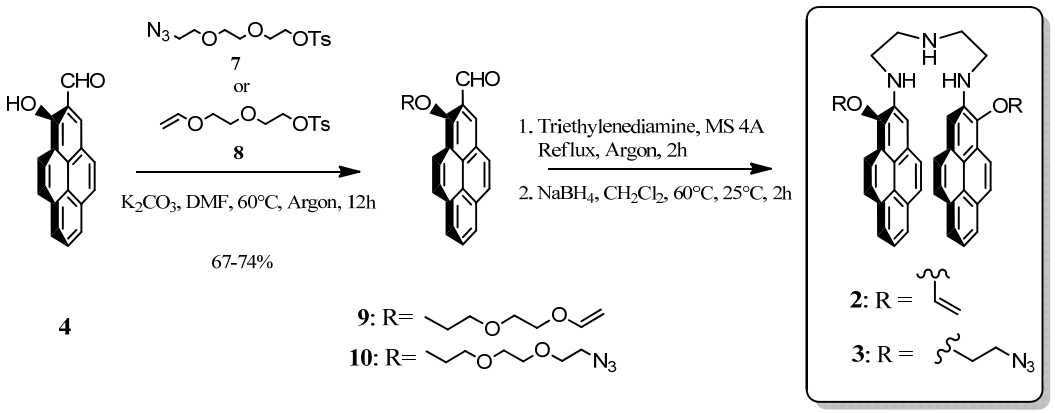

Figure 3.5: Synthesis of the bispyrenes **2** and **3** from the disubstituted precursor **4**.

This convergent strategy to prepare bispyrene-based cross-linker may be used in the future in various others applications.

3.3 Bispyrene derivative 2 used as a mechanical sensor included in poly(acrylamide) hydrogels

The use of fluorescent molecules whose emission properties can be modulated by external stimuli (such as pH, temperature or ionic concentrations) is a powerful tool in the field of sensor device applications.[17-19] Bispyrene-containing molecular systems have been studied extensively because they demonstrated distinctive monomer and excimer emissions (figure 3.1). Two pyrene units are attached at both ends of a short chain that responds to stimuli; in water, the hydrophobic pyrene units induce a folding and the formation of an excimer characterized by a long-wavelength emission band at 460-540 nm when excited at 342 nm. When an adequate stimulus is applied, the bispyrene molecule is forced into an extended conformation that disrupts the excimer band. Only monomer fluorescence at 370-420 nm in purple-blue which arises from locally excited pyrene chromophores is observed. High sensitivity, selectivity, fast response time, flexibility and experimental simplicity are the main advantages of this molecular sensor.

In our case, the chemical mechanical sensor that we used is composed of two pyrene rings both linked together through a polyammonium bridge. Each pyrene unit was attached to

reactive functions through a linker (figure 3.2). These reactive functions must allow covalent binding of the bispyrene entity into 3D matrices as poly(acrylamide) hydrogel (PAM). Compression of this bispyrene **2** containing materials may lead to a switch of fluorescence emission.

3.3.1 Optimization to get a viscous-elastic and stretchable PAM hydrogel

The polymer used as a mechano-transductive matrix for the bispyrene should be transparent to UV-visible wavelengths allowing spectroscopic measurements, resist to stretching at 50% of initial dimension and should be mostly elastic (reversible) up to 50% stretching. For these reasons, the system that we chose for testing our mechanical sensor was the poly(acrylamide) hydrogel (PAM) formed by free radical polymerization in water (figure 3.6).

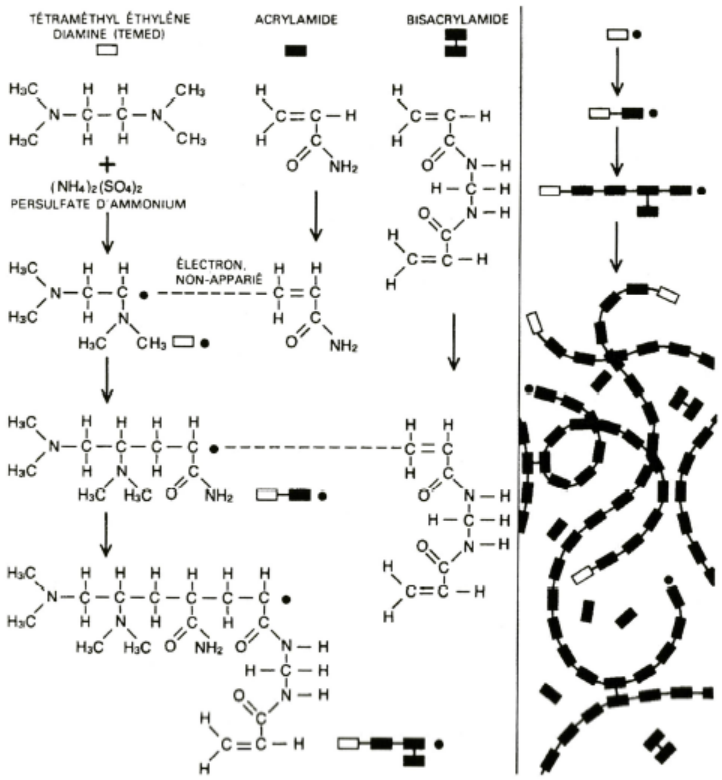

Figure 3.6: (left) Molecular mechanism of the poly(acrylamide) gel formation in presence of acrylamide, bisacrylamide, tetramethylethylendiamine (TEMED) and ammonium persulfate (APS); (**right**) Schematic representation of the polymerization and crosslinking of PAM hydrogel.[20]

All hydrogels studied were formed in 3.5 cm of diameter glass petri dishes by addition of the reactants in the sequence showed in Table 3.1 and stirring vigorously between each step. Figure 3.6 represents schematically the chemical reactions taking place during the gel formation.

The PAM gel is polymerized through a radical chain reaction. The first step corresponds to the activation of the tetramethylethylenediamine (TEMED) by the ammonium persulfate (APS) which results in a molecule with one unpaired electron. This activated molecule reacts with an acrylamide molecule which is also activated at its turn. When the acrylamide units are still growing, the active site moves to the free side. The bisacrylamide, which consists in two acrylamide units linked together, is incorporated into growing chains, cross-linking the polymers. The polymer has a gel complex topology formed with ramifications and interconnections.

Compound	**1.** Acrylamide 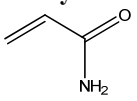	**2.** Bis-acrylamide 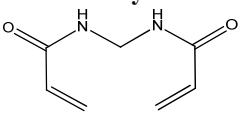	**3.** Water H_2O	**4.** Tetramethyl-ethylenediamine **(TEMED)** 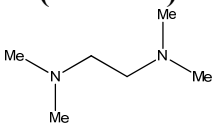	**5.** Ammonium peroxodisulfate **(APS)** $(NH_4)_2S_2O_8$
Role	*Monomer*	*Cross-linker*	*Solvent*	*Catalyst*	*Initiator*
Amount	800µL of 40wt% in water	133.3µL of 5mg/mL in water	800µL	4.8µL	66.6µL 54mg/mL in water

Table 3.1: Optimized conditions of PAM hydrogel preparation used in our study. The numbers next to the compound name show the order of introduction.

Different mechanical properties can be obtained by varying the amount of each reactants, in particular the ratio and the concentration of acrylamide and bisacrylamide. Cedric Vogt, PhD student at INSERM UMR 977 of Strasbourg, optimized the gel composition to get a transparent and elastomeric gel. These conditions are gathered in Table 3.1 and described in details in chapter 6. From a practical point of view, the PAM hydrogel formation begins within a few minutes after the successive addition of the following reagents, in the proportion indicated in Table 3.1: acrylamide, bisacrylamide, water, TEMED and APS. It is important to note that the third constituent added to the gelating solution is pure water: we decided to introduce later the bispyrene cross-linker at this step, dissolved in MilliQ water.

Finally, the samples are left covered overnight at room temperature and then allowed to swell in water. Excess of monomer and unbound chains are removed by changing the bath water every hour during 8 hours. Size stability is reached after about 24 h. The resulting PAM hydrogel is then cut with a blade and despite many problems to handle and adapt it into a stretching device (see the chapter 2 "Materials and Methods") and stretch without breaking it, we observed that this gel was stretchable at least five times at 50% of its initial length.

3.3.2 Bispyrene 2 cross-linked in the poly(acrylamide) hydrogel

The cross-linkable bispyrene **2** is pH responsive and its solubility varies with the pH: at low pH, the triamine spacer is highly charged and therefore the compound **2** become more soluble in aqueous medium than at basic pH. To be introduced into the PAM architecture, the bispyrene **2** was added into the 800 µL of water used as the third reagent in the preparation of the PAM hydrogel (see Table 3.1 above). Two solutions of bispyrene **2** (0.1 mg/mL) at pH 1 and pH 14 were prepared and exposed to a UV lamp emitting at 360 nm (see figure 3.7a). The aim of these measurements is to have reference spectra of the two limit conformation of the bispyrene **2**. The acid solution of bispyrene **2** appears violet and the basic one is blue-green. Thus, the proportion of the two conformations ("opened" and "closed") of the bispyrene structure in each solution is not the same. This difference of behaviour can be explained by the protonation of the diethylenetriamine spacer in acid condition: the spacer adopts a linear conformation to pull away the positive charges of the three ammonium groups (figure 3.7c). Thus, the emission of fluorescence observed from the acid solution is identical to the one recorded from an isolated pyrene ring (figure 3.7b): three intense and characteristic peaks identified at 395, 375 and 420 nm explain the resulting violet color (figure 3.7a). At pH 14, the hydrophobic effect occurs and the two pyrene rings are close together leading to the very broad fluoresecent excimer emission at 480 nm, responsible of the green color (figure 3.7b). We assumed that if we are able to prepare a PAM hydrogel containing the bispyrene **2** under its closed conformation and linked in the polymeric architecture, by stretching of this material, we can switch the closed conformation to the opened one.

According to the previous part 3.3.1 of this chapter 3, the preparation of the suitable PAM hydrogel require to mix successively together the acrylamide, the bisacrylamide and the water solution, containing the bispyrene **2** in our case. All solutions were adjusted at pH 14 before polymerization. Then, TEMED and APS were added and the radical polymerization occurred overnight. The resulting PAM hydrogel was washed up to no fluorescence emission

was detected in the washing water. The so-washed gel was still emitting fluorescence, proving the covalent grafting of bispyrene **2** in the PAM structure, but the color emitted was blue sky when exposed to a UV lamp (360 nm), which is the characteristic color of the opened conformation of bispyrene **2** (figure 3.8a). Using an optical probe specially dedicated to the measurement of the fluorescence of material, we recorded the fluorescence emission spectra of the PAM hydrogel containing bispyrene **2**. As expected, the spectra observed is similar to the one measured with the bispyrene **2** in pH 1 solution (figure 3.8b). Therefore, the bispyrene **2** has adopted an opened conformation during the PAM polymerization process.

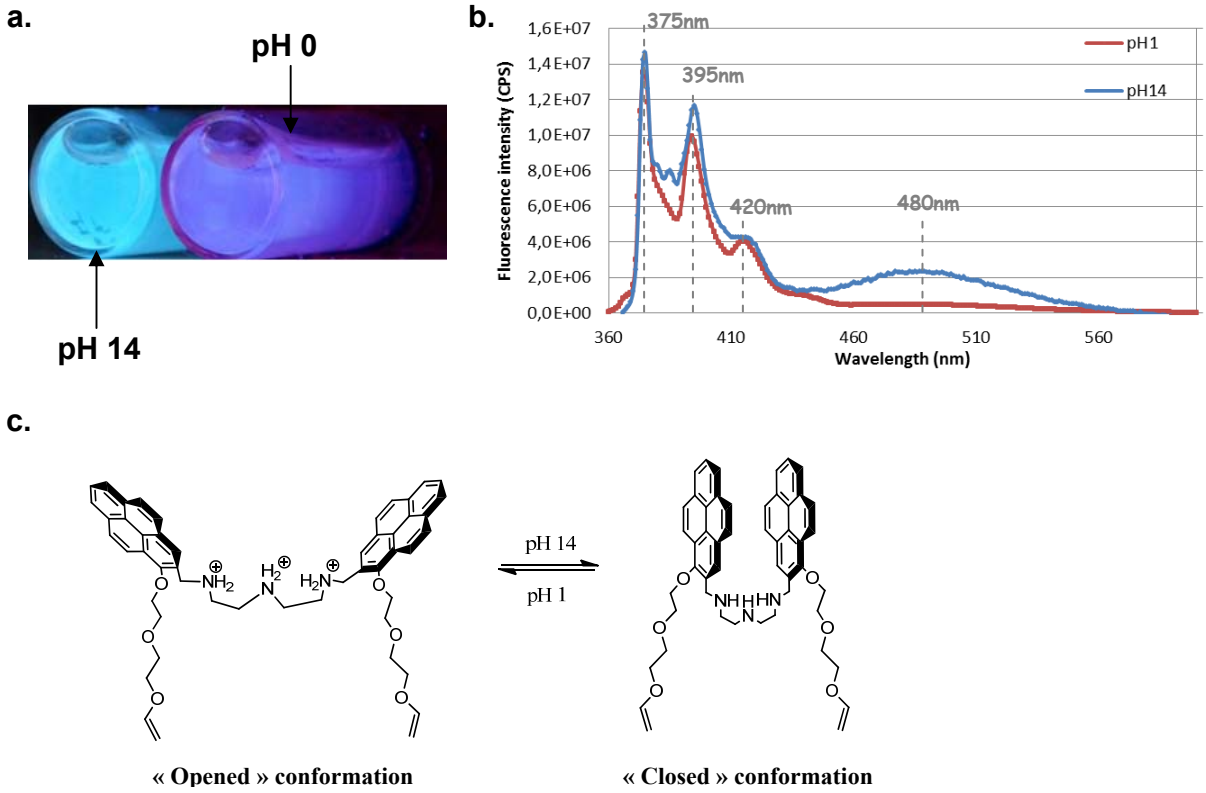

Figure 3.7: (**a**) Pictures of the bispyrene **2** in aqueous solutions (0.1 mg/mL) at pH 1 and pH 14 when exposed to a UV lamp (360 nm); (**b**) Fluorescent emission spectra of bispyrene **2** solutions at pH 1 and pH 14 when excited at 342 nm; (**c**) Schematic representation of the equilibrium between the "opened" and "closed" conformation of the bispyrene **2**, according to the pH.

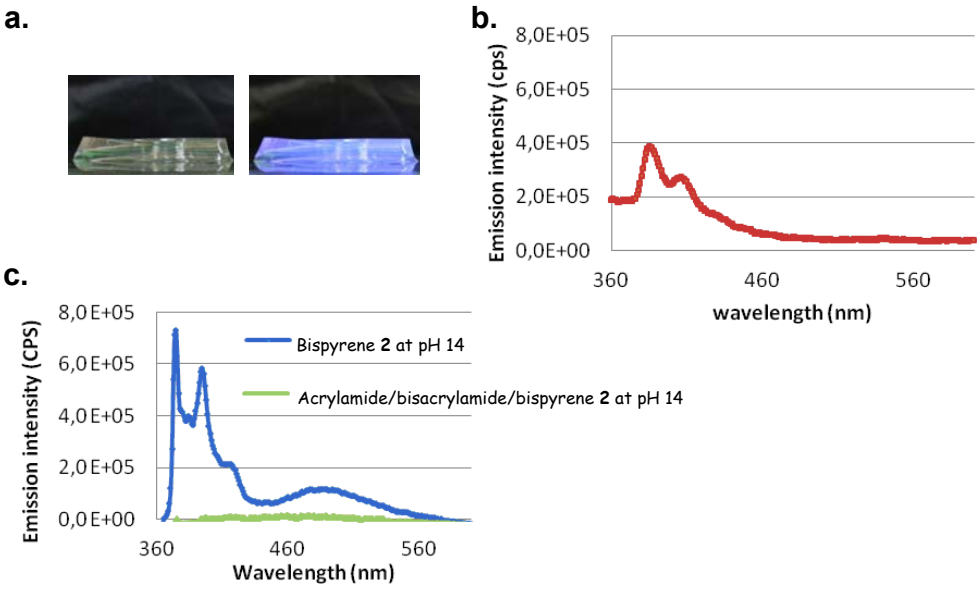

Figure 3.8: (**a**) Pictures of the PAM hydrogel containing the bispyrene **2** exposed to sunlight (left) and under a UV lamp at 360 nm (right); (**b**) Fluorescence emission spectra of the PAM hydrogel containing the bispyrene **2** excited at 342 nm; (**c**) Fluorescence emission spectra of the bispyrene **2** in aqueous solution (0.1 mg/mL) (blue curve) and in presence of acrylamide and bisacrylamide (green curve), both at pH 14.

To understand why the bispyrene **2** conformation switches from the closed conformation to the opened one, we measured the fluorescence emission spectra of the bispyrene **2** at pH 14, in presence of acrylamide and bisacrylamide compounds. We observed a complete lost of fluorescence emission (figure 3.8c). We assigned this result to a quenching fluorescence effect coming from the acrylamide or bisacrylamide. It must be noted that this phenomena has been already reported in the literature[21] and can be explained by the possible stacking of acrylamide or bisacrylamide molecule between the two pyrene rings.

3.4 Conclusion

In the part 3.3.2 of this chapter, we studied the design and the preparation of poly(acrylamide) hydrogel containing the bispyrene **2** covalently attached into the polymeric architecture as mechanotransduction system. Yet the polyacrylamide gels could not be stretched without breaking them (however, an alternative of this problem is described in chapter 6). The amount of fluorescent bispyrene **2** which is added to the hydrogel was optimized and allowed us to measure the fluorescence intensity signal by a spectrofluorometer. Unfortunately, despite that the bispyrene **2** is readily incorporated into the

PAM network, this sensor **2** cannot play the wished role because it is mainly present in the open conformation in the resulting PAM hydrogel. We thus failed to use it as mechano molecular sensor in the chosen hydrogel matrix.

Yet, the bispyrene molecules can also be a pH sensor. We thus decided to make use of this molecule as pH sensor in one-pot morphogen self-constructed films that were introduced in 2011 by our team. The idea is to buildup covalent cross-linking films by the electro control Huisgen click chemistry reaction between modified polyelectrolytes and homobifuntional spacers in the presence of a catalyst which is generated after applying an electric potential. Thus, we have prepared the bispyrene 3 described in the previous part 3.2, as homobifunctional cross-linker and pH sensors. The work represent the part 3.6 of this chapter 3 and have been recently published in Soft Matter.

3.5 References

(1) Engler, A. J.; Sen, S.; Sweeney, H. L.; Discher, D. E. Matrix elasticity directs stem cell lineage specification *Cell* **2006**, 126, 677-689.

(2) Discher, D. E.; Janmey, P.; Wang, Y.-l. Tissue Cells Feel and Respond to the Stiffness of Their Substrate *Science* **2005**, 310, 1139-1143.

(3) Rief, M.; Gautel, M.; Oesterhelt, F.; Fernandez, J. M.; Gaub, H. E. Reversible unfolding of individual titin immunoglobulin domains by AFM *Science* **1997**, 276, 1109-1112.

(4) Kellermayer, M. S. Z.; Smith, S. B.; Granzier, H. L.; Bustamante, C. Folding-unfolding transitions in single titin molecules characterized with laser tweezers *Science* **1997**, 276, 1112-1116.

(5) del Rio, A.; Perez-Jimenez, R.; Liu, R.; Roca-Cusachs, P.; Fernandez, J. M.; Sheetz, M. P. Stretching single talin rod molecules activates vinculin binding *Nature* **2009**, 323, 638-641.

(6) Zhang, X.; Rehm, S.; Safont-Sempere, M. M.; Wurthner, F. Vesicular perylene dye nanocapsules as supramolecular fluorescent pH sensor systems *Nat. Chem.* **2009**, 1, 623-629.

(7) Pérez-Gonzalez, R.; Machi, L.; Inoue, M.; Sanchez, M.; Medrano, F. Fluorescence and conformation in water-soluble bis(pyrenyl amide) receptors derived from polyaminopolycarboxylic acids *Journal of Photochemistry and Photobiology A: Chemistry* **2011**, 219, 90-100.

(8) Kanai, M.; Hirano, T.; Azumaya, I.; Okamoto, I.; Kagechika, H.; Tanatani, A. Solvent-dependent conformational and fluorescence change of an N-phenylbenzohydroxamic acid derivative bearing two pyrene moieties *Tetrahedron* 68, 2778-2783.

(9) Nagata, Y.; Nishikawa, T.; Suginome, M. Solvent-dependent fluorescence and circular dichroism properties of poly(quinoxaline-2,3-diyl)s bearing pyrene pendants *Chemical Communications* 48, 11193-11195.

(10) Toda, M.; Ogawa, N.; Itoh, H.; Hamada, F. Unique molecular recognition property of bis-pyrene-modified β-cyclodextrin dimer in collaboration with γ-cyclodextrin *Analytica Chimica Acta* **2005**, 548, 1-10.

(11) Narita, M.; Mima, S.; Ogawa, N.; Hamada, F. Fluorescent molecular sensory system based on bis pyrene-modified gamma-cyclodextrin dimer for steroids and endocrine disrupters *Analytical Sciences* **2001**, 17, 379-385.

(12) Shiraishi, Y.; Ishizumi, K.; Nishimura, G.; Hirai, T. Effects of metal cation coordination on fluorescence properties of a diethylenetriamine bearing two end pyrene fragments *Journal of Physical Chemistry B* **2007**, 111, 8812-8822.

(13) Yang, J.-S.; Lin, C.-S.; Hwang, C.-Y. Cu2+-Induced Blue Shift of the Pyrene Excimer Emission: A New Signal Transduction Mode of Pyrene Probes *Organic Letters* **2001**, 3, 889-892.

(14) Winnik, F. M. Photophysics of preassociated pyrenes in aqueous polymer solutions and in other organized media *Chemical Reviews* **1993**, 93, 587-614.

(15) Zhou, Y.; Wang, F.; Kim, Y.; Kim, S. J.; Yoon, J. Cu2+-Selective Ratiometric and "Off-On" Sensor Based on the Rhodamine Derivative Bearing Pyrene Group *Organic Letters* **2009**, 11, 4442-4445.

(16) Pengo, P.; Polizzi, S.; Battagliarin, M.; Pasquato, L.; Scrimin, P. Synthesis, characterization and properties of water-soluble gold nanoparticles with tunable core size *Journal of Materials Chemistry* **2003**, 13, 2471-2478.

(17) de Silva, A. P.; Gunaratne, H. Q. N.; Gunnlaugsson, T.; Huxley, A. J. M.; McCoy, C. P.; Rademacher, J. T.; Rice, T. E. Signaling Recognition Events with Fluorescent Sensors and Switches *Chemical Reviews* **1997**, 97, 1515-1566.

(18) Balzani, V.; Credi, A.; Raymo, F. M.; Stoddart, J. F. Artificial molecular machines *Angewandte Chemie-International Edition* **2000**, 39, 3349-3391.

(19) Czarnik, A. W., *Fluorescent Chemosensors for Ion and Molecular Recognition*. ACS: Washington, DC, 1993; Vol. 538.

(20) Tanaka, T. Gels *Scientific American* **1981**, 244, 124-138.

(21) Stramel, R. D.; Nguyen, C.; Webber, S. E.; Rodgers, M. A. J. Photophysical Properties of Pyrene Covalently Bound to Poly-Electrolytes *Journal of Physical Chemistry* **1988**, 92, 2934-2938.

3.6 Investigations of bispyrene 3 as homobifunctionnal cross-linker and local pH sensor of polyelectrolyte based films

Article 1:

"Morphogen-driven self-construction of covalent films built from polyelectrolytes and homobifunctional spacers: buildup and pH response"

Article by César Rios, Gaulthier Rydzek, Prasad Polavarapu, Jean-Nicolas Tisserant, Jean-Claude Voegel, Bernard Senger, Philippe Lavalle, Benoît Frisch, Pierre Schaaf, Fouzia Boulmedais, Loïc Jierry published in *Soft Matter*, **2012**, 8, 10336.

Soft Matter

Dynamic Article Links

Cite this: *Soft Matter*, 2012, **8**, 10336

www.rsc.org/softmatter

PAPER

Morphogen-driven self-construction of covalent films built from polyelectrolytes and homobifunctional spacers: buildup and pH response†

Gaulthier Rydzek,‡[abc] Prasad Polavarapu,‡[a] César Rios,‡[a] Jean-Nicolas Tisserant,[a] Jean-Claude Voegel,[bc] Bernard Senger,[bc] Philippe Lavalle,[bc] Benoît Frisch,[de] Pierre Schaaf,*[ae] Fouzia Boulmedais[ae] and Loïc Jierry*[ae]

Received 1st June 2012, Accepted 3rd August 2012
DOI: 10.1039/c2sm26272j

Self-construction of films using polyelectrolytes bearing complementary chemical groups is a recent emerging concept in the coating field. Herein, we describe the one-pot morphogen film self-construction through formation of covalent bonds between polyelectrolytes and homobifunctional spacers by Huisgen click-chemistry. One-pot solution of poly(acrylic acid) bearing alkyne groups (PAA-Alk), bisazides ethylene glycol (Az-EG_n-Az) spacers and $CuSO_4$ was brought into contact with a gold electrode. Cu(I), the morphogen, was generated electrochemically from Cu(II) at the electrode/one-pot solution interface. The PAA-Alk/Az-EG_n-Az film buildup was investigated by varying the length of the EG_n spacer ($n = 2$, 13 and 50) leading to different growth rates. By increasing the pH of the solution, a reversible swelling of the films (up to 400% for $n = 13$ or 50) is obtained due to electrostatic repulsion between PAA chains. Further investigations on film swelling were performed by using PAA-Alk and an original bisazide spacer based on two pyrene units connected by a triamine spacer (Az-bispyrene-Az). This spacer has the property to adopt an extended conformation under acidic conditions and a "stacked" conformation under basic conditions, which both can be monitored by fluorimetry. Despite the mechanical tension due to film swelling at basic pH, bispyrene spacers adopt a stacked conformation. This allowed us to monitor the pH within PAA-Alk/Az-bispyrene-Az films. The pH remains fairly stable and below the pK_a of PAA when the pH of the contacting solution varies from pH 5 to pH 7 and increases above pH 8, which explains why film swelling takes place essentially above pH 8.

1. Introduction

Research in surface coating is a field that finds many applications in areas ranging from anti-corrosion, sensors, optical devices, biomaterials, and membranes up to tissue engineering. Among the different methods developed to build nanometric sized films onto a substrate, the step-by-step deposition process is probably one of the most prominent. The first example of step-by-step construction of electrostatically interacting molecules concerned polyelectrolytes and bolaform molecules of opposite charges.[1] This process was rapidly extended to polyelectrolyte multilayers which result from the alternated deposition of polyanions and polycations.[2] Many studies have demonstrated the feasibility and efficiency of this procedure for different applications such as surface treatments,[3] optical coatings,[4] separation processes[5] and biomaterials,[6] to cite only a few examples. However, this process suffers from two main drawbacks which limit its industrial applications: the films obtained are usually weakly resistant to external stimuli (high ionic strength, pH changes or strong mechanical forces for instance) and the process is time consuming. Covalent crosslinking between polyelectrolytes during the step-by-step process or at the end of the buildup was introduced to render the film robust.[7] To circumvent the second drawback, we have recently introduced the concept of one-pot morphogen-driven self-construction based on the reaction between two polymers that form covalent bonds in the presence of a catalyst.[8]

By producing the catalyst at the surface of the substrate, the film buildup is obtained and takes place exclusively on the

[a]*Centre National de la Recherche Scientifique, Unité Propre de Recherche 22, Institut Charles Sadron, 23 rue du Loess, 67034 Strasbourg Cedex 2, France*
[b]*Institut National de la Santé et de la Recherche Médicale, Unité 977, 11 rue Humann, 67085 Strasbourg Cedex, France*
[c]*Université de Strasbourg, Faculté de Chirurgie Dentaire, 1 place de l'Hôpital, 67000 Strasbourg, France*
[d]*Laboratoire de Conception et Application de Molécules Bioactives, UMR 7199, CNRS/Université de Strasbourg, Faculté de Pharmacie, 74 route du Rhin, 67401 Illkirch Cedex, France*
[e]*International Centre for Frontier Research in Chemistry, 8 allée Gaspard Monge, 67083 Strasbourg, France*

† Electronic supplementary information (ESI) available: Chemical modification of PAA, syntheses of homobifunctional spacers and bispyrene units, fluorescence measurements, and Fig. S-1 to S-9. See DOI: 10.1039/c2sm26272j

‡ These authors contributed equally.

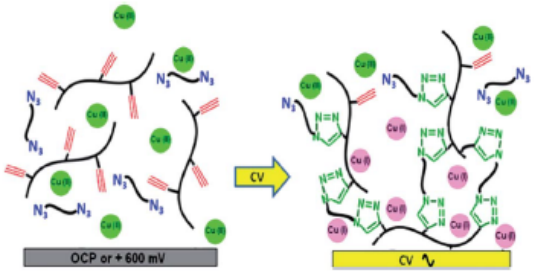

Scheme 1 Schematic representation of a one-pot self-construction of a PAA-Alk/Az-EG$_n$-Az film using electrotriggered click chemistry. Cu(I), a catalyst of the reaction, is produced at the electrode by electro-reduction of Cu(II) present in solution by application of a cyclic voltammetry between −350 mV and 600 mV (*vs.* Ag/AgCl, scan rate 50 mV s^{-1}). The morphogen Cu(I) induces the formation of triazole groups between PAA-Alk and Az-EG$_n$-Az spacers.

substrate. The catalyst then plays the role of a morphogen. We used Huisgen's click reaction between azide and alkyne groups catalyzed by Cu(I) to demonstrate the validity of this concept.[9] Copper ions (I), which play the role of morphogens, were generated electrochemically from Cu(II) at the interface in the simultaneous presence of two types of poly(acrylic acid) chains, one type bearing azide and the other alkyne groups. Caruso and collaborators have recently introduced a similar concept named Continuous Assembly of Polymers (CAPs) based on atom transfer radical polymerization.[10] In the present work, we investigated the one-pot morphogen-driven film construction of poly(acrylic acid) chains bearing alkyne groups (PAA-Alk) and ethylene glycol spacers bearing azide groups on both sides (Az-EG$_n$-Az) (Scheme 1). The film buildup was by far not obvious because the two ends of the bifunctionalized spacers could react with the same polymer chain and thereby become unavailable to continue the self-construction process. By using a functionalized spacer, this approach of buildup represents an easy way to design stimuli-responsive films as illustrated herein. The film buildup and morphology were investigated respectively by quartz crystal microbalance with monitored dissipation (EC-QCM-D) and by atomic force microscopy (AFM). The length of the Az-EG$_n$-Az spacers (n = 2, 13 and 50 EG units) had an influence on the film growth rate. Due to electrostatic repulsion between PAA chains, PAA-Alk/Az-EG$_n$-Az films swell in a reversible manner in response to a pH change of the solution in contact with them. In order to get a better understanding of the swelling/deswelling behaviour, an original bispyrene spacer Az-bispyrene-Az was used with PAA-Alk. A change in the fluorescence of bispyrene molecules is observed when they switch from a "stretched" to an "unstretched" conformation. This property allows us to also monitor the pH within the PAA-Alk/Az-bispyrene-Az film *versus* the pH of the contacting solution.

2. Materials and methods

Chemicals

Poly(ethyleneimine) (PEI, M = 750 000 g mol^{-1}, CAS 18197-8) and copper(II) sulfate pentahydrate ($CuSO_4 \cdot 5H_2O$, 99.99% purity, M = 249.69 g mol^{-1}, CAS 7758-99-8) were purchased from Aldrich and used as received. Poly(acrylic acid) functionalized by alkyne groups (PAA-Alk) at 5% were described according to Rydzek *et al.*[11] Bisazide ethylene glycol (EG) spacers Az-EG$_n$-Az (with n = 2, 10 and 50) were prepared respectively according to Bonger *et al.*,[12] El Haitami *et al.*,[13] and Xu *et al.*[14] The chemical structure of PAA-Alk and the different Az-EG$_n$-Az spacers are represented in Scheme 2. Synthesis of the Az-bispyrene-Az spacer and azide-free bispyrene spacer is described in Section 1 of the ESI.† All solutions were prepared with ultra pure water (Milli-Q Plus system, Millipore, Billerica, MA) and adjusted at pH 4 using 0.1 M HNO_3.

Electrochemical-quartz crystal microbalance with dissipation monitoring (EC-QCM-D)

The electrochemical-quartz crystal microbalance (EC-QCM-D) experiments were performed on a Q-Sense E1 apparatus from Q-Sense AB (Gothenburg, Sweden) by monitoring the changes in the resonance frequency f and the dissipation factor D of an oscillating quartz crystal upon adsorption of a viscoelastic layer.[15,16] The quartz crystal was excited at its fundamental frequency (5 MHz), and the measurements were performed at the first, third, fifth and seventh overtones corresponding to 5, 15, 25 and 35 MHz, respectively. The thickness was estimated using the 3rd, 5th and 7th overtones. The EC-QCM-D measurement is sensitive to the amount of water associated with the adsorbed molecules and senses the viscoelastic changes in the interfacial material.[15] The thickness of the adsorbed layers can be estimated using the viscoelastic Voigt model.[17] For this evaluation, the fluid density (1009 kg m^{-3}), fluid viscosity (0.91 mPa s^{-1}) and layer density (1000 kg m^{-3}) were kept constant. The Q-Sense Electrochemistry Module, QEM 401, allows simultaneous QCM and electrochemistry measurements. Either a gold-coated QCM sensor from Q-Sense AB (Gothenburg, Sweden) or an ITO-coated QCM sensor from Microvacuum (Budapest, Hungary) acted as the working electrode. A platinum counter-electrode on the top wall of the chamber and a no-leak Ag/AgCl reference electrode fixed in the outlet flow channel were used respectively as counter and reference electrodes. Before the buildup of the polymer film, and in order to test the quality of the EC-QCM-D cell, a capacitive current and a faradic current of the following solution were recorded: a Tris–$NaNO_3$ buffer solution prepared from tris(hydroxy-methylaminomethane) (Tris, 5 mM) and sodium nitrate ($NaNO_3$, 0.15 M) was adjusted at pH 7.4 and used to measure the capacitive current of the EC-QCM-D cell. 1 mM

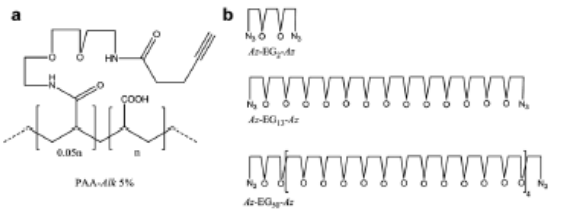

Scheme 2 Chemical structures of (a) PAA-Alk and (b) the homo-bifunctional spacers Az-EG$_n$-Az, with n = 2, 13 and 50, involved in the self-construction of films.

of potassium hexacyanoferrate(II) was prepared in Tris–$NaNO_3$ buffer solution and brought in contact with the crystal to monitor its cyclic voltammogram.

Film buildup procedure

Film self-constructions were performed either on a bare gold or ITO QCM crystal. Gold and ITO coated crystals were cleaned by dipping during 15 min in a 50% (v/v) 1 M sodium hydroxide/hydrogen peroxide mixture. This cleaning step was followed by a rinsing step with distilled water. The substrate was brought in contact during 5 min with a PEI solution (1 g L^{-1} in water, pH 7.0) followed by a rinsing step with a $CuSO_4$ solution (0.6 mM, pH 4). This step was done to obtain an initial electrostatic adsorption and promote further film buildup. Then a mixture of PAA-Alk at 1 g L^{-1}, homobifunctional azide spacers at 2 mM and $CuSO_4$ at 0.6 mM, prepared in Milli-Q water and adjusted at pH 4, was injected at a flow rate of 0.1 mL min^{-1}. After the electrostatic adsorption of PAA-Alk (on the precursor layer of PEI) and a stabilization of 5 min, a cyclic voltammetry between −350 mV and +600 mV with a 50 mV s^{-1} scan rate was applied during 90 min.

Film washing procedure

Since copper ions are known to interact with PAA and bispyrene groups, self-constructed films were washed during 30 min using a 0.02 M EDTA solution at pH 4 with a flow rate of 1 mL min^{-1}. This procedure allows us to successfully remove all copper ions from the assemblies.[8]

Atomic force microscopy (AFM) measurements

AFM images were obtained in contact mode under liquid conditions with the Nanoscope IV from Bruker (Santa Barbara, CA). The images were carried out with silicon nitride cantilevers with a spring constant of 0.03 N m^{-1} (model MSCTAUHW, Bruker, CA). Several images were performed over a given surface area. These scans had to give reproducible images to ascertain that there was no sample damage induced by the tip. Deflection and height mode images were scanned simultaneously at a fixed scan rate (2 Hz) with a resolution of 512 × 512 pixels. Data evaluation was performed with the NanoScope software version 5.31r1 (Bruker). Profilometric section analyses of a scratched film allowed us to determine precisely the quality of the film and its thickness over the scanned area. Achieved with a plastic cone tip, scratches were always imaged perpendicular to the scan axis to obtain profiles corresponding to a cross section along this axis. A mean thickness of the scratched film was determined by measuring it at least on three different areas. For all the observations, the samples were kept under liquid conditions.

Fluorescence measurements

Fluorescence intensity of Az-bispyrene-Az in solution and of self-constructed PAA-Alk/Az-bispyrene-Az films, built on ITO substrates, was recorded using a FluoroMax-4 Spectrofluorometer from HORIBA Jobin Yvon equipped with a fiber optic probe. Light is focused from the excitation spectrometer onto the optical fiber and then directed to the sample. Fluorescence emission from the sample is measured directly through the optical fiber. Measurement details concerning fluorescence are given in the ESI.†

3. Results and discussion

Self-construction of PAA-Alk/Az-EG_n-Az films

The self-construction of PAA-Alk and Az-EG_n-Az spacer films was first investigated by EC-QCM-D varying the length of the spacer. The chemical structures of PAA-Alk and Az-EG_n-Az spacers are represented in Scheme 2. The buildups have been performed at pH 4 in the simultaneous presence of PAA-Alk, Az-EG_n-Az spacer and 0.6 mM of $CuSO_4$. The film thickness was determined by means of the Voinova model[17] (Fig. 1), using the frequency shifts and the dissipations (Fig. S-1, ESI†).

It is noticeable that the application of cyclic voltammetry (CV) between −350 mV and +600 mV (*vs.* Ag/AgCl) results in a continuous film buildup for the three studied systems PAA-Alk/Az-EG_2-Az, PAA-Alk/Az-EG_{13}-Az and PAA-Alk/Az-EG_{50}-Az. After the first 20–30 min, the film buildup becomes linear (Fig. S1, ESI†). Electrostatic interactions between PAA-Alk and the precursor layer of PEI might influence the film growth in the first few minutes of the buildup. To analyze these results, one must keep in mind that EC-QCM-D measures the hydrated thickness of the film related to its hydrated mass. The repulsion between PAA chains, decreasing the rate of the buildup, could explain the lower film thickness obtained with the shortest EG spacer. What is more surprising is that the same thickness is found in the case of films constructed with Az-EG_{13}-Az and Az-EG_{50}-Az. In fact the buildup of our films occurs at pH 4 where PAA-Alk is still partially ionized so that the chain should have a high persistence length (locally more or less linear) with statistically one alkyne group separated from another one by twenty carboxylic groups (the grafting ratio of PAA-Alk is 5%). Thus it appears difficult for a short spacer to link itself two times to the same polymer. On the other hand, for longer spacers the two azide functions could react with the same PAA-Alk chain and thereby become unavailable to continue the self-construction

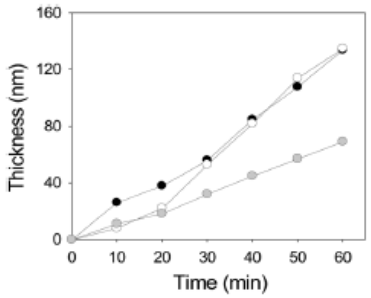

Fig. 1 Evolution of the film thickness of (●) PAA-Alk/Az-EG_2-Az, (○) PAA-Alk/Az-EG_{13}-Az and (●) PAA-Alk/Az-EG_{50}-Az as a function of the application time of CV. The mixture solution of PAA-Alk and Az-EG_n-Az, prepared in 0.6 mM $CuSO_4$ aqueous solution and adjusted at pH 4, was injected at a 0.1 mL min^{-1} flow rate. The film thickness is calculated using the Voinova model[17] from EC-QCM-D data.

process. Another explanation might be that the reactivity of both ends of the spacers decreases when the spacer chain length increases due to a smaller accessibility because it is hidden in a random coil. But, as far as the film thickness is concerned, these effects can be compensated by a longer end-to-end spacer length which leads to a higher hydration mass of the film, since oligo and polyethylene glycol chains are well known to be highly hydrated. These phenomena might be simultaneously in competition and explain the similar growth rate between Az-EG_{13}-Az and Az-EG_{50}-Az spacers. These observations are in agreement with the results of El Haitami *et al.*[13] investigating a step-by-step buildup of the same PAA-Alk/Az-EG_n-Az system. In this study, for a given number of deposition steps, the film thickness, measured by QCM-D, increased by increasing the spacer length from Az-EG_2-Az to Az-EG_{13}-Az but decreased slightly with Az-EG_{50}-Az.

Reversible swelling and topography of the films

In order to study the robustness of the films, we investigated their behaviour under pH cycles. Indeed, PAA based films are known to be pH responsive[12] since their carboxylic groups can undergo deprotonation when the pH of the contacting solution is higher than its pK_a (of 4.5). At a basic pH, the electrostatic repulsion between PAA chains induces a swelling of the films. We first changed the pH of the contacting solution back and forth between pH 3 and 9. Table 1 summarizes the normalized frequency shift and dissipation relative to the third harmonic, measured by QCM-D, and the thickness, calculated from QCM-D data and measured by AFM, of PAA-Alk/Az-EG_n-Az films at pH 3 and 9. PAA-Alk/Az-EG_n-Az films (with $n = 2$ and 13) show a reversible increase of the frequency shift under pH changes from 3 to 9 corresponding to a reversible film swelling (Fig. S-2 and S-3, ESI†). Interestingly, in the case of PAA-Alk/Az-EG_{50}-Az films, a strong decrease of the third frequency shift is observed when the pH is increased from 3 to 9 (Fig. S-4, ESI†). Correlatively the frequency of higher harmonics is no longer measured by the apparatus. Such a decrease of the frequency shift is fully compatible with a film that becomes extremely thick.[14] All these results indicate a high film stability with no loss of material under pH changes, signature of covalent links between the constituting PAA chains. Longer EG spacers lead to higher rises of the dissipation factor when the pH is increased (Table 1). At pH 9, the amount of water in the films depends on the distance between the PAA chains and thus on the length of the spacer.

Table 1 Normalized frequency shift and dissipation, measured at 15 MHz by EC-QCM-D, thicknesses, calculated from EC-QCM-D data and measured by AFM and RMS, determined by AFM, of PAA-Alk/Az-EG_2-Az, PAA-Alk/Az-EG_{13}-Az and PAA-Alk/Az-EG_{50}-Az films at pH 3 and 9 (90 min application time of CV)

	$-\Delta f/\nu$ (Hz) at 15 MHz	$\Delta D\nu$ (10^{-6}) at 15 MHz	d_{QCM} (nm)	d_{AFM} (nm)	RMS (nm)
PAA-Alk/Az-EG_2-Az					
pH 3	361	20	43	90	25
pH 9	558	54	103	166	42
PAA-Alk/Az-EG_{13}-Az					
pH 3	941	19	150	155	14
pH 9	2448	263	540	567	91
PAA-Alk/Az-EG_{50}-Az					
pH 3	1079	15	174	—	—
pH 9	280	851	608	—	—

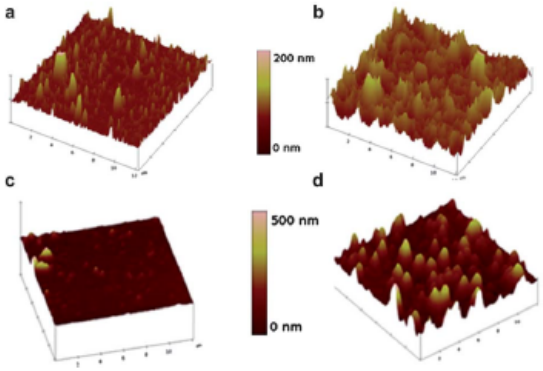

Fig. 2 Typical AFM height 3D images (12 μm × 12 μm), obtained in contact-mode, of (a and b) PAA-Alk/Az-EG_2-Az and (c and d) (PAA-Alk/Az-EG_{13}-Az) films observed in a liquid state at pH 3 (a and c) and pH 9 (b and d).

The effect of the swelling on the self-constructed films was also observed by AFM in the liquid state. After 90 min of self-construction, the topography and the thickness of PAA-Alk/Az-EG_2-Az and PAA-Alk/Az-EG_{13}-Az films were determined at pH 3 and 9. The PAA-Alk/Az-EG_{50}-Az film was too soft to be imaged at both pH values. The large dissipation factor value recorded by QCM-D indicated a strong hydration of the film, responsible for its softness. PAA-Alk/Az-EG_n-Az films (with $n =$ 2 and 13) appear both homogeneous with a high roughness (RMS) respectively of 25 nm and 14 nm at pH 3 that increases to 42 and 91 nm at pH 9 (Fig. 2). The high roughnesses are due to the large number of spikes which seem to correlate with the use of bifunctional EG spacers, as it was observed by El Haitami *et al.*[13] The buildup mechanism is the result of the interplay between the reactivity of the spacers and their local diffusion processes but we do not know the buildup mechanism in more detail. It would thus be highly speculative to give an explanation for the difference in the roughness observed for the films corresponding to EG_2 and EG_{13}. By scratching the film, AFM images allow us to determine its thickness at pH 3 and 9 (Fig. S-5, ESI†). The PAA-Alk/Az-EG_n-Az film thickness increases about 2-fold from 90 to 166 nm for $n = 2$ and about 4-fold from 155 to 567 nm for $n = 13$. The swelling of the (PAA-Alk/Az-EG_n-Az) film induces a 2- to 7-fold increase of the film roughness, respectively for $n = 2$ and $n =$ 13. For both films, a larger film thickness is determined by QCM-D rather than by AFM. Indeed, high film roughness increases hydrodynamic thickness compared to the core thickness determined by AFM (Table 1).

By gradually increasing the pH of the contacting solution, the normalized frequency shift of PAA-Alk/Az-EG_{13}-Az (Fig. 3a) and PAA-Alk/Az-EG_{50}-Az films (Fig. S-4, ESI†) increases gradually because of the film swelling. Both film thicknesses, calculated from QCM-D data, increase slightly with pH, up to pH 8 where a strong increase is observed (Fig. 3b). Above pH 9 no major thickness change takes place anymore. It appears that

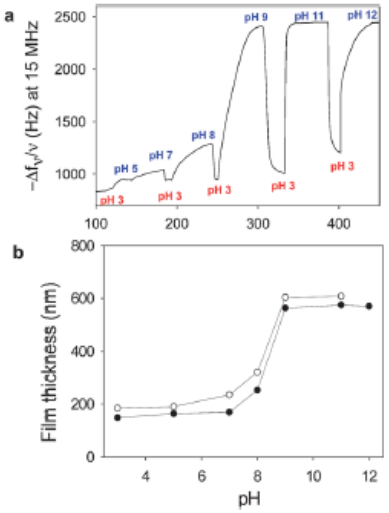

Fig. 3 (a) Evolution of the opposite of the normalized frequency shift, measured at 15 MHz ($\nu = 3$) by EC-QCM-D, of a PAA-Alk/Az-EG_{13}-Az film brought into contact with different aqueous solutions from pH 3 to 12. (b) Evolution of (PAA-Alk/Az-EG_{13}-Az) (●) and (PAA-Alk/Az-EG_{50}-Az) (○) film thickness, calculated from EC-QCM-D data, as a function of the pH solution.

the pH at which the strong swelling takes place is independent of the spacer length.

Considering that the pK_a of carboxylic groups in solution is close to 4.5,[18] it was not expected that swelling takes place essentially between pH 8 and 9. It must be noted that recently, in the case of crosslinked polyethyl(acrylic acid) based capsules, swelling has been reported at a pH higher than 9.[19] In our case, this could be due to two phenomena: (i) strong interactions between carboxylic groups which are known to increase the pK_a value or (ii) a non-sensitivity of the local pH within the film when the solution in contact is below pH 8.

Properties of self-constructed PAA-Alk/Az-bispyrene-Az films

The first part of our study suggests that the architecture of the self-constructed films undergoes a mechanical tension due to swelling when exposed to basic conditions. To investigate the mechanical constraints applied on the spacer when the pH increases, we designed and prepared an original homobifunctional spacer based on a bispyrene unit, named Az-bispyrene-Az (Scheme 3). The syntheses of the Az-bispyrene-Az and azide-free bispyrene compounds are given in Section 1 in the ESI.† These molecules are known to adopt two conformations depending on the pH: at low pH, an unstacked conformation due to electrostatic repulsion between protonated nitrogen atoms and at high pH, a stacked conformation due to π–π interactions and hydrophobic effects.[20] Such molecular stacking directly influences the fluorescence behaviour of the molecule. In solution, Az-bispyrene-Az shows the expected evolution of the fluorescence intensity when the pH increases from 2 up to 9 (Fig. S-6a, ESI†). At low pH, the Az-bispyrene-Az spacer displays mainly monomer fluorescence emission at 385 and 405 nm (with

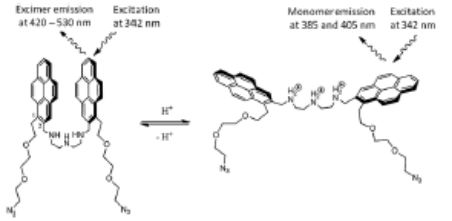

Scheme 3 Chemical structure and conformation changes from stacked (left) to unstacked (right) states of the Az-bispyrene-Az spacer in an aqueous solution. At low pH, a broad fluorescence emission signal due to the excimer (stacked state) is observed between 420 and 530 nm. At high pH, two main fluorescence emission wavelengths are observed at 385 nm and 405 nm. The fluorescence excitation wavelength is at 342 nm.

$\lambda_{excitation}$ = 342 nm) which arises from locally excited pyrene chromophores due to the extended conformation. When the pH increases, the monomer fluorescence of the Az-bispyrene-Az spacers gradually decreases and a new broad excimer emission in blue-green appears as well as an increase of fluorescence at 420–530 nm due to the stacked conformation. From the changes observed in the fluorescence intensity ratio between excimer and monomer peaks respectively at 480 and 383 nm, we can obtain a calibration curve of the ratio *versus* the pH of the solution (Fig. S-6b, ESI†). Many bispyrene molecules are described in the literature for applications as a pH probe[21] or metal ion sensor[22] in aqueous solution. Monopyrene-labelled polyelectrolytes have been widely used to study polyion complexes in solution,[23] polyelectrolyte conformations in films,[24] electron transfer,[25] polarity,[26] changes of the molecular structure under stress[27] of multilayer films or capsules.

However, no use of bispyrene covalently linked to a film or a material from each pyrene molecule has been reported so far. This lack can be explained by the synthetic difficulty to isolate a 1,2-difunctionalized pyrene ring as a unique compound (without contaminating regioisomers). To this end, self-construction of a PAA-Alk/Az-bispyrene-Az film was performed under the same conditions as PAA-Alk/Az-EG_n-Az films but in a water–ethanol 50/50 (v/v) solution because of the low water solubility of bispyrene spacers (Fig. S-7, ESI†). A continuous and nearly linear film buildup was observed during the CV application. When an azide-free bispyrene is used instead of Az-bispyrene-Az, no self-construction of the film occurs. After 90 min of buildup, non-scratched and scratched PAA-Alk/Az-bispyrene-Az films were characterized by AFM (Fig. S-8, ESI†). At pH 3, the film covers the whole surface of the substrate. It appears possible to prepare functionalized self-constructed films by using bispyrene containing spacers. Many spikes appear to extend over almost 40 nm and render the film rough as observed for PAA-Alk/Az-EG_n-Az films. At pH 3 for a thickness of 40 nm, the roughness (RMS) is of 12 nm. When the film is brought into contact with a solution at pH 9, the thickness increases about 3-fold to 130 nm and the roughness increases at 17 nm. As far as film construction and swelling is concerned, one can conclude that the Az-bispyrene-Az linkers behave similarly to Az-EG_n-Az linkers. In contrast, when the pH is switched between pH 3 and 9, the normalized frequency shift exhibits an unexpected swelling/deswelling behaviour.

When the pH is decreased from 9 to 3, a rapid decrease of the opposite of the normalized frequency shift is observed, signature of a film shrinking (Fig. 4a). The expected film shrinking is followed by a slow swelling during 35–40 min before stabilization. On the other hand when the pH increases from 3 to 9, the film swells rapidly (increase of the opposite of the normalized frequency shift). The film swelling is slowed down during almost 10 min, again with an "unexpected" behavior before rapidly reaching a plateau (Fig. 4b). We can notice that the overall timescale of the film shrinking is much longer compared to its swelling. These two observations could be explained by an "antagonist motion" of the PAA chains and bispyrene units, components of the film, during the pH switching (Scheme 4). When the PAA-Alk/Az-bispyrene-Az film is at pH 3, the carboxylic groups of PAA are mainly in their protonated form and bispyrene molecules are in their unstacked conformation because of the protonated amines. When the pH is changed from 3 to 9, the deprotonation of the carboxylic groups leads to an electrostatic repulsion between PAA chains inducing the swelling of the film. This repulsion is in competition with conformational motions of bispyrene molecules going from an unstacked (at pH 3) to a stacked (at pH 9) state, which leads to a reduction of the spacer arms between PAA chains. Indeed according to experiments performed with EG spacers, a reduction of the spacer arm should lead to a thinner film thickness. This shortening of the spacer arm seems to be as fast as the electrostatic repulsion between PAA chains inducing the small film shrinking observed after the initial swelling (Fig. 4b). When the film is brought back at pH 3, the shrinking of the film conflicts the "opening" of bispyrene entities, which again leads to an unexpected behaviour of the shrinking process.

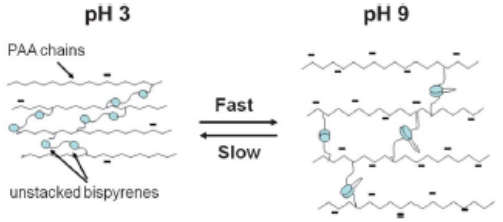

Scheme 4 Schematic representation of PAA-Alk/Az-bispyrene-Az films at pH 3 and 9. At pH 3, the PAA chains are less negatively charged and can get closer to each other whereas the amine functions of bispyrene spacers are protonated, leading to an opened form of the molecule. At pH 9, the bispyrene spacers adopt their unstacked conformations whereas the deprotonated carboxylic groups of PAA lead to electrostatic repulsion between the polymer chains.

To check this interpretation, we measured the fluorescence emission spectra of the PAA-Alk/Az-bispyrene-Az film at pH 3 and 9 (Fig. 5a). The fluorescence of the film was measured at the excitation wavelength of 342 nm with a fluorimeter equipped with an optical fiber probe (experimental details are given in Section 2 of the ESI†). When the pH is increased from 3 to 9, one

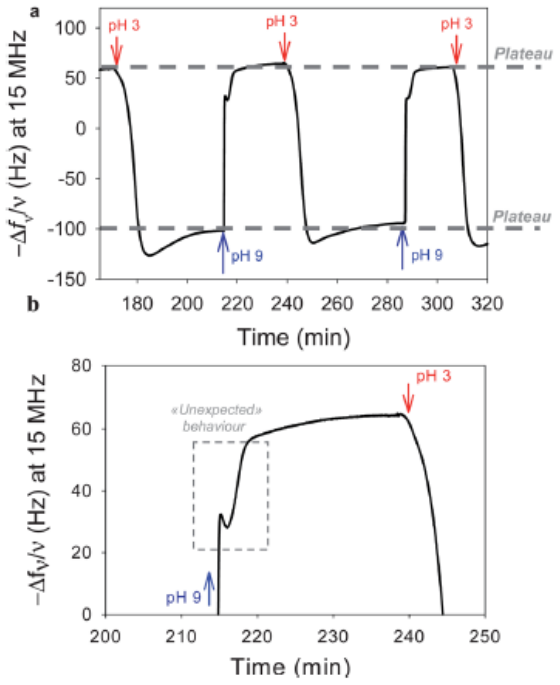

Fig. 4 (a) Evolution of the opposite of the normalized frequency shift, measured at 15 MHz ($\nu = 3$) by EC-QCM-D, as a function of time of the PAA-Alk/Az-bispyrene-Az film during pH changes. Red and blue arrows indicate the injection of pH 3 and pH 9 solutions respectively. (b) is a zoom in of (a) showing a small film shrinking after the initial swelling.

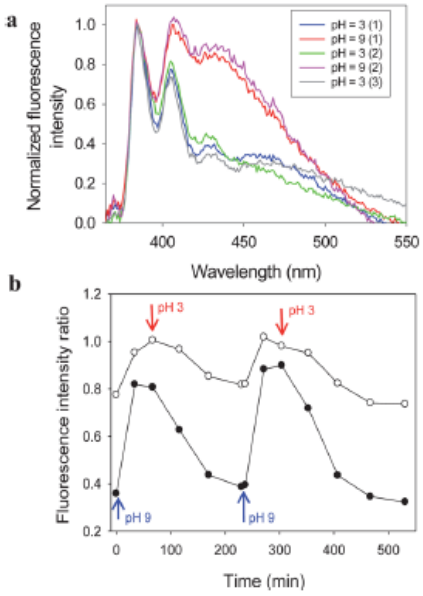

Fig. 5 (a) Normalized fluorescence emission spectra of a PAA-Alk/Az-bispyrene-Az film measured alternately at pH 3 and 9; (b) evolution of the fluorescence intensity ratios of the PAA-Alk/Az-bispyrene-Az film (●) between the excimer peak at 435 nm and the monomer peak at 385 nm and (○) between the two monomer peaks (405 and 385 nm) as a function of time during pH changes. Red and blue arrows indicate the injection of the pH 3 and pH 9 solutions respectively.

observes an increase of the emission intensities at 405 and 435 nm with respect to 385 nm. The very broad emission observed at 435 nm is assigned to the excimer formation of bispyrene into the PAA-Alk/Az-bispyrene-Az film. This is an indication of the stacked state of bispyrene. When the film is brought back from pH 9 to pH 3, two emission peaks at 385 and 405 nm are mainly observed. Bispyrene spacers are in the unstacked state. It is interesting to note that changes in the fluorescence intensity spectra are reversible with respect to pH switches. The fluorescence intensity ratios of the excimer (ratio between the peak at 435 nm and the monomer peak at 385 nm) and of the monomer (ratio between both monomer peaks at 405 and 385 nm) allow us to monitor the conformation of the bispyrene spacer at each pH change. An opening of the bispyrene molecule corresponds to a decrease of the fluorescence intensity ratio of the excimer. The timescale of bispyrene conformation changes is not the same when the pH increases or decreases (Fig. 5b). When the pH of the contacting solution decreases from 9 to 3, the "opening" of the bispyrene of the film is much slower than the reverse process, when the film is put back at pH 9 (200 min compared to 30 min). This is in agreement with the interpretation of the QCM-D signals. When the pH is switched from 3 to 9, the slow shrinking of the film that occurs in the first few minutes after the pH change seems to be due to the fast stacking of bispyrene. The rapid appearance of excimer after the pH change from 3 to 9 seems to invalidate the hypothesis that the unexpected effect observed (Fig. 4b) is due to complexation between the ammonium in the Az-bispyrene-Az spacer and the carboxylic groups of the PAA, and in any case proves that the dominant effect is the bispyrene stacking. When the pH is switched from 9 to 3, the slow swelling period observed after the first shrinking step should be due to the opening of the bispyrene unit. This hypothesis may be true if we assume that the motion of the bispyrene molecules are governed by their pH behavior and not the electrostatic forces inside the film generated by the repulsion between the PAA chains. Our initial aim was to check if the repulsion between PAA chains is sufficient to unstack the bispyrene molecules. Thus, this seems not to be the case. The π–π stacking appears more energetic than the repulsive forces resulting from PAA electrostatic repulsion. At equilibrium, the conformation of bispyrene spacers is thus solely governed by the pH within the film.

Then, we monitored the fluorescence spectrum of the PAA-Alk/Az-bispyrene-Az film at different pH and determined the fluorescence intensity ratio of bispyrene excimer and monomer (Fig. S-9, ESI†). When shifting from pH 3 to 4, a small increase of the fluorescence intensity ratio of the excimer is observed. It stabilizes up to almost pH 7 and increases strongly between pH 8 and 9. As the conformation of bispyrene is mostly sensitive to the pH within the PAA-Alk/Az-EG$_n$-Az film and not to the mechanical stress due to the film swelling, pH can be monitored. To this aim, a calibration curve of fluorescence intensity ratio of bispyrene excimer free in solution *versus* pH was plotted (Fig. S-6, ESI†). This curve allows us to associate the fluorescence intensity ratio of bispyrene excimer of the film with a pH value that corresponds to the pH within the film. Fig. 6 represents the pH within the film *versus* the pH of the contacting solution. We can notice that for a pH lower than 8 the internal pH of the film is lower by about 4 units than the pH of the contacting solution. The pH within the film remains fairly stable

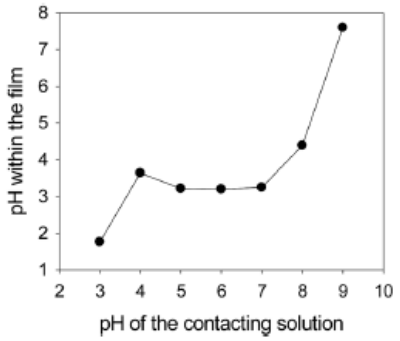

Fig. 6 Evolution of the pH within the PAA-Alk/Az-bispyrene-Az film as a function of the pH of the contacting solution. The pH within the film was determined by the fluorescence intensity ratio of excimer (435 nm) and monomer (385 nm) of the bispyrene spacer included in the film (Fig. S-9, ESI†), and the calibration curve of the fluorescence intensity ratio of excimer and monomer of the bispyrene spacer in solution *versus* pH of the solution (Fig. S-6, ESI†).

and lower than the pK_a of PAA for pH of contacting solution ranging from 5 to 7. This explains why the film swelling takes place essentially above pH 8 (Fig. 3b). This phenomenon was also described for polyelectrolyte multilayers.[28,29]

4. Conclusions

Herein, we investigated the one-pot morphogen film buildup of PAA chains with homobifunctional spacers by using electro-controlled Huisgen 1,3-cycloaddition. We proved that such architectures lead to films which rapidly cover the whole surface. The PAA-Alk/Az-EG$_n$-Az film thickness increases with the length of the Az-EG$_n$-Az spacer. By increasing the pH of the solution in contact, PAA-Alk/Az-EG$_n$-Az films swell because of the electrostatic repulsions between PAA chains. A reversible swelling/shrinking of the films is obtained by pH switching between 3 and 9. Film thicknesses increase slightly with pH up to 8 where a strong increase is observed. Above pH 9, no changes take place anymore. By using a pH sensitive homobifunctional spacer based on a bispyrene unit, we noticed that despite the mechanical tension accompanying the film swelling, bispyrene spacers adopt a stacked conformation due to the pH within the film. The local pH in the film is fairly stable between pH 5 and almost pH 7 explaining why the film swelling takes place essentially above pH 8.

Acknowledgements

We gratefully acknowledge Karim Benmlih and Joseph Hemmerlé for the design of the adaptative fluorescence device. G.R. was supported by a fellowship from the "Ministère de la Recherche et de la Technologie". C.R. was supported by a fellowship from International Center for Frontier Research in Chemistry (icFRC) and the "Ministère de la Recherche et de la Technologie". This work was supported by ANR grants (BIO-STRETCH ANR-10-BLAN-0818 and CLICK MULTILAYER ANR-07-BLAN-0169).

Notes and references

1 G. Decher and J. D. Hong, *Makromol. Chem., Macromol. Symp.*, 1991, **46**, 321.
2 G. Decher, *Science*, 1997, **277**, 1232.
3 Z. Z. Wu, J. Walish, A. Nolte, L. Zhai, R. E. Cohen and M. F. Rubner, *Adv. Mater.*, 2006, **18**, 2699; D. G. Shchukin, M. Zheludkevich, K. Yasakau, S. Lamaka, M. G. S. Ferreira and H. Möhwald, *Adv. Mater.*, 2006, **18**, 1672.
4 D. M. DeLongchamp and P. T. Hammond, *Chem. Mater.*, 2004, **16**, 4799.
5 Z. J. Sui and J. B. Schlenoff, *Langmuir*, 2004, **20**, 6026; N. A. Kotov, S. Magonov and E. Tropsha, *Chem. Mater.*, 1998, **10**, 886.
6 B. Thierry, P. Kujawa, C. Tkaczyk, F. M. Winnik, L. Bilodeau and M. Tabrizian, *J. Am. Chem. Soc.*, 2005, **127**, 1626; C. Vodouhê, M. Schmittbuhl, F. Boulmedais, D. Bagnard, D. Vautier, P. Schaaf, C. Egles, J.-C. Voegel and J. Ogier, *Biomaterials*, 2005, **26**, 545.
7 G. Decher, J. Schmitt, L. Heiliger and H.-U. Siegmund, European Patent, EP647467, 1995; J. J. Harris, P. M. DeRose and M. L. Bruening, *J. Am. Chem. Soc.*, 1999, **121**, 1978; A. Schneider, G. Francius, R. Obeid, P. Schwinté, J. Hemmerlé, B. Frisch, P. Schaaf, J.-C. Voegel, B. Senger and C. Picart, *Langmuir*, 2006, **22**, 1193; G. K. Such, J. F. Quinn, A. Quinn, E. Tjipto and F. Caruso, *J. Am. Chem. Soc.*, 2006, **128**, 9318.
8 G. Rydzek, L. Jierry, A. Parat, J. S. Thomann, J.-C. Voegel, B. Senger, J. Hemmerlé, A. Ponche, B. Frisch, P Schaaf and F. Boulmedais, *Angew. Chem., Int. Ed.*, 2011, **50**, 4374.
9 H. C. Kolb, M. G. Finn and K. B. Sharpless, *Angew. Chem., Int. Ed.*, 2001, **40**, 2004.
10 D. Mertz, C. J. Oehs, Z. Zhu, L. Lee, S. N. Guntari, G. K. Such, T. K. Goh, L. A. Connal, A. Blencowe, G. G. Qiao and F. Caruso, *Chem. Commun.*, 2011, **47**, 12601.
11 G. Rydzek, J. S. Thomann, N. Ben Ameur, L. Jierry, P. Mésini, A. Ponche, C. Contal, A. E. El Haitami, J.-C. Voegel, B. Senger, P. Schaaf, B. Frisch and F. Boulmedais, *Langmuir*, 2010, **26**, 2816.
12 K. M. Bonger, R. J. B. H. N. van den Berg, L. H. Heitman, A. P. Ijzerman, J. Oosterom, C. M. Timmers, H. S. Overkleeft and G. A. Marel, *Bioorg. Med. Chem.*, 2007, **15**, 4841.
13 A. E. El Haitami, J. S. Thomann, L. Jierry, A. Parat, J.-C. Voegel, P. Schaaf, B. Senger, F. Boulmedais and B. Frisch, *Langmuir*, 2010, **26**, 12351.
14 L. Q. Xu, F. Yao, G. D. Fu and E. T. Kang, *Biomacromolecules*, 2010, **11**, 1810.
15 K. A. Marx, *Biomacromolecules*, 2003, **4**, 1099.
16 F. Höök, J. Vörös, M. Rodahl, R. Kurrat, P. Boni, J. J. Ramsden, M. Textor, N. D. Spencer, P. Tengvall, J. Gold and B. Kasemo, *Colloids Surf., B*, 2002, **24**, 155.
17 M. V. Voinova, M. Rodahl, M. Jonson and B. Kasemo, *Phys. Scr.*, 1999, **59**, 391.
18 M. Fujiwara, R. H. Grubbs and J. D. Baldeschwieler, *J. Colloid Interface Sci.*, 1997, **185**, 210; J. E. Gebhardt and D. W. Furstenau, *Colloids Surf.*, 1983, **7**, 221.
19 V. Kozlovskaya, A. Shamaev and S. A. Sukhishvili, *Soft Matter*, 2008, **4**, 1499.
20 X. Zhang, S. Rehm, M. M. Safon-Sempere and F. Würthner, *Nat. Chem.*, 2009, **1**, 623.
21 Y. Shiraishi, Y. Tokitoh and T. Hirai, *Org. Lett.*, 2006, **8**, 3841.
22 F. Sancenon, A. B. Descalzo, J. M. Lloris, R. Martinez-Manez, T. Pardo, M. J. Segui and J. Soto, *Polyhedron*, 2002, **21**, 1397.
23 S. Holappa, L. Kantonen, T. Andersson, F. Winnik and H. Tenhu, *Langmuir*, 2005, **21**, 11431.
24 J. Park and P. T. Hammond, *Macromolecules*, 2005, **38**, 10542.
25 C. Tedeschi, L. D. Li, H. Möhwald, C. Spitz, D. von Seggern, R. Menzel and S. Kirstein, *J. Am. Chem. Soc.*, 2004, **126**, 3218.
26 C. Tedeschi, H. Möhwald and S. Kirstein, *J. Am. Chem. Soc.*, 2001, **123**, 954.
27 J. Fruh, R. Kohler, H. Möhwald and R. Krastev, *Langmuir*, 2010, **26**, 15516.
28 E. Kharlampieva and S. A. Sukhishvili, *Langmuir*, 2003, **19**, 1235.
29 T. Mauser, C. Déjugnat and G. B. Sukhorukov, *Macromol. Rapid Commun.*, 2004, **25**, 1781.

3.6.1 Supporting Information to article 1

SECTION 1: Syntheses of PAA-*Alk* and homobifunctionnal spacers

General Informations

All starting materials were obtained from commercial suppliers and were used without further purification. ^{1}H NMR and ^{13}C NMR spectra were recorded on Bruker Advance DPX400 (400 MHz) spectrometers. The NMR chemical shifts are reported in ppm relative to tetramethylsilane ($CDCl_3$ or MeO-d_4) or tert-butanol (1.24 ppm) in D_2O (s:singlet, t:triplet, q:quadruplet, dd:doublet of doublet, br:broad). Infrared spectra were obtained on a Thermo Electron Corporation Nicolet 380 FT-IR equipped with ATR. Merck RP-18 F254S plates were used for analytical thin layer chromatography. Silica gel 60 (particle: 40 – 60 □m) was used for flash chromatography.

Synthesis of PAA-*Alk* 5%. PAA- Alk 5 % was synthesized according to Rydzek, G.; Thomann, J. S.; Ben Ameur, N.; Jierry, L.; Mésini, P.; Ponche, A.; Contal, C.; El Haitami, A. E.; Voegel, J.-C.; Senger, B.; Schaaf, P.; Frisch, B.; Boulmedais, F. Langmuir **2009**, 26, 2816–2824.

Synthesis of bispyrene has been prepared according to Shiraishi, Y.; Tokitoh, Y.; Hirai, T. Org. Lett. **2006**, 17, 3841-3844.

Synthesis of *Az*-Bispyrene-*Az*. 1-(2-(2-(2-azidoethoxy)ethoxy)ethoxy)pyrene-2-carbaldehyde (**3**). To a solution of 100 mg (0.41 mmol) of compound **1** (Y. Zhou et *al*., *Org. Lett.* 2009, **11**, 4442-4445) in 5 mL DMF was added 561 mg (4.06 mmol, 10 eq) of K_2CO_3 under argon. To this bright red solution, 147 mg (0.45 mmol, 1.1 eq) of tosylate **2** in 1 mL DMF was added slowly and heated at 60 ^{o}C during overnight. Water was added and solvent evaporated under reduced pressure. The residue was extracted with CH_2Cl_2 (3 times) and the combined organic phase was washed with water, dried over MgSO4, solvent evaporated to give yellowish residue. This was flashed in a silica gel column eluting with 0-3 % ethyl acetate in CH_2Cl_2 to get 110 mg (67 %) of product **3** as light brown semi solid (contains little tosylate starting material). ^{1}H NMR (400 MHz, $CDCl_3$) : δ = 10.82 (s, 1H), 8.47 (s, 1H), 8.36 (d, ^{3}J = 9.0 Hz, 1H), 8.08 (d, ^{3}J = 7.5 Hz, 1H), 8.04 (d, ^{3}J = 7.5 Hz, 1H), 8.03 (d, ^{3}J = 9.0 Hz, 1H), 7.95 (t, ^{3}J = 7.5 Hz, 1H), 7.90 (d, ^{3}J = 9.0 Hz, 1H), 7.85 (d, ^{3}J = 9.0 Hz, 1H), 4.40 (m, 2H), 3.93 (m, 2H),

3.75 (m,2H), 3.72 (m, 2H), 3.68 (t, ^{3}J = 5.0 Hz, 2H), 3.38 (t, ^{3}J = 5.0 Hz, 2H); ^{13}C NMR (100 MHz, $CDCl_3$) : δ = 190.9, 155.7, 131.8, 131.6, 128.9, 127.9, 127.5, 127.5, 127.3, 127.1, 126.1, 125.3, 125.2, 124.5, 124.3, 123.5, 121.2, 70.8, 70.6, 70.2, 70.0, 50.7; MS (ESI) m/z calcd for $C_{23}H_{21}N_3NaO_4$ $[M + Na]^+$ = 426.14, found 426.00; IR (neat, cm^{-1}) : 2921, 2853, 2100, 1683, 1123.

N1-((1-(2-(2-(2-azidoethoxy)ethoxy)ethoxy)pyren-2-yl)methyl)-N2-(2-((1-(2-(2-(2-azidoethoxy) ethoxy)ethoxy)pyren-2-yl)methylamino)ethyl)ethane-1,2-diamine (***Az*-bispyrene-*Az***). A stirring solution of 110 mg (0.27 mmol, 2 eq) of Pyrene derivative (**3**) and 14 mg (15 µL, 0.14 mmol) of diethylenetriamine in 12 mL CH_2Cl_2 with few molecular sieves was refluxed for 2.5 h under argon. The reaction mixture was cooled down and filtered off the molecular sieves and the filtrate evaporated. To this semi oily yellow residue 13 mL ethanol and 31 mg (0.82 mmol, 6 eq) of $NaBH_4$ were added and heated at 60 ^{o}C for 4 h and stirring continued for 16 h at room temperature. Solvent was evaporated under reduced pressure and the residue was taken into CH_2Cl_2, washed with 1 M NaOH solution (3 times), water and concentrated by evaporation to give impure compound ***Az*-bispyrene-*Az*** as light orange semisolid. This compound was used without further purifications. ^{1}H NMR (400 MHz, $CDCl_3$) : δ = 8.36 (d, ^{3}J = 9.0 Hz, 2H), 8.11 (m, 4H), 8.03 (m, 4H), 7.92 (m, 6H), 4.22 (m, 6H), 4.00 – 3.30 (m, 22H), 2.81 (m, 8H); ^{13}C NMR (100 MHz, $CDCl_3$) : δ = 155.7, 144.7, 131.0, 130.9, 128.6, 127.4, 127.3, 127.0, 125.9, 124.0 – 125.5 (5C), 121.3, 70.7, 70.6, 70.0, 69.1, 68.7, 50.7, 50.6; MS (Maldi-TOF) m/z calcd for $C_{50}H_{56}N_9O_6$ $[M + H]^+$ = 878.435, found 878.669; IR (neat, cm^{-1}) : 2924, 2868, 2104, 1123.

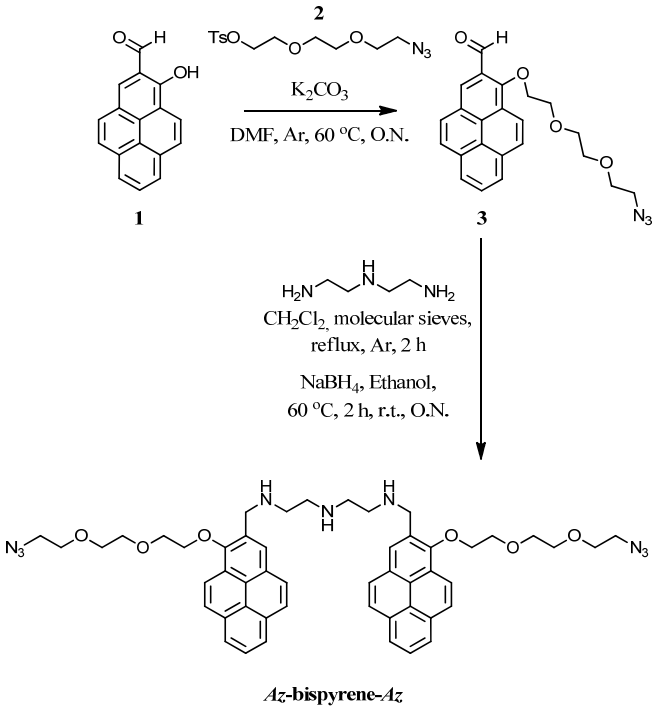

SECTION 2: Fluorescence measurements on the film PAA-*Alk*/*Az*-Bispyrene-*Az*.

All fluorescence intensities were measured by using the spectrofluorometer FluoroMax-4 from HORIBA JOBIN YVON at 432 nm of excitation wavelength. Emission fluorescence intensity of the film **PAA-*Alk*/*Az*-Bispyrene-*Az*** film was measured as follows:

1. The self-constructed **PAA-*Alk*/*Az*-Bispyrene-*Az*** film was prepared on an ITO substrate by using the EC-QCM-D according to the description process given in the Materials and Methods section of the article. To measure fluorescence, the buildup of the film studied was stopped when $\Delta f_v/v$ corresponding to the third overtones reached -950 Hz by the QCM.
2. The ITO substrate covered with the **PAA-*Alk*/*Az*-Bispyrene-*Az*** film was dipped in 15 mL of MilliQ solution at desired pH (this pH was obtained by using diluted solutions of HCl and NaOH).
3. The ITO substrate was deposited on a microscope glass slide with the film on the top. Then, the film was covered with another, thinner glass slide. This system was maintained in a home-made adaptor allowing fixing both the ITO substrate and an optical fiber. Thus, reproducible experiments have been performed.

4. The optical fiber F-3000, purchased from HORIBA JOBIN YVON, was fixed in our home-made adaptor and put in contact with the top glass slide on the ITO substrate by using a micrometer screw (see picture below).
5. Excitation of the film at 342 nm and fluorescence emission was done through the optical probe into a dark room.

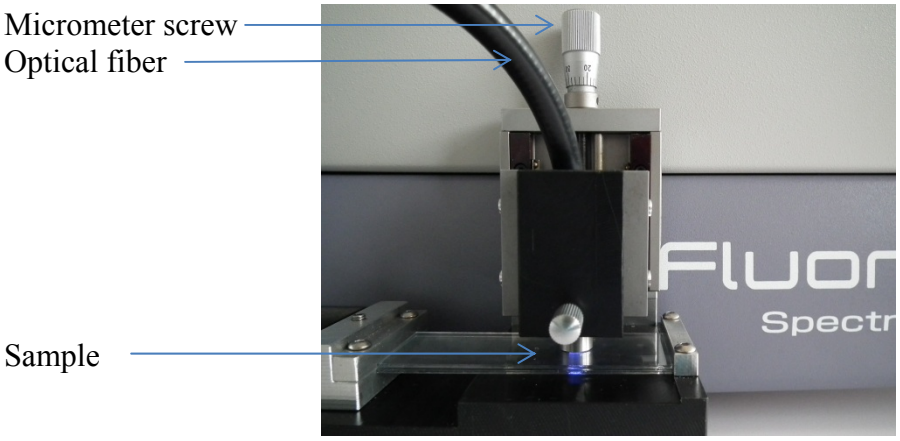

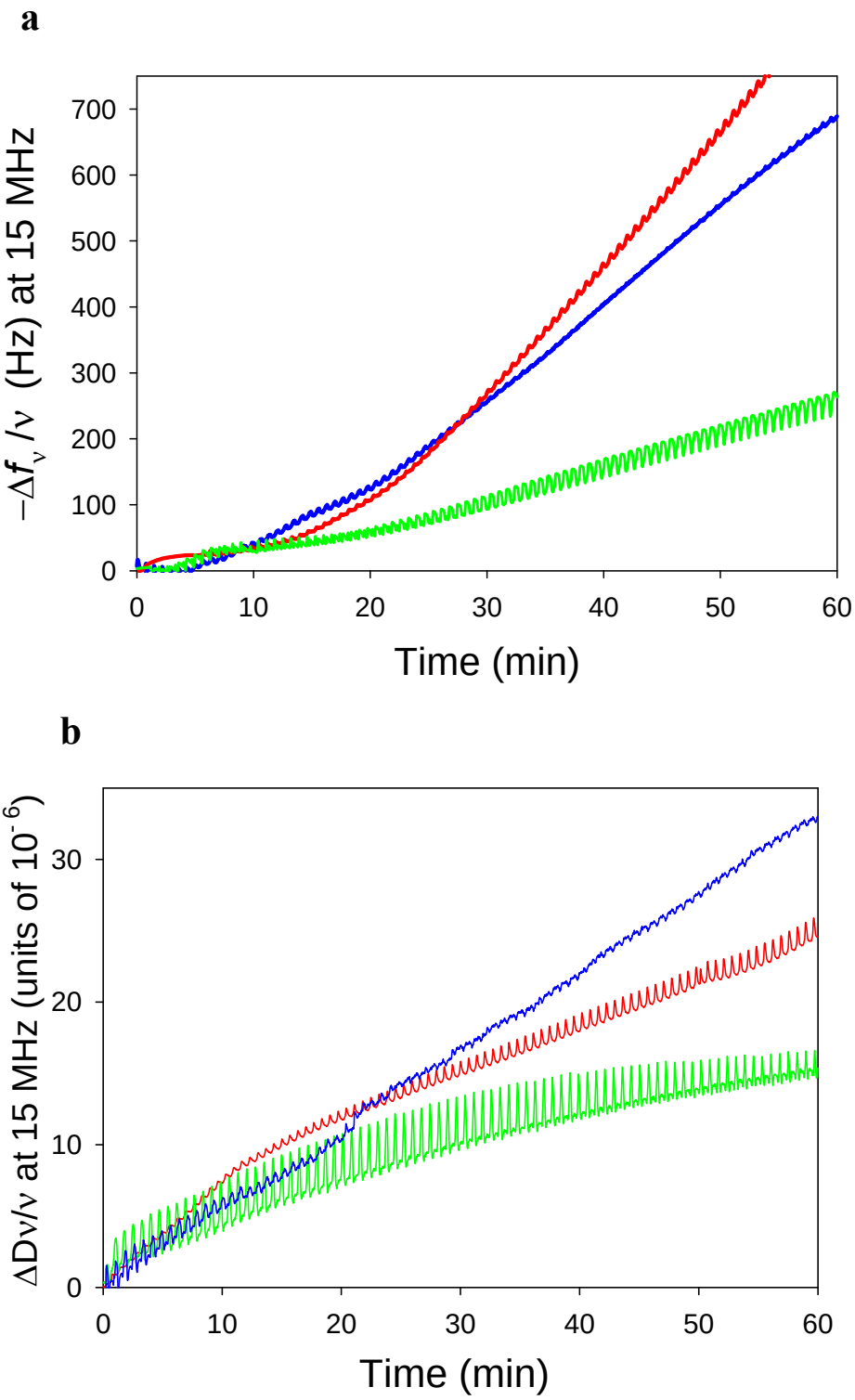

Fig. S-1 Evolution of the opposite of the normalized frequency shift (**a**) and dissipations (**b**), measured at 15 MHz (ν = 3) by EC-QCM, during the self-construction of PAA-*Alk*/*Az*-EG_2-*Az* (green line), PAA-*Alk*/*Az*-EG_{13}-*Az* (red line) and PAA-*Alk*/*Az*-EG_{50}-*Az* films (blue line). A mixture solution (PAA-*Alk*, *Az*-EG_n-*Az* and $CuSO_4$) is in contact with the gold substrate (QCM crystal) and a cyclic voltammetry (CV) between -350 mV and + 600 mV (vs Ag/AgCl, scan rate of 50 mV/s) is applied. The film is built on a PEI pre-coated surface.

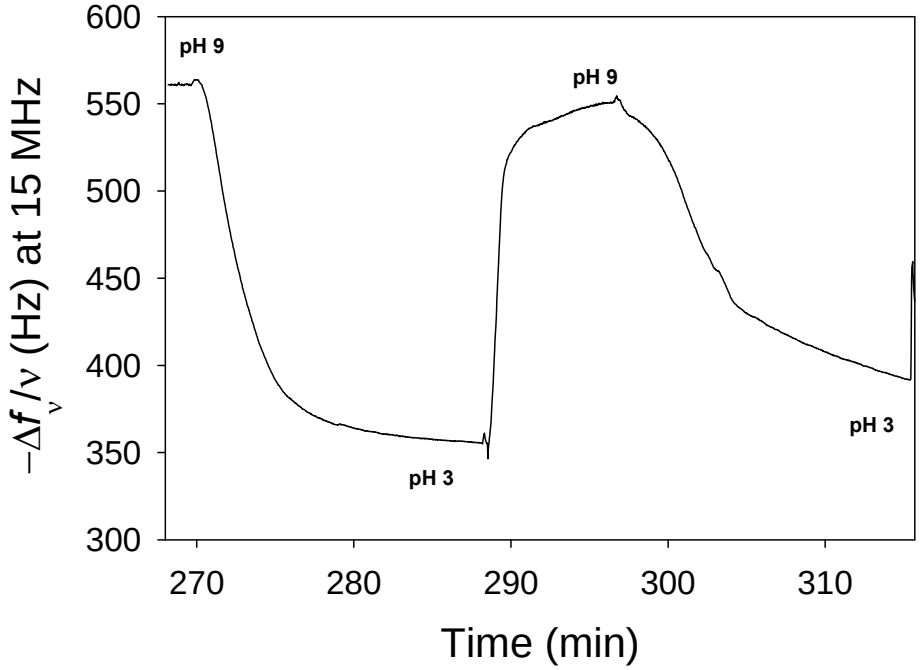

Fig. S-2 Evolution of the opposite of the normalized frequency shift, measured at 15 MHz (ν = 3) by EC-QCM-D, of PAA-*Alk*/*Az*-EG_2-*Az* film during pH changes back and forth from 9 to 3. After the film buildup on a PEI precoated surface, aqueous solutions at pH 9 and pH 3 were put into contact alternately with the film under a flow rate of 1 mL/min. The swelling and shrinking recorded are attributed to reversible deprotonation/protonation of the carboxylic functions of PAA.

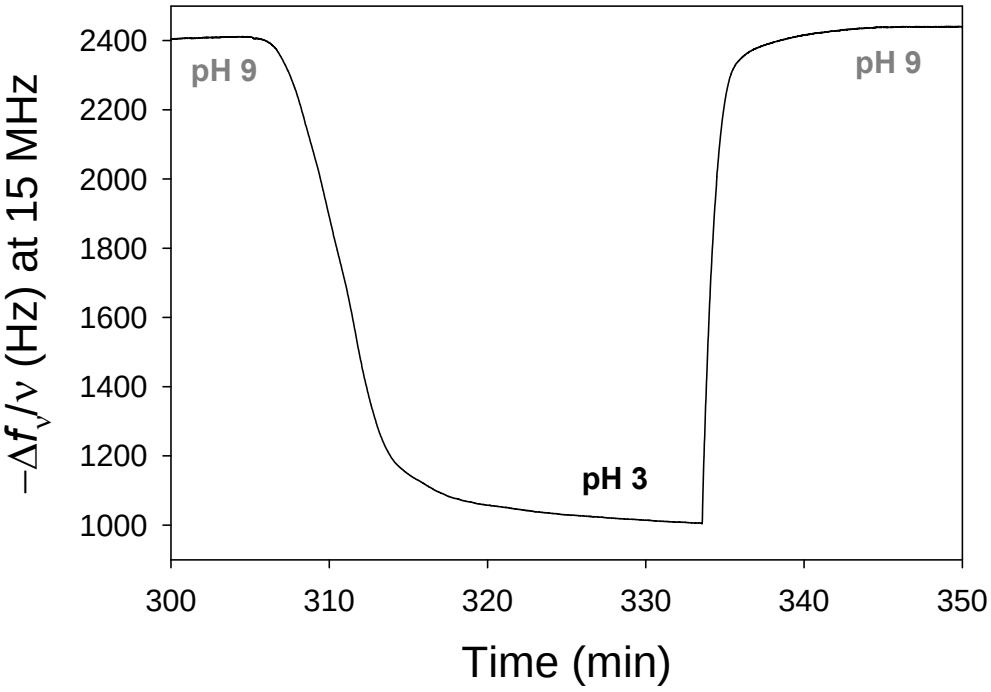

Fig. S-3 Evolution of the opposite of the normalized frequency shift, measured at 15 MHz (ν = 3) by EC-QCM-D, of PAA-Alk/*Az*-EG_{13}-*Az* film during pH changes back and forth from 9 to 3. After the film buildup on a PEI precoated surface, aqueous solutions at pH 9 and at pH 3 were put into contact alternately with the film under a flow rate of 1 mL/min. The swelling and shrinking recorded are attributed to reversible deprotonation/protonation of the carboxylic functions of PAA.

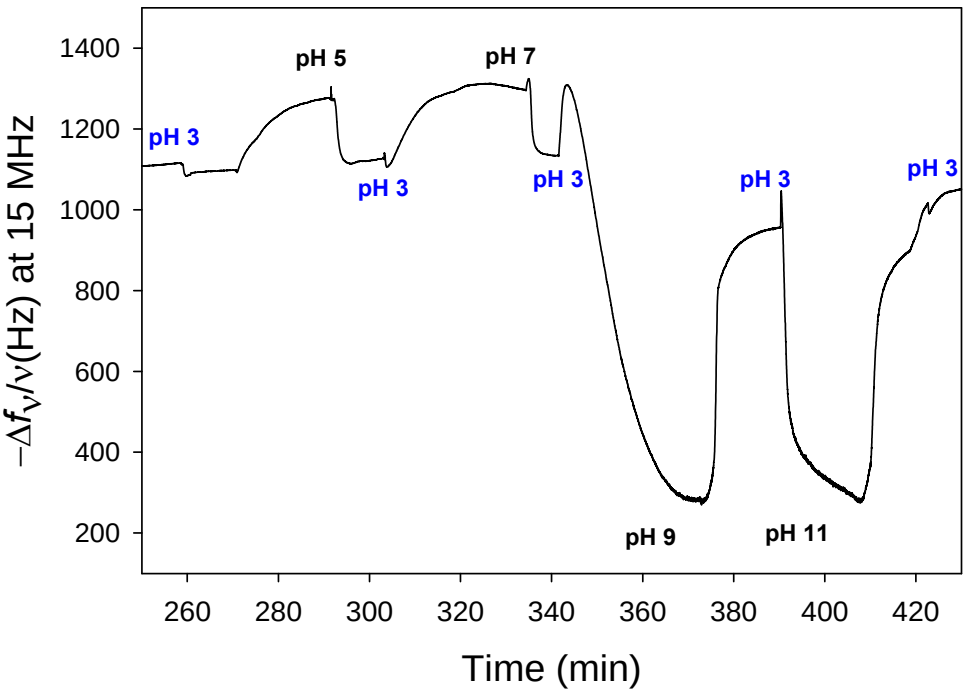

Fig. S-4 Evolution of the opposite of the normalized frequency shift, measured at 15 MHz (ν = 3) by EC-QCM-D, of a PAA-*Alk*/*Az*-EG_{50}-*Az* film during gradual pH increase from pH 3 to pH 11. After the film buildup on a PEI precoated surface, aqueous solutions at different pH were put into contact alternately with the film under a flow rate of 1 mL/min. After an expected increase of the frequency shift with the increase in pH, one observes a strong decrease of the frequency shift when the pH increases at pH 9 and 11. Correlatively the frequency of higher harmonics is no longer measured by the apparatus. Such a decrease of the frequency shift is fully compatible with a film that becomes extremely thick (Xu, F. Yao, G. D. Fu, E. T. Kang, *Biomacromolecules*, **2010**, *11*, 1810).

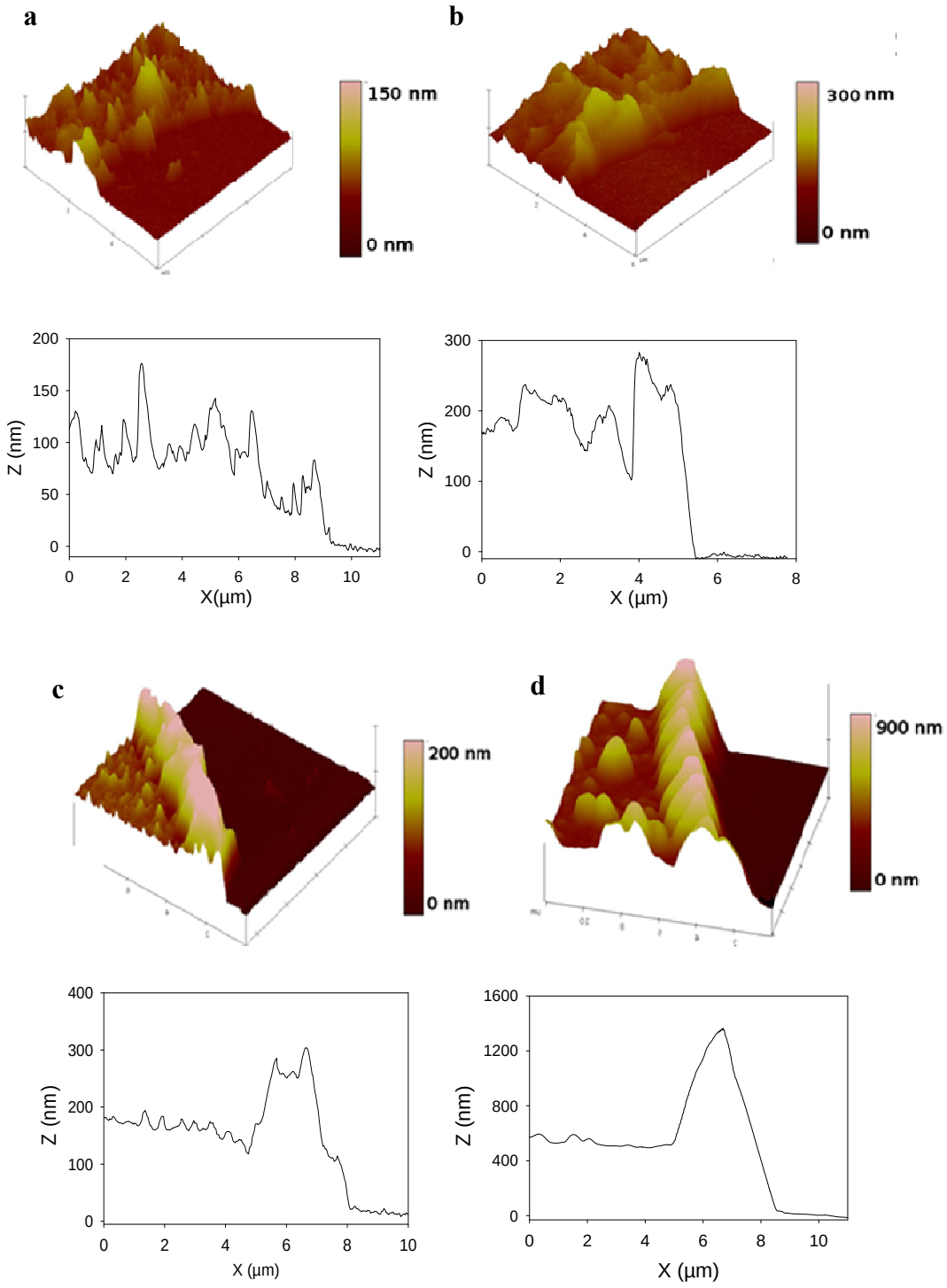

Fig. S-5 Typical AFM height 3D images (12 µm × 12 µm) and their corresponding profilometric sections profiles of scratched (**a**, **b**) (PAA-*Alk*/*Az*-EG_2-*Az*) and (**c**, **d**) (PAA-*Alk*/*Az*-EG_{13}-*Az*) films obtained, in contact-mode, observed in liquid state at pH 3 (**a**, **c**) and pH 9 (**b**, **d**).

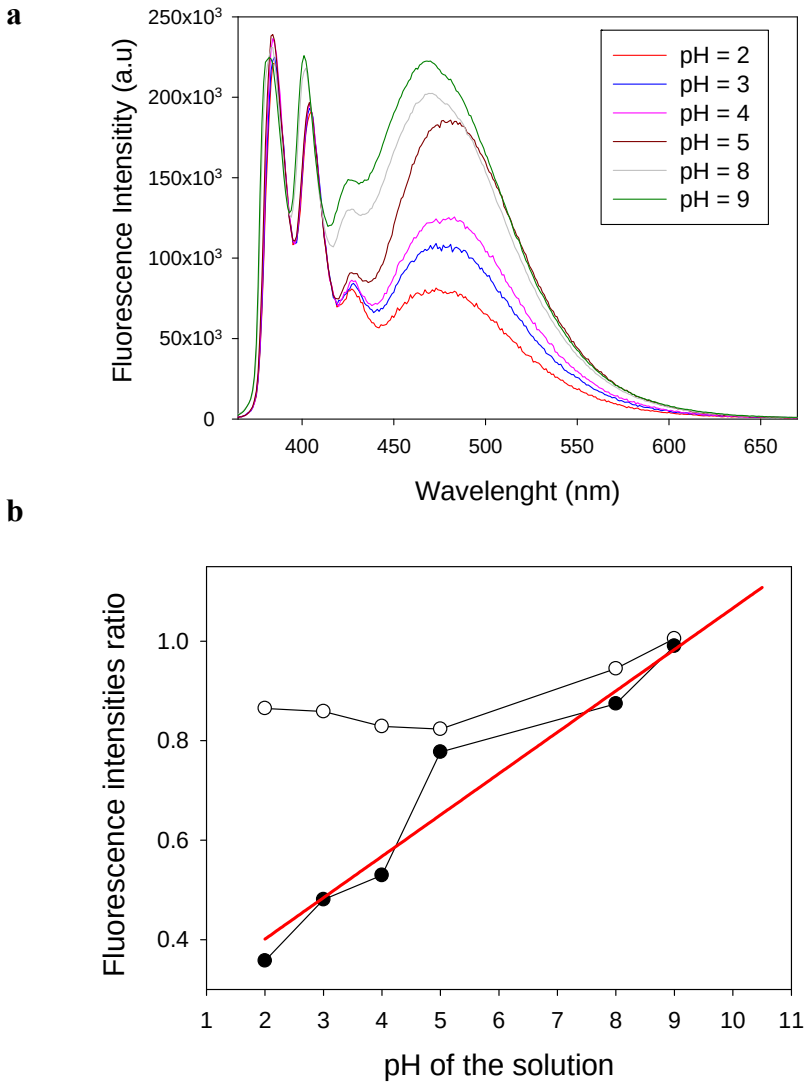

Fig. S-6 (**a**) Fluorescence emission spectra of *Az*-bispyrene-*Az* molecule in solution measured at different pH with an excitation wavelength of 342 nm. The concentration of *Az*-bispyrene-*Az* was 0.2 mg/mL prepared in a 80:20 (v/v) water/ethanol solution. (**b**) Evolution of fluorescence intensities ratios of *Az*-bispyrene-*Az* in solution (●) between the excimer (480 nm) and a monomer (383 nm) peaks and (○) between the two monomer peaks (404 and 385 nm) as a function of pH. A calibration curve (red curve) can be plotted with the following equation: $Fluorescence\ Intensity\ Ratio\ of\ excimer = 0.0832 \times pH + 0.2347$ ($R^2 = 0.977$).

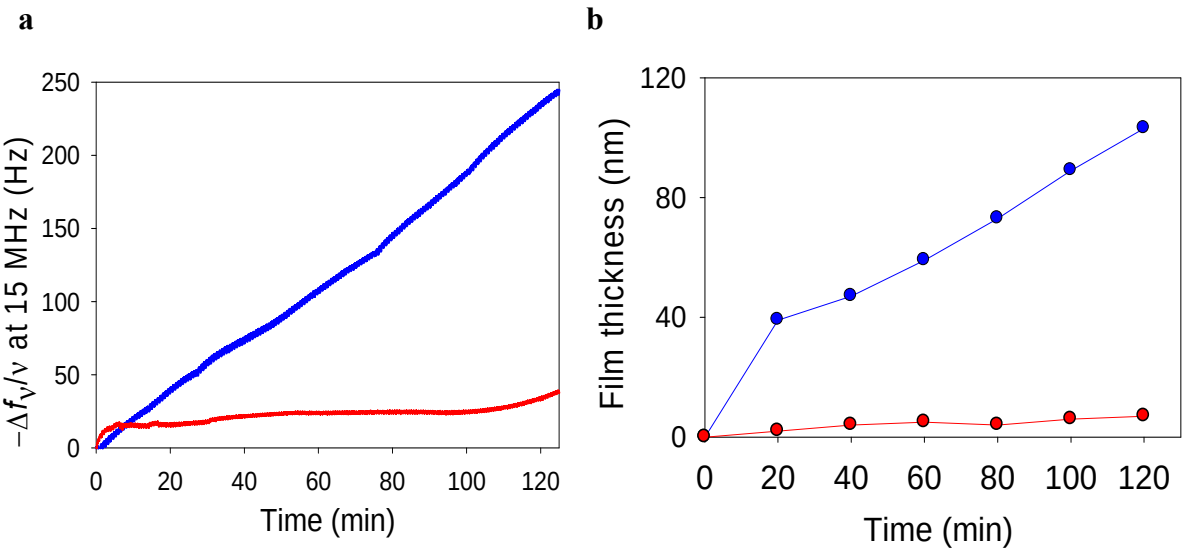

Fig. S-7 (**a**) Evolution of the opposite of the normalized frequency shift, measured at 15 MHz (ν = 3) by EC-QCM-D, as a function of time in the presence of (PAA-*Alk*/*Az*-bispyrene-*Az*) mixture (blue line) and of (PAA-*Alk*/azide-free bispyrene) mixture (red line) during the CV application between -350 mV and +600 mV (vs Ag/AgCl, scan rate of 50 mV/s). (**b**) Evolution of the calculated thicknesses of PAA-*Alk*/*Az*-bispyrene-*Az* film (blue line) and PAA-*Alk*/azide-free bispyrene mixture (red line). The film thickness was calculated using the Voigt model (M. V. Voinova, M. Rodahl, M. Jonson, B. Kasemo, Physica Scripta **1999**, 59, 391) from EC-QCM-D data. The mixture solutions were prepared at pH 4 in water/ethanol 50/50 (v/v) solution with 0.5 g/L of polymer and of *Az*-bispyrene-*Az* and 0.6 mM of $CuSO_4$. The film is built on a PEI precoated surface.

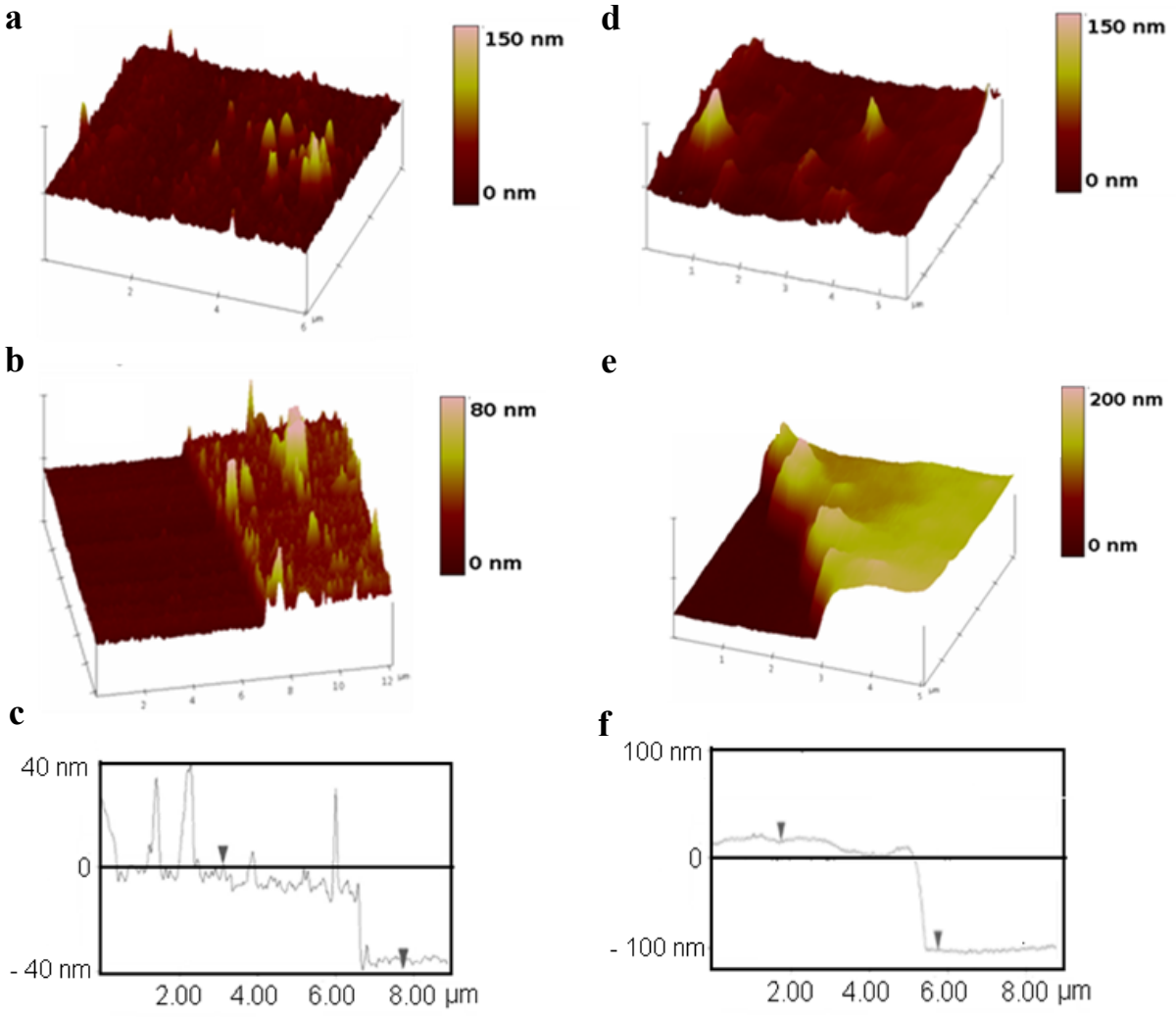

Fig. S-8 AFM 3D images of (**a**, **d**) non-scratched (6 µm × 6 µm) and (**b**, **e**) scratched (12 µm × 12 µm) PAA-*Alk*/*Az*-bispyrene-*Az* film with (**c**, **f**) their respective profilometric sections obtained in AFM height mode in liquid state at pH 3 (**a**, **b**, **c**) and pH 9 (**d**, **e**, **f**).

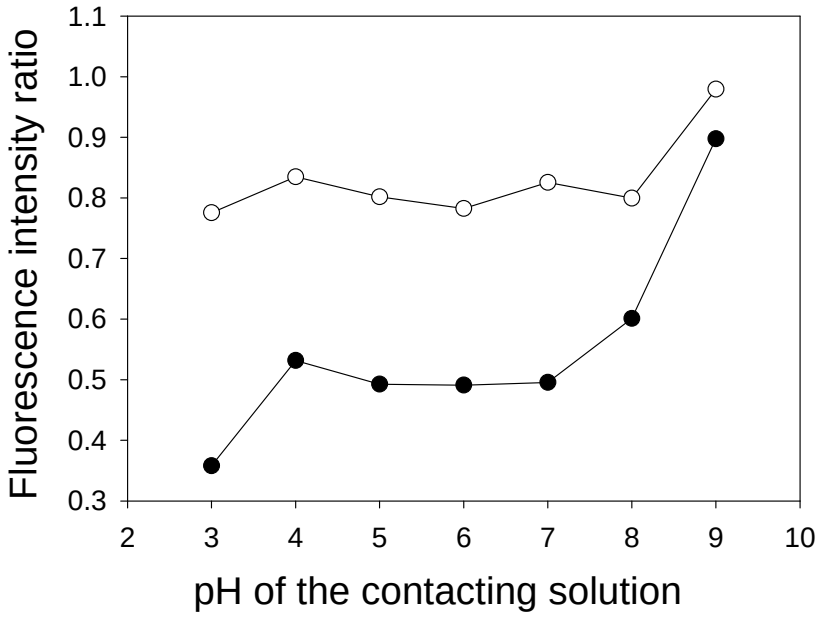

Fig. S-9 Evolution of fluorescence intensity ratios of self-constructed PAA-*Alk*/*Az*-bispyrene-*Az* film (●) between the excimer (435 nm) and a monomer (385 nm) peaks and (○) between the two monomer peaks (405 and 385 nm) as a function of pH. PAA-*Alk*/*Az*-bispyrene-*Az* film was built on an ITO coated QCM crystal. The film was dipped into 15 mL Milli Q water at the different pH values during at least 2 h before measurement of the fluorescence intensity at an excitation wavelength of 432 nm.

Chapter 4

Covalent modifications of poly(dimethylsiloxane) substrate to design reversible chemo-mechanoresponsive surfaces

4.1 Introduction

Mechanosensitive transduction processes are frequently encountered in nature.[1-3] For instance, carnivorous plants or *Mimosa Pudica* species (also commonly called *Sensitive* or *Touch-me-not*) are considered as mechanoresponsive living organisms: in both cases, a mechanical stimulation, like touching or vibrations, induces chemical transformations[4] (figures 4.1a and 4.1b). In the case of cell adhesion on a substrate, the transfer of information going from a mechanical stimulation to a chemical recognition is now well understood and accepted by the community.[5] Indeed, it has been demonstrated that when the stretching of specific proteins occurs, buried recognition sites called cryptic sites, are exhibited, leading to the formation of focal adhesion.[6, 7] At the molecular scale, another example is the assembly-disassembly cycle of the actin polymer responsible of the internal architecture of cells.[8] This process is under the control of the interaction between the talin protein and vinculin, its natural ligand.[9] This interaction occurs only when talin is mechanically stretched as depicted in figure 4.1c.[10] The cryptic binding site of the vinculin ligand is so "discovered" and the interaction between the receptor and its ligand is allowed. This binding between talin and vinculin, only possible when talin is unfolded through a mechanical stretching initiates a chemical process which is the actin cytoskeleton polymerization.

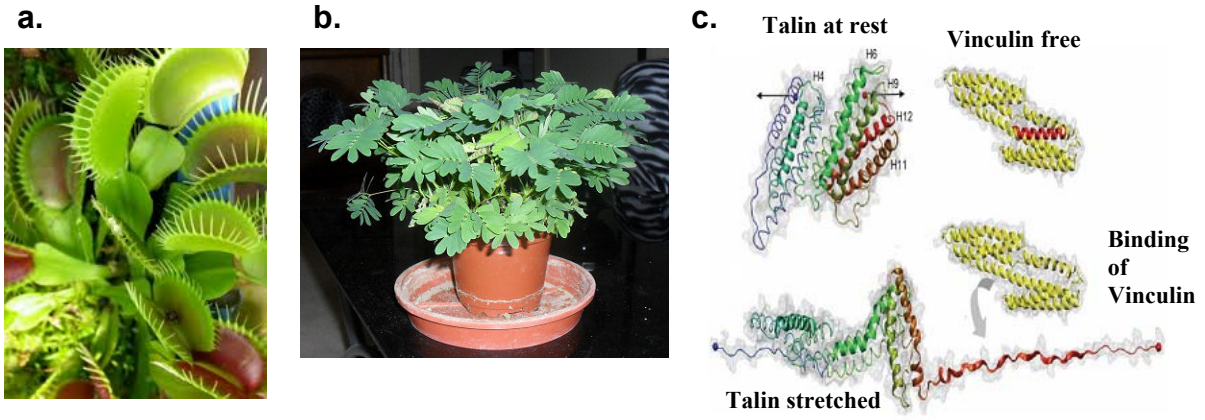

Figure 4.1: (**a**) The snap traps of this carnivorous plant, called *Dionaea muscipula*, close rapidly when the sensitive hairs on the leaf lobes are mechanically triggered[11]; (**b**) *Mimosa pudica* is mechanosensitive plant native from South America and Central America: its leaves fold inward and droops when touched or shaken, re-opening minutes later[12]; (**c**) Schematic representation of the talin unfolding when stretched, allowing the binding with vinculin ligand through the accessibility of a cryptic site.[10]

Inspired from this idea, our group developed recently several strategies based on multilayer films to design mechanoresponsive materials. Thus, it was introduced the first example of bio-inspired films becoming enzymatically active under stretching[13] and more recently cyto-mechanoresponsive.[14] In these both approaches, active compounds are embedded in a polyelectrolyte multilayer and a mechanical stretching of the architecture renders the compounds accessible to their environment. However, none of these alternatives allows designing **fully reversible systems**. Thus there is still a further stage to go and designing reversible chemo-mechanoresponsive materials remains a challenging project. To take up this challenge, herein I will describe our work concerning the design of cryptic site surfaces that reproduce closely the behavior of the cryptic site proteins. This concept is schematically represented in figure 4.2.

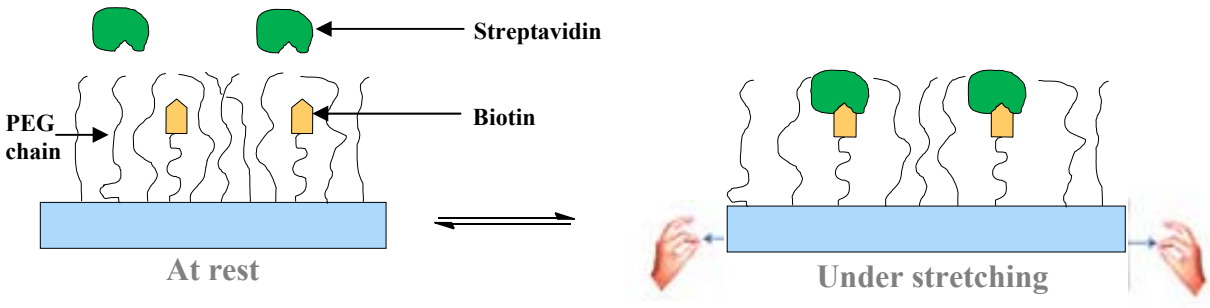

Figure 4.2: Schematic representation of the reversible cryptic site mechanoresponsive surface. At rest (left side), due to the high density of PEG chains grafted onto the substrate, the ligand (biotin) are not accessible to their receptor (Streptavidin). Under stretching (right side), the PEG chain density decreases, rendering the ligand (biotin) accessible.

Our goal is to design a material able to switch its ability to adsorb specifically a protein according to the level of stretching. Indeed, currently the control of protein adsorption on all kind of surfaces is an important issue in the field of biomaterial development since this interaction is involved in biocompatibility processes.[15-17] We used the Streptavidin-biotin system as model of couple ligand – receptor. To reach our goal, the surface of a selected elastomer will be modified with poly(ethylene oxide) (PEG) chains to get PEG brushes, rendering it antifouling. Despite the simultaneous presence of biotin groups on this surface, the Streptavidin should not interact with them. When this elastomeric material is stretched in a longitudinal direction, the density of PEG brushes decreases and then the protein can recognize its natural ligand. When return at rest, the PEG chains on the surface should

sterically push away the streptavidin from the biotin, leading to a reversible mechanoresponsible process.

In the first part of this chapter 4, I will present the different elastomeric silicone substrates chosen (Scheme 4.1). A long part is dedicated to the description of the PDMS Sylgard-184 which is the silicone substrate we entirely prepared and characterized (Part 4.2). Then, the oxydation of the silicone substrate, based on the UV-Ozone (UVO) treatment, will furnish hydroxyl groups on the surface (Part 4.3). Silanization with a mercaptosilane derivative on this so-prepared hydroxylated silicone substrate will lead to a thiol-coverage layer (Part 4.4). By using the thiol-ene click reaction between SH groups and maleimide moieties, PEG chains and biotin entities will be covalently grafted on the silicone. Finally, stretching experiments will constitute the last part of this chapter (Part 4.5).

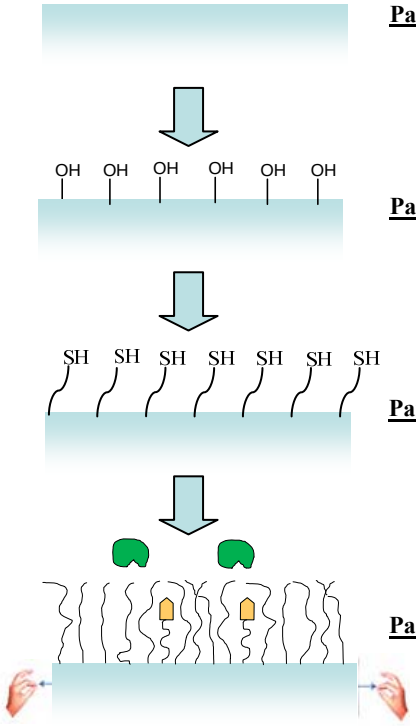

Scheme 4.1: Schematic representation of the different parts 4.2, 4.3, 4.4 and 4.5 constituting the plan of the chapter 4.

It must be noted that during my PhD work, a similar topic was developed by my group in collaboration with Dr Vincent Roucoules from the *Institut de Science des Matériaux de*

Mulhouse (IS2M). This project was running by using another strategy based on the use of polymer plasma technique.[18]

4.2 Choice of the elastomeric substrate: the PDMS

The choice of the substrate is of crucial importance for our project. It must fulfill the following conditions:

- To be transparent to UV and allow fluorescent measurements (no absorption in UV and no fluorescent emission).
- To be an elastomer (stretchable up to 100% at least).
- To be chemically modified on surface (allowing covalent grafting).
- Commercially available (and cheap also) or easy to prepare.

Thus, the PDMS, or also commonly called silicone, appeared as an ideal candidate. Several commercial sources of silicone sheets can be found. We decided to work with two kinds of silicone substrates: the commercially available silicone sheet from Specialty Manufacturing Inc. (SMI, Michigan, USA) and a home-made silicone Sylgard-184 prepared from starting compounds purchased from Dow Corning. The silicone sheet SMI is well known in my group because already used in other projects involving multilayer film buildup. It is a stretchable elastomer, displaying low auto-fluorescent and guaranteed filler free by the provider. It can be purchased in large amounts in an A4 format sheets, with a thickness of 250 µm. The silicone Sylgard-184 is a PDMS largely described in the literature and used as an elastomeric biomaterial.[19-21] We decided to prepare our own silicone to control the size of the resulting silicone sheet. In particular, the thickness of the silicone layer is important for fluorescence measurement and adaptability into our home-made stretching device. The stretching ability of the silicone sheet is also dependent of the thickness: thinner silicone sheets lead to higher stretching level. Furthermore, preparing our own silicone reduces the risk of adsorbed contamination on the surface. Smooth and defect free silicone surfaces can also be expected from the home-made silicone sheet.

In the next part of this chapter 4 is reported a short description of PDMS, its principle of synthesis and the preparation of the PDMS Sylgard-184.

4.2.1 The PDMS Sylgard-184: presentation, principle of synthesis and preparation

4.2.1.1 Introduction

Since their introduction in the 1960s, silicone rubbers have steadily gained market share from porcelain and glass as outdoor insulation and protective materials.[22] One of the most used silicone rubbers is PDMS, which are synthetic polymers containing repetitive units of Si-O in the principal chain and presents organic groups linked to the silicium atom by a Si-C bond (figure 4.3).[21]

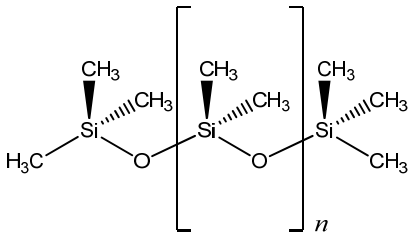

Figure 4.3: Chemical structure of a poly(dimethylsiloxane) chain: Si-O bonds ensure the backbone of the polymer and all the methylene groups are responsible of the strong and characteristic hydrophobic property of PDMS. *n* is the repeating unit.

There exists a variety of silicones, depending on the chemical structure, that can present linear molecules (fluids) or small macromolecular networks after reticulation (solids). In our case, the reticulated PDMS is of course the most interesting one.

4.2.1.2 Methods and mechanism of PDMS reticulation

In order to obtain a cross-linked elastomer based on poly(dimethylsiloxane), different methods can be used as for example γ irradiation, electron beam, ultra violet, polycondensation or hydrosilylation. In my project, we used the hydrosilylation reaction which consists in the addition of a hydrogen silane bond (Si-H) across an unsaturated double bond[23] (Scheme 4.2).

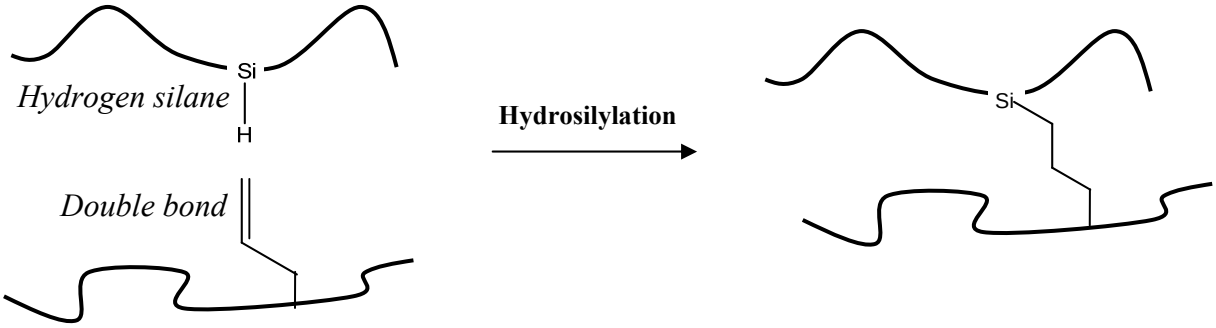

Scheme 4.2: General scheme of hydrosilylation reaction between hydrogen silane and unsaturated bond on two different PDMS chains. The product of this reaction leads to a new Si-C bond formation ensuring the cross-linkage between PDMS chains and the reticulation of the material.

This reaction is typically catalyzed by late transition metals such as rhodium (Rh), palladium (Pd) and platinum (Pt), the last one is an extremely active catalyst thus commonly used. The best known hydrosilylation catalyst is the Speier's catalyst which is a solution of hexachloroplatine acid (H_2PtCl_6) in isopropanol.[24] In the last years, another active catalyst have appeared in the literature, the Karstedt's catalyst which is a Pt(0) complex coordinated with divinyltetramethyldisiloxane (figure 4.4).[25] This catalyst is more reactive than the Speier one. Therefore we used it in the preparation of our PDMS substrate.

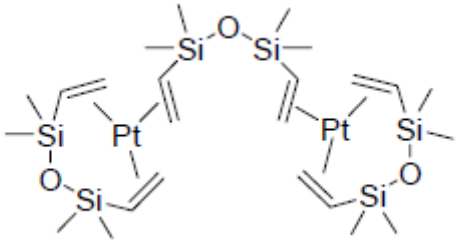

Figure 4.4: Molecular structure of the Karstedt's catalyst, based on Pt(0).

The catalytic mechanism of hydrosilylation involving the Karstedt's catalyst is commonly accepted and called the Chalk-Harrod mechanism.[26] This mechanism consists of catalytic cycles of oxidation addition and reductive elimination (figure 4.5)

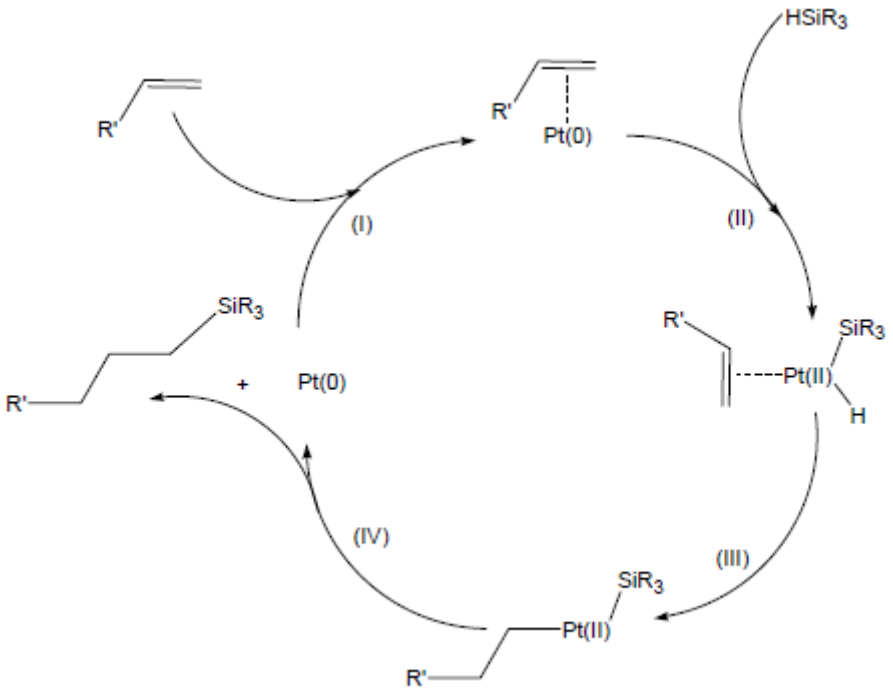

Figure 4.5: Chalk-Harrod mechanism for the catalytic cycle of hydrosilylation of olefins using the Karstedt's catalyst.

The first step of the catalytic cycle (step I in figure 4.5) is the coordination of the Pt(0) with the olefin followed by the oxidant addition of the $HSiR_3$ (step II) producing a Pt(II) complex. Then, the coordinated olefin in the complex migrates between the Pt-H bond (migratory insertion) (step III). The last step (step IV) is the reductive elimination with the generation of Pt(0) which can coordinate with another olefin and continue the catalytic cycle.

4.2.1.3 The PDMS Sylgard-184

In our experiments, PDMS were made by mixing a viscous *base* and *curing agent* of Sylgard-184 (see chapter 2 *Materials and Methods*). The *base* is a poly(dimethyl-methylvinylsiloxane) prepolymer containing also a small amount of platinum (Pt), the Karstedt's catalyst, and the *curing agent* is a mixture of vinyl-endcapped PDMS precursors and poly(dimethyl-hydrogenosiloxane) as cross-linkers[27] (figure 4.6a). Upon mixing together, the so-called curing process is started; the vinyl groups and the hydrosilane hydrogens undergo a hydrosilylation reaction in presence of Pt catalyst, which results in highly cross-linked three-dimensional networks.

a. **b.**

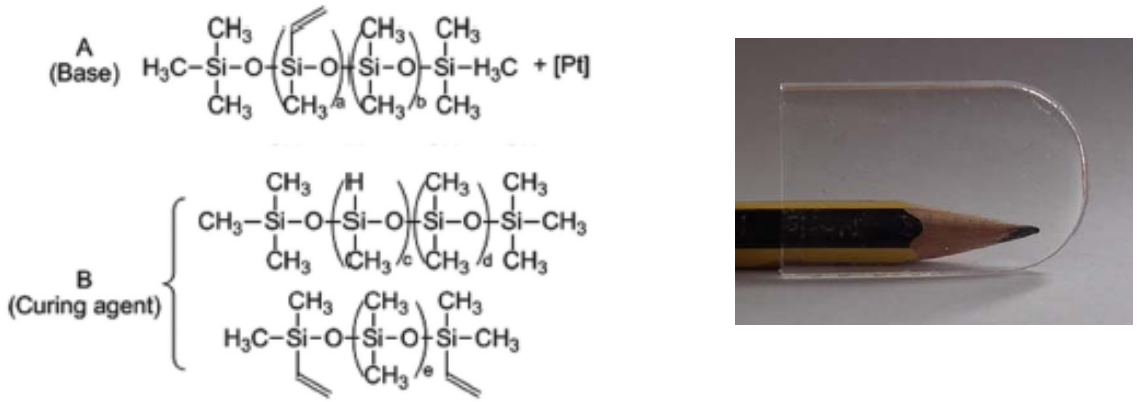

Figure 4.6: (**a**) Composition and chemical structure of the Base (A) and the Curing agent (B) purchased from Dow Corning; (**b**) Picture of a home-made thin subtrate of PDMS Sylgard-184.

Following this procedure, we were able to prepare silicone sheet having different sizes going from 6 x 2 cm^2 for the smaller size to 15 x 5 cm^2, according to the moulds used (figure 4.6b). The minimun thickness of film prepared was 1 mm. Then, the silicone may be cut out with a cutter to get the desired dimensions of substrate.

4.3 Chemical modification of the PDMS surface

There exist mainly three different kinds of methods to modify the PDMS surface. These are gas-phase processing, wet chemical methods and a combination of both.[28]

- Gas-phase processing methods include plasma oxidation, ultraviolet irradiation (UVO), chemical vapor deposition (CVD) and sputter coating of metal compounds.
- Wet chemical methods include layer-by-layer (LBL) deposition, sol-gel coatings, silanization, dynamic modification with surfactants and protein adsorption.
- Finally, the combination of gas-phase and wet chemical methods include silanization, LBL, graft polymerization methods on PDMS pretreated by methods such as UV or plasma oxidation.

The UVO equipment was readily available in our group, thus we chose to modify the PDMS surface by using this technique of irradiation. In comparison to plasma treatment, the UVO process is nearly an order of magnitude slower in terms of the time required to achieve

the same results.[29] However, one main advantage of UVO treatment methods is the better control of the oxidative process: formation of holes on the surface or cracks due to over-oxydation of silicone can be avoided by controlling the exposition time of UVO.[30] Another important benefit is the simple way to use the UVO device. There is no need to make vacuum or requirement of gas such as oxygen. All the oxidation treatments by UVO on silicone substrates were done in normal conditions (atmospheric pressure and room temperature).

4.3.1 Principle of the UVO oxidation process of silicone surface

UVO treatment is a photosensitized oxidation process in which the surface of the treated PDMS is excited and/or dissociated by the absorption of two short-wavelength UV radiations. Two distinct UV lamps equip the UVO device. Atomic oxygen is generated when molecular oxygen is dissociated by λ1 = 185 nm and in presence of molecular oxygen (O_2, coming from the air), the ozone molecule (O_3) is formed. A second UV wavelength of λ2 = 254 nm radiation creates radicals species by reaction with organic matter, such as the methyl groups in the case of the PDMS.[29] These radicals react with ozone to form simple oxidized and volatile molecules (such as carbon dioxide), which desorbs from the surface, leading mainly to silanol groups (figure 4.7).

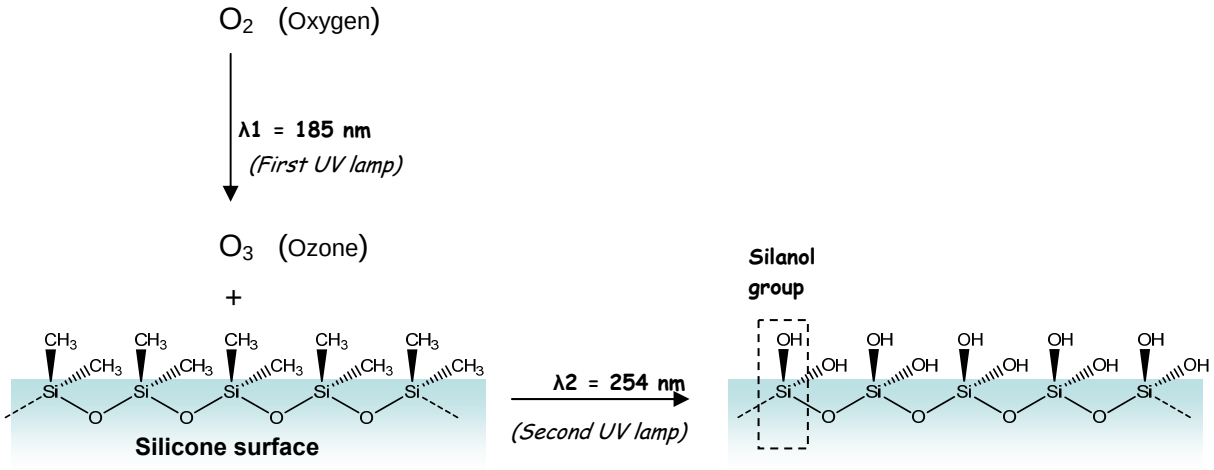

Figure 4.7: Schematic and simplified representation of the PDMS oxidation under UVO treatment: A first lamp emits at λ1 = 185 nm and induces the formation of ozone (O_3). Then, a second lamp (λ2 = 254 nm) forms radicals with methyl groups on the surface of silicone. Reaction between these radicals and O_3 lead to the formation of silanol groups responsible of the high hydrophilic features of the oxidized PDMS surface.

4.3.2 Results of the chemical modifications and characterization of the silicone surface

It must be noted that the data shown in the following part 4.3.2.1 relative to the characterization of oxidized PDMS surfaces are also presented in more detailed in chapter 6. Indeed, this strategy of PDMS modification was also efficiently used in another project of my PhD.

4.3.2.1 UVO oxidation of silicone SMI and PDMS Sylgard-184

As mentioned in the beginning of this chapter 4, two kinds of PDMS were used in our study, both fillers free: a first one was purchased from SMI, and a second one named PDMS Sylgard-184, prepared from starting precursors provided by Dow Corning. First of all, we studied the influence of the exposition time of PDMS under UVO on the formation of silanol groups and potentially presence of cracks. I remind here that this oxidation step of the silicone substrate will allow the next silanization step. Silanol groups formed through UVO treatment will change the initial hydrophobic surface of PDMS to hydrophilic. This was evaluated through contact angle measurement. In figures 4.8a and 4.8b are shown the evolution of contact angles of water on silicone sheets SMI and PDMS Sylgard-184 respectively according to the UVO exposition time.

The contact angle measurements have been done from the unexposed silicone sheets and every 15 minutes of UVO treatment, up to 120 minutes. Starting from highly hydrophobic surface of SMI and PDMS Sylgard-184, 98° and 107° respectively, we observe in both cases a roughly linear decrease of the contact angle up to 8-10° after two hours of UVO treatment (see also figure 4.8c). The surfaces become more and more hydrophilic with the increase of the exposition time of UVO.

It is well know that the hydrophilic feature of these PDMS surfaces are temporary: after an oxidation treatment, the surface recovers its hydrophobicity with time due to the migration of short and uncrosslinked PDMS chains from the bulk to the surface.[30-32] Therefore, the next FTIR-ATR measurements and the silanization step, described later in the part 4.4, were done immediately after this UVO treatment.

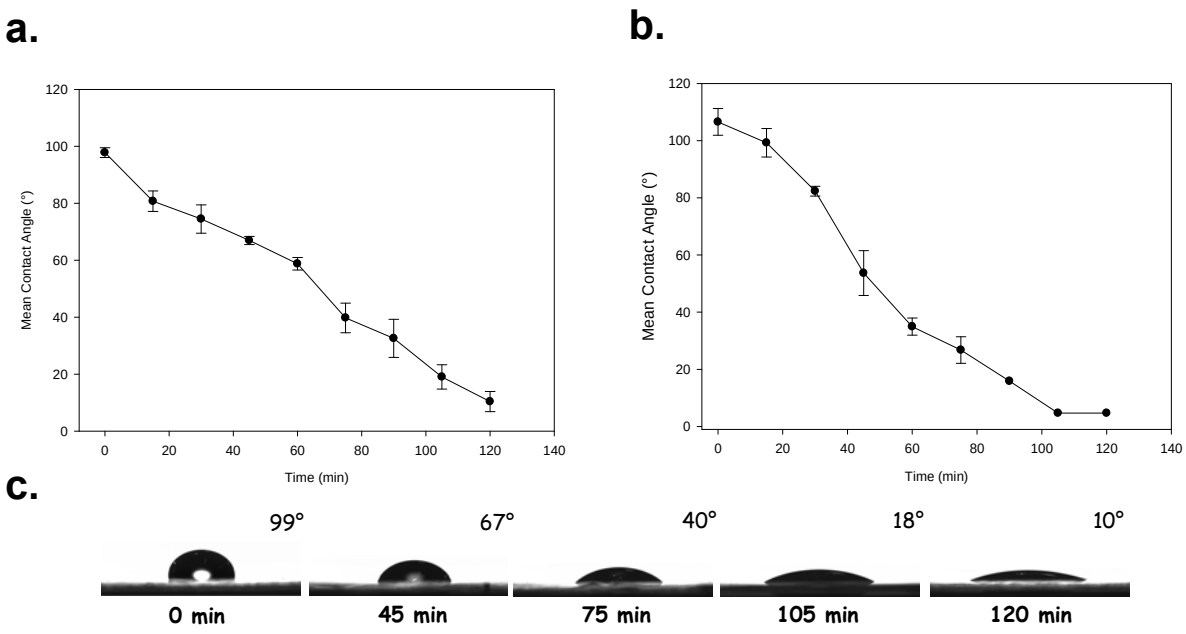

Figure 4.8: Evolution of the contact angle of water (**a**) on silicone SMI and (**b**) PDMS Sylgard-184 surfaces exposed to UVO treatment at different times up to 120 minutes. All the contact angle measurements have been done directly after UVO oxidation. Error bars correspond to at least three measurements realized on various areas of the silicone surface; (**c**) Images of water droplet on SMI untreated by UVO and treated during 45, 75, 105 and 120 minutes. The number on the top of each droplet indicates the contact angle measured.

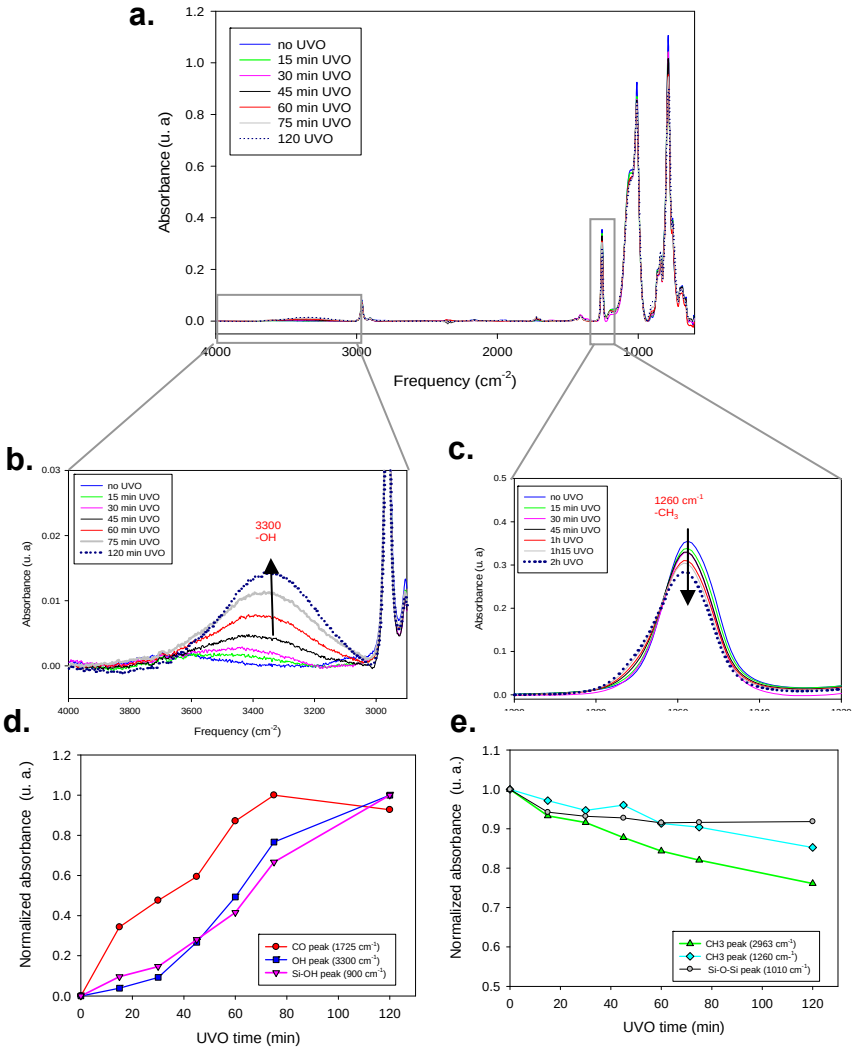

Figure 4.9: (**a**) Overlapping of the FTIR-ATR spectra of the silicon surface (SMI) at different times of UVO exposition; (**b**) Increasing of the band intensity localized at 3300 cm^{-1} with the UVO exposition time going from 0 to 120 min; (**c**) Decreasing of the band intensity localized at 1260 cm^{-1} with the UVO exposition time going from 0 to 120 min; (**d**) Evolution of the normalized IR vibration bands localized at 3300, 1725 and 900 cm^{-1}; (**e**) Evolution of the normalized vibration bands localized at 2963, 1260 and 1010 cm^{-1}.

The origin of this increasing hydrophilic feature with the exposition time of UVO can be explained by analysing FTIR-ATR spectrum of the treated silicone surface. A complete study about the UVO treatment on PDMS Sylgard-184 monitored by several techniques of analysis, in particular FTIR-ATR, has been reported by Genzer and collaborators.[29] In agreement with this previous work, the monitoring of the FTIR-ATR spectra at different time of UVO exposition show the formation of polar groups, such as hydroxyl and carbonyl

derivatives. In figures 4.9a, 4.9b and 4.9c is presented the overlapping of all the IR spectra measured on Silicone SMI at different exposition times of UVO: 15, 30, 45, 60, 75 and 120 minutes.

As expected, a large band at 3300 cm^{-1} is growing with the increasing exposition time of UVO (figure 4.9b). The evolution of the normalized absorbance of this band is represented in figure 4.9d. This vibration band is assigned to the stretching band of the OH bond, probably due to the formation of the silanol groups. In the same time, we can observe a decrease in the intensities of characteristic bands of the $–CH_3$ such as 1200 cm^{-1}, corresponding to the symmetric deformation band of the C-H bond (figure 4.9c), 2960 and 1010 cm^{-1} (see figure 4.9e) corresponding to the asymmetric CH_3 vibrations. In figure 4.9d is also shown the evolution of the normalized absorbance of bands at 1725 cm^{-1} and 900 cm^{-1}. These bands are attributed to a vibration of the carbonyl groups and to the stretching vibration of Si-O in silanol groups, respectively. Both of them display an increasing intensity of their band when the time of UVO exposition increases too, indicating the formation of hydroxyl, aldehyde or carboxylic groups during the reaction of oxidation. However, between 60 and 120 minutes of UVO exposition, the normalized absorbance band intensity at 1725 cm^{-1} decreases slightly, meaning that a small proportion of carbonyl groups disappear, probably because of CO or CO_2 compounds that desorb from silicone. Therefore, according to the results obtained by contact angle measurements and FT-IR studies, we can conclude that more the SMI silicone layer is exposed to UVO more the surface has a hydrophilic feature due to more hydroxyl group's formation. All these observations are similar to those reported by Genzer on the PDMS Sylgard-184.

Before proceeding to the silanization step, we stretched the oxidized silicone sheet (SMI and Sylgard-184) up to 100% of its initial length with a home-made stretching device (see chapter 2 *Material and Methods*). This level of stretching is considered as suitable to observe a mechanotransductive effect. The silicone is stretched in only one (longitudinal) direction and observed by scanning electron microscopy (SEM). Our goal is to detect the eventually silica-like layer formed during the UVO treatment: when this layer is stretched, cracks must appear on the silicone surface. It must be noted that in some cases, the observation of very large crack formation can also be done with an optical microscope.

a.

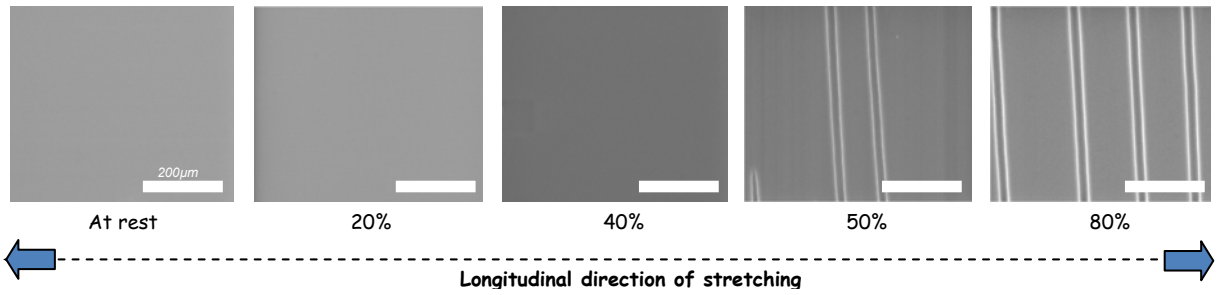

b.

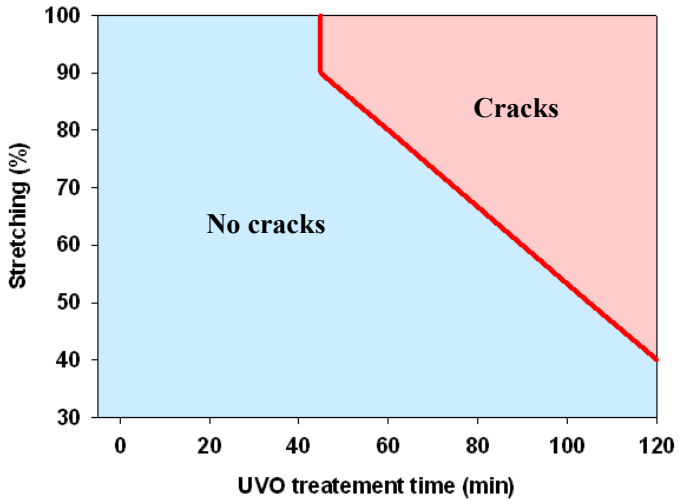

Figure 4.10: (**a**) Series of SEM images of silicone surfaces exposed to 105 minutes of UVO at rest and stretched at 20%, 40%, 50% and 80%. The white bar scale indicates 200µm; (**b**) Diagram showing the presence (red area) or absence (blue area) of cracks observed on silicone surface (SMI) exposed to a given UVO time and after stretching at a given level.

The use of SEM allows discerning the cracks at the microscopic size. We analysed several SEM images (1 x 1 mm^2) of silicone sheets exposed to various UVO treatment times up to 120 minutes. A series of SEM images of silicone sheets exposed to UVO during 120 minutes and stretched at 20%, 40%, 50% 80% is shown as a characteristic example in figure 4.10a. In this case, appearance of cracks occurred after 50% of stretching. Stretching up to 50% of the initial length of the silicone sheet leads to more cracks formation, as expected. We did not stretch more than 100% because it happened sometimes that at this level of stretching, the silicone break into two pieces. Gathering all our observations did by SEM on silicone exposed at different times of UVO, we established the diagram shown in figure 4.10b. Two

distinct areas in the diagram appear clearly: a blue one where no cracks can be observed by SEM for a given UVO time and after a given stretching level, and a pink one where crack formation occurs. These two areas are separated by almost a straight red line. Under 50 minutes of UVO, we did not observe any cracks on exposed silicone after stretching up to 100%. Over 50 minutes of UVO, the more the exposition time is important, the more cracks are observed at lower level of stretching. This means that formation of the silica-like layer is mainly formed from this time limit of 50 minutes. It must be noted that three successive stretching at a given levels do not change the result observed on the SEM images after only one stretching. Furthermore, in our case, the UVO process was independent of the origin of the silicone sheet used because we obtained exactly the same diagram (figure 4.10b) with the PDMS Sylgard-184 than with the silicone SMI.

4.4 Silanization step: introduction of thiol groups onto oxidized silicone surface

Surface silanization can be performed on various substrates provided they can contain surface hydroxyl groups which will react with alkoxysilanes to form covalently siloxane bonds to the underlying substrate.[28] By using the commercially available 3-mercaptopropyltrimethoxysilane (MPS), thiol groups can be introduced onto the oxidized silicone surfaces (figure 4.11) described above.

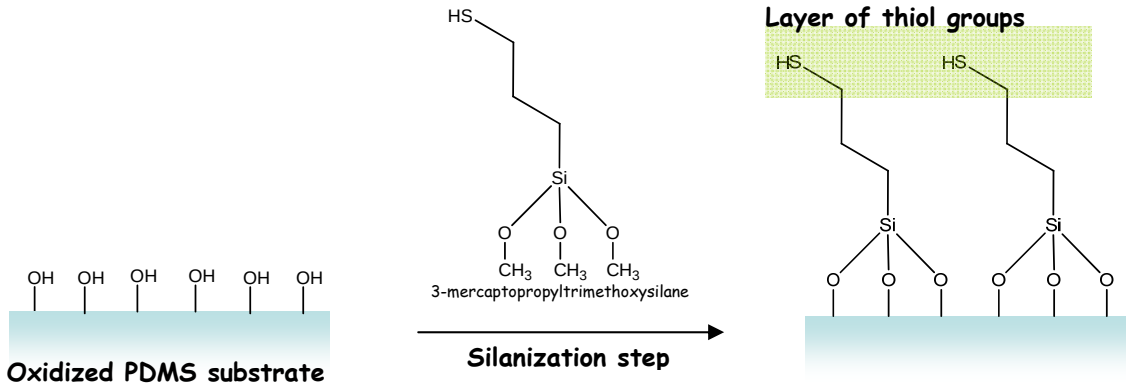

Figure 4.11: Schematic representation of the silanization step from the oxidized PDMS sheet. The use of 3-mercaptopropyltrimethoxysilane compound allows the introduction of a layer of thiol groups onto the surface.

These thiol groups are interesting chemical function that can react rapidly with double bonds at room temperature and without secondary products formation.[33] This reaction is

considered as “click reaction” and has been used to introduced PEG chains and biotin groups on silanized silicone surface, as described later in part 4.5.

4.4.1 Chemical modification process and characterization of the PDMS surface with thiols groups

Immediately after the activation of the 18 x 18 mm^2 PDMS surfaces (SMI or PDMS Sylgard-184) with 90 minutes of UVO, the sample was brought in contact with methanolic solution containing 1 % v/v of 3-mercaptopropyltrimethoxysilane and stirred gently overnight at room temperature. Then, the silicone sheet was washed three times with methanol during 1 hour under stirring, changing the solvent every 15 minutes and then kept in methanolic solution. These conditions, described in more details in chapter 2 *Material and Methods*, have been optimized to get a surface of silicone still transparent and not rough, according to visualization through optical microscopy.

Contact angle and FTIR measurements were carried out to characterize the modified PDMS surface with thiol groups.

A contact angle of 78° ± 8° has been measured after the silanization step. This high value can be explained by the disappearance of hydroxyl groups and the presence of propyle chains bearing the thiol group on the silane derivative used. This value is in agreement with the ones reported in literature on PDMS.[34]

The transmission FTIR-ATR spectrum of the silanized PDMS surfaces show the disappearance of the Si-OH vibrationnal peak between 3700 and 3100 cm^{-1} (figure 4.12). This first observation indicates the successful covalent linkage of the trimethoxy functional group of the MPS to both SMI and Sylgard-184. Furthermore, a characteristic vibrationnal band is observed at 2850 cm^{-1}. This band is not present in the FTIR-ATR spectra of the UVO treated silicone surface, and is assigned to symmetric stretch of the bond CH_2-SH. Thus, we considered that there is no ambiguity about the coverage of thiol groups on the PDMS surface, coming from the covalent grafting of MPS.

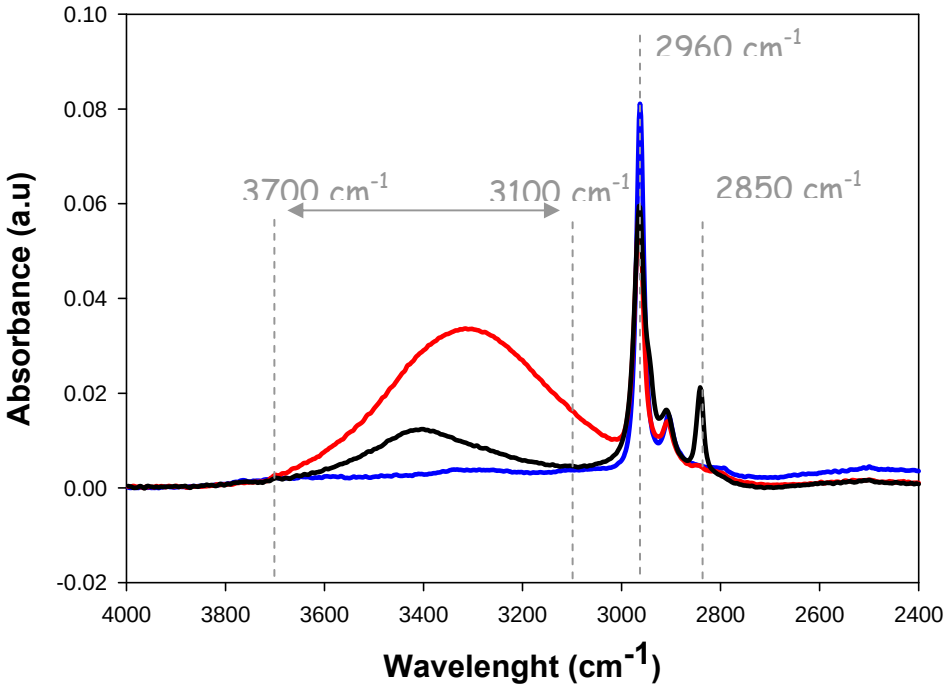

Figure 4.12: Transmission FTIR-ATR spectra of an unmodified PDMS Sylgard-184 (blue line), modified PDMS after 90 minutes of UVO treatment (red line) and after the thiol silanization step (black line).

No significant differences between the silanization of PDMS Sylgard-184 and SMI were observed by FTIR-ATR study. In the next part of this chapter 4, all experiments described were done on silicone SMI, except when mentioned.

4.5 Grafting of biotine groups and PEG brushes on PDMS surfaces

As described in the introduction of this chapter, the presence of thiol-covered surfaces allows using the covalent coupling reaction with maleimide derivatives: this reaction was chosen because of its simplicity and efficiency to occur and also because of the commercial availability of compounds such as PEG-Mal and Biotin-Mal derivatives (figure 4.13). Different molecular weights of PEG-Mal were used in this project: 2000, 5000 and 10 000 Dalton corresponding to a number of ethylene oxide groups of 50, 125 and 250 units. The maleimide function is linked to the biotin group through a short ethylene oxide spacer composed of two units. This molecule is denoted as Biotin-Mal.

The thiol-ene click reaction corresponds to a Michael addition of the sulfur atom on the 1,4-conjugated system of the maleimide group. The resulting product is formed in an irreversible way.

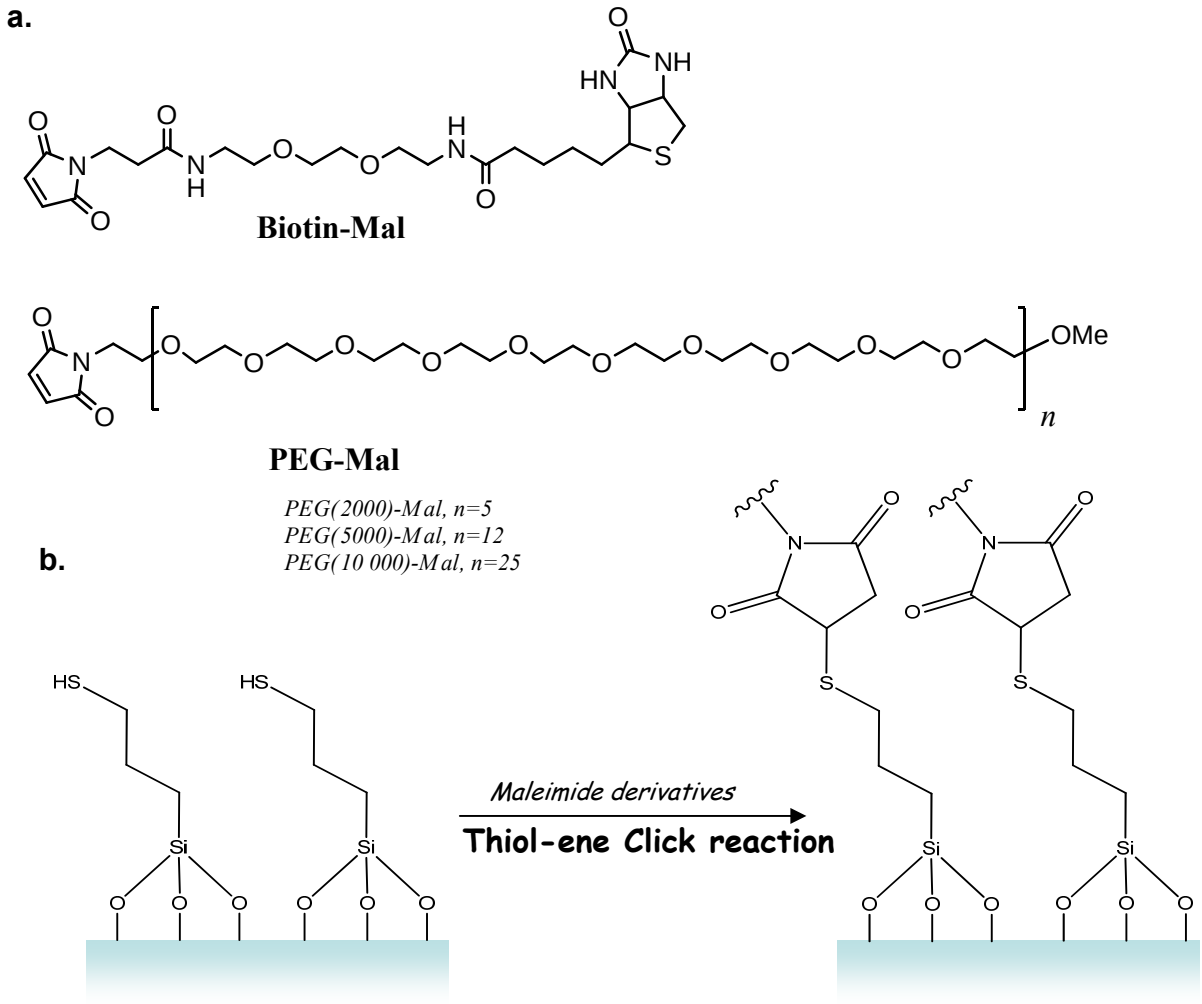

Figure 4.13: (**a**) Chemical structure of PEG-Mal derivatives (PEG2000, PEG5000 and PEG10 000) and Biotin-Mal; (**b**) Thiol-ene reaction between the thiol groups on silicone surface and free maleimide derivatives in solution.

4.5.1 Covalent grafting of Biotin groups on silanized PDMS surfaces

First of all, we grafted the Biotin-Mal compounds onto the silanized PDMS surface. Our goal in this step was to check the validity of our grafting conditions. For the rest of this chapter, before all experiment series, we will shortly describe the experimental procedure used to modify the silicone substrate, to adsorb the Streptavidin^{FITC} and the fluorescent measurement set-up when necessary. Indeed, these conditions changed sometimes according to the experiments.

4.5.1.1 Experimental procedure

After UVO treatment during 90 minutes and further modification of the surface with thiol groups the substrates were treated with a 5 mM TCEP solution prepared in PBS buffer at pH 7.4 for 30 min to break the possible disulfide bridges.[35] After that, the samples were washed three times with PBS buffer. Quickly, solutions of 0.1 mg/mL, 0.6 mg/mL and 1.5 mg/mL of Biotin-Mal prepared in PBS buffer at pH 7.4 were added on the modified surface leaving the reaction between the thiol and maleimide groups to occur overnight at room temperature. The samples were then rinsed three times with PBS buffer and stocked in the same buffer until use.

4.5.1.2 Protein adsorption

The sample was then carefully placed on a homemade electric stretching device (see chapter 2 *Materials and Methods*) and adapted to a fluorescence microscope. Their edges were protected with a PDMS STATIS before they were tight on the stretching support. A 0.1 mg/mL Streptavidin^{FITC} solution prepared in TRIS buffer at pH 7.4 was added on the sample's surface for 10 min. Then, it was rinsed three times with TRIS buffer followed by the fluorescence measurements.

4.5.1.3 Fluorescence measurements

The experiments were carried out using an inverted light microscope (Nikon Microphot-FXA, Japan) equipped with a mercury lamp and operating between 470 nm and 490 nm for excitation and above 500 nm for detection. The measurements were done using a ×10 dry objective and a digital camera with 20 s times of exposure under a hydrated state.

Before bringing Biotin-Mal in contact with the modified silicone, this last one was treated with a reductive agent, the tris(2-carboxyethyl)phosphine hydrochloride (TCEP), to reduce the disulfure bonds that may have been formed in contact with air. We tested three different concentrations of Biotin-Mal in buffer (PBS buffer at pH 7.4) 0.1, 0.6 and 1.5 mg/mL, to determine the optimum grafting conditions. The efficiency of this grafting was evaluated by using Streptavidin^{FITC}, the natural protein-receptor of the biotin ligand, and the fluorescence emission on the silicone was measured with a fluorescent microscope. Without contact with the Streptavidin^{FITC}, a residual fluorescence was measured, mainly due to the slight light present in the room and also because of auto-fluorescence of the silicone. This value has always been measured before all our emission fluorescence experiments. In figure 4.14 are shown two typical images of silicone sheets with and without contact with Streptavidin^{FITC}. When excited with UV, the surface of biotinylated silicone that was in contact with the labeled Streptavidin appears green. We observed a non-homogeneous distribution of the fluorescence all over the silicon surface probably due to irregularities coming from the native silicone. The quantification of the fluorescence level was done by using the software ImageJ® with a size of images 800 x 600 µm^2. The results obtained with the three solutions of Biotin-Mal are gathered in figure 4.15.

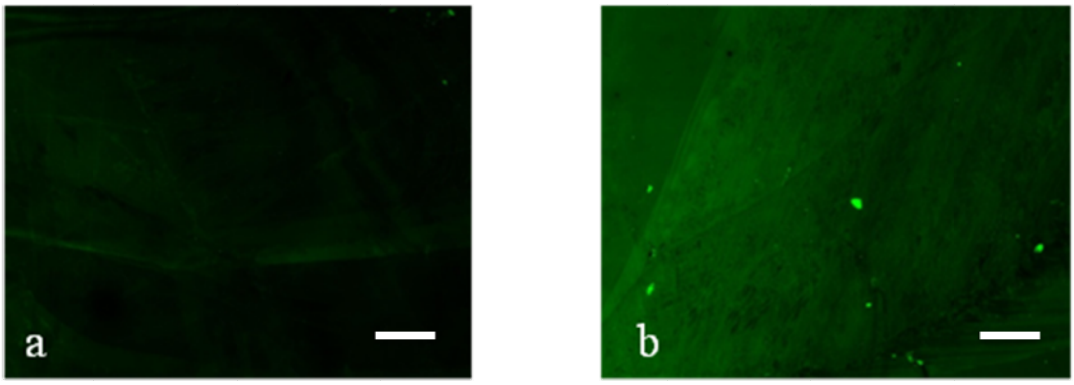

Figure 4.14: Fluorescence images of SMI silicone surface before contact with Streptavidin^{FITC} solution (**a**) and after contact with 1.5 mg/mL of Biotin-Mal (**b**). Bar scale equals to 100 µm.

In all experiments presented in figure 4.15, the residual emission of fluorescence was measured before contact with Streptavidin^{FITC}. This residual fluorescence emission is almost constant in all measurements and represents the black bars in the histogram. We can observe that a small non-specific adsorption of Streptavidin^{FITC} occurs on unmodified silicone, and also on silicone after silanization with the thiol derivative. An increase of this adsorption is

measured when the silicon surface has been treated with Biotin-Mal solutions: higher concentrations of Biotin-Mal lead to higher adsorption of Streptavidin^{FITC}. This corresponds to an increase of the grafted biotin density leading to a higher amount of Streptavidin anchored on the surface. However, between 0.6 and 1.5 mg/mL of Biotin-Mal, the increase of Streptavidin^{FITC} adsorption is not really important: 1350 and 1420 a.u. respectively. One can assume that we have reached almost the maximum grafting level of biotin groups onto the surface, in our conditions. **Thus, the concentration of 1.5 mg/mL of Biotin-Mal will be kept for the rest of this chapter 4**.

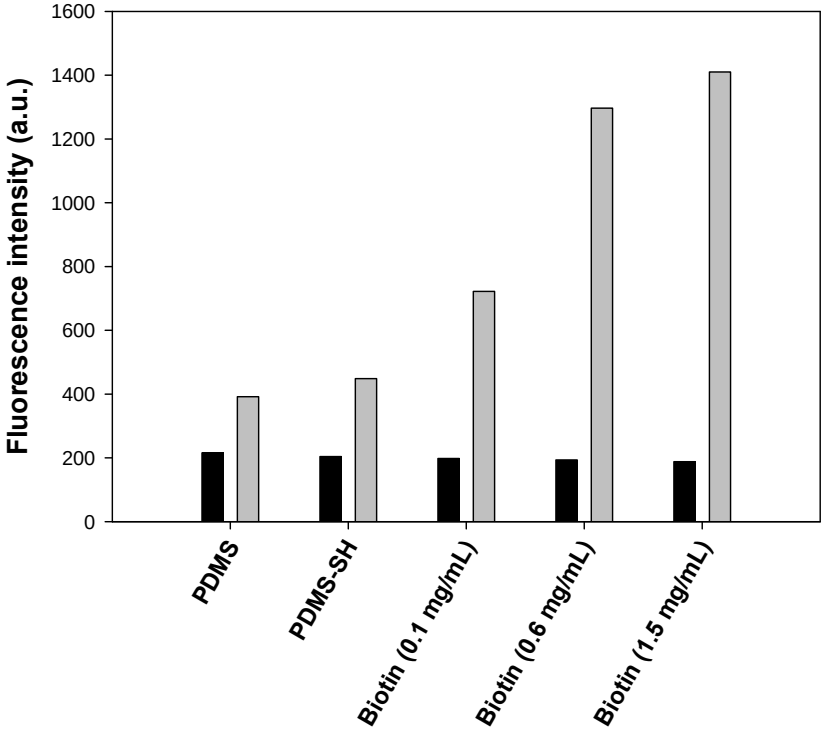

Figure 4.15: Fluorescence emission intensities measured on silicone surfaces when exposed to UV between 470 nm and 490 nm. Black bars correspond to values measured before contact with Streptavidin^{FITC} (auto-fluorescence), and the grey bars correspond to fluorescence after contact with the Streptavidin^{FITC}.

4.5.2 Effect of stretching and irreversibility of the Streptavidin anchored

Our goal is to develop substrates that become reactive to Streptavidin under stretching. We prepared a silicone surface functionalized with biotin from a 1.5 mg/mL Biotin-Mal solution as just described. This surface was brought in contact with Streptavidin^{FITC} before rinsing with 10 mM TRIS buffer solution. The fluorescence was then measured. The substrate was then stretched from 0% up to a stretching degree of 50% by stretching steps of 10%. No

Streptavidin^{FITC} was added. Figure 4.16 shows the evolution of the measured fluorescence as a function of the stretching degree. One observes a strong increase of the fluorescence after addition of Streptavidin^{FITC} as already described. The fact that one does not reach the same level of signal as in figure 4.15 may be due to the different amplification factor of the camera during use. One can assume, in first approximation, that the fluorescence intensity decreases linearly with the stretching degree, reaching a decrease of 25% for a stretching degree of 50%. This effect can be attributed to a change of the fluorophore density with the stretching degree. This "dilution" effect has to be taken into account when analyzing our results.

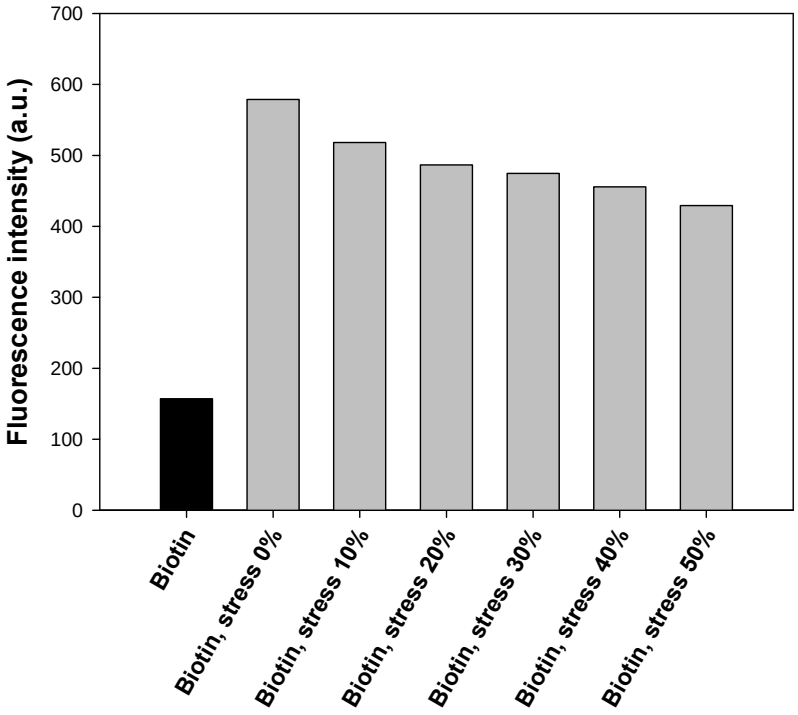

Figure 4.16: Evolution of the fluorescence intensity as a function of the stretching degree measured on a sample functionalized with biotin groups and brought at rest in contact with Streptavidin^{FITC}. The sample is then stretched at different stretching degrees. The black bar represents the fluorescence intensity measured on the biotinilated sample before contact with Streptavidin^{FITC}.

Next we wanted to verify the irreversibility of the biotin/Streptavidin interaction during stretching/unstretching cycles. Indeed, this ligand/receptor interaction is known to be one of the strongest non-covalent interactions in biology.[36] We thus used a biotinylated substrate prepared in the same conditions as just described. We brought this substrate in contact with the Streptavidin^{FITC} solution for 10 minutes, rinsed the substrate with TRIS

buffer. We then measured the fluorescence intensity of the substrate during the different steps of 4 stretching/unstretching cycles. The results are summarized in figure 4.17.

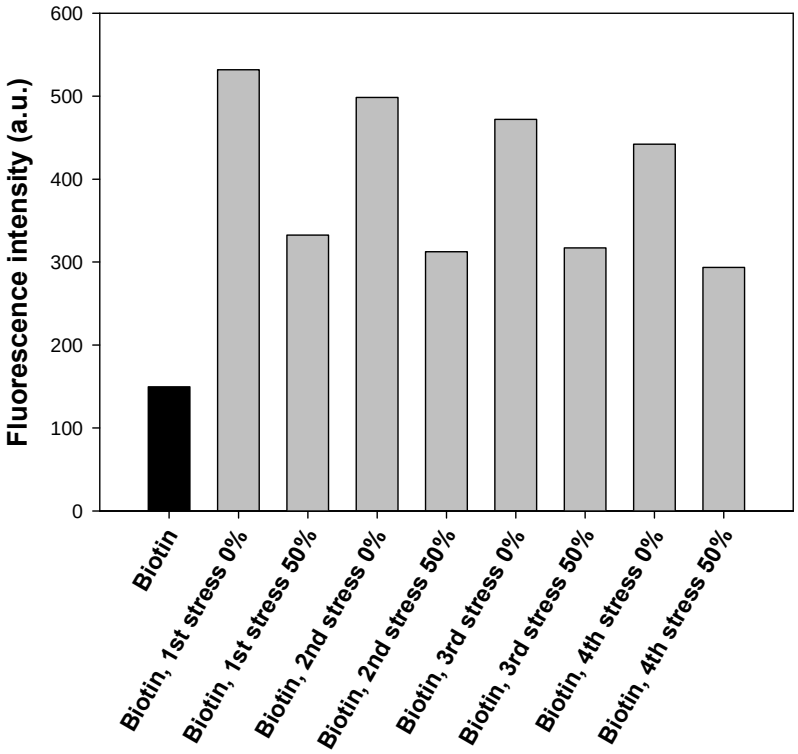

Figure 4.17: Evolution of the fluorescence intensity of a silicone substrate covered with biotin and brought initially, at rest, in contact with a Streptavidin^{FITC} solution. Four stretching/unstretching cycles are performed during this experiment. The black bar corresponds to the fluorescence of the substrate at rest before contact with the Streptavidin^{FITC} solution.

After the initial contact of the substrate with the Streptavidin^{FITC} solution, followed by a rinsing with buffer, the surface did no more come in contact with the fluorescent protein. The fluorescence of the substrate must thus decrease or remain constant. One observes that each stretching at 50% of the substrate is accompanied by a significant decrease of the order of 35% of the fluorescence intensity. This decrease is partly due to a decrease of the Streptavidin^{FITC} density over the substrate. Yet, it cannot be entirely attributed to this effect. Indeed, we have seen that density changes can account for a decrease of 25% of the fluorescence. The remaining 10% could originate from some desorption of Streptavidin from the surface during stretching. Such a desorption could be due to the fact that despite a decrease of the streptavidin density, stretching is accompanied by a shrinking in the direction perpendicular to the stretching direction. This effect may induce lateral interactions between

Streptavidin molecules which could eventually lead to some desorption. This interpretation is corroborated by a small decrease of the fluorescence intensity after returning to the non-stretched state when compared to the fluorescence intensity measured in the first non-stretched state. A similar effect is observed during the next stretching/unstretching cycles. Another interpretation of the continuous decrease of the fluorescence intensity observed in the non-stretched states during consecutive stretching/unstretching cycles and also of the higher decrease of the fluorescence during stretching when compared to that expected from simple Streptavidin dilution, might be some bleaching. Indeed, each experiment necessitates the sample to be irradiated so that some bleaching always exists.

One can thus conclude that the biotin/Streptavidin interactions are extremely strong even on our substrates and that if desorption occurs during stretching/unstretching cycles due to lateral Streptavidin interaction, it must be small. By stretching the substrate to 50%, if the biotin/Streptavidin interaction is irreversible, one can expect a decrease of the fluorescence of the order of 25-30%.

4.5.3 Simultaneous grafting of PEG2000 chains and biotin groups on the substrate

To reach the goal of our project, we must anchor biotin groups covalently onto the silicone surface but also graft a suitable density of PEG chains to get PEG brushes that hide the biotin groups and thus render the surface antifouling at rest. The biotin groups should become accessible when this density of PEG chains is decreased by stretching the substrate.

We first decided to modify the silicone surface with the simultaneous presence of Biotin-Mal and PEG-Mal in solution. We first chose PEG-Mal of 2000 Da as molecular weight, the concentration of Biotin-Mal was kept equal to 1.5 mg/mL. We chose this molecular weight because preliminary results of the group of Vincent Roucoules from Mulhouse working on a similar issue but with another grafting method of the PEG found that, in their case, PEG 2000 was optimal.[37] Various concentrations of PEG-Mal were investigated: 60 mg/mL, 120 mg/mL and 180 mg/mL. These solutions were prepared in PBS buffer at pH 7.4 and then added onto the silanized PDMS surface in the unstretched state. The experimental procedure for the substrate functionalization, the interaction of the substrate with Streptavidin^{FITC} and the following fluorescence measurements were performed in a similar way as described for entirely biotinylated substrates besides the replacement of the Biotin-MAL solution by mixed solutions of 1.5 mg/mL Biotin-Mal + 60 mg/mL PEG(2000)-

Mal, 1.5 mg/mL Biotin-Mal + 120 mg/mL PEG(2000)-Mal or 1.5 mg/mL Biotin-Mal + 180 mg/mL PEG(2000)-Mal prepared in PBS buffer at pH 7.4.

Substrate fluorescence intensities have been measured at rest and at a stretching degree of 50%. Furthermore, we measured the fluorescence intensities before and after contact with Streptavidin^{FITC}. All results are gathered in figure 4.18.

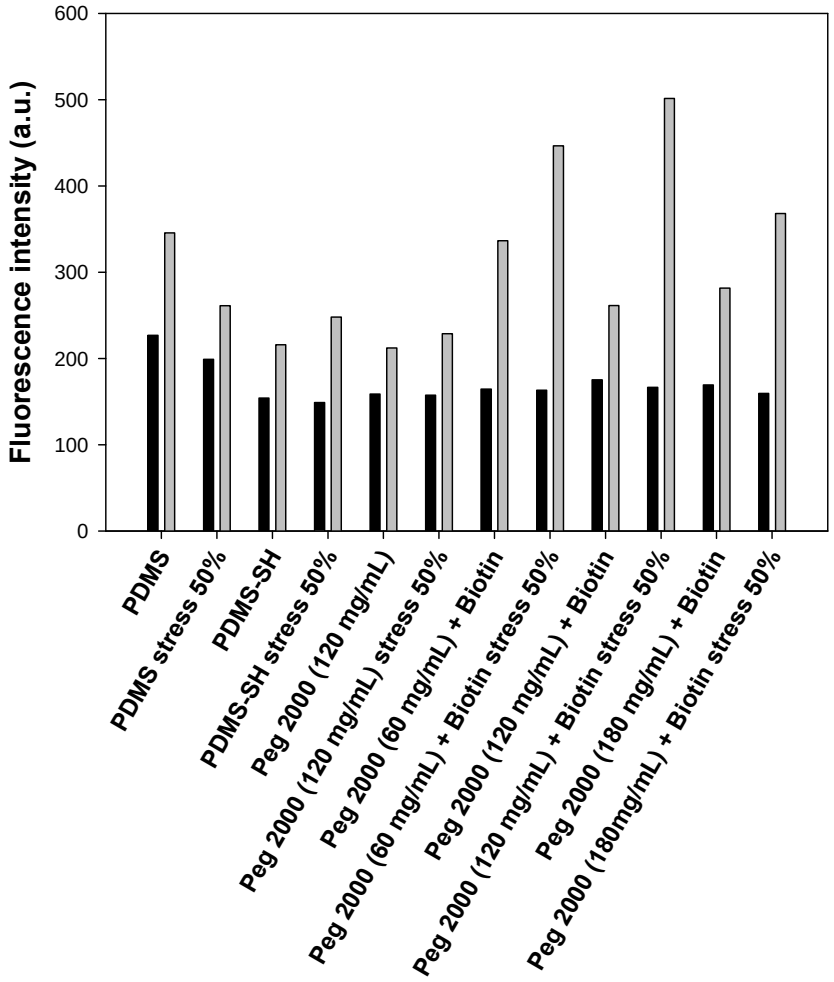

Figure 4.18: Fluorescence intensities of treated silicone surfaces (SMI) with (grey bars) or without (black bars) treatment with Streptavidin^{FITC}, at rest or at a stretching degree of 50%. For one kind of experiment set, two different silicone sheets were used (at rest and when stretched at 50%).

Each pair of reported values in figure 4.18 corresponds to an independent experiment. The black bars represent the fluorescence of the substrate before being in contact with Streptavidin^{FITC} (auto-fluorescence). One observes that the auto-fluorescence of treated PDMS is almost independent of the performed treatment and is, in our case, of the order of 150 a.u. It represents a significant part of the measured intensity and must thus be taken into

account for the interpretation of the data. The unmodified PDMS shows a significant adsorption of Streptavidin^{FITC} at rest: a fluorescence intensity value of 345 a.u. (arbitrary unit) is measured, compared to the residual fluorescence measured at 226 a.u. Next we brought the functionalized PDMS with thiol groups (SH) in contact with Streptavidin^{FITC}. The silanized PDMS surface seems more antifouling than the unmodified PDMS with a very low level of fluorescence measured (215 a.u.) at rest and a slight increase when stretched (247 a.u.). Almost the same amount of Streptavidin is adsorbed on the PDMS treated with 120 mg/mL of PEG(2000)-Mal. It is important to note that when the pegylated surface of PDMS is stretched, no additional unspecific adsorption of Streptavidin^{FITC} occurs. Next we modified the silanized PDMS with the simultaneous presence of Biotin-Mal (1.5 mg/mL) and PEG(2000)-Mal in solution at different PEG concentrations: 60 mg/mL, 120 mg/mL and 180 mg/mL. In all cases, at rest, one observes a higher fluorescence after contact with Streptavidin^{FITC} than for the biotin free substrate. This shows that none of our surface totally hinders the Streptavidin to access the biotin through the PEG layer. The smallest Streptavidin adsorption is obtained when the surface is functionalized with a 120mg/mL PEG solution. In this case the fluorescence increase corresponding to specific Streptavidin^{FITC} interaction with biotin represents of the order of 50% of the non-specific adsorption. When these substrates where stretched at 50% and brought in contact with Streptavidin^{FITC} one always observes a strong increase of the fluorescence intensity. This clearly shows that new biotin groups become accessible to Streptavidin. These surfaces thus act as cryptic site surfaces by exhibiting ligands under stretching. The optimal cryptic site surface is obtained from the 120mg/mL PEG solution. In this case the Streptavidin interaction is reduced at rest and maximum under stretching.

Next we wanted to investigate the reversibility of our system during stretching/unstretching cycles. We prepared a system in the optimal conditions reported above. After bringing the system stretched at 50% in contact with a Streptavidin^{FITC} solution and rinsing, we performed two stretching/unstretching cycles, measured the fluorescence intensity at each step without never bringing the substrate in contact with Streptavidin^{FITC} again. The results are summarized in figure 4.19.

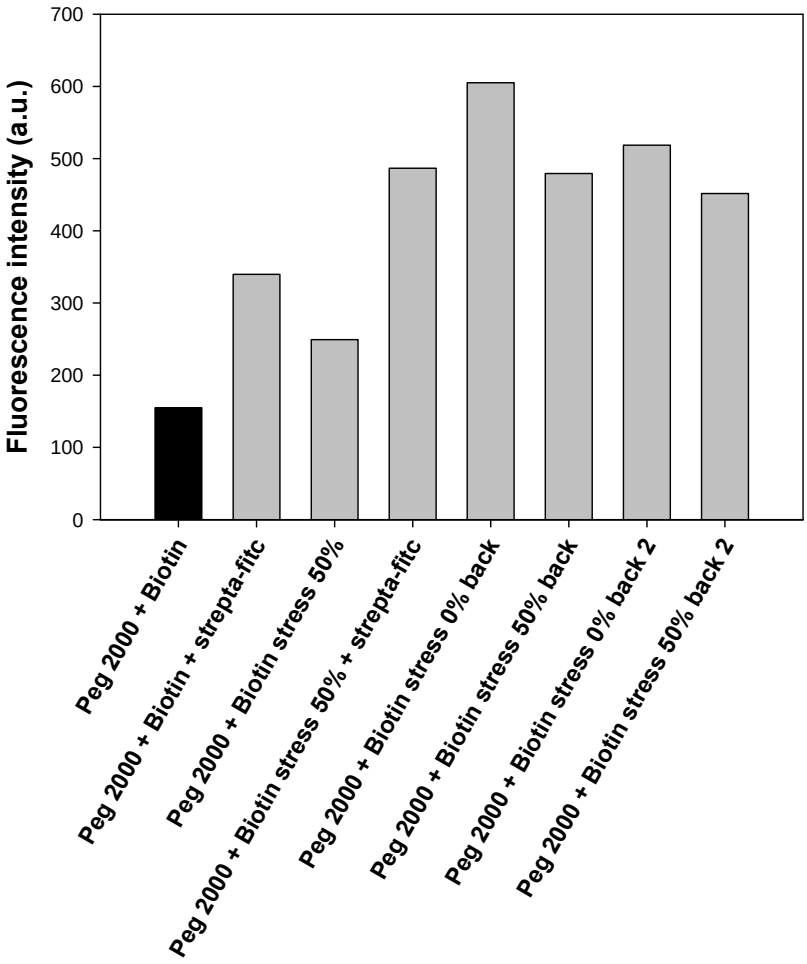

Figure 4.19: Evolution of the fluorescence intensity at the different steps of two stretching/unstretching cycles of the system biotin-streptavidin when biotin is embedded within a PEG 2000 brush. Sample in contact with streptavidin (gray bars) and without streptavidin (black bars). Streptavidin was added two times, first in the unstretched state and then after stretching the substrate for the first time at 50%.

One observes an increase of the fluorescence during each return from the stretched to the non-stretched state. This increase is smaller than the 25% expected due to the density change consecutive to a change of the substrate area accompanying the return to the non-stretched state. This shows that there must be a small desorption of Streptavidin during this return to the non-stretched state but this desorption must be small. **The system appears essentially as irreversible**: once Streptavidin has interacted with biotin, the interaction cannot be removed through a return to the non-stretched state. This result is confirmed in the second stretching/unstretching cycle.

4.5.4 Different attempts to increase the density of grafted PEG chains

The substrate obtained with the optimal grafting conditions were neither totally Streptavidin repulsive at rest nor was the interaction with Streptavidin reversible with respect to stretching/unstretching cycles. This can be attributed to a too small PEG density grafted on the substrate. We thus tried to increase the density of PEG chains. To do that we investigated two ways. First, we realized the entire chemical functionalization of the silicone surface under stretching at 60%. Another strategy investigated was to use longer PEG chains instead of PEG(2000)-Mal.

4.5.4.1 Covalent grafting of PEG chains and biotin groups on stretched silicone

In the literature, Genzer et al. have reported that the chemical functionalization of silicone sheets can lead to higher active group densities when the silicone sheet is functionalized under stretching instead in the non-stretched state.[38] Thus, we thought to oxidize, to silanize and to let react the PEG(2000)-Mal chains and the Biotin-Mal on a silicone stretched at 60% of its initial length. The coupling reaction onto the silicone substrate was done with 1.5 mg/mL of Biotin-Mal and 120 mg/mL of PEG(2000)-Mal simultaneously present in solution. The experimental procedure was similar to that reported above. Figure 4.20 compares the fluorescence intensities measured on substrates functionalized at 60% of stretching with regularly functionalized (non-stretched state) substrates. Functionalization at a stretching degree of 60% seems to increase the Streptavidin interaction of the surface at rest. **This procedure does thus not improve the anti-fouling character of our system at rest and was thus not retained.** We nevertheless verified the reversibility of the biotin/Streptavidin interaction on this system by performing a stretching/unstretching cycle. The results are given in figure 4.21. As previously, one observes that once the interaction took place at 50% of stretching between biotin and Streptavidin, no significant reduction of the fluorescence is observed during retraction and stretching again. This shows that in this case too, the interaction is irreversible.

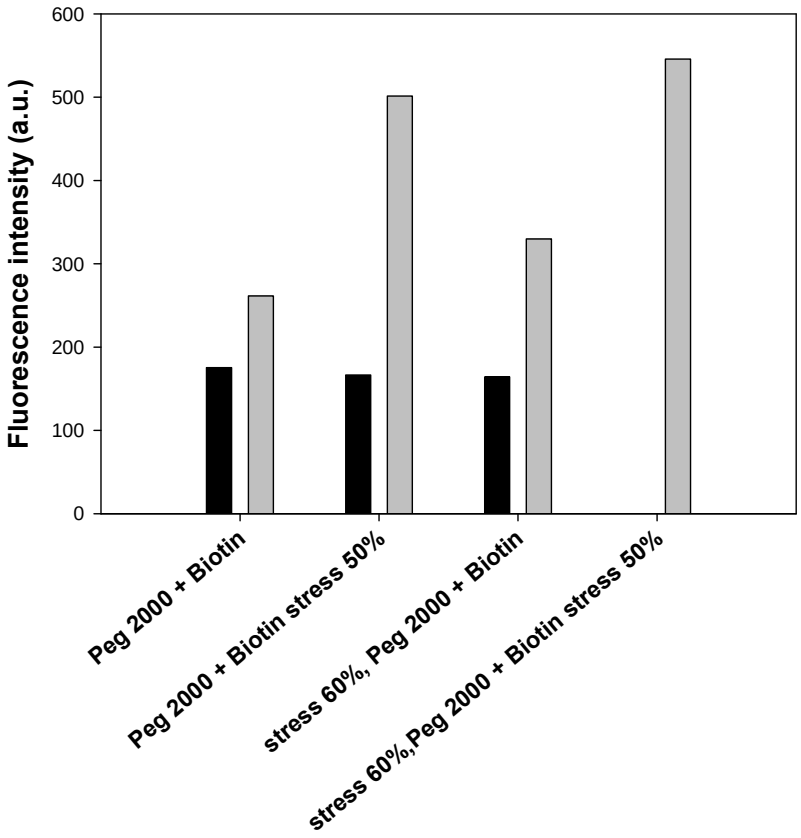

Figure 4.20: Comparison of the fluorescence intensities after contact with Streptavidin^{FITC} of silicone sheets functionalized at rest and stretched at 60%. Black bars correspond to the fluorescence measured before contact with Streptavidin^{FITC} (auto-fluorescence).

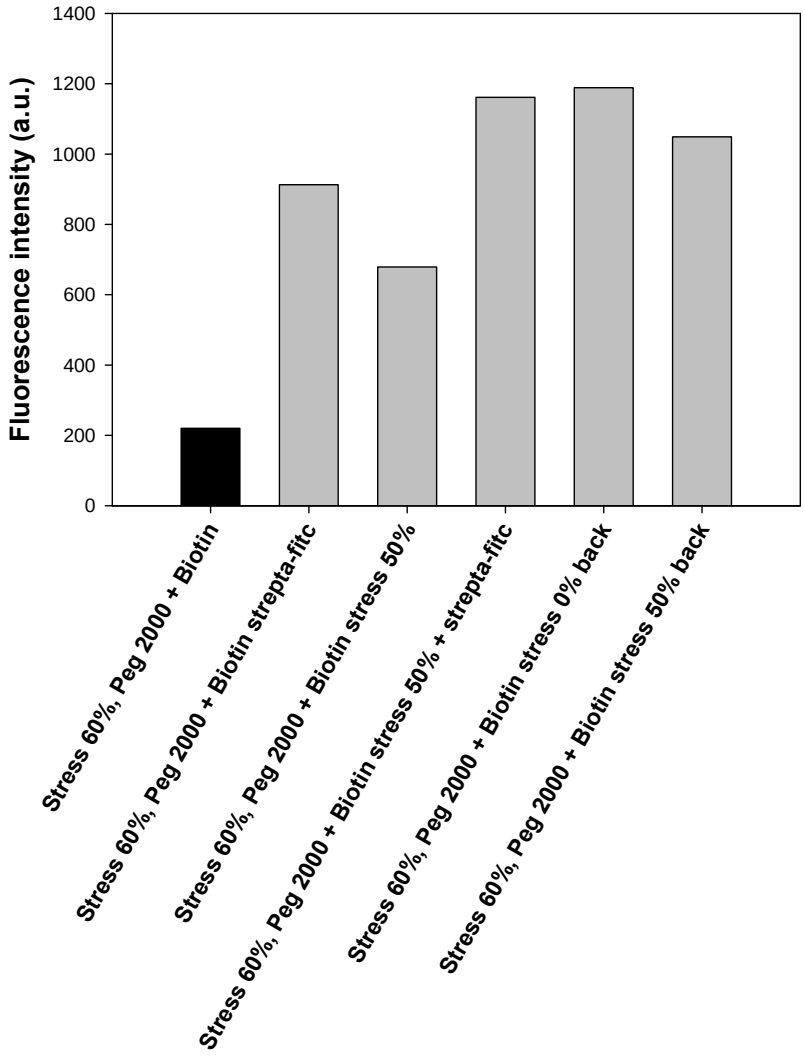

Figure 4.21: Evolution of the fluorescence intensity of a system functionalized under stretching at 60% during a stretching/unstrteching cycle. The black bar represents the auto-fluorescence of the substrate.

4.5.4.2 Effect of the PEG chain length

Next we tried to improve the characteristics of our system by increasing the PEG chain length. We used PEG(5000)-Mal and PEG(10000)-Mal which correspond respectively to 125 and 250 monomer units. The experimental conditions to functionalize the silicone surface with PEG(5000)-Mal and PEG(10000)-Mal were the same as those described above with PEG(2000)-Mal, except that the concentration of the PEG chains of the solution was 300 and 600 mg/mL for the PEG(5000)-Mal and the PEG(10000)-Mal respectively, instead of 120 mg/mL for the PEG(2000)-Mal. By using these mass concentrations, the molar concentrations are the same in each case. Comparison of the influence of the PEG chain-length is presented in figure 4.22. Fluorescence intensities coming from the adsorption of Streptavidin^{FITC} adsorbed onto the modified silicone surface were measured at rest and when the substrates were stretched at 50%.

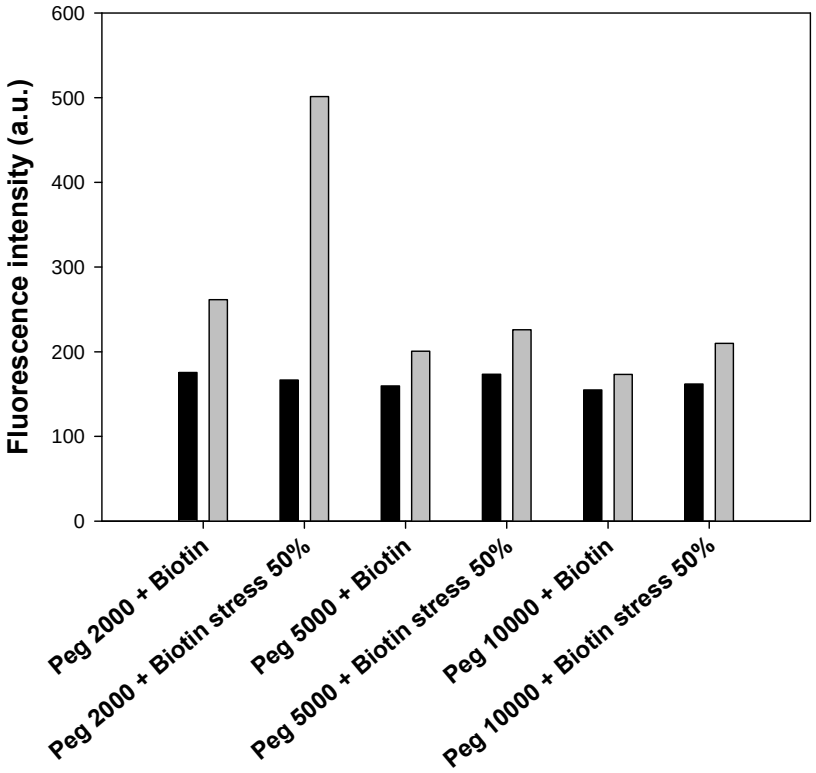

Figure 4.22: Fluorescence emission intensities measured onto silicone substrate before contact with the Streptavidin^{FITC} solution (black bars) and after contact and rinsing (grey bars). Silicone substrates were functionalized with different lengths of PEG-Mal: PEG(2000)-Mal, PEG(5000)-Mal and PEG(10000)-Mal. The measurements have been done at rest and stretched at 50%.

At rest, the silicone surfaces modified with the two longer PEG chains (PEG5000 and PEG10000) displayed a better antifouling effect than the substrate corresponding to PEG2000: lower values of fluorescence intensities, 200 and 173 a.u., are measured when using PEG(5000)-Mal and PEG(10000)-Mal respectively. These levels of fluorescence observed are very close to the residual one measured before contact with the Streptavidin^{FITC} solution. Thus, these surfaces are both almost completely antifouling to Streptavidin adsorption. When stretched at 50%, almost no additional fluorescence intensity is measured compared to the unstretched state. Increasing the PEG chain length seems thus not to be good way to go and we discarded this strategy.

4.5.4.3 Sequential grafting of PEG and biotin in a stretched state

Next we tried to graft sequentially PEG 2000 and biotin. Three different attempts were performed:

Sample A: the PDMS surface was treated with UVO for 1h30 followed by the functionalization with thiols groups. The substrate was then brought in contact with a 120 mg/mL solution of PEG 2000 during 2 h at room temperature. After this time the substrate was rinsed with buffer, stretched 1.5 times its initial length (50% stretching degree) followed by the addition of a 1.5 mg/mL solution of Biotin-Mal for 2 h at room temperature. Finally the sample was returned to its non-stretched state.

Sample B: the PDMS surface was treated with UVO for 1h30 followed by the functionalization with thiols groups. Then the substrate was stretched 1.4 times its initial length (stretching degree of 40%) and brought in contact with a 120 mg/mL solution of PEG 2000 during 1 h at 60°C. This was followed by the addition of a 1.5 mg/mL solution of Biotin-Mal that remained in contact with the substrate during 1h still at 60°C. Finally the sample was returned to its non-stretched state.

Sample C: The PDMS surface was stretched 1.6 times its initial length. It was then treated by UVO for 1 h and funtionalized with thiol groups. The functionalized substrate stretched at 60% was then brought in contact with a PEG 2000 solution at a concentration of 120 mg/mL at room temperature overnight. The surface was then brought a second time in contact with a similar PEG solution during 9h at 60°C. Then the substrate, still stretched at 60%, was brought in contact with a 1.5 mg/mL Biotin-Mal solution overnight and at room temperature. Finally the sample was returned to the non-stretched state.

The fluorescence after contact of these samples with Streptavidin^{FITC} is represented in figure 4.23.

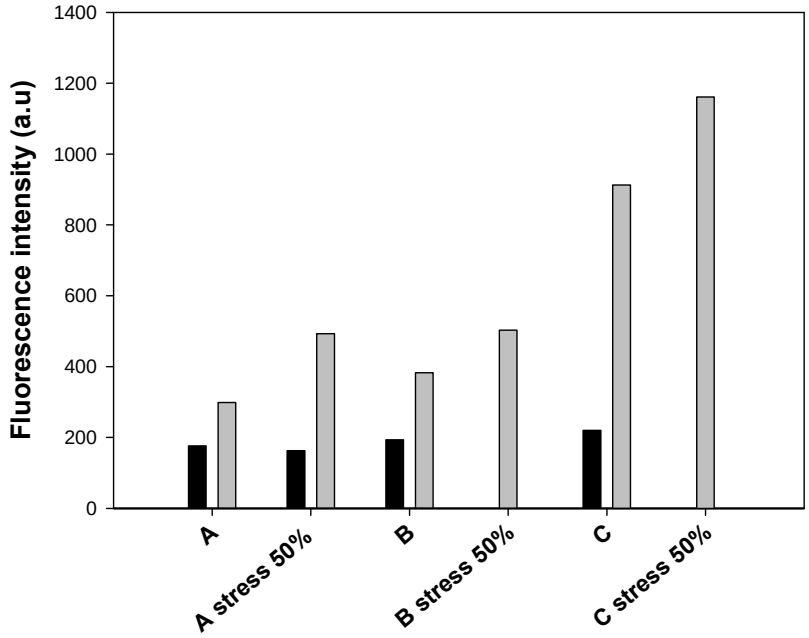

Figure 4.23: Fluorescence intensity after contact with Streptavidin^{FITC} of three substrates at rest and under 50% stretching. Once stretched, each substrate is brought again in contact with the Streptavidin^{FITC} solution and rinsed with buffer. The construction of the different samples is described in the text above.

One observes that none of the three buildup conditions is satisfactory. None of these buildup procedures renders the substrate anti-fouling with respect to Streptavidin, all show a cryptic site behavior but to a relatively modest degree. Out of the three buildup conditions, the most optimal one is that where one first grafts the PEG chains with the substrate at rest and then one grafts the biotin on the pegylated surface that is stretched at 60%. Yet because there was no real improvement compared to the simultaneous grafting of both PEG and biotin from a single solution, we did not pursue this strategy.

4.5.4.4 Sequential grafting of biotin and PEG

In these experiments, Biotin-Mal was first grafted on the samples followed by the grafting of the PEG chains, both procedures taking place in the non-stretched state. We tried the grafting of PEG of different molecular weights : 2000, 5000 and 10000 respectively. The

concentration of the Biotin-Mal solution was 1.5 mg/mL and the grafting reaction took place overnight at room temperature. The substrate was then rinsed with PBS buffer at pH 7.4 and brought in contact with a reductive agent, the tris(2-carboxyethyl)phosphine hydrochloride (TCEP), for 30 min to reduce the disulfure bonds that may have been formed in contact with air. Later, a PEG solution (concentration: 120, 300 and 600 mg/mL of PEG(2000)-Mal, PEG(5000)-Mal and PEG(10000)-Mal respectively) was added letting the reaction occurs overnight and at room temperature. The results are given in figure 4.24.

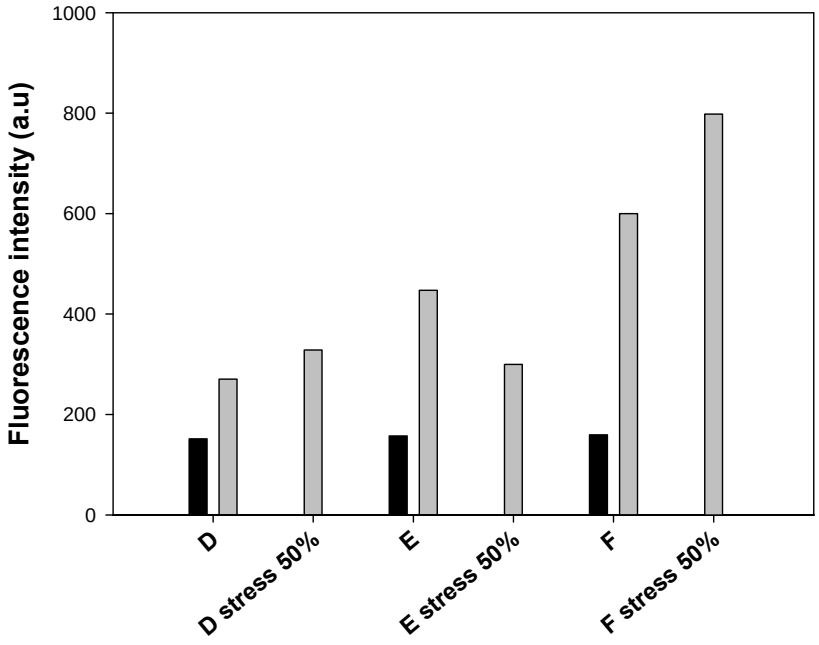

Figure 4.24: Fluorescence intensity after contact with Streptavidin^{FITC} for three different conditions of film preparation: PDMS surfaces were functionalized with UVO 1h30 min and thiols groups. Later, a 1.5 mg/mL solution of Biotin-Mal was added on the modified PDMS overnight and room temperature followed by the addition of PEG solution of 120 mg/mL PEG 2000 (sample D), 300 mg/mL PEG 5000 (sample E) and 600 mg/mL PEG 10000 (sample E) respectively overnight and at room temperature.

Here too, none of the substrates improves the expected characteristics when compared to the samples where both compounds are grafted simultaneously.

4.6 Conclusion

In this chapter we tried to design cryptic site surfaces by functionalizing silicone sheets with PEG brushes into which were incorporated biotin groups. The requirements for

the ideal cryptic substrate are to be anti-fouling, in particular with respect to the receptor of the ligand, to render the ligands accessible to the receptor under stretching and finally that the receptor/substrate interaction be reversible during stretching/unstretching cycles. Our strategy was based on the use of UV Ozone treatment of the silicone sheets for further chemical grafting of the substrate. We first determined the UVO treatment conditions such that one does not form a silica layer that breaks under stretching. This is a required condition for the further development of cryptic site surfaces. We succeeded in this way. We then silanized this surface and anchored thiol groups on the substrate. We then used a Michael addition between thiol groups and maleimide groups to graft modified PEG chains and modified biotin groups on the surface. We tried a large variety of strategies to graft both entities. The optimal strategy found within all that were tried was the simultaneous grafting of both the PEG chains and the biotin groups with a PEG molecular weight of 2000. This system, and most of the investigated systems, behaves as cryptic site surfaces. Yet they are all imperfectly anti-fouling with respect to Streptavidin. The major issue that is to be solved is that of the reversibility of the interaction. Up to now our systems behave totally irreversibly with respect to the streptavidin/substrate interaction. These results are to be compared to those obtained by Bacharouche et al.[18] following a similar strategy as the one developed here but by using polymer plasma for the silicone treatment instead of UV Ozone. Bacharouche et al. found a system that is cryptic and that seems totally reversible with respect to stretching/unstretching cycles. Yet it would be of interest to compare the two approaches by performing experiments strictly in a similar way (interaction with Streptavidin, rinsing conditions…). One of the largest difficulties of these studies is that one cannot get access to the surface densities of the grafted groups. This renders us largely blind so that it is difficult to improve the grafting procedure. Next studies need to address first this point.

4.7 References

(1) Vogel, V.; Sheetz, M. Local force and geometry sensing regulate cell functions *Nature Reviews Molecular Cell Biology* **2006**, 7, 265-275.

(2) Bustamante, C.; Chemla, Y. R.; Forde, N. R.; Izhaky, D. Mechanical processes in biochemistry *Annual Review of Biochemistry* **2004**, 73, 705-748.

(3) Gillespie, P. G.; Walker, R. G. Molecular basis of mechanosensory transduction *Nature* **2001**, 413, 194-202.

(4) Coutand, C. Mechanosensing and thigmomorphogenesis, a physiological and biomechanical point of view *Plant Science* **2010**, 179, 168-182.
(5) Vogel, V. Mechanotransduction involving multimodular proteins: Converting force into biochemical signals *Annual Review of Biophysics and Biomolecular Structure* **2006**, 35, 459-488.
(6) Vogel, V.; Thomas, W. E.; Craig, D. W.; Krammer, A.; Baneyx, G. Structural insights into the mechanical regulation of molecular recognition sites *Trends in Biotechnology* **2001**, 19, 416-423.
(7) Vakonakis, I.; Staunton, D.; Rooney, L. M.; Campbell, I. D. Interdomain association in fibronectin: insight into cryptic sites and fibrillogenesis *EMBO J.* **2007**, 26, 2575-2583.
(8) Critchley, D. R. Focal adhesions - the cytoskeletal connection *Current Opinion in Cell Biology* **2000**, 12, 133-139.
(9) Izard, T.; Vonrhein, C. Structural basis for amplifying vinculin activation by talin *Journal of Biological Chemistry* **2004**, 279, 27667-27678.
(10) del Rio, A.; Perez-Jimenez, R.; Liu, R.; Roca-Cusachs, P.; Fernandez, J. M.; Sheetz, M. P. Stretching single talin rod molecules activates vinculin binding *Nature* **2009**, 323, 638-641.
(11) Forterre, Y.; Skotheim, J. M.; Dumais, J.; Mahadevan, L. How the Venus flytrap snaps *Nature* **2005**, 433, 421-425.
(12) Braam, J. In touch: plant responses to mechanical stimuli *New Phytologist* **2005**, 165, 373-389.
(13) Mertz, D.; Vogt, C.; Hemmerle, J.; Mutterer, J.; Ball, V.; Voegel, J.-C.; Schaaf, P.; Lavalle, P. Mechanotransductive surfaces for reversible biocatalysis activation *Nat. Mater.* **2009**, 8, 731-735.
(14) Davila, J.; Chassepot, A.; Longo, J.; Boulmedais, F.; Reisch, A.; Frisch, B.; Meyer, F.; Voegel, J.-C.; Mesini, P. J.; Senger, B.; Metz-Boutigue, M.-H.; Hemmerle, J.; Lavalle, P.; Schaaf, P.; Jierry, L. Cyto-mechanoresponsive Polyelectrolyte Multilayer Films *J. Am. Chem. Soc.* **2012**, 134, 83-86.
(15) Ratner, B. D.; Bryant, S. J. Biomaterials: Where we have been and where we are going *Annu. Rev. Biomed. Eng.* **2004**, 6, 41-75.
(16) Mendes, P. M. Stimuli-responsive surfaces for bio-applications *Chemical Society Reviews* **2008**, 37, 2512-2529.
(17) Mano, J. F. Stimuli-Responsive Polymeric Systems for Biomedical Applications *Advanced Engineering Materials* **2008**, 10, 515-527.

(18) Bacharouche, J.; Badique, F.; Fahs, A.; Spanedda, M. V.; Geissler, A.; Malval, J. P.; Vallat, M. F.; Anselme, K.; Francius, G.; Frisch, B.; Hemmerle, J.; Schaaf, P.; Roucoules, V. Biomimetic Cryptic Site Surfaces for Reversible Chemo- and Cyto-Mechanoresponsive Substrates *Acs Nano* **2013**, 7, 3457-3465.

(19) Whitesides, G. M. The origins and the future of microfluidics *Nature* **2006**, 442, 368-373.

(20) Ikada, Y. Surface Modification of Polymers for Medical Applications *Biomaterials* **1994**, 15, 725-736.

(21) Colas, A.; Curtis, J., *Silicone biomaterials: history, chemistry & Medical Applications of Silicones*. Second ed.; Elsevier: Ratner, London, 2004; p 697-706.

(22) Hillborg, H.; Gedde, U. W. Hydrophobicity changes in silicone rubbers *IEEE Trans. Dielectr. Electr. Insul.* **1999**, 6, 703-717.

(23) Lewis, L. N.; Stein, J.; Gao, Y.; Colborn, R. E.; Hutchins, G. Platinum catalysts used in the silicones industry. Their synthesis and activity in hydrosilylation *Platinum Met. Rev.* **1997**, 41, 66-75.

(24) Mehl, G. H.; Saez, I. M. Polyhedral liquid crystal silsesquioxanes *Applied Organometallic Chemistry* **1999**, 13, 261-272.

(25) Ojima, I.; Li, Z.; Zhu, J., Recent Advances in the Hydrosilylation and Related Reactions. In *The Chemistry of Organic Silicon Compounds*, John Wiley & Sons, Ltd: 2003; pp 1687-1792.

(26) Chalk, A. J.; Harrod, J. F. Homogeneous Catalysis. II. The Mechanism of the Hydrosilation of Olefins Catalyzed by Group VIII Metal Complexes *Journal of the American Chemical Society* **1965**, 87, 16-21.

(27) Wu, Y.; Huang, Y.; Ma, H. A Facile Method for Permanent and Functional Surface Modification of Poly(dimethylsiloxane) *Journal of the American Chemical Society* **2007**, 129, 7226-7227.

(28) Zhou, J.; Ellis, A. V.; Voelcker, N. H. Recent developments in PDMS surface modification for microfluidic devices *Electrophoresis* **2010**, 31, 2-16.

(29) Efimenko, K.; Wallace, W. E.; Genzer, J. Surface Modification of Sylgard-184 Poly(dimethyl siloxane) Networks by Ultraviolet and Ultraviolet/Ozone Treatment *Journal of Colloid and Interface Science* **2002**, 254, 306-315.

(30) Berdichevsky, Y.; Khandurina, J.; Guttman, A. s.; Lo, Y. H. UV/ozone modification of poly(dimethylsiloxane) microfluidic channels *Sensors and Actuators B: Chemical* **2004**, 97, 402-408.

(31) Hillborg, H.; Ankner, J. F.; Gedde, U. W.; Smith, G. D.; Yasuda, H. K.; Wikstrom, K. Crosslinked polydimethylsiloxane exposed to oxygen plasma studied by neutron reflectometry and other surface specific techniques *Polymer* **2000**, 41, 6851-6863.

(32) Hillborg, H.; Gedde, U. W. Hydrophobicity recovery of polydimethylsiloxane after exposure to corona discharges *Polymer* **1998**, 39, 1991-1998.

(33) Hermanson, G. T., *Bioconjugate Techniques*. (Second Edition) ed.; Academic press: New York, 2008; p 130-131.

(34) Branch, D. W.; Wheeler, B. C.; Brewer, G. J.; Leckband, D. E. Long-term stability of grafted polyethylene glycol surfaces for use with microstamped substrates in neuronal cell culture *Biomaterials* **2001**, 22, 1035-1047.

(35) Burns, J. A.; Butler, J. C.; Moran, J.; Whitesides, G. M. Selective Reduction of Disulfides by Tris(2-Carboxyethyl)Phosphine *Journal of Organic Chemistry* **1991**, 56, 2648-2650.

(36) Michael Green, N.; Meir Wilchek and Edward, A. B., Avidin and streptavidin. In *Methods in Enzymology*, Academic Press: 1990; Vol. 184, 51-67.

(37) Geissler, A.; Vallat, M. F.; Fioux, P.; Thomann, J. S.; Frisch, B.; Voegel, J. C.; Hemmerle, J.; Schaaf, P.; Roucoules, V. Multifunctional Stretchable Plasma Polymer Modified PDMS Interface for Mechanically Responsive Materials *Plasma Processes and Polymers* **2010**, 7, 64-77.

(38) Genzer, J.; Efimenko, K. Creating long-lived superhydrophobic polymer surfaces through mechanically assembled monolayers *Science* **2000**, 290, 2130-2133.

Chapter 5

Polyelectrolyte multilayers with mechanically modulable enzymatic activity (article in preparation)

5.1 Introduction

Chemo-mechanoresponsive materials constitute a new class of materials that respond chemically to a mechanical stress. This domain has largely been initiated by the groups of Moore and Sotos[1, 2] who incorporated polymers that contain mechanophores into polymeric matrices. Mechanophores are molecules that undergo a chemical reaction when brought under stretching. This usually results in a colour change in the material at regions of high stress. The first reported example of such material is that of poly(methyl methacrylate) matrices into which poly(methyl acrylate) chains that contain spiropyrane were incorporated.[2] Recently, using a *gem*-dichlorocyclopropanated indene incorporated into a cross-linked poly(methylacrylate) material, the group of Moore reported a new material which under compression releases protons (mechanogenerated acid).[3] This is due to a force dependent rearrangement that results in proton elimination.

The development of chemo-mechanoresponsive materials relies on mechanotransduction processes. Such processes are also widely used in Nature, in particular by cells when sensing their environment.[4] Usually Nature does not directly use internal chemical reactions in molecules to transform a mechanical signal into a chemical response but rather less energy demanding processes such as small conformational changes of proteins.[5] Stretching domain-proteins can lead, for example, to a sequential unravelling of different domains as it is observed in fibronectin or to the exhibition of cryptic sites that become then active.[6] Enzymes constitute a class of proteins that act through a precise topology of the different constituting groups of their active site. Moreover dynamic fluctuations of enzyme conformations appear also to play an important role in their activity. It is thus reasonable to assume that enzyme activity can be modulated by applying a mechanical stress on them.[5] Such a stress should be able to modify both the conformation of the enzyme as well as the dynamics of their structural fluctuations. This was confirmed by Tseng at al. who used a DNA molecular spring that was coupled on two positions of an enzyme, guanylate kinase, to create a protein-DNA chimera.[7] Depending of the ligation position of the DNA and its length, and thus on the stress exerted on the enzyme, they found that the enzyme activity was reduced and the reduction activity was stronger for shorter DNA (larger strength exerted by the DNA on the enzyme).

Based on this simple idea, modifying the enzymatic activity by applying a mechanical tension on an enzyme, we propose to create mechano-modulable enzymatic active materials by covalently incorporating enzymes into stretchable polymeric films. This requires that the

films be elastic, that the enzymes remain active in the film and that the enzyme substrate is able to diffuse in the film in order to react with the enzyme. We propose to use exponentially growing polyelectrolyte multilayers into which are embedded enzymes to fulfil these requirements. Indeed, polyelectrolyte multilayers are known to preserve enzymatic activity, to be stretchable[8] and to be easily processed. They are obtained by the alternate deposition of polyanions and polycations onto a solid substrate. We used poly-(L-lysine)/hyaluronic acid (PLL/HA) as exponentially growing multilayer because it is the exponentially growing film that is best known.[9] As we will see, in order to obtain mechano-responsiveness the multilayer has to be cross-linked and the enzymes have to be covalently anchored onto the cross-linked multilayer. As enzyme we have used β-galactosidase. This enzyme was selected because it is a tetramer comprised of four polypeptide chains (monomers) held together through non-covalent interactions[10] (see figure 5.1).

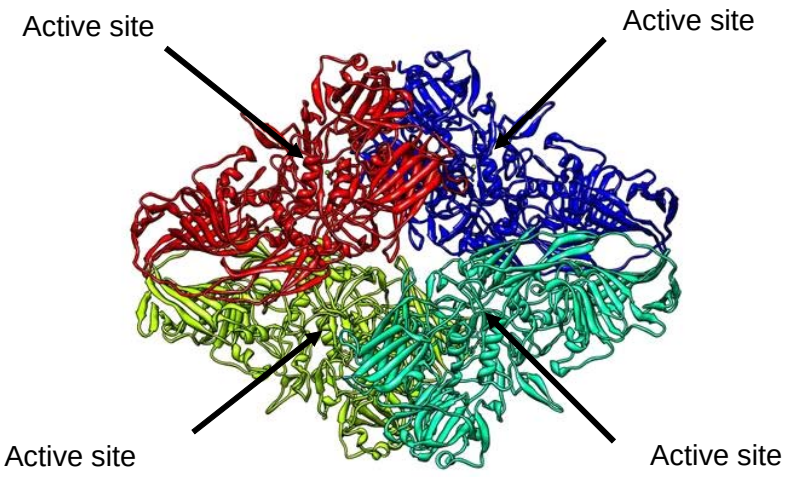

Figure 5.1: Image of the β-galactosidase from *Escherichia coli* with the location of the active sites. Taken from ref[10].

Each monomer is made up of five domains, domain 3 having an α/β barrel structure with the active site located at the C-terminal end of the barrel. The enzyme has four active sites that are located at the barrel in domains 3, including residues belonging to loops of domains 1 and 5 from the same monomer and residues from domain 2 belonging to a different monomer. The structure of the enzyme and more particularly of the enzymatic active site is anticipated to be particularly sensitive to mechanical stresses exerted onto the enzyme in particular because it involves several enzyme components. As substrate we used fluorescein di(β-D-galactopyranoside) (FDG) which is transformed into fluorescein and β-D-

galactopyranoside through a reaction enzymatically triggered by β-galactosidase (see figure 5.2). The reaction can thus be followed by monitoring the fluorescence of the solution in contact with the film.

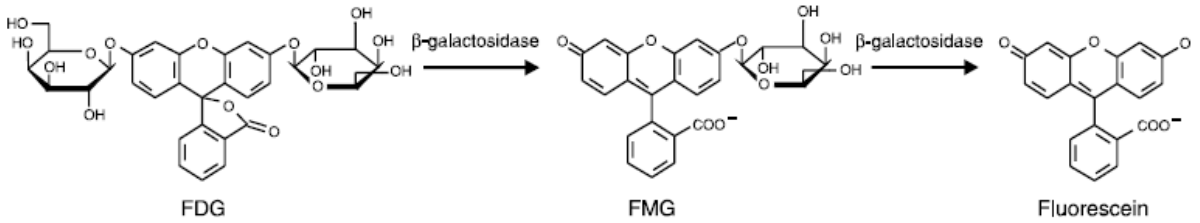

Figure 5.2: Reaction of FDG leading to fluorescein in the presence of β-galatosidase

5.2 Results

Our first goal was to prepare cross-linked polymeric films that are both stretchable and enzymatically active. In previous studies it was shown that PLL/HA multilayers can be deposited on silicone substrates in a step-by step manner.[8] The film thickness grows exponentially with the number of deposition steps and reaches of the order of 7 μm after 24 PLL/HA deposition steps.[9] We used a similar deposition procedure here (see supporting information S4.1). Once built, the film was brought in contact with a β-galactosidase solution whose concentration was 0.5 mg/mL. Using fluorescein labelled β-galactosidase we could show that the enzymes diffuse within 60 minutes (contact time of the film with the solution) into the whole multilayer film (figure 5.3). When this film was brought in contact with a FDG solution at 0.5 mg/mL we observed a linear increase with time of the fluorescence in the solution contacting the film (figure 5.4). This indicates that the enzymes remain active in the multilayer, in accordance with previous studies on other enzyme/multilayer systems.[8] When this system was stretched no change in the fluorescence rate production in solution was observed under stretching (figure 5.5). This is anticipated since PLL/HA behaves as a viscoelastic liquid.[11]

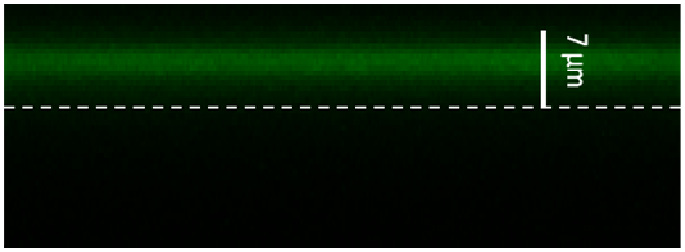

Figure 5.3: Confocal microscope section (x,z) images of $(PLL/HA)_{24}$ multilayer films deposited on silicone sheets brought in contact with a β-Gal^{FITC} solution at 0.5 mg/ml. The image was taken 60 minutes after contact between the film and the enzyme solution. The thickness of the film is around 7 µm. The dashed lines indicate interfaces between silicone sheet and multilayer film. This figure shows that the enzymes diffuse into the whole film.

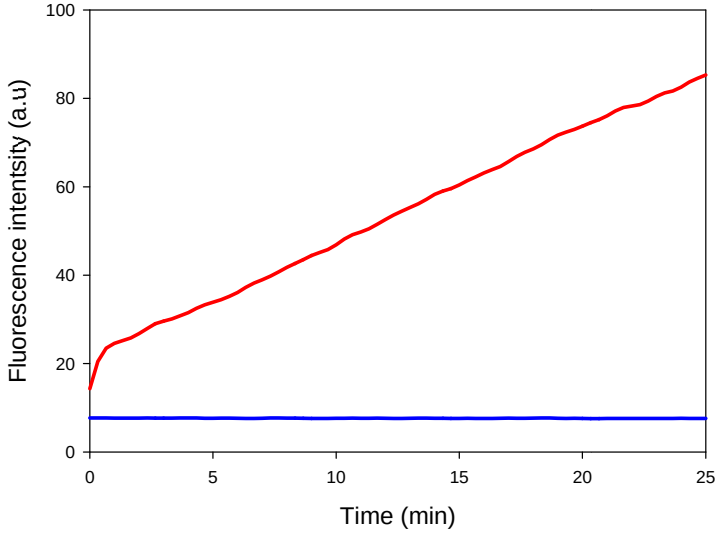

Figure 5.4: Evolution with time of the fluorescence intensity measured in solution due to the loaded enzymes in the $(PLL/HA)_{24}$ films (red curve) before cross-linking, (blue curve) after EDC/NHS cross-linking. One observes that before cross-linking, the enzymes remain active in the multilayer and after cross-linking the film becomes totally inactive enzymatically.

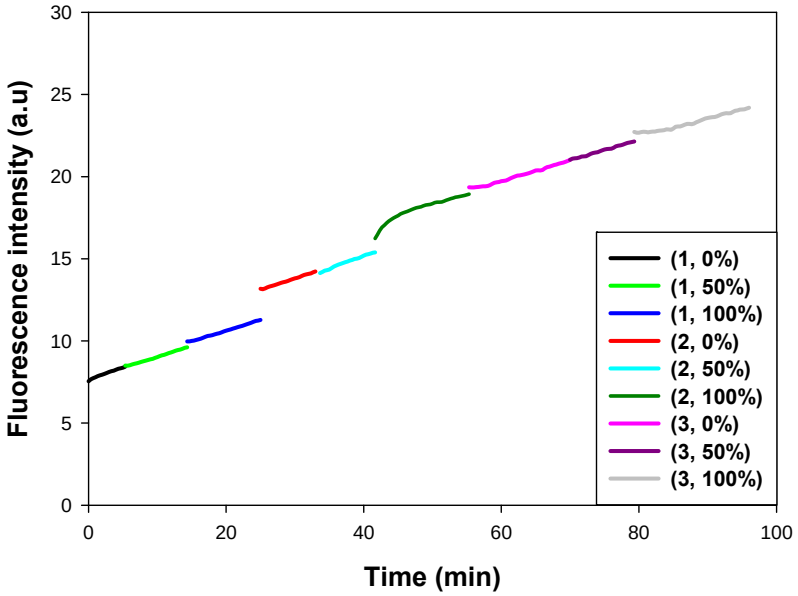

Figure 5.5: Evolution with time of the fluorescence in solution for a film $(PLL/HA)_{24}$-β-Gal in the presence FDG. The film is stretched at various stretching degrees. No change in the fluorescence rate increase is observed when the stretching degree of the film is changed. (X,Y%): X represents the stretching cycles number and Y represents the stretching degree within the cycle.

Next, we cross-linked the film through carbodiimide chemistry by bringing it in contact with an EDC-NHS solution. This procedure is known to cross-link the PLL/HA film by formation of amide bonds.[12] We first optimized the cross-linking conditions by changing the EDC concentration and the cross-linking time with the goal to obtain a film that is stretchable up to a stretching degree of 100% without crack formation. We found that the optimum conditions are 20 mmol EDC, 50 mmol NHS with a cross-linking time of 15 hours at 4°C (see table S1 in supporting information). This led to films which can be stretched up to 160% without breaking. Under stretching, the film remained firmly attached to the silicone substrate. These conditions were used throughout the whole study. When this procedure was applied on a film containing β-galactosidase, no enzymatic activity was observed anymore (see figure 5.4). This may be due to the fact that cross-linking the film also affects the enzymes internally which should greatly modify their conformation, their conformation fluctuations and thus also their catalytic activity.

In order to circumvent these difficulties we proceeded in two steps. We modified PLL chains chemically by grafting on them thiopyridone groups leading to PLL-S-TP. The grafting

ratio was 27%. The enzymes were modified by grafting maleimide groups through their free lysines (β-Gal-mal). The average grafting ratio was 70%. Details of the chemical modifications of both PLL and β-gal are given in supporting information S1. We constructed PLL-S-TP/HA films onto silicone substrates similarly to PLL/HA multilayers. The films were then reticulated through the EDC/NHS cross-linking chemistry before enzyme incorporation. We then brought the cross-linked PLL-S-TP/HA films in contact with β-Gal-mal enzyme solution. We first verified that the enzymes diffuse into the film, a result that is by far not obvious since the film is already reticulated. This was verified by using β-Gal-mal enzymes labelled with fluorescein isothiocyanate (FITC) (figure 5.6).

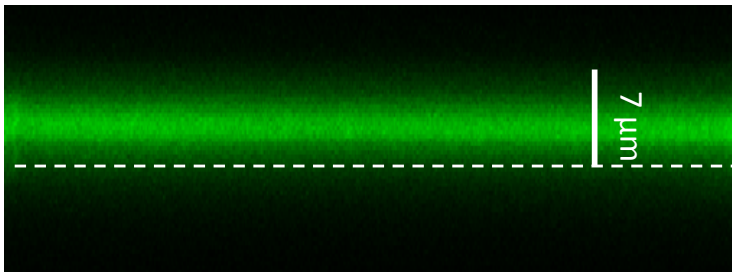

Figure 5.6: Confocal image of a $(PLL\text{-}S\text{-}TP/HA)_{24}$ film cross-linked with EDC-NHS and then brought in contact with β-Gal-mal^{FITC} before cross-linking by addition of TCEP

The film appears green over 7 µm, a thickness that corresponds typically to that of a $(PLL/HA)_{24}$ multilayer. By comparing the fluorescence intensity in the film and in different solutions we could estimate the enzyme concentration in the film to be of the order of 854 µg/mL. This value is to be compared to 0.5 mg/mL in solution (More details are given in supporting information S4.6). The multilayers thus act as a concentrating media as it was observed for non-cross-linked PLL/HA multilayers.[13] When this film is brought in contact with a FDG solution, fluorescence in solution increases linearly with time showing again that the film remains enzymatically active. When this film is stretched at 50% and later at 100%, no significant change in the fluorescence rate in solution is observed (see figure 5.7). Thus, even when the film is cross-linked but the enzyme is not coupled to the film, the enzymatic activity of the film is not affected by stretching.

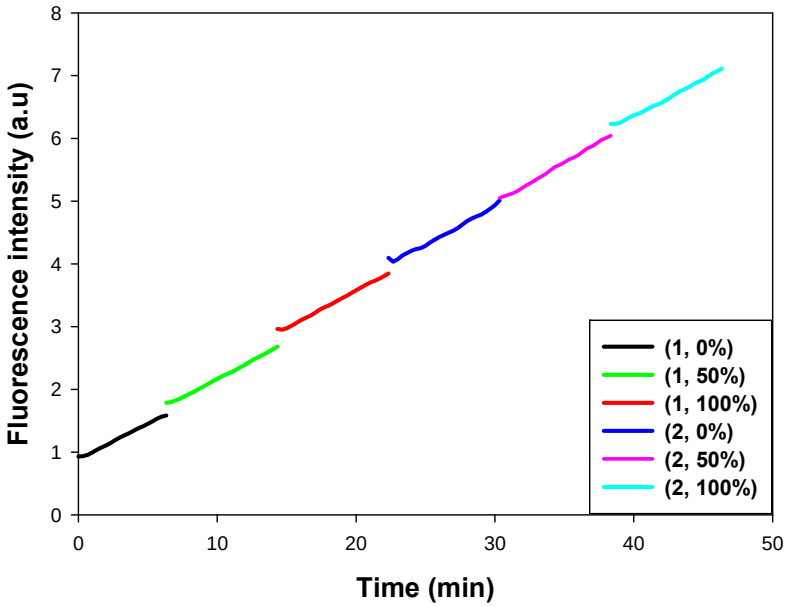

Figure 5.7: Evolution with time of the fluorescence intensity measured in solution due to the loaded enzymes in the reticulated PLL-S-TP/HA films. The modified enzyme β-Gal-mal is not yet coupled with the thiols groups present in the modified PLL, therefore there's no changing in the catalytic activity after stetching the PDMS. (X,Y%): X represents the stretching cycles number and Y represents the stretching degree within the cycle.

We then brought the film in contact with 3, 3′, 3″-phosphanetriyltripropanoic acid (TCEP), a reducing agent that deprotects the thiopyridone groups into thiols which then react with the maleimide groups anchored on the proteins. This reaction then covalently couples the enzymes onto the multilayer matrix. The deprotection reaction was followed by absorption spectroscopy at 343nm in the contacting solution (see figure 5.8).

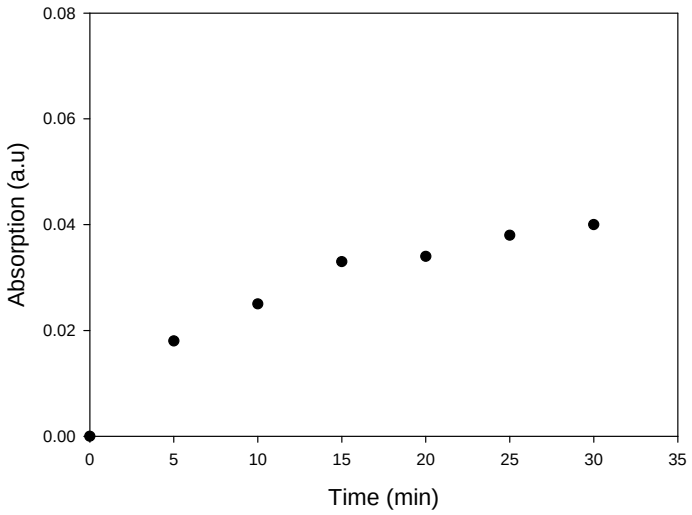

Figure 5.8: Deprotection of the thyopiridone groups in contact with TCEP followed by UV spectroscopy at 343 nm wavelength. The reaction takes place over 30 minutes.

The increase in absorption corresponds to the release of the pyridinone molecules in solution. We found that the reaction takes place during approximately 30 minutes. We thus always kept this coupling time for all the experiments. We also tried to verify the coupling of the enzymes onto the PLL-S-TP/HA matrix by using fluorescence recovery after photobleaching experiments (FRAP) (see figure S7 in Supporting Information). We found that the fraction of mobile enzymes is for β-Gal-mal^{FITC} and β-Gal^{FITC} 34% and 42% respectively. These results are very similar which indicates almost the same number of immobile between the modified or unmodified enzymes throught the PEM film. It thus seems that the β-Gal^{FITC} non-cross-linked enzyme is firmly attached to the PLL-S-TP/HA network, eventually through strong electrostatic interactions with PLL-S-TP. We thus rely on the reduction of thiopyridone and the high reactivity of thiol groups with maleimide groups to argue that the enzymes are covalently linked to the cross-linked PLL-S-TP/HA film.

Films containing covalently attached β-Gal-mal enzymes were then brought in contact with FDG and stretched in a stepwise manner up to 100%. Figure 5.9 shows a typical evolution of the fluorescence during such a process.

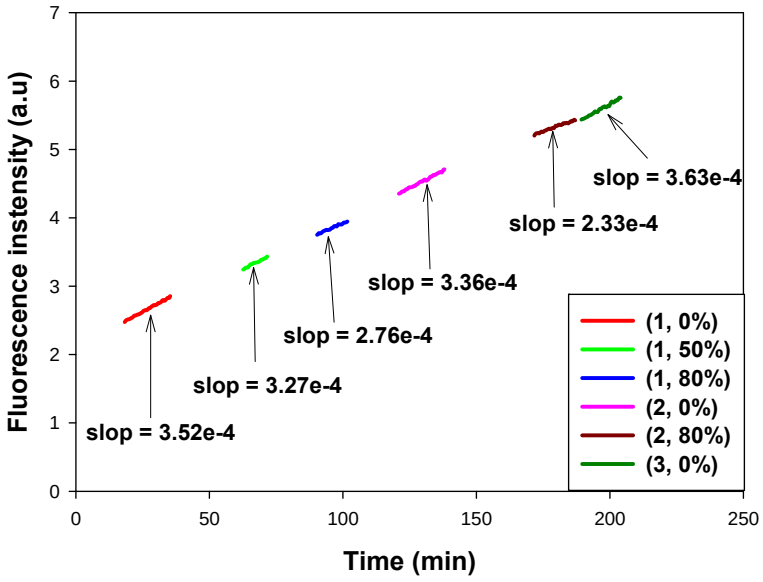

Figure 5.9: Evolution with time of the fluorescence intensity measured in solution due to the loaded cross-linked and in the reticulated PLL-S-TP/HA films.Evolution of the fluorescence intensity in the solution as a function of time during a stretching/unstretching cycle. The rate of fluorescence increase is given for each stretching degree. (X,Y%): X represents the stretching cycles number and Y represents the stretching degree within the cycle.

First one observes that the films remain enzymatically active in the non stretched state. Under stretching, the fluorescence production rate in the solution decreases when the stretching degree is increased. This evolution of the fluorescence production rate is different from that observed with non-crosslinked enzymes where the fluorescence production remained almost constant or even increased slightly under stretching. A summary of the obtained results is found in figure 5.10 where one plots the fluorescence rate as a function of the stretching degree, the rate being normalized to the rate measured initially in the non-stretched state. It clearly appears that stretching the film with the crosslinked enzymes affects the enzyme activity. One can speculate about the origin of the reduced enzymatic activity, one highly probable reason being a change of the enzyme conformation, yet this is impossible to prove with our experimental set-ups. The decrease of the film activity becomes particularly important at stretching degrees higher than 50%. We reached 32±10% reduction of the fluorescence production at a stretching degree of 80-85%. Due to a constant or even small increase of the production under stretching for non cross-linked films one can conclude that the mean enzyme activity is decreased by more than 32% at 80% of stretching. This

reduction of the enzyme activity is to be compared to the values of the reduction of the activity of guanylate kinase found by Tseng et al. using the DNA molecular spring method and which, to our knowledge, is the only example where the enzymatic activity has been quantitatively measured for enzymes under mechanical forces.[7] Depending upon the DNA length, these authors found a decrease of the catalytic rate constant k_{cat} entering in the Michaelis-Menten equation from 9.6 to 6.4 for short DNA (high stress exerted on the enzyme) and from 9.3 to 8.8 for a longer chain DNA (low stress exerted on the enzyme). It is also found that the application of a mechanical stress decreases the binding affinity of the enzymes for ATP and GMP, the two substrates involved in the reaction up to 20%. The reduction of the catalytic rate constant up to 30% is of the same order of magnitude as that found in our experiments.

Next we investigated the reversibility of the activity change. The films were stretched at 80 or 100% and then returned to the non stretched state. Figure 5.10 shows that returning to the non stretched state leads to an increase of the order of 15% of the fluorescence rate production. When repeated a second time, the stretching/unstretching process leads again to a decrease/increase of the fluorescence production rate. This shows that the stretch-induced change of the enzymatic activity is partially reversible. These results show the enzymatic mechano-responsive character of the film.

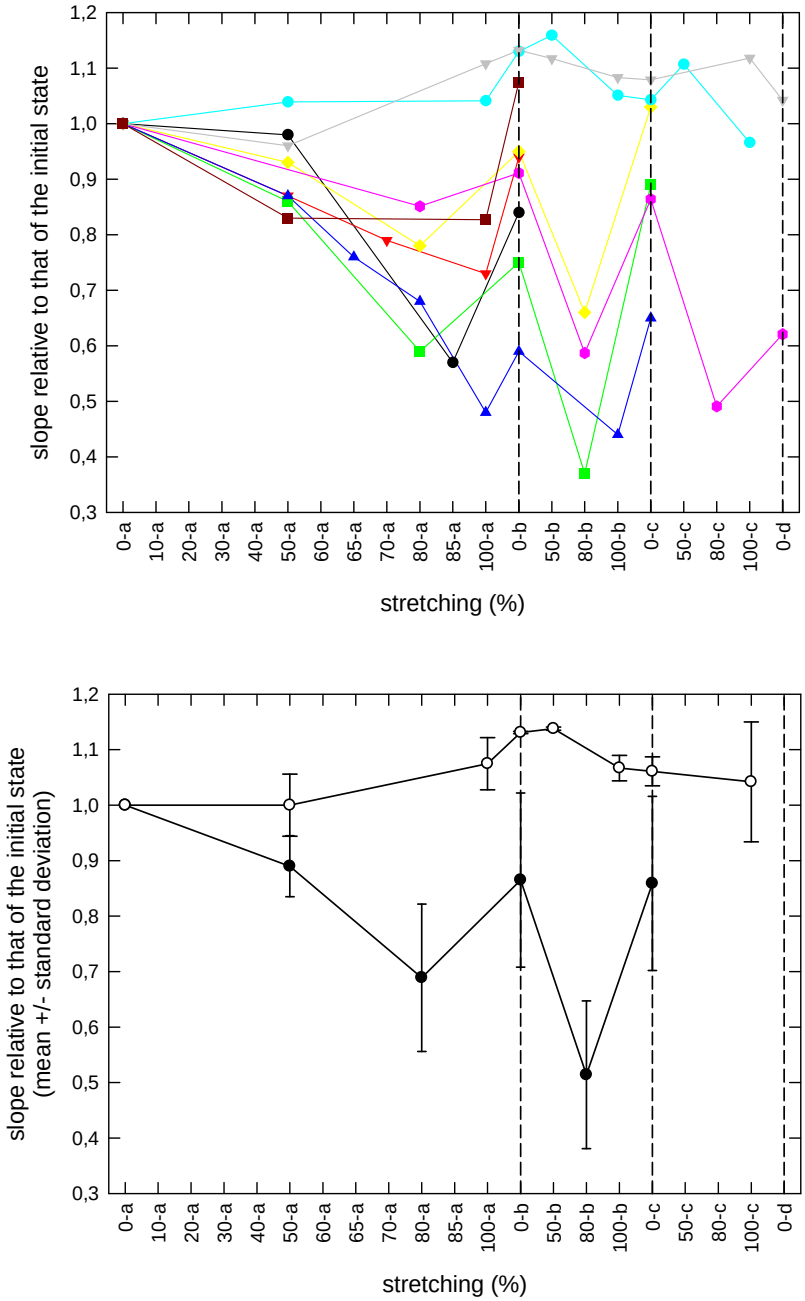

Figure 5.10: (Upper figure): Evolution of the relative fluorescence production rate at different stretching degrees. Each colour represents an individual experiment. The two upper curves correspond to experiments in which the enzyme was not coupled to the PLL/HA network. (lower figure) : evolution of the mean values of the fluorescence rate production at different stretching degrees corresponding to the experiments shown on the upper figure.

5.3 Conclusion

The large variability of the reduction of the enzymatic activity that we find between different experiments may be due to the large number of parameters entering in the preparation process of the sample and the experimental difficulties related to the fact that the stretching-unstretching process is only partially reversible. When the unstretched prepared sample is introduced in the clamps, unavoidably the film becomes locally slightly folded which introduces local mechanical stresses. Moreover, slight temperature changes during the film preparation might slightly influence the film structure, the reticulation reactions which in turn influence the enzyme behaviour.

In 2009 our group presented a first enzymatic mechano-responsive film[8], yet it was based on a totally different principle. It was based on embedding an enzyme, alkaline-phosphatase, into a PLL/HA multilayer which was then capped by a linearly growing multilayer, namely poly(styrene sulfonate)/poly(diallyl dimethyl ammonium). This latter film played the role of barrier towards fluorescein di-phosphate (FDP), a substrate of alkaline-phosphatase. By stretching the film, the barrier remained tied towards FDP but some enzymes became exhibited through the barrier so that the reaction took place. When returning to the non stretched state, the enzymes were hidden again by the barrier, at least to a large extent, so that the systems appeared fairly reversible. The present system, which could at first sight appear quite similar to the one developed by Mertz *et al.* relies in fact on totally different physical grounds and is by far more general in its principle. The system presented here is based on a conformational change of the enzymes under stretching. Even if we could not directly prove this conformational change of the enzymes under stretching, it appears as the only explanation for our observations. The system presented here opens the route towards a class of materials whose active sites have their conformations modified and thus their activity changed under tensile stress. Our goal is now to generalize this concept to other enzymes and other supporting hydrogels.

5.4 References

1. Hickenboth, C. R.; Moore, J. S.; White, S. R.; Sottos, N. R.; Baudry, J.; Wilson, S. R., Biasing reaction pathways with mechanical force. *Nature* **2007,** *446*, 423-427.

2. Davis, D. A.; Hamilton, A.; Yang, J. L.; Cremar, L. D.; Van Gough, D.; Potisek, S. L.; Ong, M. T.; Braun, P. V.; Martinez, T. J.; White, S. R.; Moore, J. S.; Sottos, N. R., Force-induced activation of covalent bonds in mechanoresponsive polymeric materials. *Nature* **2009,** *459*, 68-72.

3. Diesendruck, C. E.; Steinberg, B. D.; Sugai, N.; Silberstein, M. N.; Sottos, N. R.; White, S. R.; Braun, P. V.; Moore, J. S., Proton-Coupled Mechanochemical Transduction: A Mechanogenerated Add. *Journal of the American Chemical Society* **2012,** *134*, 12446-12449.

4. Orr, A. W.; Helmke, B. P.; Blackman, B. R.; Schwartz, M. A., Mechanisms of mechanotransduction. *Developmental Cell* **2006,** *10*, 11-20.

5. Vogel, V.; Sheetz, M., Local force and geometry sensing regulate cell functions. *Nature Reviews Molecular Cell Biology* **2006,** *7*, 265-275.

6. Vogel, V., Mechanotransduction involving multimodular proteins: Converting force into biochemical signals. In *Annual Review of Biophysics and Biomolecular Structure*, Annual Reviews: Palo Alto, 2006; Vol. 35, pp 459-488.

7. Tseng, C. Y.; Wang, A.; Zocchi, G., Mechano-chemistry of the enzyme Guanylate Kinase. *Epl* **2010,** *91*.

8. Mertz, D.; Vogt, C.; Hemmerle, J.; Mutterer, J.; Ball, V.; Voegel, J. C.; Schaaf, P.; Lavalle, P., Mechanotransductive surfaces for reversible biocatalysis activation. *Nature Materials* **2009,** *8*, 731-735.

9. Picart, C.; Mutterer, J.; Richert, L.; Luo, Y.; Prestwich, G. D.; Schaaf, P.; Voegel, J.-C.; Lavalle, P., Molecular basis for the explanation of the exponential growth of polyelectrolyte multilayers. *Proceedings of the National Academy of Sciences of the United States of America* **2002,** *99*, 12531-12535.

10. Jacobson, R. H.; Zhang, X. J.; DuBose, R. F.; Matthews, B. W., Three-dimensional structure of beta-galactosidase from E. coli. *Nature* **1994,** *369*, 761-766.

11. Picart, C.; Sengupta, K.; Schilling, J.; Maurstad, G.; Ladam, G.; Bausch, A. R.; Sackmann, E., Microinterferometric study of the structure, interfacial potential, and viscoelastic properties of polyelectrolyte multilayer films on a planar substrate. *Journal of Physical Chemistry B* **2004,** *108*, 7196-7205.

12. Richert, L.; Boulmedais, F.; Lavalle, P.; Mutterer, J.; Ferreux, E.; Decher, G.; Schaaf, P.; Voegel, J. C.; Picart, C., Improvement of stability and cell adhesion properties of polyelectrolyte multilayer films by chemical cross-linking. *Biomacromolecules* **2004,** *5*, 284-294.

13. Vogt, C.; Ball, V.; Mutterer, J.; Schaaf, P.; Voegel, J. C.; Senger, B.; Lavalle, P., Mobility of Proteins in Highly Hydrated Polyelectrolyte Multilayer Films. *Journal of Physical Chemistry B 116*, 5269-5278.

14. Hermanson, G. T., Zero-length crosslinkers - EDC plus sulfo-NHS. In Bioconjugate Techniques (Second Edition), Academic Press: New York, 2008; pp 219-223.

15. Bacharouche, J.; Badique, F.; Fahs, A.; Spanedda, M. V.; Geissler, A.; Malval, J. P.; Vallat, M. F.; Anselme, K.; Francius, G.; Frisch, B.; Hemmerlé, J.; Schaaf, P.; Roucoules, V., Biomimetic Cryptic Site Surfaces for Reversible Chemo- and Cyto Mechanoresponsive Substrates. *ACS Nano* **2013,** *(in press)*.

16. Picart, C.; Mutterer, J.; Arntz, Y.; Voegel, J. C.; Schaaf, P.; Senger, B., Application of fluorescence recovery after photobleaching to diffusion of a polyelectrolyte in a multilayer film. *Microscopy Research and Technique* **2005,** *66*, 43-57.

5.5 Supporting Information

S1. Chemicals and chemical modifications of polymers and enzymes

S1.1 Chemicals

The polyelectrolytes Poly(L-lysine) (PLL, *Mw* = 2.60 x 10^4 Da) and hyaluronic acid (HA, *Mw* = 1.32 x 10^5 Da) were purchased from Sigma Aldrich and Lifecore Biomedical respectively. Coupling agents as *N*,*N*′-Dicyclohexylcarbodiimide 99% (DCC), *N*-(3-Dimethylaminopropyl)-*N*′-ethylcarbodiimide hydrochloride ≥98% (EDC), *N*-Hydroxysuccinimide sodium salt 98% (NHS), and *N*-Hydroxysulfosuccinimide sodium salt (sulfo-NHS) ≥98% were all purchased from Sigma Aldrich. The enzyme *β*-Galactosidase from *Escherichia coli* Grade VI, lyophilized powder, 250-600 units/mg protein and the enzyme substrate fluorescein di(β-D-galactopyranoside) (FDG) were purchased from Sigma Aldrich. 2,4,6-Trinitrobenzenesulfonic acid (TNBS), Tris(2-carboxyethyl)phosphine hydrochloride powder, ≥98% (TCEP), tris(hydroxymethyl)aminomethane (TRIS) and 4-(2-Hydroxyethyl)piperazine-1-ethanesulfonic acid (HEPES), sodium chloride (NaCl), sodium bicarbonate ($NaHCO_3$) anhydrous solvents for synthesis dichloromethane (CH_2Cl_2), *N,N*-Dimethylformamide (DMF) were all purchased from Sigma Aldrich. Dialysis cellulose ester membrane (MWCO 3500 Da) was purchased from Roth and Bicinchoninic Assay protein quantification kit was purchased from Uptima (Montlouçon, France). Thiopyridone mercaptopropionic acid (TP-MPA) was synthesized by the procedure described by Xie et al.[1]. Maleimide succinimide ester was synthetized by the procedure described by Thibaudeau et al.[2]. Poly(dimethylsiloxane) PDMS sheets of 250 µm of thickness (Specialty Manufacturing Inc., Saginaw, Michigan, United States) and circular glass slides of 12 mm of diameter, 150 µm of thickness and less than 1 nm of roughness (Menzel-Gläser, Braunschweig, Germany) were chosen as substrates for the construction of polyelectrolyte multilayer films.

S1.2 Chemical modification of PLL with thiopyridone protecting groups (PLL-S-TP)

The modified poly(L-Lysine) with thiopyridone groups (PLL-S-TP) was obtained in a two step reaction. The first step consists in the activation of the thiopyridone mercaptopropionic acid (TP-MPA) with the *N*-Hydroxysuccinimide (NHS) followed by the second step where the amines of the PLL will make a nucleophilic attack on the activated acid cited before.

S1.2.1 First step: activation of the TP-MPA acid with NHS

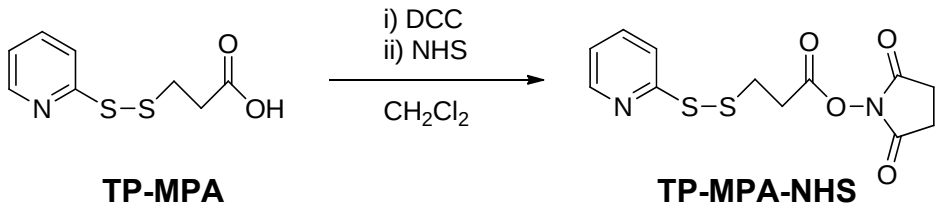

TP-MPA **TP-MPA-NHS**

The TP-MPA (186 mg, 0.864 mmol) was dissolved in 8 mL of CH_2Cl_2 followed by the addition of DCC (178 mg, 0.864 mmol, 1 eq) and NHS (99 mg, 0.864 mmol, 1eq). The reaction was stirred at room temperature for 24 h. The solution was filtered and the solvent was removed under pressure until dryness to obtain a yellow solid compound TP-MPA-NHS in a quantitative yield which will be used in the next step without further purification. The characterization of this compound is described in Xie et al.[1]

S1.2.2 Second step: coupling reaction between TP-MPA-NHS and the PLL

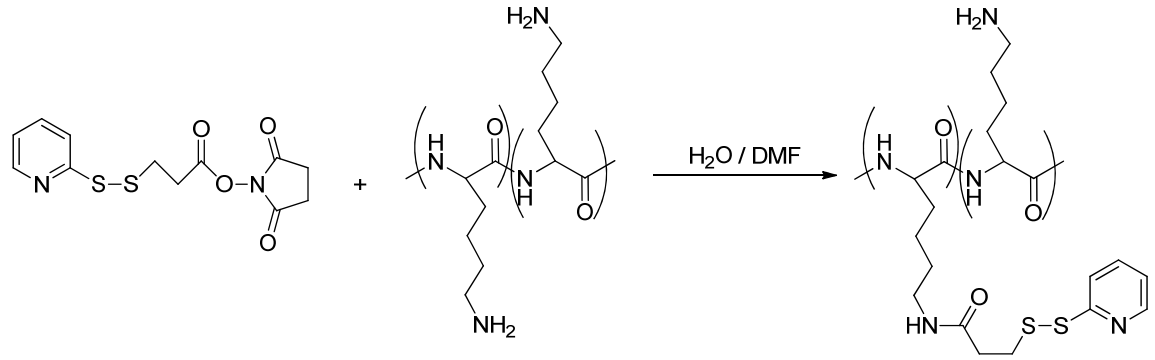

TP-MPA-NHS **PLL** **PLL-S-TP (27%)**

The PLL (300 mg, 1.44 mmol) was dissolved in 15 mL of Milli-Q water followed by the addition of a solution of TP-MPA-NHS (269.9 mg, 0.864 mmol, 0.6 eq) in 3 mL of DMF. The reaction was stirred at room temperature for 24 h. The solution was filtered and dialyzed (cellulose ester membrane (MWCO 3500 Da)) against a 2 L solution of NaCl 0.30 M for 1 day at 4°C and then changed two times against 2 L of Milli-Q water for another 2 days at 4°C. Lyophilisation of the solution afforded PLL-S-TP as a white like foam with a 75 % yield.
^{1}H NMR (D_2O, 400 MHz, δ ppm): 8.20 (br s, 1H, Ar), 7.75 (br s, 2H, Ar), 7.20 (br s, 1H, Ar) 4.25 (br s, 1H, CαH), 3.05 (br s, 2H, CH_2 thiopyridyl), 2.99 (br s, 4H, $NHCH_2CH_2CH_2$), 2.60 (br s, 2H, CH_2 thiopyridyl) 1.85 (br m, 6H $CH_2CH_2CH_2$), 1.40 (br s, 6H, $CH_2CH_2CH_2$).

By comparison of the integration of one aromatic signal and the integration of the broad singlet at 4.25 (H on the carbon α of the lysine amino acid), the percentage of modification on the PLL by thiopyridone groups is be estimated to be 27%

S1.3 Chemical modification of β-Galactosidase with maleimide groups (β-Gal-mal)

S1.3.1 Chemical modification

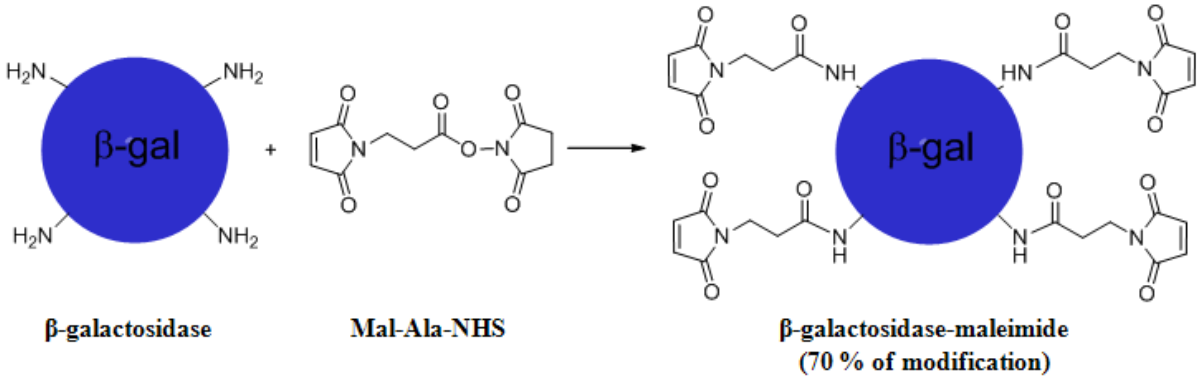

β-Galactosidase from *Escherichia coli* (7 mg, 1.61×10^{-5} mmol) was dissolved in 1 mL of $NaHCO_3$ 0.1 M at pH 8.5 followed by 4 mL of HEPES 50 mM at pH 6. Then, 500 µL of a 1 mg/mL (0.5 mg, 1.87×10^{-3} mmol) 3-(Maleimido)propionic acid N-succinimidyl ester (Mal-Ala-NHS) solution in DMF is added to the β-Galactosidase solution and stirred at room temperature for 3h. The solution was dialyzed (cellulose ester membrane (MWCO 10 000 Da)) against a 2 L solution of 50 mM HEPES and two times against a 2 L solution 10 mM HEPES pH 6 at 4°C for 3 days. Aliquots of 250 µL were prepared and conserved at -20°C. The modified enzymes with thyopiridone groups were not lyophilized after chemical modification. The reason to avoid the lyophilisation of the modified enzyme is the loss of enzymatic activity detected in previous experiments after this treatment.

S1.3.2 Determination of the modified enzyme concentration

We used the bicinchoninic acid (BC) Assay test to determine the concentration of the solutions of the modified enzyme[3]**.** A fresh set of protein standards, from 20 µg/mL to 1 mg/mL, were prepared using the Bovine Serum Albumin (BSA) at 2 mg/mL. Solutions of the sample β-Galactosidase-maleimide and the control β-Galactosidase at 1 mg/mL were prepared and then diluted to 0.25 mg/mL in an aqueuse solution of $NaHCO_3$ 0.1M at pH 8.5. 100 µL of each standard, control and sample were then pipettes in test tubes. Then 2 mL of BC Assay

reagent (mixture of 50 parts of bicinchoninic acid and 1 part of $CuSO_4$) were added to the test tubes, mixed and incubated at 60°C for 20 min. All the test tubes were mixed at room temperature and their optical absorbance read at 562 nm against the blank $NaHCO_3$ in a 96 well cell plate. Then the proteins concentration can be calculated with a reference curve obtained for a standard protein (figure S1). Finally, we obtained a concentration of 0.4 mg/mL for β-Gal-mal and 0.5 mg/mL for β-Gal.

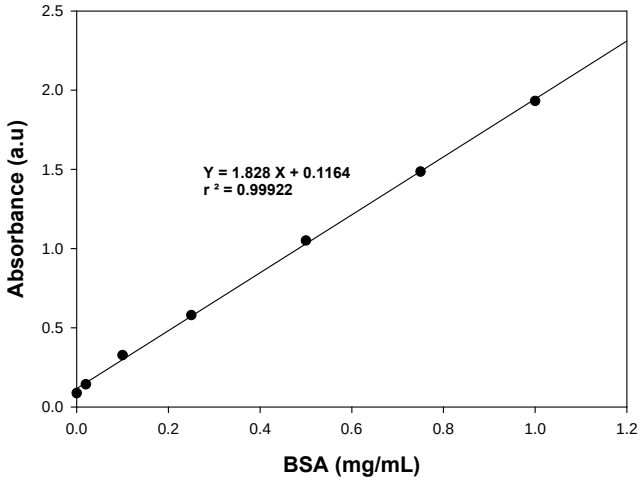

Figure S1: Calibration curve to determine the concentration of enzymes before and after the chemical modification. Each black point corresponds to a measurement of the absorbance of different standard solution concentration and the black line is the linear regression of these values.

S1.3.3 Verification of the catalytic activity of the modified enzyme

The enzymatic activity of the β-Gal-mal was verified against the unmodified enzyme β-Gal in presence of the substrate fluorescein di(β-D-galactopyranoside) (FDG). The principle of this experiment is the hydrolysis in 2 steps of the FDG in the presence of the enzyme to obtain fluorescein (Scheme S1).

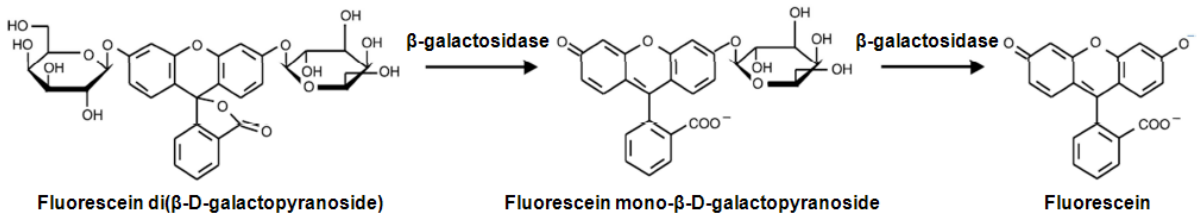

Scheme S1: Sequential hydrolyse reaction of the FDG by the β-Galactosidase

This fluorescent product is detected as a function of time giving the enzymatic kinetics with a multidetector Spectrofluorimeter SAFAS Xenius XC equipped with microplates reader ($\lambda_{ex/em}$: 495 nm / 519 nm). In a 96 well cell plate, we added 200 µL of FDG at 0.071 mg/mL and 50 µL of the enzymes separately at 0.0048 mg/mL. Then, the catalytic activity was recorded with the spectroflorimeter SAFAS. The results are presented in figure S2 where the slope of the curve indicates the activity of the enzymes. The activities for the unmodified and modified enzymes are 0.08 a.u and 0.02 a.u respectively. β-Gal-mal appears thus 4 times less active than non modified β-Gal. There was thus a loss in the enzymatic activity of the β-Gal after the chemical modification.

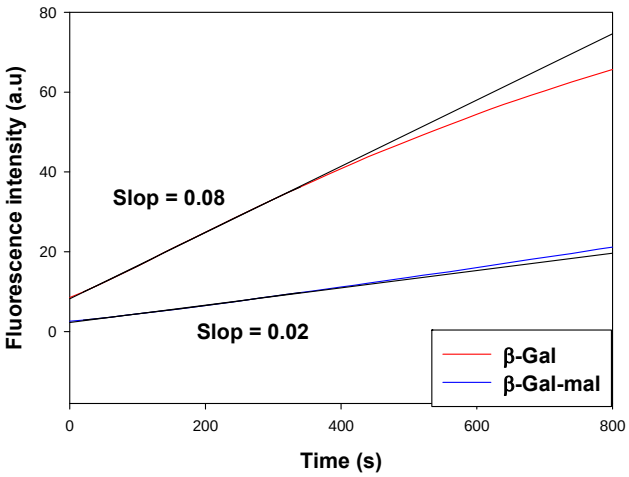

Figure S2: Comparison of the enzymatic activity between the modified and unmodified enzyme β-Galactosidase. The black lines represent the linear regression curves for a same period of time.

S1.3.4 Free-amines TNBS test

The grafting rate on the modified β-Gal with maleimide groups was obtained using the 2,4,6-Trinitrobenzenesulfonic acid (TNBS) also known as picrylsulfonic acid. This test consists in the complexation between the picrylsulfonic acid and the primaries amines groups that are present on the protein to form a highly chromogenic derivative[4] (**Scheme S2**).

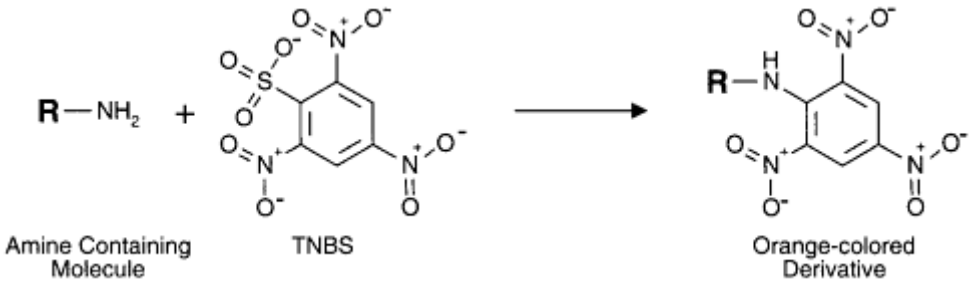

Scheme S2: TNBS may be used to detect or quantify amine groups through the production of a chromogenic derivative.

Different concentrations of glycine (standard) were prepared ranging from 10^{-1} mM to 10^{-3} mM in 0.1 M of $NaHCO_3$ at pH 8.5 from glycine 1 mM. 1 mL of the standard solutions was mixed with 25 µL of a 30 mM picrylsulfonic acid solution. In the same way, 300 µL of the control β-Gal and sample β-Gal-mal at 0.1 mg/mL in 0.1 M of $NaHCO_3$ pH 8.5 and 7.5 µL of a picric sulfonic acid solution were added into the eppendorfs. They were incubated for 40 min at room temperature. After that 200 µL of the standards, control and sample were transferred into a 96 cells well plate and the optical absorption was measured at 420 nm in a Spectrofluorimeter SAFAS. In figure S3, the lysine concentration can be calculated with a reference curve obtained for a standard acid amine glycine. The grafting rate was calculated from the relation:

$$\boldsymbol{GR = \frac{modified\ groups}{total\ groups} = \frac{total\ group - non\ modified\ groups}{total\ groups}}$$

where: total and non modified groups represents the UV absorbance of the β-Gal and β-Gal-mal respectively.

A grafting rate of 70% was obtained after modification of the β-Gal with maleimide groups.

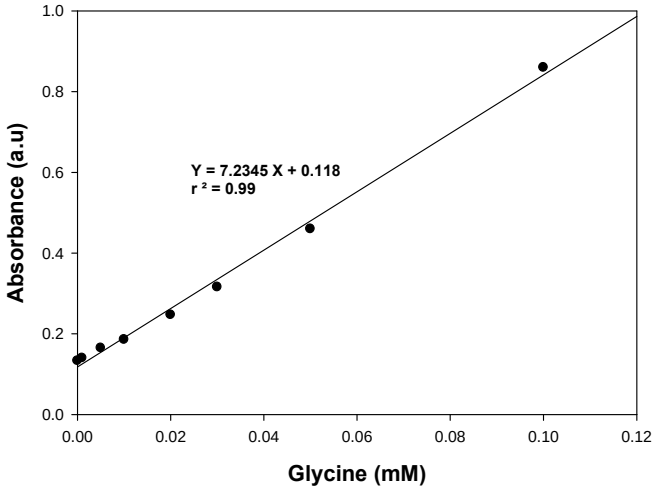

Figure S3: Calibration curve to determine the grafting rate of maleimide groups on the β-Gal-mal. Each black point corresponds to a measurement of the absorbance of different standard Glycine concentration solution and the black line is the linear regression of these values.

S1.4 Chemical modification of enzymes with fluorophores

S1.4.1 Chemical modification of β-Gal with FITC (β-Gal^{FITC})

3.1 mg of β-Gal was disolve in 3 mL of 100 mM $NaHCO_3$ buffer at pH 8.5 followed by the addition of 3.75 µg of FITC in methanol solution. The reaction mixture was stirred for 3 h at room temperature and dialysed with a cellulose ester membrane (MWCO 3500) against a 2L solution of NaCl 0.3 M for 8 h and finally with 2L of Milli-Q water for another 24h. Lyophilisation of the solution afforded 2.5 mg of β-Gal^{FITC} as a yellow powder.

S1.4.2 Chemical modification of β-Gal-mal with FITC (β-Gal-mal^{FITC})

2 mg of β-Gal-mal was disolve in 3 mL of 100 mM $NaHCO_3$ buffer at pH 8.5 followed by the addition of 3.75 µg of FITC in methanol solution. The reaction mixture was stirred for 3 h at room temperature and dialysed with a cellulose ester membrane (MWCO 3500) against a 2L solution of NaCl 0.3 M for 8 h and finally with 2L of Milli-Q water for another 24h. Lyophilisation of the solution afforded 1.7 mg of β-Gal-mal^{FITC} as a yellow powder.

S2. Stretching device

Figure S4 represents the homemade stretching device used for the experiments. It is made on stainless steel and it allows stretching manually the sample in an unaxial direction. The silicone sheet covered with the enzymatic active film is inserted in two jaws. These jaws can be moved continuously one with respect to the other. This stretching device is inserted in a black support made of poly(methylmethacrylate). This support was conceived to use the minimum amount of enzyme substrate (FDG). It also allows taking fluorescence measurements in the solution with a multidetector Spectrofluorimeter SAFAS Xenius XC equipped with microplates reader ($\lambda_{ex/em}$: 495 nm / 519 nm) without any interference of the stretching device.

The stretching rate (α) is defined by the relation $\alpha = (l - l_0)/l_0$ where l and l_0 represent respectively the length of the stretched and unstretched states. All the experiments were done at room temperature with the PEM coated silicone side facing down.

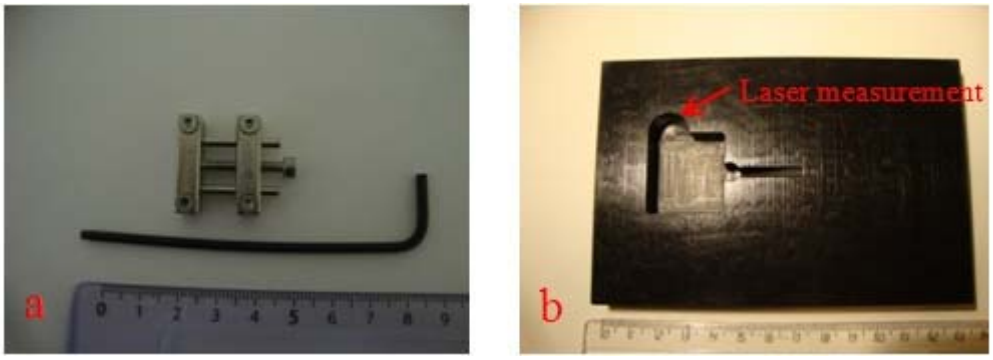

Figure S4: a) Device used for the stretching of modified silicone sheets. The silicone sheet is placed between the two clams and stretched manually. b) The black support where the red arrow indicates the fluorescence measuring with a spectrofluorimeter microplate reader.

S3. Experimental methods

S3.1 Spectrofluorometer with microplate reader

A multidetector Spectrofluorimeter SAFAS Xenius XC equipped with microplates reader was used to follow the catalytic activity of enzymes within the polyelectrolyte multilayer films supported on silicone sheets in contact with its substrate FDG ($\lambda_{ex/em}$: 495 nm / 519 nm). Thyopyridone group deprotection of PLL-S-TP were also monitored by UV experiments at 343 nm.

S3.2 Confocal laser scanning microscope (CLSM)

Confocal laser scanning microscope (CLSM) observations of polyelectrolyte multilayer films were carried out with a Zeiss LSM 510 microscope using a x 40/1.3 oil immersion Objective and with 0.43 μm z-section intervals. FITC fluorescence was detected after excitation at λ = 488 nm with a cut-off dichroic mirror of 488 nm and an emission band-pass filter of 505–530 nm (green emission). An average of three images in the same location was acquired at 256x256 pixels. Virtual film section images were taken from the film in the presence of liquid (NaCl 0.15 / TRIS 10 mM), hence allowing the determination of the thickness of the film. All the experiments are performed in the presence of liquid (0.15 M NaCl/10 mM Tris, pH =7.4) and the multilayer films were never dried.

S4. Mechanoresponsive film construction

S4.1 Multilayer film construction

Multilayers films were built with an automated dipping robot (Riegler & Kirstein GmbH, Berlin, Germany) on silicone sheets SMI of 254 μm thickness or microscope slides. Silicone sheets of 18×18 mm^2 were previously cleaned with ethanol and then extensively rinsed with water. The polyelectrolytes used for the construction of the multilayers were dissolved in a 0.15 M NaCl solution prepared with ultrapure water (18.2 MΩ.cm Milli-Q plus system, Millipore) and used at a concentration of 1 mg/mL. Silicon substrates were first dipped in a PLL solution (polycation) for 4 min. Then, two rinsing steps were performed by dipping the sheets two times for 5 min in 0.15 M NaCl solution. The polyanion (HA) was then deposited in the same manner. The buildup process was pursued by the alternated deposition of PLL and HA. After deposition of *n* bilayers, the film is denoted $(PLL/HA)_n$. We used films constituted of 24 PLL/HA "bilayers". In the case of the $(PLL\text{-}S\text{-}TP/HA)_{24}$ film construction, the same protocol was used changing the polycation by PLL-S-TP.

S4.2 Reticulation conditions of the PLL/HA films by EDC/NHS

We first determined the best reticulation conditions of PLL/HA multilayers with the goal to obtain a film that can be stretched without cracking. The PLL/HA films were constructed as reported above. The last layer constituted of PLL^{FITC} (PLL labelled with

fluorescein) was deposited manually under similar conditions. The pH of a 0.15 mol/L NaCl solution was adjusted to 5.5. The presence of TRIS is to be avoided because TRIS contains primary amines which can react during the film cross-link. The slightly acidic conditions constitute a good compromise between activation of the carboxylic acid groups through EDC and a good amide formation rate[5]. Different reticulation conditions using different EDC and sulfo-NHS conditions were then tested in order to fulfil the non-cracking condition up to a stretching rate of at least 100% observed by fluorescence optical microscopy.

Reticulation was realized by bringing a $(PLL/HA)_{24}/PLL^{FITC}$ film in contact with a solution containing both EDC and NHS for a given cross-linking time at 4°C. At the end of the cross-linking step the film was rinsed 3 times during 1h with a NaCl solution. The last rinsing step was performed with a NaCl/TRIS, pH 7.4 buffer solution. In order to determine the ultimate stretching degree before cracking, the cross-linked films were fixed in a home-made stretching device and observed under an epifluorescence microscope. The obtained results are summarized in table S1 below.

Test n°	[EDC] (10^{-3} mol/L)	[sulfo-NHS] (10^{-3} mol/L)	Cross-linking time (hours)	Critical stretching rate (± 5%)
1	200	50	1	44 %
2	200	50	2	32 %
3	200	50	19	18 %
4	2	0.5	2	No crack
5	20	50	15	161 %
6	50	50	15	68 %
7	100	50	15	54 %
8	20	50	19	163 %
9	40	50	19	76 %
10	50	50	19	69 %

Table S1: Summary of the experiments performed to determine the optimal conditions of the PLL/HA film cross-linking through EDC/sulfo-NHS. The columns [EDC] and [sulfo-NHS] corresponds to the molar concentrations by mixing EDC and sulfo-NHS. The critical stretching degree was evaluated optically.

Francius et al. have shown that the EDC and sulfo-NHS concentrations corresponding to tests 1 and 3 lead to a maximum of cross-linking after 18 hours[6]. It appears that for sample 3 prepared with 19 hours of cross-linking, the critical stretching degree (stretching degree at

which one observes the first cracks) is very small. A stretching of 18 % already leads to cracks perpendicular to the along the entire film in test n° 3. When the concentration of both compounds is divided by a factor of 100 and the cross-linking time is reduced to 2h (sample n°4), the films do not break up to a stretching degree of 250 % (the highest stretching degree that is reachable experimentally). Yet it is expected that this sample is almost identical to the native one *i.e.* almost not reticulated. When [sulfo-NHS] = 50 mM and 40 ≤ [EDC] ≤ 100 mM, cracks appear at stretching degrees comprised between 50 and 80 % (figure S5). Yet, to obtain a stretching degree that exceeds 100 %, the EDC concentration had to be reduced to 20 mM (samples 5 and 8). Diminishing the cross-linking time from 19 to 15h does not seem to change significantly the result. Finally by using [sulfo-NHS] = 50 mM and [EDC] = 20 mM and a reaction time of 15 hours, a critical stretching degree of 160 % could be obtained. These are the conditions that were used throughout this study.

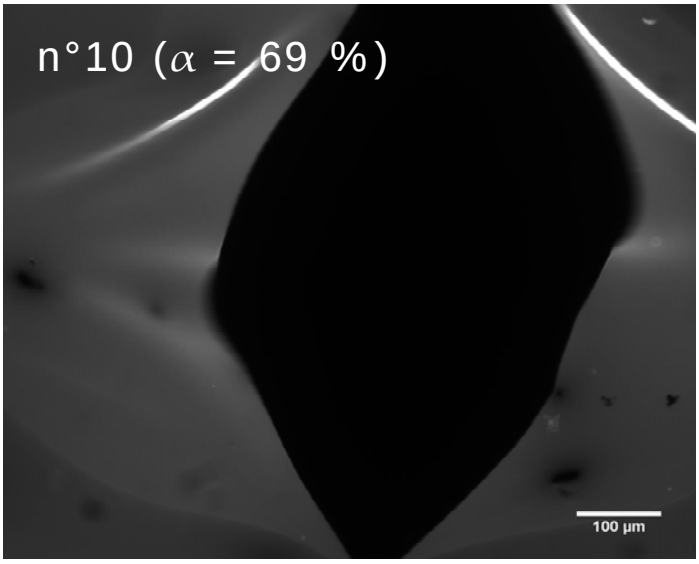

Figure S5: Image realized by epifluorescence microscopy of the surface of sample 10 of table S1. The film is stretched and cracks appear at a stretching degree of 69%. The stretching is performed along the direction indicated by the length bar. The image is in grey levels corresponding to an excitation wavelength between 465-495 nm and emission wavelength between 515-555 nm.

S4.3 Deprotection of thyopiridone groups on PLL-S-TP

The sample was put in the home made stretching device that was previously coated with parafilm to prevent leaking of the aqueous solution after its addition. A 100 µL β-Gal-

mal (0,4 mg/mL) in NaCl/TRIS solution was added on the sample containing the cross-link polyelectrolyte multilayer film (PLL-S-TP/HA) supported on PDMS for 1h. Later, the enzyme solution was pippeted and replaced by 150 µL of TCEP 1 mM solution prepared in NaCl/TRIS at (t = 0). Sampling 150µL of TCEP solution was done every 5 min and replaced by other 150 µL of TCEP solution. UV measurements at 343 nm wavelength were performed with a multidetector Spectrofluorimeter SAFAS Xenius XC equipped with microplates reader in a 96 well-cell-plate with 100 µL of the sampling solution for each period of time and total time of 30 min. Full deprotection of thyopiridone groups are completed after 30 min of treatment with TCEP solution (figure 8 in the publication).

S4.4 Cross-linking of the enzyme β-Galactosidase-maleimide within the PEM film

The reticulated PEM film on silicone sheets was placed in a homemade stretching device. The homemade device was held together tightly with clips that were previously coated with parafilm to prevent leaking of the aqueous solution after its addition. 100 µL of β-Gal-mal at 0.4 mg/mL prepared in NaCl/TRIS buffer solution was then added for 1h. The modified enzyme was later pippeted and replaced by 200 µL of 1 mM TCEP prepared in 0.15 M NaCl/10 mM TRIS buffer solution for 30 min. Finally, the PEM film was rinsed with the buffer solution 0.15 M NaCl / 10 mM TRIS at pH 7.4.

S4.5 Enzymatic kinetics

The sample in the homemade stretching device was placed in the black support and then 3.8 mL of FDG at 0.5 mg/mL prepared in the buffer 0.15 M NaCl / 10 mM TRIS at pH 7.4 solution was added. The fluorimetric measurements were then taken with a Spectrofluorimeter SAFAS Xenius XC ($\lambda_{ex/em}$: 495 nm / 519 nm**)** at different stretching rates. The linear regime of the catalytic activity was chosen to plot the data (figure 4, 5, 7, and 9).

S4.6 Determination of the amount of β-Gal-mal enzymes present in the cross-linked PLL-S-TP/HA film.

We adapted a method developed by Vodouhe et al.[7] to determine the amount of β-Gal-mal enzymes present in the cross-linked PLL-S-TP/HA film.

After PLL-S-TP/HA film construction, cross-linking the film through 20 mM EDC / 50 mM NHS solution as described above, the film was brought in contact with an ethanolamine 1 M solution prepared in 0.15 M NaCl for 40 min. This treatment will desactivate the still active carboxylique groups within the film. Later, a 400 µL of β-Gal-mal^{FITC} solution at 0.5 mg/mL was added for 1 h, after that the enzyme solution was pippeted and replaced by 500 µL of 1 mM TCEP solution for 30 min. Finally, the PEM film was rinsed with the buffer solution 0.15 M NaCl / 10 mM TRIS at pH 7.4. Several images were then taken by confocal microscopy of the film at different locations in order to determine the mean fluorescence and thickness in the film equals to 1272 a.u and 7 µm respectly.

We then removed the film from the confocal microscope and replaced it with a glass slide onto which we deposited 100 µL of β-Gal-mal^{FITC} at 0.5 mg/mL solution. Successively, the concentration of the β-Gal-mal^{FITC} was diluted with the addition of NaCl/TRIS solution. For each concentration, the fluorescence was measured in the solution again by using the confocal microscope with the same experimental parameter setups as for the measurements in the film. This allowed determining a calibration curve (figure S6) and we could calculate the concentration of β-Gal-mal^{FITC} inside the polyelectrolyte multilayer using the fluorescence value recorded in the film. Finally, the concentration of β-Gal-mal^{FITC} in the PLL-S-TP/HA film was about 0.85 mg/mL, when 400 µL of β-Gal-mal^{FITC} at 0.5 mg/mL were deposited on it.

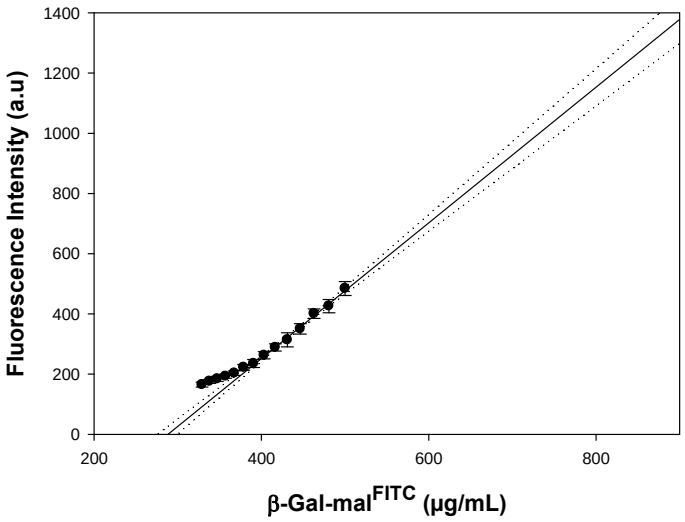

Figure S6: Calibration curve for the determination of the β-Gal-mal concentration in the PLL-S-TP/HA cross-linked film. The equation of the curve is I = 2.25 C – 648.92, where I is the fluorescence intensity in a.u and C the concentration of β-Gal-mal^{FITC} in µg/mL. The linear regression (black line) was done with a confidence interval of 95% (doted points).

S5. Fluorescence Recovery After Photobleaching experiments.

In order to verify if the enzymes are covalently coupled to the cross-linked (PLL-S-TP/HA)$_{24}$ film we performed Fluorescence Recovery After Photobleaching (FRAP) experiments. These experiments were performed according to a procedure described by Picart et al.[8]

After PLL-S-TP/HA film construction, cross-linking the film through 20 mM EDC / 50 mM NHS solution as described above, the film was brought in contact with an ethanolamine 1 M solution prepared in 0.15 M NaCl for 40 min. This treatment will desactivate the still active carboxylique groups within the film. Later, a 400 µL of β-Gal-mal^{FITC} solution at 0.5 mg/mL was added for 1 h, after that the enzyme solution was pippeted and replaced by 500 µL of 1 mM TCEP solution for 30 min. Finally, the PEM film was rinsed with the buffer solution 0.15 M NaCl / 10 mM TRIS at pH 7.4. The same protocol was used using β-Gal^{FITC} instead of β-Gal-mal^{FITC}.

The bleaching and imaging of the resulting polyelectrolyte film were performed on a Zeiss LSM 510 confocal microscope equipped with an argon laser (488 nm). During observation, the glass slides coated with the films were placed in a homemade sample holder filled with 1 mL of TRIS-buffered 0.15 M NaCl solution, in order to avoid drying of the film. A ×10 objective lens with a numerical aperture of 0.3 (Zeiss Plan Neofluar) was used. The

numerical zoom was fixed to ×2 in order to define a 460 × 460 µm^2 image (L = 460 µm). The area of an image was virtually subdivided into N × N = 512 pixels × 512 pixels. z-sections of the films were also obtained after deconvolution and reconstruction of (x, y) stacked images.

The FRAP protocol was as follows: First, a pre-bleach image of the sample was recorded. Then, using the bleaching tool of the software (Carl Zeiss AIM 510 version 3.2), we selected a circular area of diameter equal to 115.17 µm. This area was then bleached by scanning it 1000 times with a laser set at its maximum power. The ×10 objective used for photobleaching yields optical sections that are thicker than the film thickness itself: from 11 µm up to more than 50 µm, depending on the value of the pinhole diameter used. Consequently, the film was bleached over its whole thickness during this procedure. The bleach time was adjusted to achieve sufficient contrast between the bleached and nonbleached regions. After the bleach, images were acquired at times ranging from ca. 10 s up to ca. 2000 s to monitor the recovery process. These images were acquired by scanning the sample with the laser power carefully chosen to have an acceptable signal-to-noise ratio while avoiding strong bleach during image acquisition ("reading" step). The data were analyzed by following the procedure described by Picart et al.(ref 8).

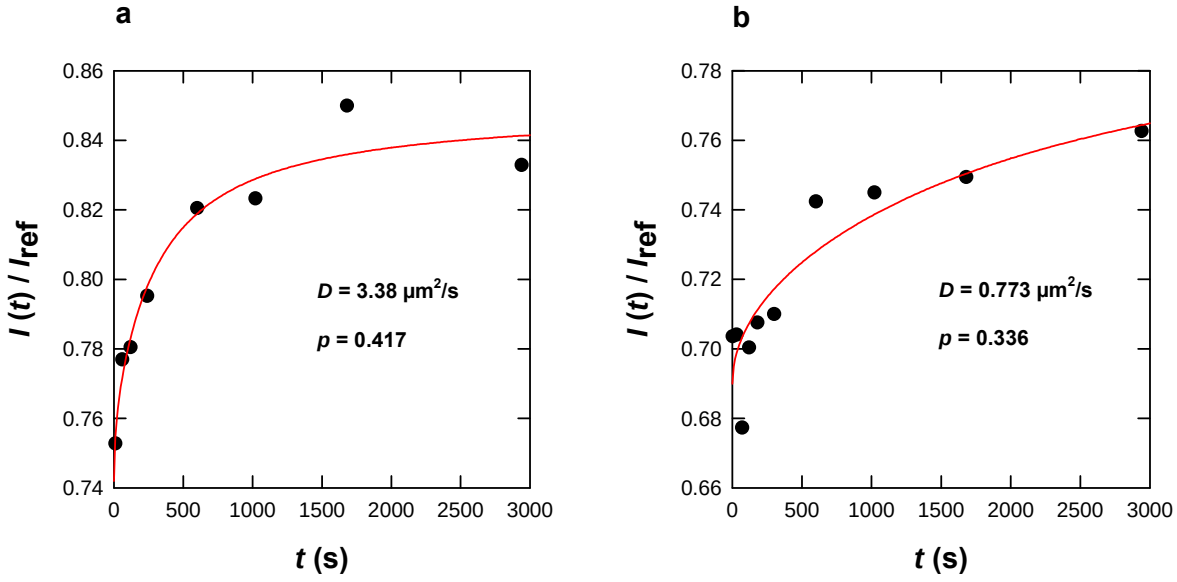

Figure S7: Fluorescence recovery intensity in function of time for a reticulated polyelectrolyte multilayer film with β-Gal^{FITC} (a) and β-Gal-mal^{FITC} (b). The mobile fraction population and the diffusion coefficient are represented by *p* and *D* respectively.

The results are shown in figure S7. We obtain a mobile fraction population for β-Gal-mal^{FITC} and β-Gal^{FITC} of 34% and 42% respectively. From these values, we cannot be sure

certainly that the enzyme is cross-linked inside the bulk. Therefore, we use, as a support, the results of the deprotection of the thiopyridone as an argument to explain the reaction between the maleimide and thiols groups present in the modified enzyme and in the PEM film respectively.

S6. References

(1) Xie, H. Z.; Braha, O.; Gu, L. Q.; Cheley, S.; Bayley, H. Single-molecule observation of the catalytic subunit of cAMP-dependent protein kinase binding to an inhibitor peptide *Chemistry & Biology* **2005**, 12, 109-120.

(2) Thibaudeau, K.; Leger, R.; Huang, X. C.; Robitaille, M.; Quraishi, O.; Soucy, C.; Bousquet-Gagnon, N.; van Wyk, P.; Paradis, V.; Castaigne, J. P.; Bridon, D. Synthesis and evaluation of insulin-human serum albumin conjugates *Bioconjugate Chemistry* **2005**, 16, 1000-1008.

(3) Smith, P. K.; Krohn, R. I.; Hermanson, G. T.; Mallia, A. K.; Gartner, F. H.; Provenzano, M. D.; Fujimoto, E. K.; Goeke, N. M.; Olson, B. J.; Klenk, D. C. Measurement of protein using bicinchoninic acid *Analytical Biochemistry* **1985**, 150, 76-85.

(4)Habeeb, A. Determination of free amino groups in proteins by trinitrobenzenesulphonic acid *Anal Biochem* **1966**, 14, 328–336.

(5) Hermanson, G. T., *Zero-length crosslinkers - EDC plus sulfo-NHS. In Bioconjugate Techniques*. (Second Edition) ed.; Academic press: New York, **2008**; p 219-223.

(6) Francius, G.; Hemmerlé, J.; Ohayon, J.; Schaaf, P.; Voegel, J.-C.; Picart, C.; Senger, B. Effect of crosslinking on the elasticity of polyelectrolyte multilayer films measured by colloidal probe AFM *Microscopy Research and Technique* **2006**, 69, 84-92.

(7) Vodouhe, C.; Le Guen, E.; Garza, J. M.; Francius, G.; Dejugnat, C.; Ogier, J.; Schaaf, P.; Voegel, J. C.; Lavalle, P. Control of drug accessibility on functional polyelectrolyte multilayer films *Biomaterials* **2006**, 27, 4149-4156.

(8) Picart, C.; Mutterer, J.; Arntz, Y.; Voegel, J. C.; Schaaf, P.; Senger, B. Application of fluorescence recovery after photobleaching to diffusion of a polyelectrolyte in a multilayer film *Microscopy Research and Technique* **2005**, 66, 43-57.

Chapter 6:

Stretchable polyacrylamide hydrogel covalently supported onto a silicone substrate: design of an ideal 3D polymeric network for mechanotransductive investigations

(article in preparation)

6.1 Abstract

Our group is in a strategy to develop chemo-mechano-responsive materials. Among the different possible ways to achieve this goal, the covalent coupling of mechano-responsive molecules into stretchable hydrogels constitutes one of the most promising option. Yet, hydrogels are usually fragile and thus difficult to stretch in particular when fixed into jaws. To circumvent this problem we propose here the first composite system made out of a silicone sheet onto which is covalently grafted a poly(acrylamide) gel that can be stretched up to 100% without breaking. This system is obtained by first treating the silicone substrate by UV ozone and then further silanizing it in order to graft acrylate groups onto the surface. The UV ozone treatment has to be optimized such as to avoid the formation of a brittle silicium oxide layer on top of the silicone substrate. The hydrogel is then formed by radical polymerization on top of the acrylate bearing surface. The conditions to obtain the poly(acrylamide) hydrogel are optimized such as to obtain the most stretchable hydrogel. The gels is characterized from a rheological point of view and has a Young modulus of the order of 5.7 kPa. The resulting system can be stretched up to 100% a large number of times and can be deformed at will without cracking the hydrogel and without altering the coupling of the gel on the silicone. This system constitutes an ideal starting material to develop hydrogel-based mechano-responsive materials.

6.2 Introduction

Smart materials are able to adapt themselves to their environment and thus are currently of considerable interest because of their potential uses in applications that range from drug delivery to camouflage systems, artificial muscles or tissue engineering.[1] Many external stimuli like pH[2, 3], temperature[4, 5], light[6, 7] or ionic strength[8, 9] may change the matter in a controlled way.[10, 11] Research that focuses on the control of the behaviour of material under mechanical deformation is a growing research field named *mechano-responsive material*.[12] To confer the property allowing the switching behaviour of the material under a mechanical stress one strategy is to insert mechano-responsive molecules into polymeric materials.[13] Mechano-reponsive molecules are force-sensitive entities able to chemically transform themselves from one molecular structure to another one under a mechanical stress, like stretching or squeezing.[14, 15] Recently, several mechano-sensitive smart materials have been described. Yet, almost all these studies have described systems able to change color when stretched.[16, 17] An important breakthrough in this field would be to tune the selectivity or the catalytic activity of a functional material, simply by stretching. To this goal, the selected material requires communicating with its environment and thus hydrogels appear as ideal candidates.[18] However, hydrogels are fragile and are not easy to handle and manipulate which are constraining practical problems met when the behaviour of these materials are studied under a mechanical stress. For example, stretching a hydrogel requires maintaining it between two crowbars which is often difficult to obtain because of the slippery feature of hydrogels. Bruns et *al*.[19] have recently reported the first mechano-sensitive polyacrylamide (PAM) hydrogel containing a green fluorescent protein (GFP) covalently attached to the polymeric network. Yet, when a very small deformation (up to 5%) is imposed to this chemical gel, little cracks appear immediately and thus no FRET signals are detected anymore. Several strategies have been investigated to get gels exhibiting high stretchability: development of hydrogels containing slide-ring polymers, branched poly(ethylene glycol) chains, double-network architectures or hybrid gels based on clay and dendritic binders.[20]

Here, we report the preparation of a robust elastomeric PAM hydrogel covalently supported on a silicone sheet. Easy and reversible stretching of the silicone sheet induces also the reversible stretching of the PAM hydrogel. This system is obtained by first functionalizing the silicone substrates by UV-Ozone (UVO) irradiation. This usually leads to the formation of a thin brittle silica layer. We first describe the optimization of the UVO treatment in such a way that stretching levels going up to 100% can be reached without seeing cracks on the

silicone surface. Next this surface is silanized in order to graft polymerisable methacrylate groups on the silicone substrate. We then show that in the presence of acrylamide and bis-acrylamide solutions, a poly(acrylamide) hydrogel can be obtained which is covalently attached to the substrate. The optimization of the acrylamide and bis-acrylamide composition is described in order to get system (silicone sheet + gel) that can be stretched up to 100% of stretching degree without inducing cracks in the gel. This gel is then characterized by rheology measurements.

6.3 Material and methods

6.3.1 Materials

Polydimethylsiloxane (PDMS) of 254 µm thick sheets Non-Reinforced Vulcanized (NRV) gloss/gloss (G/G) was purchased from Specialty Manufacturing Inc. (SMI) Saginaw, Michigan. Acrylamide powder 98,5% was purchased from Acros Organics. Acrylamide solution 40%, for electrophoresis, sterile-filtered, bis-acrylamide (N,N' methylenebisacrylamide) 99%, *N*,*N*,*N*′,*N*′-Tetramethylethylenediamine (TEMED) 99%, Ammonium persulfate (APS) 99% and Acetone technical grade were purchased from Sigma Aldrich. 3-(trimetoxysilyl)propylmethacrylate 97% was purchased from Alfa Aesar. Milli-Q water with a resistivity of 18.2 MΩ cm^{-1} was used to prepare the different aqueous solutions.

UV-ozone. An UV-ozone Pro Cleaner Bio Force Nanosciences machine that has a mercury vapor lamp wavelength of 254 nm and 185nm with an UV intensity of 14.76 mW/cm^2 at 1 cm of distance from the sample was used for the measurements.

Contact angle measurements. Contact angle measurements were carried out using the DIGIDROP-GBX® coupled with a charge-coupled device CCD Camera and a total volume of 6 µL high-purity water dropwise. Measurements were made on both sides of the drop and were averaged. A series of three experiments were carried out for each treatment.

Infra-red spectroscopy. An FT-IR spectrometer Bruker Vertex 70 equipped with DTGS detector and an ATR (attenuated total reflectance) germanium crystal accessory was used for IR spectroscopy measurements. All spectra were acquired at 4 cm^{-1} resolution over 20 scans between a range of 4000 cm^{-1} and 600 cm^{-1}.

Optical microscopy. White light microscopy images were captured with inverted optical microscope Nikon Eclipse TE200 using a 40x objective lenses. Images were acquired with Nikon Digital Camera DS-Qi1Mc (with NIS-Elements software). Pictures were processed with ImageJ (http://rsb.info.nih.gov/ij/).

Environmental Scanning Electron Microscopy. PDMS's surface images were obtained by environmental scanning electron microscopy (ESEM, FEI Quanta 400) after placing the sample in a stretching home device machine (see Methods part below).

Rheometer. The rheological studies were carried out at 25°C using a controlled-stress rotational rheometer ThermoScientific-Haake Mars III with 35 mm diameter plate-plate geometry. The water evaporation of the hydrogels was avoided using a cover designed as a solvent trap. The Haake Rheowin-4 software was used for controlling the rheometer and analyzing experimental data. Hydrogel samples for rheological measurements were prepared by casting (pouring) the reaction mixture (described below) into a glass mold of cylindrical shape and, after polymerization, disk-shaped samples are obtained (diameter 35 mm matching the size of the measuring geometry, thickness c.a. 3-4 mm).

Preliminary oscillatory experiments were performed for each sample to determine the linear regime i.e. the stress range for which the storage modulus (G') and loss modulus (G'') do not depend on the applied stress (see figure S3 in supporting information). Then, the viscoelastic behavior in the linear regime was characterized by studying the variation of G' and G" for frequency sweeps ranging from 10 Hz to 0.01 Hz (100 rad/s to 0.1 rad/s). Creep-recovery experiments were also performed in the linear regime to confirm if the hydrogel adopt a viscous, an elastic or a viscoelastic behavior.

6.3.2 Methods

PAM gels preparation. Polyacrylamide gels were prepared using acrylamide, bisacrylamide (cross-linking monomer), tetramethylethylenediamine (TEMED) and ammonium persulfate (APS). These chemicals were all purchased from Sigma Aldrich except for the acrylamide and used for preparation of gels. The acrylamide solution was a commercial 40 % solution (400 g/L, 5.63 mol/L) which was diluted with ultra-pure water to reach the desired concentration. Bisacrylamide and persulfate solutions were prepared

extemporaneously at concentrations of 5 g/L (0.03 mol/L) and 54 g/L (0.24 mol/L) respectively using ultra-pure water. TEMED was used without dilution.

To prepare a polyacrylamide gel, a given volume of each reagent was successively introduced in a container in the following order: acrylamide, bisacrylamide, TEMED and finally the persulfate salt. The introduced volumes of reactants were always calculated to reach final concentrations of 0.03 mol/L for TEMED and 0.01 mol/L for ammonium persulfate. The mixture was vigorously shaken between each addition. For example, the polymerizable mixture could contain 400 µL 20 % acrylamide solution, 33 µL bisacrylamide solution, 1.8 µL TEMED and 25 µL ammonium persulfate solution, leading to a gel preparation containing 2.82 mol/L acrylamide, $2.2*10^{-3}$ mol/L bisacrylamide, 0.03 mol/L TEMED and 0.01 mol/L APS.

Preparation of PAM hydrogel covalently linked on silicone sheet. The surface of a PDMS (3cm x 1cm x 0.2cm) was activated in the UVO machine during the desired time. The silicone sheet was then gently transferred into a petri glass dish with the activated face up. A 10% (v/v) fresh solution of 3-(trimethoxysilyl)propylmethacrylate in acetone was added until the silicone's surface was fully covered. It was left at room temperature on a horizontal agitation plate for 1h and finally rinsed with a large amount of acetone. The silicone sheet was then dried with N_2 gas and put into another petri glass dish. A solution mixture of acrylamide (3 mL of 40wt% aqueous solution), bisacrylamide (498 µL of 5 mg/mL aqueous solution), MilliQ-water (3 mL), TEMED (18µL) and the initiator APS (249 µL of 54 mg/mL aqueous solution), one after the other in this order, were added covering the surface of silicone sheet. The solution is then mixed using a pasteur's pipette without making air bubbles. This was left at room temperature without stirring. The polymerization reaction occurs during 12 hours. Finally the hybrid system of silicone-hydrogel was taken out with a scalpel.

Stretching device. The homemade stretching device used for the experiments of the PDMS surface modification with hydrogels is presented in Supporting Information. It is made of stainless steel and it allows stretching manually the sample in uniaxial direction. Pictures are given in figure S1 in Supporting Information (SI). The level of stretching is expressed as the percentage of the initial length: for instance, stretch at 100% means to double the initial length of the material.

6.4 Results and discussion

6.4.1 Design of the PAM hydrogel supported covalently on silicone sheet

PAM hydrogel is a polymeric network built from acrylamide and bisacrylamide mixtures by radical polymerisation in water.[21] The buildup is initiated with the radical initiator ammonium persulfate (APS) in the presence of tetramethylethylendiamine (TEMED): the TEMED reacts with APS to form *in situ* radical species which are the real initiators of the polymerisation. To anchor a PAM hydrogel onto a silicone surface, it is necessary to graft covalently polymerizable groups on this surface. Thus, polyacrylamide chains can start from the surface and meet some others growing PAM chains in solution and finally create the polyacrylamide network. The modification of the silicone sheet could be done in two steps according to methods described in the literature. Treatment by UV-ozone (UVO) provides a highly hydrophilic silicone surface due to the formation of silanol groups (Scheme 6.1a). To ensure a robust bonding between the PAM hydrogel and silicone, it is important to define the best conditions providing the higher density of hydroxyl groups without loosing the elasticity of the oxydized silicone surface. Then, this surface can be silanizated with 3-(trimethoxysilyl)propylmethacrylate leading to a surface covered with a layer of polymerisable methacrylate groups. Finally, PAM hydrogel polymerisation can be initiated on this modified silicone surface leading to a macroscopic hybrid material constituted of a layer of PAM gel covalently linked on a layer of silicone (Scheme 6.1b) and which can be stretched up to 100%.

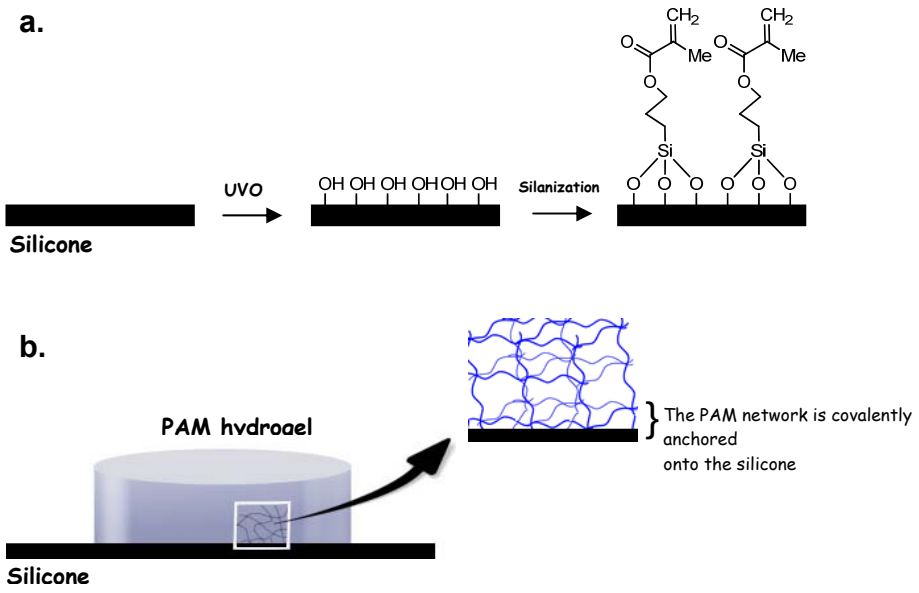

Scheme 6.1: General overview of the synthetic approach to get a stretchable silicone-PAM hydrogel material; (**a**) The silicone sheet is oxydized by using UVO treatment and then silanized with 3-(trimethoxysilyl)propylmethacrylate; (**b**) The polymeric chains of the PAM gel are covalently linked to the surface of the silicone.

First of all, we determined the optimum ratio between acrylamide and bisacrylamide to get a PAM hydrogel that does not break when stretched up to 100%. Next, the conditions of UVO treatment on the silicone were optimized providing a high density of hydroxyl groups without formation of a silicium oxide layer which would crack under stretching. Introduction of methacrylate groups on the silicone substrate was done through silanization. Next, the PAM gel is formed on the functionalized silicon surface.

6.4.2 Elastomeric PAM preparation

Before preparing PAM covalently anchored on functionalized silicone sheets we first determined the optimum acrylamide/bis-acrylamide ratio and concentration in order to obtain a handable and least fragile hydrogel. Because the hydrogels could not be inserted into jaws without breaking, we could not perform ultimate tensile strain measurements. We thus relied on a qualitative determination to evaluate if the gels are fragile or stretchable. This was done by stretching them by hand and appreciating the ultimate tensile strain. We kept the proportion of TEMED and APS constant and equal to 0.03 mol/L for TEMED and 0.01 mol/L for ammonium persulfate. Table 6.1 summarizes the obtained results.

[A+B](g/100mL)	A/B=60	A/B=1000	A/B=5000
5	1.1 kPa Fragile	(n.d.) Cannot be handled	(n.d.) Cannot be handled
10	16.5 kPa Fragile	0.7 kPa Fragile	(n.d.) Fragile
15	17.5 kPa Fragile	2.8 kPa Fragile	(n.d.) Fragile
20	17.5 kPa Fragile	5.7 kPa **Stretchable 150%**	(n.d.) Fragile
40	(n.d.) Fragile	50.9 kPa Stretchable 80%	5.6 kPa Stretchable 80%

Table 6.1: Summary of the results of the qualitative tests and the Young moduli E determined of the investigated gels from the storage modulus G' when $f \rightarrow 0$. (n.d.) represent systems for which G' depended upon f at small value of f so that the relation between G' and E could not be used. We varied the acrylamide (A) and bisacrylamide (B) concentrations as well as their ratio. Upper line corresponds to the Young modulus determined by dynamic rheology. By fragile we mean that rapid rupture occurs after stretching by less than a few percent. When stretchable, we give the ultimate tensile strain that is roughly estimated from experiments made by hand.

We performed rheological characterizations of several series of hydrogels prepared at different acrylamide/bisacrylamide ratio (A/B = 60, 1000, 5000) and different acrylamide+bisacrylamide concentrations (5, 10, 15, 20 and 40 wt%). Dynamic rheological properties (storage moduli (G'), loss moduli (G'')) were studied through oscillation experiments as a function of frequency, and additional information was gained from creep-recovery experiments. Furthermore, the Young moduli were determined from the value of G' extrapolated at $f \rightarrow 0$ (hydrodynamic regime) by using the relation E=3.G'. The raw data from which the Young moduli were determined are given in supporting information S2. The values of the Young moduli are given in table 6.1 when determined.

All the hydrogels prepared at the highest bisacrylamide content (A/B = 60) and at different concentrations (5, 10, 15, 20 wt%) exhibit somewhat similar rheological behaviors. As an example figure S2 shows the results obtained for the 15 wt% hydrogel. It can be observed that: (i) the elastic modulus G' is much higher than the viscous modulus G" over the entire range of oscillation frequency; (ii) G' does not depend on the oscillation frequency; (iii) G" is also almost independent of frequency. In addition, the phase difference between stress and strain is very low, $\delta < 3°$, i.e. $\tan \delta$ is close to 0 (data not shown). All these features

correspond to a nearly-perfect elastic material. This is confirmed by the creep-recovery analysis (figure S2) as shown by the very fast and constant deformation under the applied stress and the almost instantaneous and complete recovery when stress is removed. Such elastic properties are expected for macromolecular systems sufficiently cross-linked. The drawback of these strong gels is their low mechanical resistance leading to a rapid rupture after stretching by less than a few percent. We also obtained a Young moduli which increased in function of the [acrylamide + bisacrylamide] concentration from 1.1 kPa to 17.5 kPa for samples ranging from 5 – 20 wt% (table 6.1).

Conversely, the hydrogels prepared at the lowest bisacrylamide content (A/B = 5000) i.e. with a low cross-linking level exhibit poor elastic properties except when the concentration is high (40 wt%). In contrast with the previous case: (i) both G' and G" vary more or less as a function of frequency, depending on the polymer concentration; (ii) G' is higher than G" only for hydrogels with the highest concentrations (20-40 wt%) whilst the behavior is dominated by the viscous properties for the lowest concentration (10 wt%). Except for the 40 wt% hydrogel with good stretching properties, the other samples of this series are clearly insufficiently chemically cross-linked and behave rather as polymer solutions. Therefore, the Young moduli was determinated only for the sample of 40 wt% which is 5.6 kPa (table 6.1).

For the hydrogels prepared at the intermediate bisacrylamide content (A/B = 1000), the main rheological characteristic are the following (only data for 20 wt% are given as an example in figure S2): (i) the elastic modulus G' is always higher than the viscous modulus G" over the entire range of oscillation frequency; (ii) G' does not depend on the oscillation frequency (for 20 and 40 wt%) or vary slightly (for 10 and 15 wt); (iii) G" increases with the frequency for all the concentration. In comparison with the first case (A/B = 60), the viscoelastic behavior is therefore characterized by a lowered elasticity and an enhanced viscous character. This is more apparent by looking at the values of the phase difference δ at low frequencies that are much higher for A/B = 1000 ($\delta \approx$ 6-30°, i.e. $\tan \delta \approx$ 0.1-0.6, data not shown) than for A/B = 60. The creep-recovery experiments confirm that the hydrogels of the A/B = 1000 series are less strong (figure S2). These gels which are less fragile and withstand higher stretching (for concentration $\geq$ 20 wt%) appear both as viscous and elastic. The Young's moduli were determined with values of 0.7 kPa to 50.9 kPa from a [acrylamide + bisacrylamide] concentration ranging from 10 - 40 wt% respectively (see table 6.1).

Because mechanoresponsive materials should be obtained by grafting mechanosensitive molecules into these gels, it is of interest to use gels with the highest

possible Young moduli that remain stretchable. From the above rheological data, it comes out that the best compromise corresponds to the hydrogel with an [acrylamide + bisacrylamide] concentration of 20g/100mL and an acrylamide/bisacrylamide concentration ratio of 1000. This gel was stretchable up to 150%. Then, this hydrogel formulation was selected for the rest of the study. Yet under this form i.e. non-supported, the gel could not be inserted into mechanical devices for further experiments. This led us to the development of gels supported by a silicone elastomer.

6.4.3 Silicone sheet modifications

Following our strategy described above, the preparation of the PAM hydrogel covalently linked onto the silicone requires the introduction of methacrylate groups on the surface of a silicone sheet. We used a filler-free PDMS purchased from SMI. Various approaches can be used to modify the silicone but in almost all of them, the first step is a surface oxidation allowing the introduction of hydroxyl groups through silanol formation. Among all the chemical or physical methods described to do that[22], the oxygen plasma treatment is the most widely used method to oxidize the surface of PDMS.[23] Highly hydrophilic surfaces can be obtained but concomitantly one observes the formation of a thin layer of silicium oxide. This thin glass-like layer is brittle and thus not suitable to design a mechanotransductive substrate. Techniques using ultraviolet (UV) is another way extensively used to render hydrophilic the PDMS surface. In particular, using UV light in combination with ozone (UVO) allows a hydroxylation of silicone surfaces similar to those obtained with an oxygen plasma treatment. Despite the fact that this method is considerably slower (from few minutes to one or two hours) than the use of plasma (from few seconds to few minutes)[24], this difference can be advantageously used. It allows to vary the time of UVO exposition to find the optimum time allowing to both oxidize the silicone surface and to avoid the formation of glass silicium oxide.[25] Designing a mechanotransductive PAM gel requires to avoiding this silica-like layer in order to avoid cracks under stretching. PAM hydrogel linked onto these parts of cracked layer would not homogeneously respond when undergoing the mechanical tension.

First, we studied the influence of exposition time of PDMS under UVO on the formation of silanol group and the presence of cracks. Figure 6.1a shows the evolution of water contact angles of silicone sheets treated by UVO for increasing times.

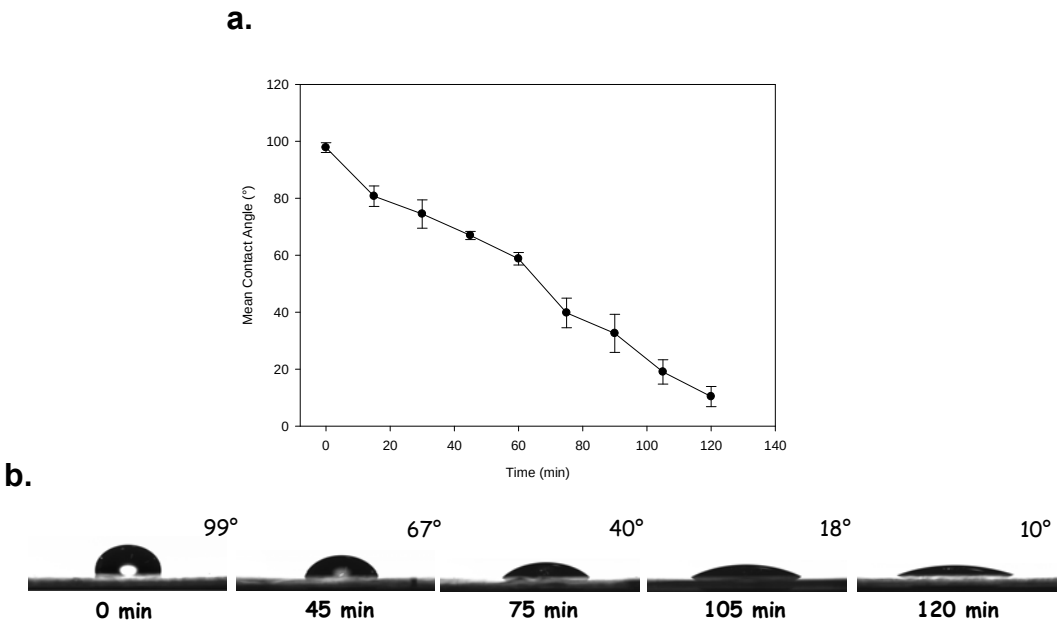

Figure 6.1: Evolution of the contact angle of water (**a**) on silicone SMI and exposed to UVO treatment at different time. All the contact angle measurements have been done directly after UVO oxidation. Error bars correspond to at least three measurements realized on various areas of the silicone surface; (**b**) Images of water droplet on SMI untreated by UVO and treated during 45, 75, 105 and 120 minutes. The number on the top of each droplet indicates the contact angle calculated.

The contact angle measurements have been done starting with an untreated silicone sheet after every 15 minutes of UVO treatment, up to 120 minutes. From a highly hydrophobic surface (contact angle of 99°), one observes a roughly linear decrease of the contact angle up to 8-10° after two hours of UVO treatment (see also figure 6.1b). The surface becomes more and more hydrophilic with the increase of the exposition time to UVO.

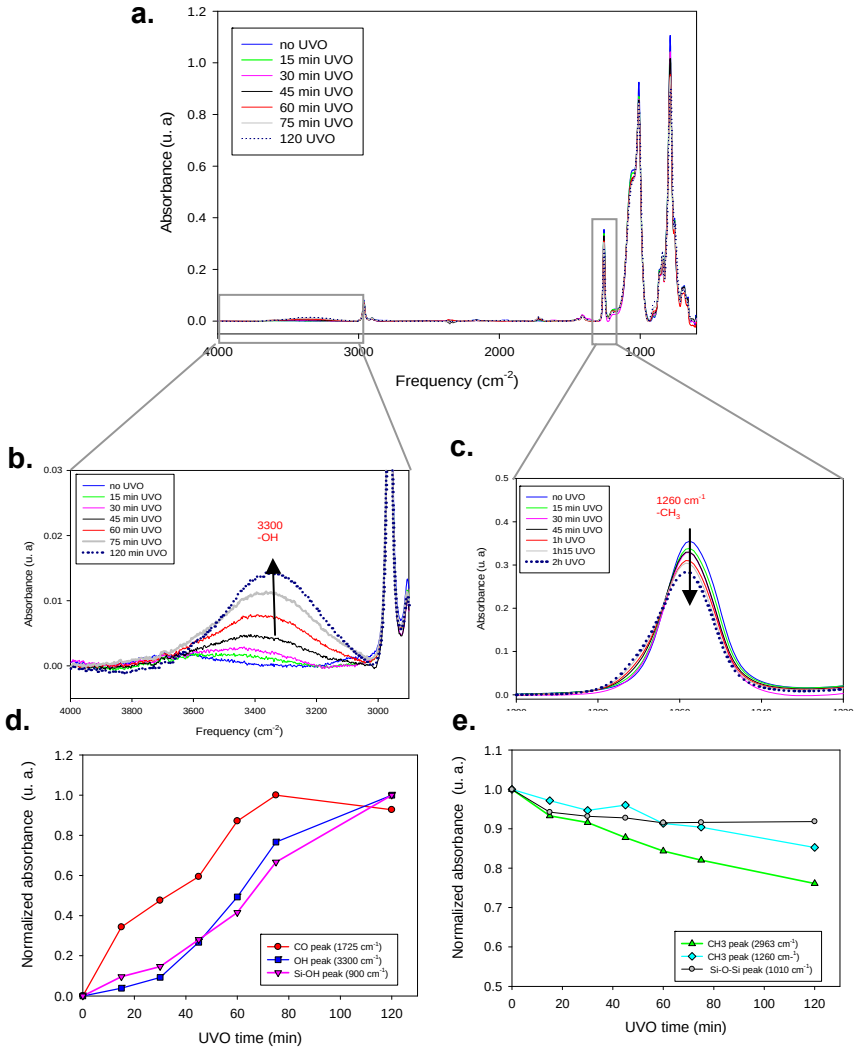

Figure 6.2: (**a**) Overlapping of the FTIR-ATR spectra of the silicon surface (SMI) at different time of UVO exposition; (**b**) Increasing of the band intensity localized at 3300 cm^{-1} with the UVO exposition time going from 0 to 120 min; (**c**) Decreasing of the band intensity localized at 1260 cm^{-1} with the UVO exposition time going from 0 to 120 min; (**d**) Evolution of the normalized IR vibration bands localized at 3300, 1725 and 900 cm^{-1}; (**e**) Evolution of the normalized vibration bands localized at 2963, 1260 and 1010 cm^{-1}.

The origin of this increasing hydrophilic feature with the exposition time of UVO can be explained by doing FTIR-ATR measurements of the treated silicone surface. A complete study about the UVO treatment on PDMS substrates monitored by several techniques of analysis, in particular FTIR-ATR, has been reported by Genzer and collaborators.[24] In agreement with their work, the monitoring of the FTIR-ATR spectra at different time of UVO exposition show the formation of polar groups, such as hydroxyl and carbonyl derivatives. In figures 6.2a, 6.2b and 6.2c is presented the overlapping of all the IR spectra measured on

silicone sheets at different exposition time of UVO: 15, 30, 45, 60, 75 and 120 minutes. As expected, a large band at 3300 cm^{-1} is growing with increasing the exposition time of UVO (figure 6.2b). The evolution of the normalized absorbance of this band is represented in figure 6.2d. This vibration band is assigned to the stretching band of the OH bond, probably due to the formation of the silanol groups. At the same time, one can observe a decrease in the intensities of characteristic bands of the $–CH_3$ such as 1200 cm^{-1} corresponding to the symmetric deformation band of the C-H bond (figure 6.2c), 2960 and 1010 cm^{-1} (see figure 6.2e) corresponding to the asymmetric CH_3 vibrations. Overlapping of FTIR spectra of all these vibration bands are given in figures S4 to S6. In figure 6.2d is also shown the evolution of the normalized absorbance of bands at 1725 cm^{-1} and 900 cm^{-1}. These bands are attributed to a vibration band of the carbonyl groups and to the stretching vibration of Si-O in silanol groups, respectively. Both of them display an increasing intensity of their band with the time of UVO exposition, indicating the formation of hydroxyl, aldehyde or carboxylic groups during the reaction of oxidation. However, between 60 and 120 minutes of UVO exposition, the normalized absorbance band intensity at 1725 cm^{-1} decrease slightly, meaning that a small proportion of carbonyl groups disappears, probably due to CO or CO_2 formation. Therefore, according to the results obtained by contact angle measurements and FTIR studies, we can conclude that the more the silicone sheet is exposed to UVO the more its surface has an hydrophilic feature due to hydroxyl groups formation.

It must be emphasized that this behaviour is very general but the exact time needed to reach a contact angle of 8-10° or the time evolution of the silanol groups depend upon the UV radiation intensity and the distance of the silicone surface from the UV source. Moreover, it is well known that the hydrophilic feature on these PDMS surfaces is temporary: after an oxidation treatment, the surface recovers its hydrophobicity with time due to the migration of short and uncrosslinked PDMS chains from the bulk to the surface.[25-27] Therefore, the FTIR-ATR measurements and the silanization process were done immediately after UVO treatment.

Before proceeding to the silanization step, we stretched the oxidized silicone sheet up to 100% of its initial length. We considered this level of stretching suitable to detect mechanotransductive effects. The silicone is stretched in only one (longitudinal) direction and observed by scanning electron microscopy (SEM). Our goal is to detect the eventually silica-like layer formed during the UVO treatment: when this layer is stretched, cracks must appear on the silicone surface. It must be noted that in some cases, the observation of very large crack formation can also be done with an optical microscope.

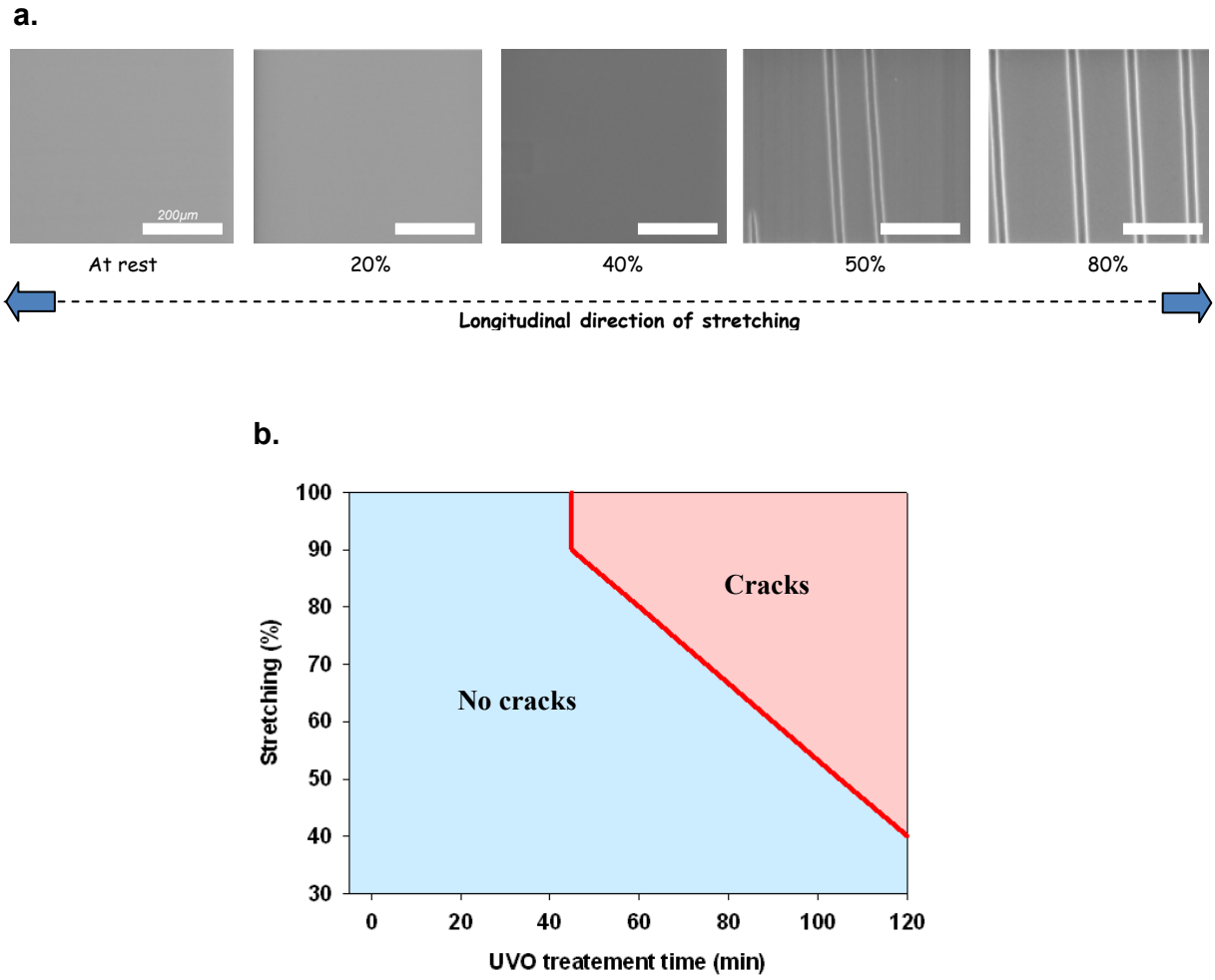

Figure 6.3: (**a**) Series of SEM images of silicone surfaces exposed to 105 minutes of UVO at rest and stretched at 20%, 40%, 50% and 80%. The white bar scale indicates 200µm; (**b**) Diagram showing the presence (red area) or absence (blue area) of cracks observed on silicone surface SMI exposed to a given UVO time and after stretching at a given level.

The use of SEM allows discerning the cracks at the microscopic size. We analysed several SEM images (1 x 1 mm^2) of silicone sheets exposed to various UVO treatment time up to 120 minutes. A series of SEM images of silicone sheet exposed to UVO during 105 minutes and stretched at 20%, 40%, 50% 80% are shown as a characteristic example in figure 6.3a. In this case, appearance of cracks occurred after 50% of stretching. Stretching at higher stretching degrees than 50% of the initial length of the silicone sheet led to more cracks formation, as expected. We did not stretch higher than 100% because it happened sometimes at this level of stretching that the silicone sheet ruptured at the crawbars. Gathering all our SEM observations of the silicones exposed at different time of UVO, we established the

diagram shown in figure 6.3b. Two distinct areas in the diagram appear clearly: a blue one where no cracks can be observed by SEM for a given UVO time and after a given stretching degree and a pink one where crack formation occurs. These two areas are separated by almost a straight red line. Below 50 minutes of UVO, we did not observe any cracks on exposed silicone for stretching degrees up to 100%. For exposition times higher than 50 minutes, cracks form at a critical stretching degree and this critical stretching degree decreases with the UV exposition time. This means that formation of the silica-like layer is mainly formed after 50 minutes of exposition time. It must be noted that the silicone sheets do not crack after one stretching process, they can be submitted to at least three stretching/unstretching cycles at the same stretching degree without showing any crack formation. More than three stretching/unstretching cycles were not tested.

6.5 Silanization and PAM hydrogel formation

Immediately after the UVO treatment, the freshly oxidized silicone sheet is fully immersed into a 10% solution of 3-(trimethoxysilyl)propylmethacrylate in acetone during one hour. Then, the silanized silicone is brought in contact with an aqueous solution containing acrylamide (A) and bisacrylamide (B) at a molar ratio of A/B=1000 and a concentration of A+B=20 g/100mL, TEMED and the initiator APS. Twelve hours after the addition of the radical initiator, the hybrid system of PAM hydrogel on silicone sheet is formed. We observed that when performing the reaction on a silicone substrate treated by UVO and silanization, the gel that form strongly adheres to the substrate (see figure 6.4a). When the same reaction is performed on a non-treated silicone the gel forms but it can easily be removed from the substrate showing that it is not covalently attached. Thickness of the PAM hydrogel does not seem to be a limiting parameter for the buildup of this system: by adding more solution of the acrylamide and bisacrylamide we obtained a grafted gel having 2 cm of thickness. By stretching this system with a home-made device (figure 6.4b et 6.4c), it was possible to reach 100% of stretching without the formation of cracks or the breaking of the gel or the silicone. The gel remained anchored on the silicone, even after five cycles of stretching/unstretching cycles between 0 and 100%. This system can be dried when standing 12 hours under a fumehood: the resulting gel become a glass-like material and strongly shrinks on itself (see figure S7). Rehydratation in deionized water allows returning to the initial size and the integrity of the system is not affected. When the silicone-PAM system is immersed in water, the gel swells up and the maximum mass of water included in the gel has been measured to be

three times the initial mass. Once again, three repeating drying and rehydration steps did not separate the PAM hydrogel from the silicone substrate. Guanidinium solution is known to break non-covalent interactions, in particular weak bonds like hydrogen bonds.[28] When the silicone-PAM gel system was immersed into a 1M solution of guanidinium chloride salt, the gel swelled strongly and in spite of 48 hours in this solution, no detachment of the gel from the silicone occurred. All these mechanical, physical and chemical tests demonstrate that the PAM hydrogel is efficiently bonded to the silicone. Delaminating experiments were impossible to investigate because the PAM gel breaks before the separation between the silicone and the hydrogel indicating the strong bond between the PAM hydrogel and the silicone.

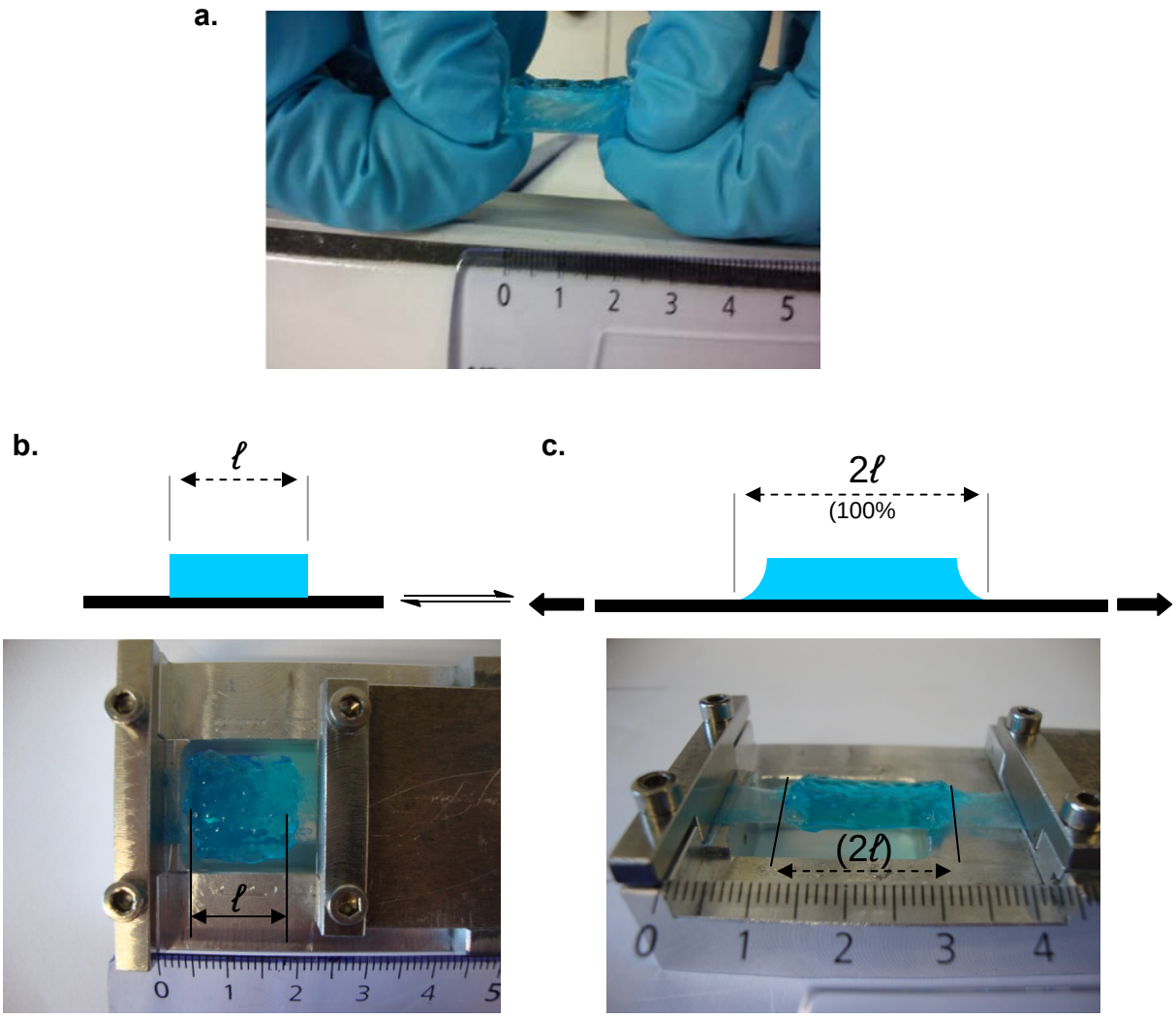

Figure 6.4: (**a**) Picture of a PAM hydrogel covalently supported on a silicone sheet and handle at both side through the non-functionnalized silicone substrate; Schematic representation and pictures of the PAM hydrogel bonded onto the silicone sheet (SMI) at rest

(**b**) and under (**c**) 100% stretch. To be visible, the PAM hydrogel has been coloured with several drops of 10 µl 1% methylene blue solutions.

6.6 Conclusion

Covalent grafting of polymers on silicone surface leading to thin film or brushes has been abundantly reported in the literature. Herein, we described the first preparation of a hybrid system constituted of a macroscopic-sized PAM hydrogel strongly supported onto a modified silicone substrate through covalent bonds. This bilayered system represents an original alternative in the development of new mechanosensitive material. Indeed, the need to design smart materials where the communication (catalysis, recognition, releasing, etc) with their surrounding environment can be controlled by stretching is of high interest. The approach proposed in this work allows the easy handling and stretching of the PAM hydrogel through the fixation of silicone into an adapted stretching device. Despite many cycles of releasing and stretching at 100%, drying and rehydrating, the PAM hydrogel stays fully bonded to the silicone surface. We believed that this idea can be helpful for the community working in smart material design.

6.7 References

(1) Yoshida, M.; Lahann, J. Smart Nanomaterials *ACS Nano* **2008**, 2, 1101-1107.

(2) Ionov, L.; Houbenov, N.; Sidorenko, A.; Stamm, M.; Luzinov, I.; Minko, S. Inverse and Reversible Switching Gradient Surfaces from Mixed Polyelectrolyte Brushes *Langmuir* **2004**, 20, 9916-9919.

(3) Burke, S. E.; Barrett, C. J. pH-Dependent Loading and Release Behavior of Small Hydrophilic Molecules in Weak Polyelectrolyte Multilayer Films *Macromolecules* **2004**, 37, 5375-5384.

(4) Motornov, M.; Sheparovych, R.; Lupitskyy, R.; MacWilliams, E.; Minko, S. Superhydrophobic surfaces generated from water-borne dispersions of hierarchically assembled nanoparticles coated with a reversibly switchable shell *Adv. Mater.* **2008**, 20, 200-205.

(5) Fulghum, T. M.; Estillore, N. C.; Vo, C.-D.; Armes, S. P.; Advincula, R. C. Stimuli-Responsive Polymer Ultrathin Films with a Binary Architecture: Combined Layer-by-Layer Polyelectrolyte and Surface-Initiated Polymerization Approach *Macromolecules* **2008**, 41, 429-435.

(6) Wu, L.; Tuo, X.; Cheng, H.; Chen, Z.; Wang, X. Synthesis, Photoresponsive Behavior, and Self-Assembly of Poly(acrylic acid)-Based Azo Polyelectrolytes *Macromolecules* **2001**, 34, 8005-8013.

(7) Zakrevskyy, Y.; Richter, M.; Zakrevska, S.; Lomadze, N.; von, K. R.; Santer, S. Stimuli-Responsive Materials: Light-Controlled Reversible Manipulation of Microgel Particle Size Using Azobenzene-Containing Surfactant *Adv. Funct. Mater.* **2012**, 22, 5064.

(8) Bajpai, A. K.; Shukla, S. K.; Bhanu, S.; Kankane, S. Responsive polymers in controlled drug delivery *Progress in Polymer Science* **2008**, 33, 1088-1118.

(9) Bawa, P.; Pillay, V.; Choonara, Y. E.; du, T. L. C. Stimuli-responsive polymers and their applications in drug delivery *Biomed. Mater.* **2009**, 4, 1-15.

(10) Stuart, M. A. C.; Huck, W. T. S.; Genzer, J.; Muller, M.; Ober, C.; Stamm, M.; Sukhorukov, G. B.; Szleifer, I.; Tsukruk, V. V.; Urban, M.; Winnik, F.; Zauscher, S.; Luzinov, I.; Minko, S. Emerging applications of stimuli-responsive polymer materials *Nature Materials* **2010**, 9, 101-113.

(11) Dipak, K. S., Smart Elastomers. In *Current Topics in Elastomers Research*, CRC Press: 2008.

(12) Weder, C. Mechanoresponsive Materials *J. Mater. Chem.* **2011**, 21, 8235-8236.

(13) Black, A. L.; Lenhardt, J. M.; Craig, S. L. From molecular mechanochemistry to stress-responsive materials *J. Mater. Chem.* **2011**, 21, 1655-1663.

(14) Davis, D. A.; Hamilton, A.; Yang, J.; Cremar, L. D.; Van, G. D.; Potisek, S. L.; Ong, M. T.; Braun, P. V.; Martinez, T. J.; White, S. R.; Moore, J. S.; Sottos, N. R. Force-induced activation of covalent bonds in mechanoresponsive polymeric materials *Nature* **2009**, 459, 68-72.

(15) Lenhardt, J. M.; Black, A. L.; Beiermann, B. A.; Steinberg, B. D.; Rahman, F.; Samborski, T.; Elsakr, J.; Moore, J. S.; Sottos, N. R.; Craig, S. L. Characterizing the mechanochemically active domains in gem-dihalocyclopropanated polybutadiene under compression and tension *Journal of Materials Chemistry* **2011**, 21, 8454-8459.

(16) Crenshaw, B. R.; Weder, C. Deformation-Induced Color Changes in Melt-Processed Photoluminescent Polymer Blends *Chemistry of Materials* **2003**, 15, 4717-4724.

(17) Sagara, Y.; Kato, T. Mechanically induced luminescence changes in molecular assemblies *Nat. Chem.* **2009**, 1, 605-610.

(18) Peppas, N. A.; Slaughter, B. V.; Kanzelberger, M. A., 9.20 - Hydrogels. In *Polymer Science: A Comprehensive Reference*, Elsevier: Amsterdam, 2012; pp 385-395.

(19) Bruns, N.; Pustelny, K.; Bergeron, L. M.; Whitehead, T. A.; Clark, D. S. Mechanical Nanosensor Based on FRET within a Thermosome: Damage-Reporting Polymeric Materials *Angewandte Chemie-International Edition* **2009**, 48, 5666-5669.
(20) Hoare, T. R.; Kohane, D. S. Hydrogels in drug delivery: Progress and challenges *Polymer* **2008**, 49, 1993-2007.
(21) Tanaka, T. Gels *Scientific American* **1981**, 244, 124-138.
(22) Zhou, J.; Ellis, A. V.; Voelcker, N. H. Recent developments in PDMS surface modification for microfluidic devices *Electrophoresis* **2010**, 31, 2-16.
(23) Vickers, J. A.; Caulum, M. M.; Henry, C. S. Generation of Hydrophilic Poly(dimethylsiloxane) for High-Performance Microchip Electrophoresis *Analytical Chemistry* **2006**, 78, 7446-7452.
(24) Efimenko, K.; Wallace, W. E.; Genzer, J. Surface Modification of Sylgard-184 Poly(dimethyl siloxane) Networks by Ultraviolet and Ultraviolet/Ozone Treatment *Journal of Colloid and Interface Science* **2002**, 254, 306-315.
(25) Berdichevsky, Y.; Khandurina, J.; Guttman, A. s.; Lo, Y. H. UV/ozone modification of poly(dimethylsiloxane) microfluidic channels *Sensors and Actuators B: Chemical* **2004**, 97, 402-408.
(26) Hillborg, H.; Gedde, U. W. Hydrophobicity recovery of polydimethylsiloxane after exposure to corona discharges *Polymer* **1998**, 39, 1991-1998.
(27) Hillborg, H.; Ankner, J. F.; Gedde, U. W.; Smith, G. D.; Yasuda, H. K.; Wikstrom, K. Crosslinked polydimethylsiloxane exposed to oxygen plasma studied by neutron reflectometry and other surface specific techniques *Polymer* **2000**, 41, 6851-6863.
(28) Yang, J. Y.; Xu, C. Y.; Wang, C.; Kopecek, J. Refolding hydrogels self-assembled from N-(2-hydroxypropyl)methacrylamide graft copolymers by antiparallel coiled-coil formation *Biomacromolecules* **2006**, 7, 1187-1195.

6.8 Supporting Information

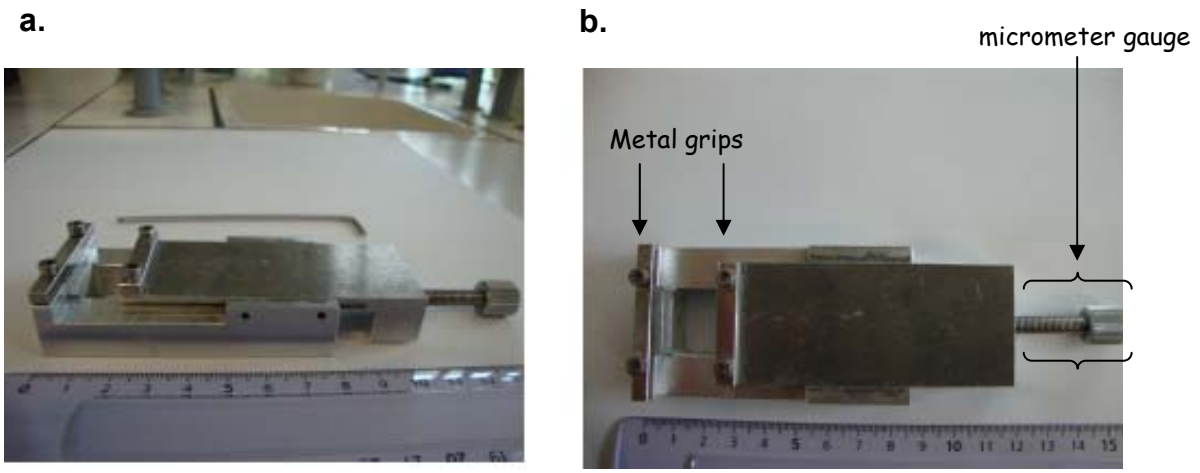

Figure S1: Lateral view (**a**) and top (**b**) view of the home-made device used for the stretching of the silicone sheet exposed to UVO and the hybrid system silicone-hydrogel. The complete device, made in stainless metal, is equipped with two metal grips allowing "to pinch" strongly the silicone for stretching experiments. A millimeter gauge is used to stretch the desired level.

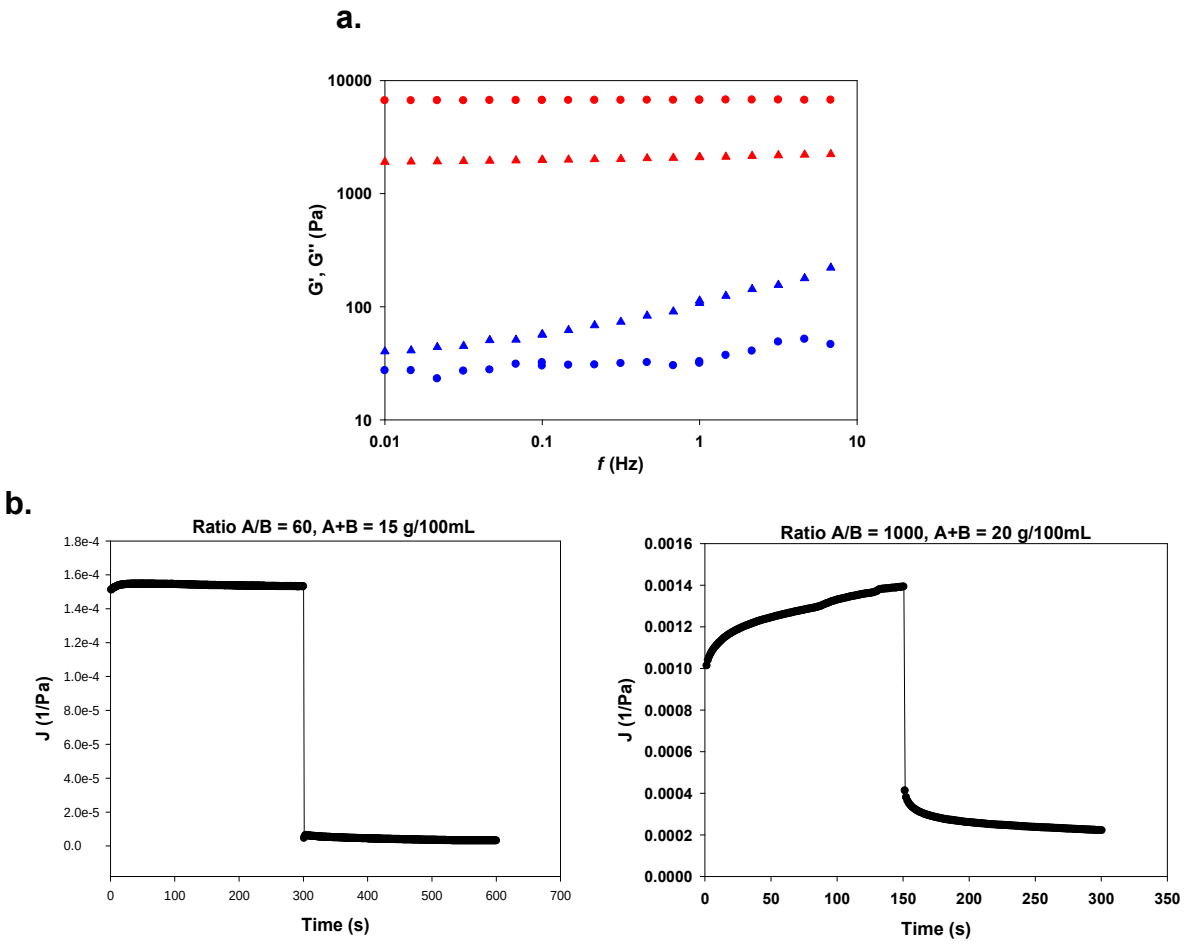

Figure S2: (**a**) Storage moduli (G', red) and loss moduli (G'', blue) of PAM hydrogels as a function of angular frequency going from 0 to 10 Hz. Dot points and triangles correspond to the PAM gel prepared from a solution of A/B=60, A+B=15g/100mL and A/B=1000, A+B=20g/100mL respectively; (**b**) Creep recovery measurements of the two PAM gel prepared from a solution of A/B=60, A+B= 15g/100mL (left) and A/B=1000, A+B= 20g/100mL (right).

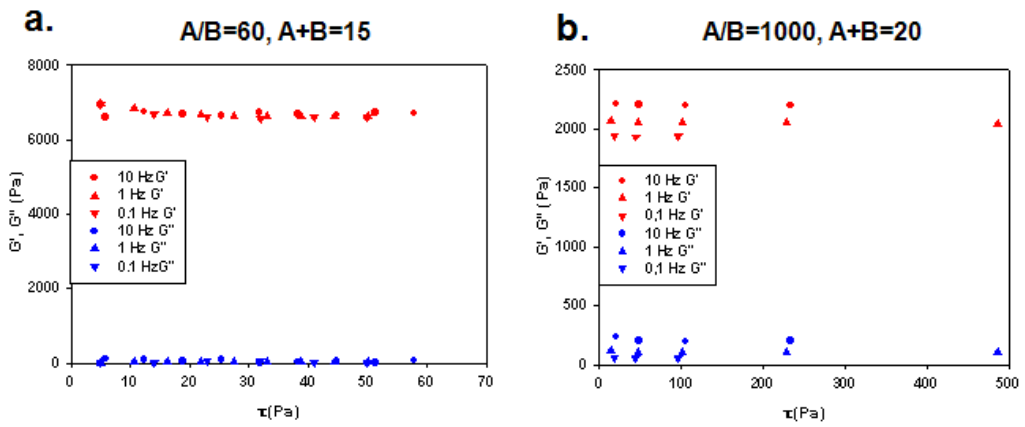

Figure S3: G' (red) and G'' (blues) values as function of an applied force (Pa), at 3 fixed angular frequencies (0.1, 1 and 10 Hz). Dot points, triangles and upside down triangle correspond to the PAM gel prepared from a solution of A/B=60, A+B=15g/100mL and A/B=1000, A+B=20g/100mL respectively. We observed a linear regime allowing to do the creep recovery experiment for the two selected PAM hydrogel (see figure S2).

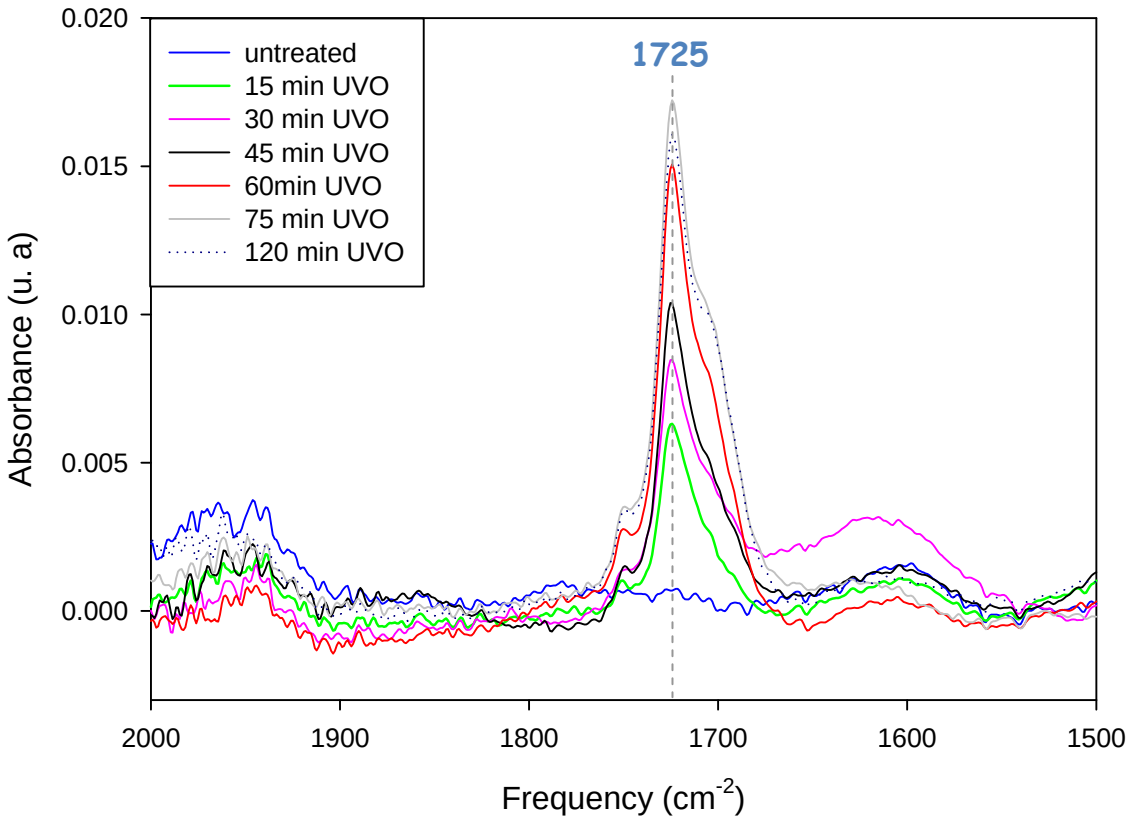

Figure S4: FTIR evolution of the absorbance vibration band observed at 1725 cm^{-1} on silicone SMI at various exposition timess of UVO: 15, 30, 45, 60, 75, 120 minutes.

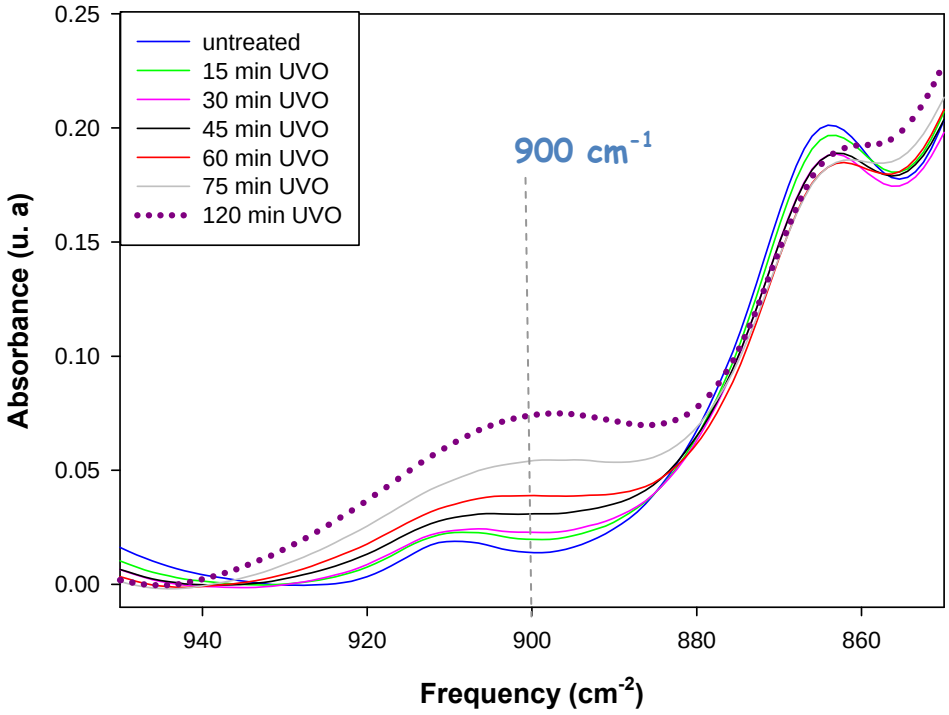

Figure S5: FTIR evolution of the absorbance vibration band observed at 900 cm^{-1} on silicone SMI at various exposition times of UVO: 15, 30, 45, 60, 75, 120 minutes.

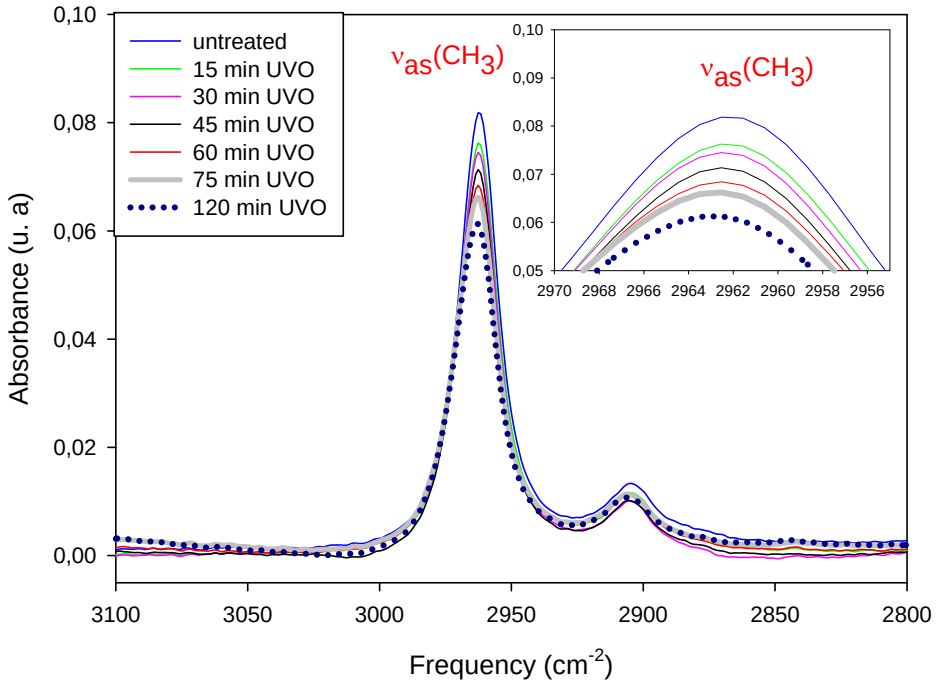

Figure S6: FTIR evolution of the absorbance vibration band observed at 2960 cm^{-1} on silicone SMI at various exposition times of UVO: 15, 30, 45, 60, 75, 120 minutes.

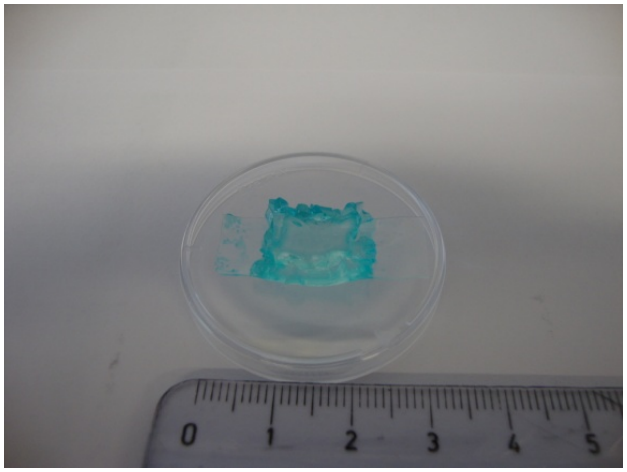

Figure S7: Picture of the PAM hydrogel-Silicone (SMI) system when the gel has been dried 12 hours under a fumehood. The PAM hydrogel has been coloured in blue by using several drops (10 µL) of 1M methylene blue solution.

Conclusion

The goal of my thesis was to develop new routes to design chemo-mechano-responsive materials, materials that respond chemically to a mechanical stress. In the past, my host group had already developed several strategies to achieve this goal, yet the designed systems are often difficult to implement or to generalize.

In the case of my work, the mechanical stress is provided by stretching the material. More precisely I was looking for materials that are inert at rest and which induce chemical reactions or trigger specific adsorption when stretched. Moreover, we were looking for systems that are reversible during stretching/unstretching cycles.

All the systems designed during my PhD thesis were based on functionalization of silicone sheets. Silicones have the great advantage to be elastic and transparent, two essential properties that are used to develop chemo-mechano-responsive materials, but they are also chemically difficult to modify. We decided to build on silicone sheets. Three different strategies were followed.

1) The first strategy is to create cryptic site surfaces by embedding ligands into PEG brushes. In order to achieve this goal we first had to chemically modify the silicone surface. This was done by UV-Ozone (UVO) treatment of the surface followed by silanization to anchor chemically active thiol groups onto the silicone substrate. The difficulty that we had to overcome was to chemically modify the silicone substrate with enough thiol groups in such a way that it does not break under stretching. The formation of cracks due to stretching is usually the case with most of the silicone surface treatments. We established an empiric and useful diagram showing the appearance of cracks according to the level of stretching and the exposition time of UVO. The modification of the silicone surface was monitored by IR, contact angle measurements and electronic microscopy. We achieved the design of a cryptic site surface by embedding biotin moieties into a PEG brush. This system was mildly interacting with Streptavidin at rest and more strongly interacting when stretched. Yet we could not succeed to create a reversible system meaning that by returning to the non-stretched state the Streptavidin remained anchored on the surface. For comparison, by using the polymer plasma technique to modify the silicone surface and the same model system (Biotin/PEG brusches/Streptavidin), Bacharouche at *al*. succeed to get a reversible behaviour of the surface. Finally, it must be noted that one major difficulty encountered in this approach

lies in the fact that one cannot measure the density of grafted groups on the surface nor of active groups after UVO treatment. This renders difficult the progress and the improvement of this system.

2) We then developed a strategy based on the covalent anchoring of enzymes into gels with the idea that, by stretching the gel, the enzymes change conformation due to applied mechanical forces and that these conformation changes alter their enzymatic activity. We used cross-linked (poly-l-lysine/hyaluronic acid) multilayers as gel. We incorporated in this film β-galactosidase that was covalently coupled to the gel. The film was deposited on a silicone sheet. We succeeded in modulating the enzyme activity in the film under stretching and this system appears as partially reversible under stretching/unstretching cycles. **This work represents the first reported system where enzymatic activity can be modulated by stretching due to modulation of the enzyme conformation**. Yet the system should still be improved. As for the cryptic site systems discussed above, one of the difficulty of this study was that we could neither directly characterize the covalent coupling degree of the enzyme to the film nor could we prove the enzymatic conformation change. This later issue still represents a real challenge for the future in surface science. Moreover, the development of these systems also requires a better characterization of these films under stretching at a nanometer scale. This will require the development of molecules that act as mechanophores and that are sensitive to a large range of stresses that are internal to the gel.

3) We made also use of the silicone functionalization by UVO to design a mixed system consisting of a silicone sheet onto which is covalently attached a polyacrylamide hydrogel with the goal to create a stretchable gel into which one can covalently fix enzymes. These enzymes can thus be put under mechanical stress. We succeeded in creating a system that can be stretched up to 150% without detachment of the gel from the silicone and without inducing cracks in the gel. This is, to our knowledge the first mixed silicone/hydrogel system reported so far. Our idea was first to incorporate into the gel mechanophores such as bispyrene molecules that change their absorption spectrum when undergoing a change from a staked to an extended conformation. Yet, after incorporation of these molecules in the gel, even at rest of the gel, the molecules were in the extended conformation so that no stretching effect could be envisioned any more. Other mechanophore systems could be envisioned in the future.

We nevertheless could make use of the bispyrene compounds as pH sensor in morphogen driven polyelectrolyte film constructions. This result was published in *Soft Matter*.

Perspectives

The development of chemo-mechano-responsive systems is in its infancy and is intimately related to that of mechano-chemistry. Up to now, mechanical forces are absent from chemistry and designing molecules or systems that induce chemical reactions under the application of a force represents a real challenge. But, why addressing this challenge? Biology offers an answer to this question. First biology was devoted to classify living species. Later emerged cell biology where it was shown that evolved living organisms are organized in cells. Then chemistry came into play where one tried to explain the cellular mechanisms entirely by chemistry. Now one discovers that chemical signals are not the only player of the biological game but that mechanical forces are also crucial for cell development and adaptation. This requires that cells convert mechanical information into chemical output and nature developed a whole bench of strategies for this purpose. What this shows is that mechanical forces are an integral part of adaptative systems. Over the last years, physical and chemical science has evolved from the understanding and from the engineering of "simple" systems towards the development of complex systems, one ultimate goal being to be able to create self-replicating, self-organizing and self-adapting systems. Mechano-chemistry will play a major role in this evolution and the systems that we are starting to develop constitute the embryos of this evolution. But there is still a long way to go.

Annex 1

Preparation of Bispyrene 2 from the intermediate 4

The description of the synthesis of the intermediate **4** is already reported in the part 3.6 of chapter 3 (supporting information).

1. Preparation of the oligoethylene glycol derivative 8

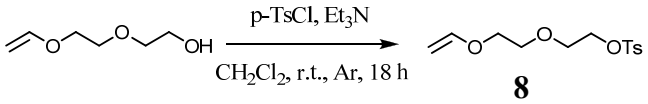

8

Procedure inspired from literature[1]: To a solution of 200 mg (1.51 mmol) of di(ethylene glycol) vinyl ether in 0.3 mL triethylamine under argon was added 298 mg (1.56 mmol, 1.03 eq) of *p*-toluenesulfonyl chloride in 0.25 mL dry CH_2Cl_2 over 5 min. The reaction mixture was stirred for 18 hours and 10 mL CH_2Cl_2 was added. The contents were washed with excess water (2 times), 5% $NaHCO_3$ solution, and water again, and dried over $MgSO_4$, filtered and the solvent evaporated to give 378 mg (87 %) of **8** as colourless liquid (contains little starting material). ^{1}H NMR ($CDCl_3$, 400 MHz) δ (ppm): 7.8 (m, 2H), 7.34 (m, 2H), 6.46 (dd, J=14.3, 6.8 Hz, 1H), 4.18 (m, 3H), 4.01 (dd, J=4.6, 2.2 Hz, 1H), 3.76 (m, 3H), 3.71 (m, 2H), 3.67 (m, 2H), 2.45 (s, 3H).

2. Substitution of the pyrene derivative 4 with the oligoethylene glycol derivative 8

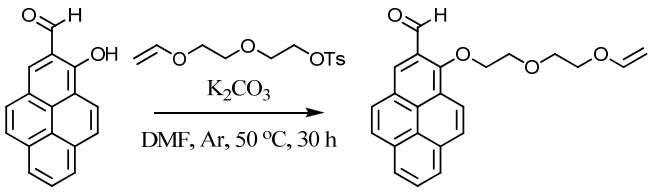

4 **9**

1-(2-(2-(vinyloxy)ethoxy)ethoxy)pyrene-2-carbaldehyde (**9**). A solution of 100 mg (0.41 mmol) of compound **4** and 561 mg (4.06 mmol, 10 eq) of K_2CO_3 in 5 mL DMF was heated at 50 °C under argon. To this bright red solution, 140 mg (0.49 mmol, 1.2 eq) of tosylate **8** in 1 mL DMF was added slowly, heating and stirring continued during overnight. Water was added and solvent evaporated under reduced pressure. The residue was extracted with CH_2Cl_2 (3 times) and the combined organic phase was washed with water, dried over $MgSO_4$, solvent

evaporated to give light green viscous liquid. This was flashed in a silica gel column eluting with CH_2Cl_2 to get 108 mg (74 %) of product **9** as light brown semi solid (contains little tosylate starting material). ^{1}H NMR ($CDCl_3$, 400 MHz) δ (ppm): 10.87 (s, 1H), 8.62 (s, 1H), 8.51 (d, J=9.2 Hz, 1H), 8.23-8.12 (m, 3H), 8.1-8.0 (m, 3H), 6.56 (dd, J=14.3, 6.8 Hz, 1H), 4.51 (m, 2H), 4.25 (dd, J=14.3, 2.2 Hz, 1H), 4.18 (m, 1H), 4.06 (dd, J=6.8, 2.2 Hz, 1H), 4.02 (m, 2H), 3.96 (m, 2H). 3.89 (m, 2H).

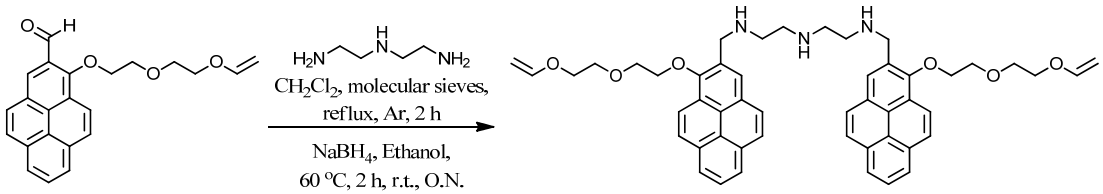

9 **2**

N1-((1-(2-(2-(vinyloxy)ethoxy)ethoxy)pyren-2-yl)methyl)-N2-(2-((1-(2-(2-(vinyloxy)-ethoxy)ethoxy)pyren-2-yl)methylamino)ethyl)ethane-1,2-diamine (**7**)[2]. A stirring solution of 108 mg (0.3 mmol, 1 eq) of Pyrene derivative (**9**) and 14 mg (15 µL, 0.135 mmol, 0.45 eq) of diethylenetriamine in 13 mL CH_2Cl_2 with few molecular sieves was refluxed for 5 h under argon. The reaction mixture was cooled down and filtered off the molecular sieves and the filtrate evaporated. To this semi oily yellow residue 13 mL ethanol and 34 mg (0.9 mmol, 6 eq) of $NaBH_4$ were added and heated at 60 ^{o}C for 4 h and stirring continued for 16 h at room temperature. Solvent was evaporated under reduced pressure and the residue was taken into CH_2Cl_2, washed with 1 M NaOH solution (3 times), water and concentrated by evaporation to give 80 mg (0.10 mmol, 77%) compound **11** as light yellow semisolid. This compound was used without further purification. ^{1}H NMR ($CDCl_3$, 400 MHz) δ (ppm): 8.62 (s, 2H), 8.51 (d, J=9.2 Hz, 2H), 8.3-8.0 (m, 12H), 6.50 (dd, J=14.3, 6.8 Hz, 2H), 4.51 (m, 4H), 4.30 (m, 28H).

References

1. Pengo, P.; Polizzi, S.; Battagliarin, M.; Pasquato, L.; Scrimin, P. *J. Mater. Chem.* **2003**, *13*, 2471-2478.

2. Shiraishi, Y.; Tokitoh, Y.; Hirai, T. *Org. Lett*. **2006**, *17*, 3841-3844.

Design of mechanoresponsive surfaces and materials

The goal of my PhD was **to develop new routes to design chemo-mechanoresponsive materials**, materials that respond chemically to a mechanical stress, in a reversible way. All the systems designed during my PhD thesis were based on the functionalization of silicone sheets. First we created *cryptic site surfaces* by embedding biotin ligands into PEG brushes. The couple streptavidin/biotin was used as a model system. At rest, the surface so-prepared was antifouling and biotin ligands were specifically recognized by the streptavidin when the surface was stretched at 50%. Unfortunately, in this first approach, the mechanosensitive surface did not lead to a reversible process. In a second approach, we modified the silicone surface by using the polyelectrolyte multilayer (PEM) film deposition. This strategy was based on the covalent cross-linking of modified enzyme, the *β*-galactosidase, into the PEM. We succeeded in modulating the enzyme activity in the film under stretching and this approach appears as partially reversible under stretching/unstretching cycles. **This work represents the first reported system where enzymatic activity can be modulated by stretching due to modulation of the enzyme conformation**. In a last approach, we also designed a mixed system consisting of a silicone sheet onto which a polyacrylamide hydrogel is covalently attached with the goal to create a stretchable gel into which one can covalently attach enzymes or chemical mechanophores. These enzymes or mechanophores can thus be put under mechanical stress. We succeeded in creating a system that can be stretched up to 50% without detachment of the gel from the silicone and without inducing cracks in the gel.
Keywords : Chemo-mechanoresponsive materials, surface modification, polydimethylsiloxane, polyelectrolyte multilayers, biocatalysis control, polyacrylamide hydrogels, polymerization, soft matter.

Conception des surfaces et des matériaux mécano-répondants

Le but de ma thèse a été de **concevoir des matériaux chimio-mécano répondants**, des matériaux capables de permettre une transformation chimique réversible lorsqu'ils sont soumis à un stress mécanique. Tous les systèmes conçus ont été développés sur des substrats en silicone. Une première approche a consisté à créer des *surfaces à sites cryptiques* où une biotine est enfouie dans des brosses de chaines de poly(éthylène glycol). Le système streptavidine/biotine a été utilisé comme modèle. Ces surfaces sont anti-adsorbantes à la streptavidine sauf lorsqu'elles sont étirées à 50% où la biotine est reconnue mais les surfaces sont non réversibles. Dans une seconde approche, nous avons modifiés la surface du silicone par adsorption d'une multicouche de polyélectrolytes. Cette stratégie est basée sur la réticulation covalente du film par l'enzyme *β*-galactosidase modifiée. Nous sommes ainsi parvenus à créer une surface présentant une activité catalytique modulable par l'étirement mécanique, et ce, d'une façon partiellement réversible. Ce travail représente **le premier exemple d'un système où une contrainte mécanique imposée à un matériau permet la déformation conformationnelle d'une enzyme et ainsi la diminution de l'activité catalytique**. Dans une dernière approche, nous avons conçu un système mixte composé d'un substrat de silicone sur lequel un gel de polyacrylamide est greffée de façon covalente. Des enzymes ou des mécanophores pourront ainsi être inclus dans le réseau polymérique du gel de polyacrylamide et être étirés. Nous sommes parvenus à préparer de tels systèmes où l'hydrogel reste solidaire du film de silicone, sans apparition de craquelures jusqu'à 50% d'étirement.
Mots-clés : matériaux chimio-mécano répondants, traitement de surface, polydiméthylsiloxane, multicouches de polyélectrolytes, biocatalyse contrôlée, hydrogels de polyacrylamides, polymérisation, matériaux mous.